

Microarray Structures for Sensing, Stimuli-
responsive Releases, Shaped Microcages and
Templating Minified Microstructures

A Thesis Submitted to the University of London for the Degree of
Doctor of Philosophy



By
Jiaxin Zhang
Queen Mary
University of London

Supervisor: Professor Gleb B. Sukhorukov

School of Engineering and Materials Science

Queen Mary University of London

February 2021

Declaration

I certify that the present work is prepared solely by me during the course of my studies at Queen Mary, University of London. It has not been submitted for a degree at this or any other University. Any words and/or figures from the work of other people are fully acknowledged according to standard referencing.

This thesis fully combines with the regulations set by the University of London and the Queen Mary, University of London.

Jiabin Zhang

February 2021

Abstract

Microarray structure plays a key role in a variety of fields ranging from optical devices, electronics to drug delivery systems due to the special periodic micropatterns, which can not only perform the capability of light diffraction, show the potential as photonic sensors, but also provide the empty space for drug loading when the highly ordered structures are microwells. Especially, the microarray structure can be transferred onto other polymers, after the introduction of microcontact printing techniques.

Inspired by the versatility of microarray structures, this work aims at exploring and expanding its potential multidisciplinary applications including multi-sensing platforms, drug delivery vehicles of microchamber array films and microcages, and structuring templates. These can be achieved by functionalizing the microarray structure with extra properties of differently structured materials including polyelectrolytes, polyester, precursor ceramics.

To provide a better understanding of the research subjects of this work, an introduction is presented at the beginning of **chapter 1**, followed by **chapter 2** of a literature review. The description of the experimental section including materials, methods and instruments is followed in **chapter 3**. The results start from **chapter 4** which investigates the possibilities of microarray structure for media, pH, ions and thermal sensing using stimuli-responsive polymers. The potential of the microarray structure for preparing drug delivery vehicles is further determined in **chapter 5**. Biodegradable polymers were fabricated into microchamber array films with the capability to efficiently encapsulate and enzymatically controlled release small hydrophilic molecules. In **chapter 6**, a novel method for preparing shape and size defined biodegradable microcages for drug delivery based on microarray structure is presented. Moreover, **chapter 7** proposed an efficient route to microfabricate proportionally minified microarray structure with the assistance of novel precursor ceramics. Finally, general conclusions of the overall results of this work along with outlooks are summarized in **chapter 8**.

Table of Contents

Abstract.....	I
Acknowledgements.....	V
List of Figures	VI
List of Tables	IX
List of Symbols and Abbreviations	X
1. Introduction.....	1
1.1. Microarray Structure.....	1
1.2. Challenges of the Versatile Applications of Microarray Structure.....	1
1.3. Motivation and Aims.....	4
2. Literature Review	7
2.1. Polyelectrolytes.....	7
2.1.1. Classification of Polyelectrolytes.....	7
2.1.2. Theory and Properties of Polyelectrolytes	9
2.1.3. Applications of Polyelectrolytes	11
2.2. Polyelectrolyte Complexes.....	12
2.2.1. Process for the Formation of PEC.....	12
2.2.2. Influencing Factors of PEC	14
2.2.3. Biomedical Applications of PEC	18
2.3. Polyelectrolyte Multilayers	20
2.3.1. Fabrication of PEM via Layer-by-Layer Technique	20
2.3.2. Driving Forces and Influence Factors of PEM assembly	22
2.3.3. Biomedical Applications of PEM.....	25
2.4. Polycaprolactone.....	29
2.4.1. The Production Methods of Polycaprolactone.....	30
2.4.2. Physicochemical and Biodegradability of Polycaprolactone	32
2.4.3. Biomedical Applications of Polycaprolactone	35
2.5. Polylactic Acid	45
2.5.1. The Production Methods of Polylactic Acid	45
2.5.2. Physicochemical Properties and Biodegradability of Polylactic Acid	48
2.5.3. Biomedical Applications of Polylactic Acid	55

2.6.	Microarray Structure.....	65
2.6.1.	The Production Method of Microarray Structure	66
2.6.2.	Rigorous Coupled Wave Analysis	71
2.6.3.	Applications of Microarray Structure	74
3.	Materials and Methods	80
3.1.	Materials	80
3.2.	Methods	82
3.2.1.	Fabrication of Patterned PDMS Stamp.....	82
3.2.2.	Preparation of Fluorescently Labelled PAH.....	84
3.2.3.	Polyelectrolyte Multilayers Preparation by Dip-coating Robot	85
3.2.4.	Printing of Polyelectrolyte Multilayer Microchamber Arrays	86
3.2.5.	Preparation of Polyelectrolyte Complex Micropillar Array Films.....	88
3.2.6.	One-dip Method for Preparing PCL/PLA Microchamber Array Films.....	89
3.2.7.	Treatments for Microarray Films.....	90
3.2.8.	Generating Fraunhofer Laser Diffraction Patterns.....	91
3.3.	Instruments	92
3.3.1.	Scanning Electron Microscopy (SEM)	92
3.3.2.	Focused Ion Beam Scanning Electron Microscopy (FIB-SEM)	97
3.3.3.	Fluorescence Spectrometer	100
3.3.4.	Fluorescence Microscopy	106
3.3.5.	Confocal Laser Scanning Microscopy (CLSM)	109
3.3.6.	Differentiated Scanning Calorimetry (DSC)	112
3.3.7.	UV-vis Spectroscopy (UV-vis)	113
4.	Microarray Films for Real-time Sensing via Diffraction Patterns	116
4.1.	Introduction	116
4.2.	Sensing of Different Environmental Stimuli.....	117
4.2.1.	Media Sensing	118
4.2.2.	pH Sensing	118
4.2.3.	Ions Sensing	128
4.2.4.	Temperature Sensing	133
4.3.	Numerical Simulations of Different Environmental Stimuli.....	137

4.4.	Conclusions	145
5.	Microchamber Array Films for Cargo Encapsulation and Release	150
5.1.	Introduction	150
5.2.	Preparation of PCL Microchamber Array Films.....	152
5.3.	Enzymatic Degradation Behaviours of PCL Microchamber Array Films.....	154
5.4.	Cargo Encapsulation in PCL and PLA Microchamber Array Films	159
5.4.1.	Encapsulation of BSA-FITC.....	161
5.4.2.	Encapsulation of CF	162
5.4.3.	Encapsulation of DEX.....	166
5.5.	Encapsulation of Small and Hydrophilic Cargos in PCL-PLA Microwell Arrays.....	169
5.6.	Enzymatic Release Behaviours of PCL-PLA (1:2) Microchamber Arrays	173
5.7.	Conclusions	176
6.	Biodegradable Microcages for Dye/Drug Encapsulation and Release	178
6.1.	Introduction	178
6.2.	Preparing Drug-loaded Microcages from Microarray Structure.....	181
6.3.	Characterization of Printing Process and Resulted Drug-loaded Microcages	183
6.4.	Release Experiment of Drug-loaded Microcages	195
6.5.	Conclusions	199
7.	Precursor Ceramics Assisted Templating of Minified Microarray Structure.....	201
7.1.	Introduction.....	201
7.2.	Replica Moulding Method for Preparing Minified Microarray Structures	204
7.2.1.	Design and Synthesis of Precursor Ceramics	206
7.2.2.	Preparation of Minified Inorganic Microarray Structures.....	207
7.3.	Characterization of Shrink-Sized Microarray Structures.....	210
7.4.	Conclusions	213
8.	General Conclusions and Outlooks	215
8.1.	Conclusions	215
8.2.	Outlooks.....	217
	References	222
	Publications.....	264

Acknowledgements

My deepest gratitude would undoubtedly go first and foremost to my PhD supervisor Professor Dr Gleb B. Sukhorukov who not only offers me the opportunities to pursue my PhD degree in QMUL but also provides a free working environment and lifestyle that enables me to learn and enjoy my research career. Moreover, he can always squeeze time from the packed schedule to discuss my experiment and follow my project. Thanks to his constant guidance both on lab work and on mental health, I can proudly note that I really enjoy my PhD life and take pride in being his PhD student in the past three years.

My sincere appreciation also goes to all the collaborators, particularly, Prof. Johannes Frueh, Dr David Gould, who inspired me and provided many suggestions on my research work. Also, I would like to express my gratitude to all the SEMS staffs, including Dr Dongsheng Wu, Dr Russell Bailey, Mr Maurizio Leo who trained and helped me a lot on various equipment, and especially to Mr Chris Mole and Mr Shafir Iqbal for their constant help with the general lab equipment use and lab management.

It is indeed honoured and lucky to be a member of Gleb's group where I can not only communicate experimental information, techniques, and ideas but also share daily life trivia, providing a nice and free research atmosphere. I wish to thank the senior group member Dr Meiyu Gai and Dr Samantha Gabriel who gave me great help at the beginning of lab work time. Besides, I would like to thank Valeriya Kudryavtseva who is knowledgeable and hard-working, encouraged and inspired me in many ways. My sincere thanks would also go to other group members, visitors to our lab, and all my friends. Officially here, I also acknowledge my funding agency Chinese Scholarship Council (CSC) (Grant No.201706630010) which funded me to study abroad for several years.

In the end, I dedicate this thesis to my beloved parents and relatives for their love and unconditional support, especially to my girlfriend Rui Sun, I can never thank her enough for her continued love, encouragement, and belief in me. I want to say I love you all very much!

List of Figures

Figure 2.1 Classification of polyelectrolytes based on the charge and position of ionic sites.	8
Figure 2.2 Structure models of polyelectrolyte complexes.	13
Figure 2.3 Schematic demonstration of the aggregation of PECs.	14
Figure 2.4 Schematic illustration of the interactions between polycations and polyanions at different pH. ..	16
Figure 2.5 Schematic illustration of the pH influence on PAA/PAH PEC in different pH conditions.	17
Figure 2.6 Schematic demonstration of PEC of cationic antimicrobial polymyxin B and anionic PSS.	19
Figure 2.7 Polyelectrolyte multilayer preparing procedures.	21
Figure 2.8 Zeta-potential as a function of layer number for coated polystyrene sulfate latex particles.	22
Figure 2.9 Illustration of polyelectrolyte configurations at the interface with different charge densities.	23
Figure 2.10 The thickness of PEM deposited under 0.1 M sodium salt of different anions.	25
Figure 2.11 The fabrication process of model drug-loaded fibroin protein/gelatin PEM and its release.	27
Figure 2.12 The process of producing drug-loaded hollow capsules and the enzymatic release.	28
Figure 2.13 The chemical structure of polycaprolactone.	30
Figure 2.14 Synthesis of polycaprolactone by the polycondensation of 6-hydroxyhexanoic acid.	31
Figure 2.15 Schematic illustration of ROP mechanisms for the ROP of lactone based on different catalysts. .	31
Figure 2.16 The enzymatic degradation of PCL film in PBS containing different lipases.	33
Figure 2.17 Accelerated degradation of PCL over 5 weeks in NaOH.	34
Figure 2.18 Schematic illustration of the preparation of PCL microspheres.	37
Figure 2.19 Schematic illustration of preparation of PCL NPs.	38
Figure 2.20 3D Scaffold-based system of tissue engineering	40
Figure 2.21 Fabrication methods for PCL scaffolds in the tissue engineering area.	41
Figure 2.22 Praziquantel loaded implants made of PEG/PCL blends.	42
Figure 2.23 The concept of PCL suture loaded with anti-inflammation drug Diclofenac.	43
Figure 2.24 SEM morphology of fabricated PCL membranes.	44
Figure 2.25 Stereoisomers of lactic acid.	45
Figure 2.26 PLA synthesis methods from poly(lactic acid).	46
Figure 2.27 Three stereoisomeric forms of lactide.	49
Figure 2.28 Biodegradation behaviours of PLA.	52
Figure 2.29 SEM images of PLA films after degradation by <i>Kibdelosporangium aridum</i> at 30°C.	54
Figure 2.30 Schematic illustration of the preparation methods of PLA micro- and nanoparticle.	57
Figure 2.31 Schematic descriptions of different methods for fabricating polymer particles.	58
Figure 2.32 Schematic descriptions of template method process and fabricated PLA microparticles.	59
Figure 2.33 Diagram of mandibular reconstruction using a PLLA mesh and bone marrow.	62
Figure 2.34 SEM images and the diameter distribution of electrospun fibres.	63
Figure 2.35 SEM images of PLA suture loaded with PM-Ds at different magnifications.	64
Figure 2.36 Implantable devices made by braiding.	65
Figure 2.37 Schematic demonstration of three forms of photolithography.	68
Figure 2.38 Interference lithography setups and representative microstructures.	69
Figure 2.39 Schematics with different processes.	70
Figure 2.40 SEM micrographs of 3D shapes.	71
Figure 2.41 Geometry of different analysed grating structure.	72
Figure 2.42 Optical microscope images showing the triggered release of MF particles into water.	75
Figure 2.43 SEM images of the microchamber array for culturing nerve cells.	76
Figure 2.44 Micropillar arrays for molecular immunodiagnosis.	76
Figure 2.45 Sensing mechanisms of the sensors based on a flat electrode and microarray electrode.	77
Figure 2.46 The specification of a silicon substrate for bacteria retention study.	78
Figure 3.1 Structural formulas of materials used in the experiment.	81
Figure 3.2 SEM images of silicon master of different specifications.	82
Figure 3.3 Schematic illustration of the preparation of patterned PDMS stamp from various templates.	84
Figure 3.4 Images of homemade Layer-by-layer dip-coating machine.	85
Figure 3.5 The process of preparing PEM microchamber arrays.	88

Figure 3.6 The process of preparing PEC micropillar arrays.	89
Figure 3.7 The process of preparing PCL or PLA microchambers.	90
Figure 3.8 The Fraunhofer diffraction pattern imaging equipment.	92
Figure 3.9 Images of FEI Inspect F scanning electron microscope.	93
Figure 3.10 Principle of the scanning electron microscope.	93
Figure 3.11 Origin and information depth of different electrons.	94
Figure 3.12 Schematic energy spectrum of electrons emitted.	94
Figure 3.13 Some atom-high energy electron interactions.	96
Figure 3.14 Primary ion beams generating secondary electrons and the collision cascade.	98
Figure 3.15 The image visualizes applications of a FIB-SEM combined system.	100
Figure 3.16 One form of Jablonski diagram for an organic molecule,	101
Figure 3.17 Chemical structure of typical fluorescent compounds.	103
Figure 3.18 Schematic illustration of fluorescence spectrometer.	104
Figure 3.19 Demonstration of Epifluorescence microscope.	107
Figure 3.20 Schematic diagram of confocal microscopy principles.	110
Figure 3.21 Different transitions between various electronic states in UV-Vis spectroscopy.	113
Figure 3.22 Optical illustration a typical of double-beam UV-vis instrument.	114
Figure 4.1 Diffraction patterns (a-d), optical micrographs (e-h) of PAA/PAH PEC micropillar arrays as a function of immersion media and solution pH.	120
Figure 4.2 SEM images of PAA/PAH PEC micropillar arrays under different conditions.	121
Figure 4.3 pH sensing behaviours of PAA/PAH PEC micropillar films triggered at different pH values.	121
Figure 4.4 The SEM images of PAA/PAH PEM microchambers of different bilayers.	126
Figure 4.5 The SEM images of the cross-section of PAA/PAH PEM microchambers.	127
Figure 4.6 The SEM images of PAA/PAH 25 bilayers PEM microchamber array film treated at different pH values.	128
Figure 4.7 Diffraction patterns and optical micrographs of PAA/PAH PEC micropillar arrays before, during and after the exposure to calcium ions.	129
Figure 4.8 Line charts of PAA/PAH PEC micropillar arrays sensing different ion of various compositions and concentrations.	132
Figure 4.9 Confocal images of PAA/PAH PEC micropillar array films under various conditions.	133
Figure 4.10 Confocal microscope images of PAA/PAH PEC micropillar arrays and PCL microchamber arrays.	135
Figure 4.11 Laser diffraction patterns (a-d), optical micrographs (e-h) and SEM images (i-l) of PCL microchamber arrays during the thermal sensing process.	136
Figure 4.12 Sketch of the diffraction grating.	139
Figure 4.13 Comparison of experimental and simulated PAA/PAH PEC micropillar array diffraction patterns of ambient state and pH 13 presence in 3D view.	140
Figure 4.14 Comparison between experimental and simulated laser diffraction patterns of microstructured PEC and PCL at varying stimuli.	141
Figure 4.15 Horizontal diffraction pattern intensity comparison between experimental and simulated data of PEC micropillar arrays in different conditions.	143
Figure 4.16 Distance changes between pattern maximums of laser diffraction patterns.	144
Figure 5.1 Schematic illustration of the fabrication of drug-loaded microchamber array films and enzymatic drug release.	153
Figure 5.2 Schematic illustration and SEM images of patterned silicon master.	154
Figure 5.3 SEM images of PCL microchamber array films of different magnification.	154
Figure 5.4 Full degradation time of PCL microchamber arrays in various lipase PS concentrations at 37°C.	155
Figure 5.5 Diffraction patterns of PCL microchamber arrays in different lipase concentration during degradation procedures.	156
Figure 5.6 SEM images and Fraunhofer laser diffraction patterns of PCL microchambers with different enzymatic degradation times at the lipase PS concentration of 0.5mg/ml.	157
Figure 5.7 SEM of 5(6)-carboxyfluorescein dye precipitates loaded in microwells with solution method.	160
Figure 5.8 SEM of 5(6)-carboxyfluorescein dye particles loading into microwells in the dry method.	161

Figure 5.9 SEM images of trapped BSA-FITC in PCL microwells.	161
Figure 5.10 CLSM images of BSA-FITC encapsulated in PCL microchamber array films.	162
Figure 5.11 SEM images of a layer of PCL film of different surface roughness on PDMS stamp after loading CF particle with dry powder loading method.	164
Figure 5.12 Encapsulation of 5(6)-CF in PCL microchamber arrays.	164
Figure 5.13 PCL microchamber arrays encapsulating 5,6-carboxyfluorescein inside microchambers.	165
Figure 5.14 Dye diffusion curve of PCL microchamber arrays encapsulated with 5(6)-carboxyfluorescein. ...	166
Figure 5.15 The SEM images of dexamethasone crystals loaded on PDMS stamp coated with PLA thin layers from different concentration of PLA chloroform solutions.	167
Figure 5.16 The optical images of dexamethasone crystals after homogenizing for different times. At each time, the drug crystals were homogenized at 5000 cycle/min for 30 seconds.	168
Figure 5.17 SEM images of dexamethasone loaded into microwells and after sealing and transferring as microchamber array films.	168
Figure 5.18 The diffusion curve of PCL blend with PLA in different ratios in PBS.	169
Figure 5.19 Encapsulation of 5(6)-CF in PCL-PLA (1:2) microchamber arrays.	170
Figure 5.20 The wall thickness of microchambers and film thickness of microchamber array films of different polymers.	171
Figure 5.21 PCL-PLA (1:2) microchamber arrays encapsulating CF particles inside microchambers.	172
Figure 5.22 Enzymatic degradation of PCL-PLA (1:2) microchambers loaded with dyes.	173
Figure 5.23 The enzymatic dye release curve of PCL-PLA (1:2) microchambers.	175
Figure 6.1 Schematically illustration in the 3D view of preparing drug-loaded microcages.	182
Figure 6.2 Schematic illustration in the cross-section view of preparing drug-loaded microcages.	183
Figure 6.3 SEM images of key stages during the preparation of microcages.	183
Figure 6.4 The specification of the PMMA template as well as the PDMS template for preparing patterned PDMS stamp.	184
Figure 6.5 Schematically illustration of the procedures for preparing microwell-patterned PDMS stamp. ...	185
Figure 6.6 DSC results of polylactic acid (PLA).	187
Figure 6.7 CLSM images of PLA microcages for confirming the encapsulation of CF model drugs.	189
Figure 6.8 After the sandwiched structure of PDMS template - polymer films - flat PDMS being heated and pressed at the different structure and lifting over the flat PDMS, the resulted structure transferred onto a glass slide by gelatin.	192
Figure 6.9 DSC results of PLA, PCL and PLA/PCL blends at different blending ratios.	193
Figure 6.10 The SEM images of printed microcages made of PLA and PLA-PCL blended polymers at different ratios.	194
Figure 6.11 Release curve of biodegradable microcages at different PLA and PCL blending ratios.	195
Figure 6.12 Optical images of CF loaded microcage of different PLA and PCL components after 4 weeks release experiment in PBS solutions at 37°C.	198
Figure 7.1 Schematic illustration of the process of preparing proportionally shrunk microarray structure. .	205
Figure 7.2 The synthesis route of inorganic ceramics.	206
Figure 7.3 Schematical demonstration of the process for fabricating ceramic microarray films.	208
Figure 7.4 The surface morphology of a,b) original patterned PDMS stamp with microwell array surface structure. c,d) micropillar array film made of UV cured precursor polymer moulded from a,b) before the tube furnace pyrolysis. e,f) the inorganic film pyrolyzed from c,d) with shrink-sized micropillar array surface structure.	210
Figure 7.5 The surface morphology of a,b) original patterned PDMS stamp with micropillar array structure. c,d) microwell array film made of UV cured precursor polymer moulded from a,b) before the tube furnace pyrolysis. e,f) the inorganic film pyrolyzed from c,d) with shrink-sized microwell array structure. g,h) new PDMS stamp with shunk micropillar array surface structure cast from e,f).	211
Figure 7.6 The surface morphology of a,b) the new patterned PDMS stamp with micropillar array structure. c,d) the new patterned PDMS stamp with microwell array structure. e,f) microwell array film made of UV cured precursor polymer moulded from a,b) before the tube furnace pyrolysis. g,h) microwell array film made of UV cured precursor polymer moulded from c,d) before the tube furnace pyrolysis.	212

List of Tables

Table 2-1 Past research on polyelectrolyte complexes and their applications in drug delivery.	20
Table 2-2 Examples of biopolymer-based multilayered films for drug delivery.	28
Table 2-3 Examples of biopolymer-based multilayered capsules for drug delivery.	29
Table 2-4 Properties of polycaprolactone.	32
Table 2-5 Different catalysts used for the production of PLA.	47
Table 2-6 General properties of a commercial amorphous PLA (96: 4 L:D ratio content).	50
Table 2-7 Properties of lactide acid polymers.	50
Table 2-8 Advantages and disadvantages of PLA micro- nanoparticles.	56
Table 2-9 PLA-based scaffolds printed with a 3D system.	62
Table 2-10 Specifications of the major lithography techniques.	67
Table 4-1 The height and diameter change of micropillar arrays under different stimuli.	132
Table 7-1 The setup details of the tube furnace for the heat treatment of UV-crosslinked film.	209

List of Symbols and Abbreviations

CF—5,6-carboxyfluorescein

CLSM—confocal laser scanning microscopy

DEX—dexamethasone

FITC—fluorescein isothiocyanate

FIB-SEM—focusing ion beam- scanning electron microscopy

LbL—layer-by-layer (technique)

M_w —molecular weight

PAA—polyacrylic acid

PCL—polycaprolactone

PDMS—polydimethylsiloxane

PEC—polyelectrolyte complex

PEM—polyelectrolyte multilayers

PEI—poly(ethylene imine)

PLA—polylactic acid

PMMA—poly(methyl methacrylate)

PDDA—poly(diallyl dimethylammonium chloride) (100~200kDa)

PSS—poly(styrene sulfonate sodium salt) (70 kDa)

PAH—poly(allylamine hydrochloride)

PLA—polylactic acid

PVA—polyvinyl alcohol

PS—polystyrene

RhB—rhodamine B

SEM—scanning electron microscopy

μ CP—microcontact printing

1. Introduction

1.1. Microarray Structure

The implantation of the periodically micropatterned surface with highly ordered surface features and well-defined dimensions is of great importance in a variety of fields ranging from lab-on-chip, sensing, electronics, optics, to microbiology biochemistry and biomedical areas and so forth. The predesigned surface structure that is either periodical in one direction or two noncollinear directions of well-defined grooves,¹ wells,² pillars³ or even chambers⁴ in microscale is named microarray structure. Generally, the microarray structures are fabricated on proper substrates such as silicon or silicon dioxide with special techniques of photolithography, selective etching and deposition and so forth.⁵ However, the expensive equipment, complex processes, strict fabrication environment standard and even experienced technician put strict limitations on its scale-up productions.⁶ One of the feasible routes to overcome the above difficulties is using the microcontact printing method that imprints and transfers the lithographed microarray structures onto other materials, resulting in reversed predesigned surface morphology.⁷ Thus, when combining the properties of both the imprinted materials and the special periodic surface micropatterns, not only the low cost and massive production of microarray structures is achieved, but also the potential application in interdisciplinary fields can be further explored and expanded.

1.2. Challenges of the Versatile Applications of Microarray Structure

The microarray structure plays an important role in the sensing areas thanks to its special periodical structure. Basically, substrates with surface structures of microarrays are capable of generating diffraction patterns when illuminated with electromagnetic waves.⁸ Laser light, a kind of precisely collimated, coherent and monochromatic electromagnetic wave, has been widely applied in various fields especially in the sensing area.⁹ Typically, diffraction of laser light has been extensively used to magnify minor differences, thus enhance the sensitivity and accuracy of sensors.¹⁰ However, though numerous diffraction-

based sensors have been proposed to measure refractive-index changes,^{11,12} particle parameters,¹³ and identify chemical compounds,^{14,15} viruses,¹⁶ etc., there are limited diffraction-based sensors for detecting thermal, ionic or pH changes. Although traditional sensors such as pH meter or mercury thermometer have already enabled common people to detect and measure normal physiochemical changes, these traditional sensors can only be used in limited range and conditions.^{17,18} While the cutting edge sensors however measure the signals required specific equipment, which is either used by specialized companies and universities only, or the high cost and non-portability (due to large optical readout systems) limit the applications of those sensors.^{19,20} An inexpensive and portable sensing platform to expand the sensing ability as well as the application area of traditional sensors is therefore needed.

In addition, film materials with microarray structures also own the potential as drug delivery vehicles. When the lithographed periodic microstructures on the substrates are micropillars, the surface morphology of imprinted materials will be reversed microwell arrays with empty space in each well, where chemical compounds can be loaded and further released through external stimulations. A similar micropackaging platform has been developed named microchamber array films,^{21,22} which is fabricated by layer-by-layer(LbL) self-assembly technique,²³⁻²⁵ enabling the encapsulation of microparticles, large molecules and hydrophobic cargos for site-specific controlled release via laser radiation.²⁶ However, the micropackaging platform above produced by LbL techniques can only manage to encapsulate cargos with high molecular weight²⁷ or small but hydrophobic molecules²⁸ due to the semi-permeability of multilayer films^{29,30} while the molecular weight of most biologically active is under 500 Da.³¹ Moreover, the inappropriate application of external triggers such as pH³², temperature³³, magnetic field³⁴, sonication³⁵ and laser light³⁶ may cause inefficiency, with the potential to induce deleterious side effects in living systems - prohibiting their applications in biological and medical fields. Therefore, the successful

encapsulation and biologically stimulated release of small hydrophilic molecules remain a significant challenge to the scientific community.

Moreover, the microarray structure can further be employed as the mould for the fabrication of identical microcages for drug delivery. It is reported that a hydrogen template with microwell array surface structure is fabricated by casting gelatin solution on photolithographed micropillar arrays, which allowed the preparation of homogeneous microparticles of predefined size and shape by filling the empty microwells with a polymer-drug solution followed with solidification.^{37,38} However, the formed microparticles are merely the blends of polymers and drugs without polymeric shells to protect the fragile cargos, which may not only lead to the drug burst release and low drug efficiency, but also induce unexpected adverse effects while delivering the active substances.³⁹ Therefore, to avoid the above defects of microparticles, microcapsules are the preferred choice as drug delivery vehicles with a variety of novel microencapsulation techniques have been developed, including the LbL self-assembly approach,^{40,41} bulk emulsification,⁴² and microfluidics.⁴³ Nevertheless, as mentioned before, LbL microcapsules have difficulties encapsulating small and hydrophilic cargo due to the semi-permeability of multilayer shells.^{30,44} Besides, the microcapsules prepared with emulsification may display poorly uniform size distributions when emulsified with standard batch high-shear mixing methodologies,⁴⁵ which will have impacts on the control of particle surface area, thus, among other factors, influencing the drug release behaviours.⁴⁶ Moreover, although microfluidic techniques can offer a promising and versatile route to prepare highly monodispersed microcapsules, the drug-loaded liquid core of the synthesized microcapsules has to be immiscible with shell material phase which puts huge limitations on the selections of active compounds to be encapsulated.⁴⁷ Therefore, an improved approach for fabricating biodegradable drug delivery vehicles that not only are capable of encapsulating small and hydrophilic molecules in a non-liquid fashion, but also have a uniformed size distribution is therefore of high demand.

Furthermore, the microarray structures also comprise the potential for microfabrication of similar geometries of proportionally minified specifications. Generally, the traditional method for obtaining proportionally minified microstructures involves the photolithography of new master templates. The most common applied top-down approach is based on photolithography with the advantages of cost-effective and fast fabrication, as the entire substrate surface is simultaneously patterned. However, the optical diffraction effect puts a limitation on the achieved lithography resolution.⁴⁸ Though the lithographed resolution can be enhanced by applying approaches of electrons or ion-based lithography to less than 50 nm, their line-by-line pattern generation process leads to a relatively small throughput.^{49,50} While the bottom-up methods that are widely employed are patterned self-assembly process using topographically/chemically patterned templating substrates and bio templates. One of the representative systems of topographically patterned substrates is block copolymer (BCP) systems, providing a versatile way to produce ordered nanoscale structures in the range of 10-200nm.⁵¹ However, the requirement of specialized polymer components and the assistance of external fields are challenging issues for most BCP-based templating schemes.⁵² Another common disadvantage of the above fabrication techniques is the requirement of expensive and unportable specialized equipment. Therefore, a cost-effective and easily accessible fabrication method that owns the possibility of large area and high-volume minified pattern fabrications is of great interest among both academia and industries.

1.3. Motivation and Aims

Inspired and motivated by both the versatility of microarray structures and the existing challenges in the sensing, drug delivery and microfabrication areas, this work aims at exploring and expanding the potential multidisciplinary applications of microarray structure by structuring different polymers with the special morphology of microarrays, thus functionalizing the microarray structure with extra properties of structured materials. The main aims of this work has been concluded into below 4 parts.

1) Microarrays for sensing environmental stimuli

Aiming at expanding the sensing capacity of microarray structures, stimuli-responsive polymers are combined with microarray structures. Stimuli-responsive polymers reacting to the chemical and physical changes of the surrounding environment such as pH value, chemical ions, media, temperature etc. have attracted significant attention over the years as smart materials in the field of drug delivery,⁵³ biochemical,⁵⁴ and sensing areas.^{55,56} These environmental changes in nature usually cannot be visualized and perceived, therefore sensors are employed to convert external chemical or physical stimuli into testable signals or changes of sensing material itself.⁵⁷ Thus, stimuli-responsive polymers become one of the best candidates for sensing applications.⁵⁸

2) Microarrays for enzymatically release small and hydrophilic cargos

The aim of solving the problem of encapsulation and release of hydrophilic cargos involves the use of both biodegradable and hydrophobic polymers, through the exploitation of the characteristic low water permeability that hydrophobic polymers possess.⁵⁹ In addition, comparing with the traditional physical triggered release, external stimuli are not required for carriers made of enzyme-degradable polymers,⁶⁰ empowering enzyme-degradable platforms to become one of the most promising systems for controlled drug delivery.⁶¹ PCL, an aliphatic and hydrophobic polymer with excellent processabilities with a low melting point,⁶² possess excellent biodegradability towards the lipase from *Pseudomonas Cepacia* (lipase PS) – a specific lipase which significantly catalyzes the degradation process of PCL compared to samples incubated in buffer alone.^{63,64} Owing to the numerous advantages including variable biodegradability, biocompatibility,^{65,66} great miscibility,⁶⁷ excellent mechanical properties,⁶⁸ PCL has been broadly selected as scaffolds for drug delivery and sustained release,^{69–71} and has been further approved by the US Food and Drug Administration (FDA) for preparing commercial products in the field of medicine and drug delivery.⁷²

3) Microarrays for preparing homogeneous biodegradable microcages

The fabrication of homogeneous drug delivery vehicles that can encapsulate small and hydrophilic molecules in a non-liquid fashion is also one of the aims of this work. Here again, the entrapment of hydrophilic small molecules is achieved by applying low water permeability materials. PLA and PCL, both of which are aliphatic and hydrophobic polymers approved by the FDA for preparing commercial products,⁷³ can be selected as candidates for preparing microcapsule shells. While the size distribution control can be achieved by taking the advantages of microarray structure that homogeneous microwells are lithographed on the surface of the special template,⁵ in which the polymers are filled, embedded and confined, resulting in identical particles of the same size and shape of the engraved microstructure.³⁸

4) Microarrays for templating proportionally minified microarray structures

To fulfil the aim of the microfabrication of microarray structures in a large area and high-volume fashion, soft lithography technique of replica moulding method is employed, which is an inexpensive and facile technique to massively transfer different types of both microscale and nanoscale microstructures onto planar, curved or other flexible substrates for many repeating times (>50) potentially at atomic level resolutions,⁷⁴ essentially based on printing, moulding and embossing with an elastomeric stamp.⁷⁵ While the proportionally minified structure can be achieved by the assistance of preceramic polymers, which can shrink to similar geometries but smaller specifications after being pyrolyzed into ceramics. With multiple times of replica moulding processes based on preceramic polymers and elastomeric stamps, the microfabrication of proportionally minified microarray structure can be successfully accomplished in a simple, cost-effective, and efficient way.

2. Literature Review

2.1. Polyelectrolytes

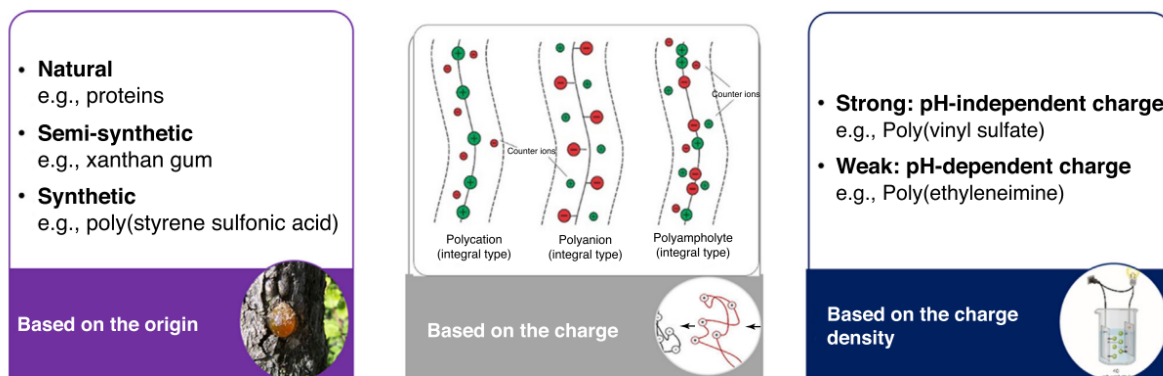
Polyelectrolytes (PEs) are a kind of polymer that is constituted with repeating units of charged electrolyte groups that can be dissociated in an ionizing solvent like water and consequently produce the corresponding charged small ions and polymeric molecules which are fully or partially charged, typically neutralized by smaller free counter ions like sodium or chloride to preserve the electroneutrality.⁷⁶ When remaining undissociated, PEs behaves similar to normal macromolecules, while a small dissociation of the ionic group would lead to intense changes in their properties. This dual character of macromolecular chain and high charge enables PEs to become one of the most attractive subjects in the scientific area for decades, especially as the stimuli-responsive polymer for sensing applications.

2.1.1. Classification of Polyelectrolytes

Typically, the polyelectrolytes are commonly classified into polycations, polyanions and polyampholyte based on the charge type of the functional groups. Polycations ionize in solution will generate positive sites along the polymer molecule, while negative sites will locate on the polymer chains of ionized polyanion; polyampholyte ionizes in solution and forms positive and negative charges along the polymer segment.⁷⁷ The most common examples of polyelectrolytes are polystyrene sulfonate (PSS), poly (allylamine hydrochloride) (PAH), polyacrylic acid (PAA), poly (diallyl dimethylammonium chloride) (PDMA) and so forth. Some biomedical molecules such as polypeptides glycosaminoglycans and deoxyribonucleic acid (DNA) are all fall into the category of polyelectrolytes. More detailed and diversified classifications are organized in Figure 2.1.

The origin base, for example, is another aspect to classify the PEs.⁷⁷ Polymers such as gelatin, chitosan, dextran, starch, nucleic acids, sodium alginate, hyaluronic acid, chondroitin sulfate are natural polyelectrolytes. While sodium dextran sulfate, xanthan gum,

pectin and cellulose-based, starch-based, dextran-based PEs are classified as chemically modified or semi-synthetic polyelectrolytes. Synthetic polyelectrolytes are dextran sulfate, poly (sodium styrene sulfonate), poly (vinyl sulfate), poly (acrylic acid-co-maleic acid), poly (p-styrene sulfonic acid), poly (methacrylic acid), poly (ethyleneimine), poly (allylamine hydrochloride) poly (acrylic acid) and so forth.



Types of polyelectrolytes

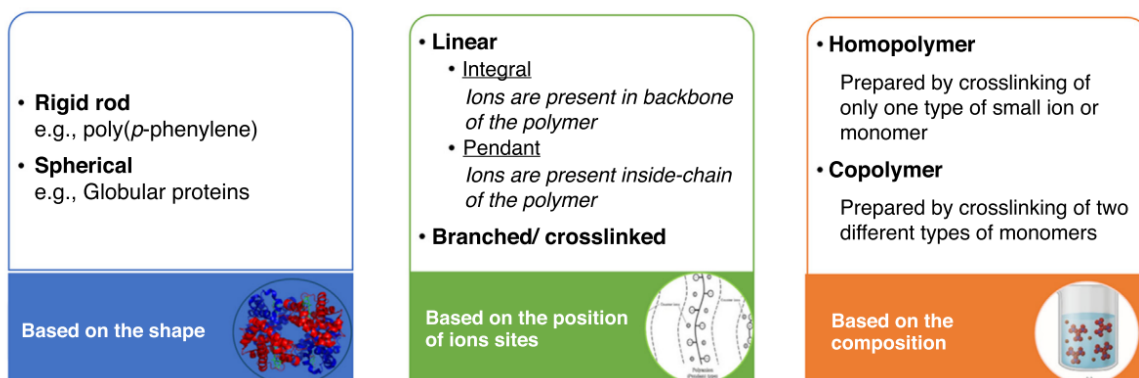


Figure 2.1 Classification of polyelectrolytes based on the charge and position of ionic sites.⁷⁷

Similar to acids and bases, polyelectrolytes can be divided into two types named “strong” and “weak” polyelectrolytes based on the charge density of the polymer chains.⁷⁸ Strong polyelectrolytes are the ones that ions can be completely dissociated in ionizing solution, whereas polyelectrolytes that are only fractionally dissociated, remaining a substantial fraction of ions bound to the polymer chains, therefore, can be sorted as weak polyelectrolytes. Moreover, the dissociation degree of weak ones can be affected by the changes of pH solutions, the concentration of counter-ions as well as the solution ionic strength, which would be introduced in the next subchapter.

Many other classification standards are considered as well. For instance, based on the shape, PEs are divided into the rigid rod and spherical shape; based on the position of ions sites, they are labelled as linear and branched or crosslinked polyelectrolytes; based on the composition, homopolymers are prepared by crosslinking of single type ions or monomer, while crosslinking two different types of monomers is therefore called copolymers.

2.1.2. Theory and Properties of Polyelectrolytes

A variety of properties of PEs, such as chain conformation, diffusion coefficients, solution viscosity, polarizability, miscibility, etc. will be significantly changed if ionic groups are introduced.⁷⁹ Specifically, ionic strength and electrostatic interaction are major influences for PEs.

The ionic strength of the PE solution can drastically influence the conformation of the polyelectrolyte. Generally, the dissolved PEs would adopt an extended and stretched conformation in a salt-free solution owing to the repulsive electrostatic force between charges along the chain. With the addition of oppositely charged counter ions, the polymer segment tends to adopt a coiled conformation due to the screening of the electrostatic interactions. If the counter ions are divalent, the ion-bridge between two ionic sites on the chain could emerge while the PE are still soluble.⁸⁰ With the increasing amount of added salt, a high volume of charge screening would lead to the precipitation of PEs from the solution. However, further increase in the concentration of the counter ions can cause a high-charge screen and redissolve the PEs.

In addition, the electrostatic interactions between polyelectrolytes, especially weak PEs, can be significantly influenced by the acid-base equilibrium, whose charge density along the polymer chain is depend on the surrounding pH environment.⁸¹ For instance, if a weak polyelectrolyte (HA) is dissolved in aqueous solutions like water, the corresponding dissociation equation of the polyelectrolyte ion pair is shown below:



Where the HA denotes a weak polyelectrolyte, which reversely dissociated into cationic H⁺ and anionic A⁻. Since the weak polyelectrolyte is only fractionally dissociated, the dissociation degree can be indicated by a special equilibrium constant called dissociation constant (K_a). The corresponding K_a is defined below:

$$K_a = \frac{[\mathbf{H}^+][\mathbf{A}^-]}{[\mathbf{HA}]}$$

Where the brackets represent the concentration of every substance. Strong polyelectrolytes own a larger dissociation constant while weak polyelectrolytes hold smaller ones whose dissociation constants (pK_a or pK_b) vary from ~2 to ~10. Generally, the higher the K_a value, the stronger the polyelectrolytes since they can be more dissociated.

The Henderson–Hassel Balch equation⁸² can describe the derivation of pH as an indicator of acidity in both biology and chemistry which can be obtained by given logarithm to the equation below:

$$pK_a = pH - \log_{10} \frac{[\mathbf{A}^-]}{[\mathbf{HA}]}$$

Where the parameter pK_a is the acid dissociation constant. Considering the charge density of the polymer chains, the Henderson–Hassel Balch equation can be modified as given:

$$pK_a = pH - n \log_{10} \frac{[\alpha]}{[1 - \alpha]}$$

Where again, pK_a denote the acid dissociation constant, n represents the extension of the polymer chains which is relating to their charge, α is the degree of protonation or occupancy.

Dissociation constant, as the equilibrium constant, is to describe the balance between the reactants and compounds, or more specifically, between the protonation and deprotonation. For polycations, when $\text{pH} < \text{pK}_a$, the nearby positively charged ions facilitate the protonation which generates an attractive potential for combining with the base group. Similarly, the neighbouring negatively charged ions could exert a repressive potential to inhibit the dissociation of polyelectrolytes when $\text{pH} > \text{pK}_a$. On the contrary, for polyanions, the dissociation behaviour influenced by pH is totally reversed.

2.1.3. Applications of Polyelectrolytes

Polyelectrolytes, as versatile polymers served as stimuli-responsive, controllable, swellable polymers, coating materials and surfactants, are welcomed in various of fields ranging from polymer science, chemical engineering, drug delivery, medicine, cosmetics, food areas and so forth. Generally, PEs manufactured into matrices, gels, drug complexes, coatings and membranes are employed as the stimuli-responsive or self-regulated controlled delivery device which would respond to specific and target physicochemical stimuli and perform designed behaviours, such as pH-dependent swell, drug delivery, sustained release.⁷⁷ Due to the bio-adhesive properties, PEs are widely applied as the matrices for oral, nasal, ocular, intra-articular and intra-tumoral administration of drugs.⁸³ Moreover, PEs can significantly influence the coagulation-flocculation processes of the mixture or dispersions, thus widely being applied as flocculants for processing and separating clay dispersions,⁸⁴ or harvesting microalgal biomass for food and feed applications.⁸⁵ In addition, PEs have proven their potentials to draw solutes in the forward osmosis process and have been proposed for the treatment of waste water.⁸⁶ Comprehensive introductions to PEs and their applications have been organized and reviewed by Rembaum.⁸⁷ Among all the applications of PEs, polyelectrolyte complexes and polyelectrolyte multilayers are the most intensively studies applications fabricated by PEs, which will be further discussed in this chapter.

2.2. Polyelectrolyte Complexes

Polyelectrolyte complexes (PEC) is obtained by the interaction between oppositely charged polyelectrolytes molecular chains. Early in the 1930s, it was already found that colloidal complexes or complex coacervates were formed when natural PEs interact with each other in solutions. Later in the 1890s, the electrostatic force was first time proposed as the driving force that led to the mutual precipitation of natural PE of oppositely charged proteins and carbohydrates.⁷⁷ While the insoluble PEC was identified in the 1960s by Michaels et al. whose pioneered studies extensively and widely revealed the properties of such complexes, including the swelling and plasticizing properties.^{88,89} After Michaels' work, the principle of PEC formation received increasing attentions due to its complicated mechanisms of both thermodynamic and kinetic factors.⁹⁰

2.2.1. Process for the Formation of PEC

The basic and crucial principle for the PEC formation is the interactions between the oppositely charged polyelectrolyte chains so that the electrostatic force can automatically attract and combine them into complexes of polyelectrolytes. Practically, based on the way that charged PEs chains contact each other, PEC is classified as bulked PEC when the interactions take place in a bulk phase (e.g., solutions), or as multilayered PEC when the complexations emerge on an interface.⁹¹ In this work, the abbreviation of PEC represents the bulk PEC while the multilayered PEC is called polyelectrolyte multilayers (PEM) which would be further introduced in subchapter 2.3.

The complexation of polyelectrolytes can occur in various charged species such as PE-PE, PE-drug, PE-nucleic acid, PE-surfactant. Though electrostatic interactions are commonly the dominant attraction force between polyanions and polycations, other factors such as hydrogen bonding,⁹² van der Waals interactions,⁹³ hydrophobic interactions⁹⁴ etc., can significantly influence the ultimate PEC structures as well. Above intermolecular chain

interactions can contribute to the formation of non-permanent networks without the assistance of chemical crosslinkers.

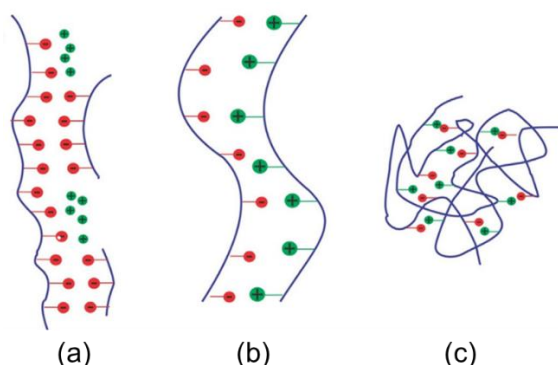


Figure 2.2 Structure models of polyelectrolyte complexes. (a)sequential model, (b) ladder-like model, (c) scrambled egg model.

Figure 2.2 schematically proposed three structural models of PEC that are commonly adopted based on the charge ratio, degree of polymerization as well as the structure of the start PEs.⁷⁷ The first one is the sequential model (Figure 2.2 a)) which is formed when the blending ratio of cationic and anionic functional group is unequal, result in nonstoichiometric complexes. The above complexes can be dispersed in water to form quasi-stable dispersions owing to the repulsion forces between charged molecules.⁹⁵ The second model is the ladder-like model with chain packed orderly as shown in Figure 2.2 b). This type of PEC can be fabricated by mixing PEs with an equal ratio at very low concentration, forming stoichiometric complexes which contain a limited number of polyelectrolyte chains. The last scrambled eggged structures of stoichiometric complexes (Figure 2.2 c)) are prepared at high PE concentration equal blending ratio and are constituted with numerous highly disordered polymer chains.⁹⁶

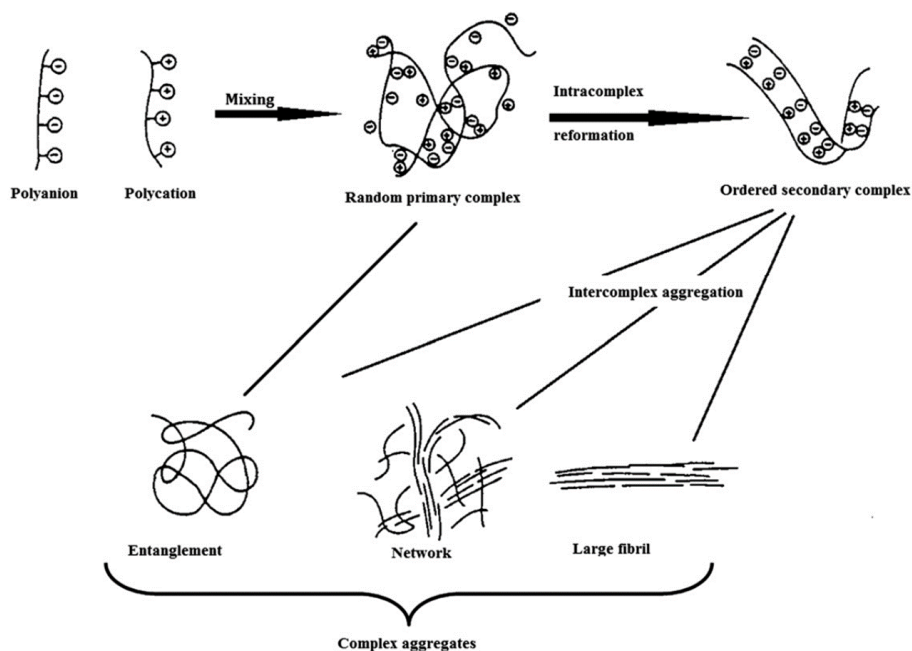


Figure 2.3 Schematic demonstration of the aggregation of PECs.

The process and mechanism of the PEC formation are generally involved three steps as schematically demonstrated in Figure 2.3.⁹⁷ The first step is the primary complex formation, where the electrostatic forces are established after the blending of oppositely charged polyelectrolyte solutions. It is noteworthy to address that this step is kinetically controlled with an extremely fast rate of within 5 μs .⁹⁰ The second step involves the formation of the new bond within intra-complexes, or the correction of the polymer chain distortions to reach an optimal new conformation. Finally, the third step is forming inter-complex aggregates where ordered secondary complexes aggregated mainly via hydrophobic interactions. The PEC precipitants can hardly be dissolved in ordinary solvents, and the molar ratio of PE components in the aggregates is almost unity.⁹⁷

2.2.2. Influencing Factors of PEC

Generally, the formation and properties of the PEC can be influenced not only by the chemical characters of the polymers themselves, such as molecular weight, charge density and stereochemical fitting, but also by the experimental conditions including the concentration and the ionic strength of the prepared polyelectrolyte solutions, the mixing

ratio of oppositely charged polyelectrolytes, and even the mixing order of the polyelectrolyte solutions.⁹⁸

As the electrostatic interaction is the primary force for the formation of polyelectrolyte complexes, there is no doubt that the concentration of salts and polyelectrolytes would have huge impacts on the interactions between polyelectrolytes and the formation and stabilities of PEC.^{99,100} It has been illustrated that the kinetics of polyelectrolytes is so complicated that it could not be explained by simply traditional kinetic schemes of first-order and second-order reactions,¹⁰¹ and it is also hard to anticipate the effect of salts during the formation of PEC since the process of complexes formed during the interaction between different characteristics of polyelectrolyte components is complicated as salts not only can reduce the interactions between oppositely charged PEs, but also can allow the PE chain rearrangement.¹⁰² In most solution systems, the concentration of salts would marginally affect the internal structure of the PEC. When the ionic strength is low, the main effect of salt is to reduce the level of polyelectrolyte aggregation. Moreover, the mass and the size of PEC particles can be controlled by salts as well.¹⁰²

The water-soluble complexes constituted by polyelectrolytes with different weak ionic groups and molecular weights at non-stoichiometric mixing ratios was successfully prepared and comprehensively studied by Tsuchida and Kabanov and coworkers^{103–105} including preparation conditions, structures, the kinetics of PEC and so forth. Basically, in the water-soluble weak polyelectrolyte systems, the addition of a small number of salts (e.g., NaCl) could compensate the charge and facilitate the formation of polyelectrolyte complex because of the rearrangement of molecule chains as well as the state of thermal dynamic equilibrium. If further increase the concentration of salts, PEC would show a shrinking effect in the basis of the shielding of charge by salts. Then, at critical ionic strength points, insoluble PEC begins to emerge and flocculate. Finally, the PEC would fully disassociate if

more salts were added to the solution. The characteristic of polyelectrolyte groups and the salts would have an influence on the range of dissolution phase of polyelectrolytes.¹⁰⁶

While in the strong polyelectrolyte systems, the mechanisms of PEC formation are different. Polyelectrolytes with strong ionic groups are more likely to form macroscopic flocculation and aggregation. Dautzenberg^{102,106} found that secondary aggregation and macroscopic flocculation would occur at higher ionic strengths at a mixing ratio below 1:1 because the major components around the PEC were screened by the electrostatically stabilizing shell. At the presence of a small amount of salts in strong polyelectrolyte complexes, not only the secondary aggregation and macroscopic flocculation were observed, but also the disintegration into subunits at low ionic strengths could be viewed.

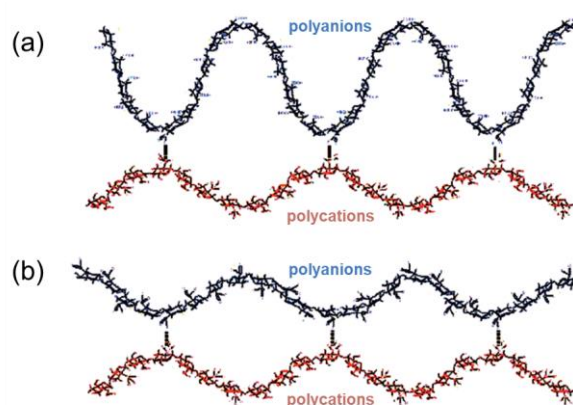


Figure 2.4 Schematic illustration of the interactions between polycations and polyanions at different pH. (a) At acidic condition;
(b) At neutral pH condition.

In addition, the properties of PEC are governed by the degree of interactions between polymers which significantly depend on the global charge density of PEs and can determine the relative proportion in the complexes. Basically, decreased charge density of polyelectrolyte chains can lead to increased proportion in the formed PEC since more polymeric chains are required to compensate with oppositely charged polymers.¹⁰⁷ Since the proportion of different components in complexes can undoubtedly influence the properties of PEC, the physicochemical conditions of the reactions play an essential role in the PEC formation. For example, one of the most important factors that can control the

complexation process is the pH value of the solution. As Figure 2.4 shows, polyanions has low charge density at acidic solutions so that more folded chains of polyanions are required to interact with polycations compared with neutral pH conditions. Moreover, the folding chains can increase the size of micropores, allowing more dissolution media and counter ions to enter, while at neutral pH, the ionic interactions are still strong so that the larger counter ions are restricted from entering.¹⁰⁸ Additionally, other secondary factors such as flexibility of polymer chains, molecular weight, substitution degree of other PEs, the nature of solvent etc., can influence the formed PEC components.⁷⁹

The pH conditions of the PEC environment can also influence the structures and properties of PEC after the preparation process. Generally, the ionizable side groups of weak polyelectrolytes can be divided into non-ionized state and ionized state in term of the pH value of the environment. For the non-ionized state, the elastic properties of the polymer main chain would be the primary factor of the swelling behaviour of polyelectrolyte, besides, just like the normal polymers, the thermal dynamics of the solvent-polymer mixture would be one of the factors as well. While if the pH value of the environment exceeds a certain threshold (e.g. dissociation constant), the side group would be ionized, and the new formed electrostatic force would contribute to the expansion of polyelectrolytes.¹⁰⁹

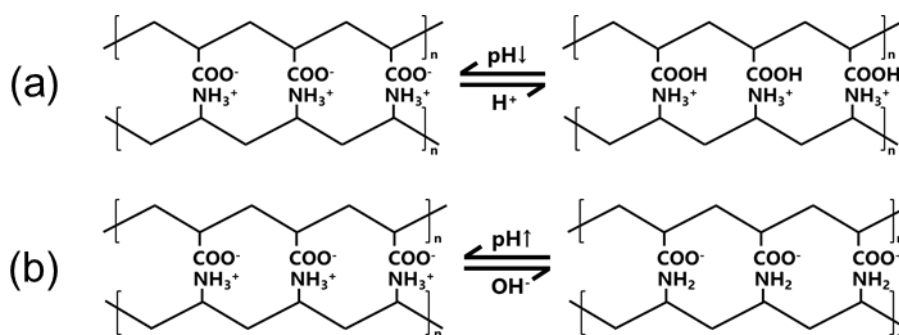


Figure 2.5 Schematic illustration of the pH influence on PAA/PAH PEC in different pH conditions. (a) In acidic condition; (b) In alkaline conditions.

For instance, PEC prepared from notable pH-responsive weak polyelectrolytes polyacrylic acid (PAA) and poly (allylamine hydrochloride) (PAH) will display shrinking and

swelling behaviours under different pH condition. Basically, the polyacrylic acid remains non-ionized when pH is lower than 4.25¹¹⁰ (the pK_a of acrylic acid), however, if the pH of the solution is above 4.25, more and more carboxylic acid groups on main chain carbon would be ionized to protons and carboxylate group, and only fractional carboxylic pairs are maintained as is shown in Figure 2.5 a). After the ionization, the negatively charged groups would repulse each other because of the electrostatic force, causing a swelling of the whole structure.¹¹⁰ Additionally, the attraction of counterion would increase the osmotic pressure and contribute to the swelling of the polymer as well. Similarly, weak polyelectrolyte PAH is also pH-responsive that when the pH value is below the pK_a of PAH (10.8), there would be an increasing number of ammonium groups which would lead to the swelling of the whole polymer structure owing to the electrostatic repulsion between the positively charged groups (Figure 2.5 b)).¹¹¹ Similarly, the enhancement of osmotic pressure would also result in the swelling of the polyelectrolytes.

2.2.3. Biomedical Applications of PEC

PEC is a versatile polymer with properties that can be manipulated in a broad range by selecting appropriate starting materials and preparation conditions and methods. The PEC formation has become an intense research focus for decades and keeps on generating increasing attentions owing to their potential applications in the fields including drug delivery, gene therapy, protein compaction, paper strength, cosmetics, and coatings.⁹¹

Especially, PEC is inherently appropriate for applications in the domain of drug delivery and pharmacy because they are generally charged, nontoxic, water-soluble polymers.¹¹² The special structure and internal interactions of PEC matrices indeed offer the possibility to encapsulate and release drugs or other active compounds. Generally, there are four ways to incorporate active substances into PEC.⁷⁶ The first and simplest way is to physically trap the active substances from the solution during the complexation processes. Second, the active substances can be absorbed from the solution and incorporated into the formed

PEC. The third route is chemically binding the active substances with one of the components of the PEC which precipitates during the complex formation. In the last case, active substances themselves are served as polyelectrolytes with either positive or negative charges and participate in the PEC formation. The release of the incorporated active compounds can be achieved with various mechanism including solution equilibration, ions exchanges, charge interaction, slow decomplexation, breakdown or degradation, or even dissolution of the complex.⁷⁶

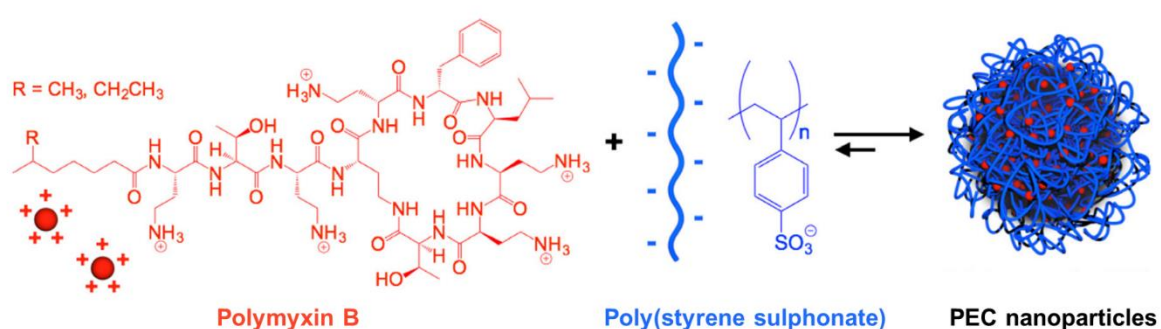


Figure 2.6 Schematic demonstration of PEC of cationic antimicrobial polymyxin B and anionic PSS.

Since charged compounds can be easily integrated into complex systems, PEC is employed as delivery vehicles and encapsulants such as proteins, enzymes etc.,¹¹³ and has been widely applied in the biomedical industries.^{114,115} For example, drug-loaded PEC matrices constituting blends of pectin, chitosan and hydrolyzed polyacrylamide can be prepared for controlling the premature solvation of the polymers and modulating the release activities of the highly hydrophilic antihistamine, diphenhydramine HCl model drug, enabling an effective site-specific and oral controlled drug delivery applications.¹¹⁶ Additionally, PEC particles assembled by antimicrobial peptide polymyxin B and poly(styrene sulphonate), as shown in Figure 2.6, were prepared for peptide delivery with antimicrobial activities of the particles performed.¹¹⁷ Diclofenac sodium was selected as the model drug to be incorporated into PEC of Carbopol and polyvinyl pyrrolidone whose controlled release behaviours were well studied.¹¹⁸ Some of the other representative drug

delivery applications of PEC that is constituted by different polyelectrolytes are listed in Table 2-1.

Table 2-1 Past research on polyelectrolyte complexes and their applications in drug delivery.

Polyelectrolyte complexes	Application
Chitosan-chondroitin-sulfate	Colon-targeted drug carrier
Chitosan-pectin	Colon-specific delivery of vancomycin
Chitosan-carboxymethyl-cashew-gum	Synthesis and thermal stability of PEC
Chitosan-carboxymethyl-cellulose	Gastric-specific delivery of clarithromycin
Chitosan-phosphorylated-chitosan	PEC hydrogel as an osteoblast carrier
Chitosan-polycarbophil	Bioadhesive controlled release delivery of insulin
Chitosan-carboxymethyl-konjac-glucomannan	Nanoparticles for sustained delivery of BSA
Trimethyl-chitosan-insulin	Self-assembled polyelectrolyte nanocomplexes for insulin delivery
Polyvinyl-pyrrolidone-carboxyvinyl	Sustained release of chlorpheniramine maleate and indomethacin
Soy-protein-poly(acrylic acid)	Interpenetrating polymer network hydrogels for colon delivery of BSA
Poly(vinyl pyrrolidone)-poly(acrylic acid)	Mucoadhesive microspheres to increase gastric residence time of acetaminophen

In addition to delivery vehicles, PEC is also appealing candidates as functional stimuli-responsive hydrogels,¹¹⁹ underwater adhesives,¹²⁰ human periodontal ligaments matrices,¹²¹ and have been used for the transplantation or tissue repairing scaffold.^{122,123} It is strongly believed that, in the future, the versatile formulation of PEC will have more applications in multiple fields owing to their unique properties of ionic interactions.

2.3. Polyelectrolyte Multilayers

Polyelectrolyte multilayers (PEM), also known as multilayered PEC, is constituted with electrostatically absorbed ordered polyanion-polycation thin layers rather than bulk complexes. The main difference between the techniques to prepare bulk PEC and PEM is that one of the complex components is fixed onto a surface or template in the interfacial complexation method, while in the solution mixing method, polyelectrolytes are blended in bulk solution.

2.3.1. Fabrication of PEM via Layer-by-Layer Technique

One of the most common techniques of interfacial complexation method for the formation of film material PEM is the simple and versatile layer-by-layer(LbL) deposition techniques which were introduced by Decher et al. in the early 1990s.²³ In most of the cases,

the growing substrates were planar interfaces made of silicon or glass. Later, Mohwald and coworkers expand the applicable interfaces of the LbL technique into organic or inorganic cores, thus the polyelectrolyte multilayered microcapsules can be fabricated after the dissolution of the template cores.^{124,125}

Generally, in this technique, as shown in Figure 2.7, suitable growth substrates are utilized to dip into polyelectrolyte solutions of designed concentration alternatively and the free polyelectrolytes in solution will complex with the oppositely charged polyelectrolyte molecules fixed on the growing substrate after the washing and removing of excessive polymer.¹²⁶ Consecutive adsorption of oppositely charged polymers results in the formation of stable polycation/polyanion bilayers during each deposition procedure. In each cycle, a small number of oppositely charged polyelectrolytes are absorbed on the former layer to reverse the surface charge of the multilayers. The thickness of polyelectrolyte multilayers ranges from several nanometers to a few microns depending on the number of layers constructed. And theoretically, the deposition procedure can be cycled as many times as designed. It has been reported that a 100.5 assembled bilayer of porous film was created by using polyelectrolytes of PAA and PAH.¹²⁷

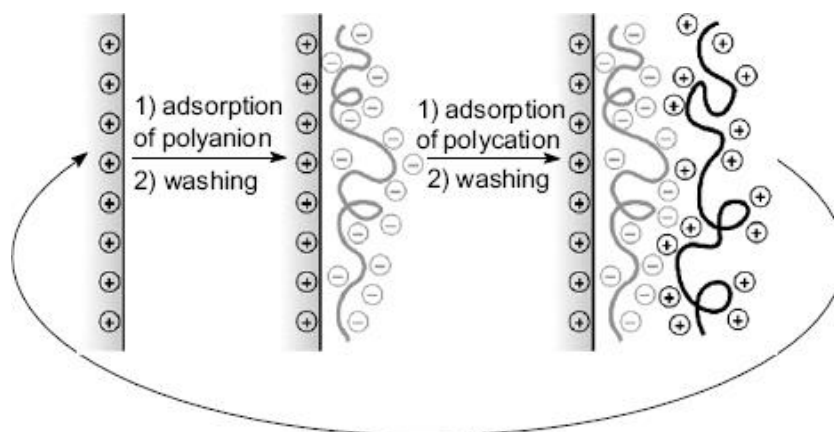


Figure 2.7 Polyelectrolyte multilayer preparing procedures.

The layer-by-layer self-assembly technique is of increasing interests as it provides a feasible route to control the thickness of the PEM on a nanometre scale when coating thin films on flat substrates or substrates with more complex shapes and to control the properties

of the multilayer film by selecting the outermost polyelectrolyte layer as well as the nature of the oppositely charged polyelectrolyte components used in the PEM formation.¹²⁸ Therefore, the versatile LbL technique can design functional ultrathin multi-layered film systems to be applied in various structural materials.¹²⁹

2.3.2. Driving Forces and Influence Factors of PEM assembly

Polyelectrolytes were absorbed onto the solid surface because of various complex intermolecular electrostatic and non-electrostatic interactions between the oppositely charged polyelectrolytes. Many intermolecular interactions dominate the LbL process whose balance would be the driven force for the multilayer formation and significantly affect the multilayer structures. Evidence showed that the charge reversion after each absorbing step is the precondition for layer-by-layer assembly and the electrostatic interactions are the main reason for forming multilayers since ζ potential changes its sign after each cycle, resulting in a kind of zigzag curve similar to the curve shown in Figure 2.8.¹³⁰

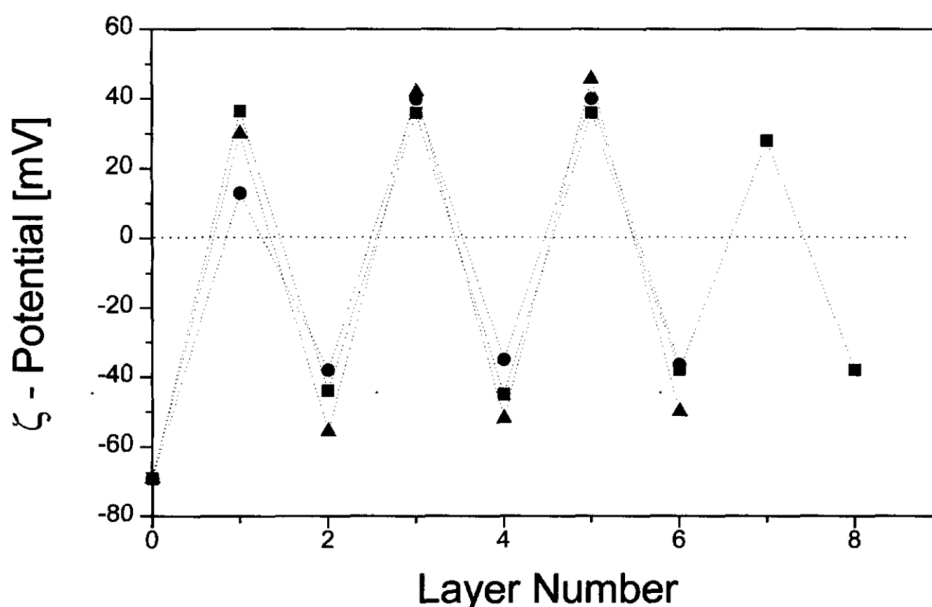


Figure 2.8 Zeta-potential as a function of layer number for coated polystyrene sulfate latex particles.

Specifically, it is required for the polyelectrolytes to reach a minimum charge density threshold to form PEM, below which the charge reversal would not be sufficient for charge overcompensation and the significant layer growth cannot be observed.^{131,132} It was found

that the combination of two nearly fully charged chain would form thick layers and their thermodynamic contributions of enthalpic and/or entropic parts have been studied and explained.^{133,134} According to their theory, if the charge density became lower, the polymer main chain would be less stiff and could not be absorbed on the surface with a flat structure but have to form a loop and tails result in the thicker multilayers. While for high charge density polyelectrolytes, most of the segment was absorbed onto a flat surface leading to thinner multilayers (shown in Figure 2.9).¹³⁵

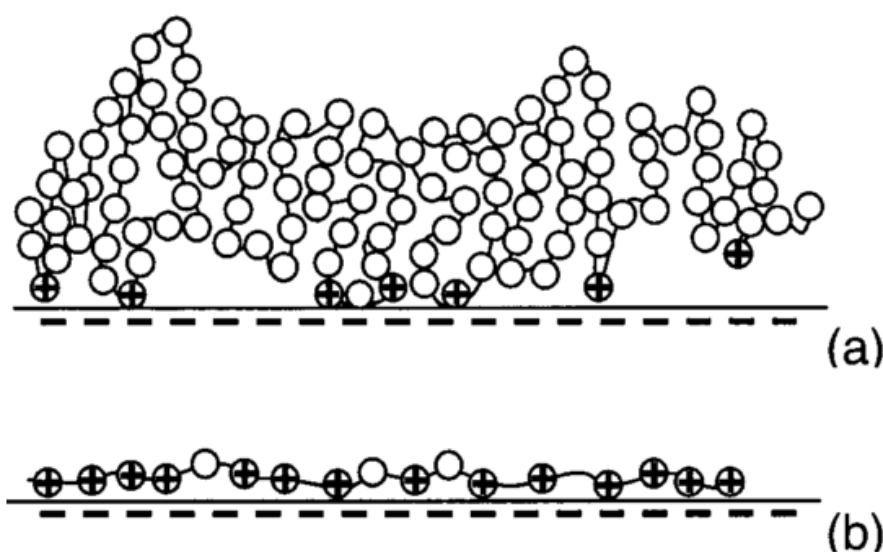


Figure 2.9 Illustration of polyelectrolyte configurations at the interface with different charge densities. (a) the low charge density of adsorbed polyelectrolytes and (b) high charge density adsorbed polyelectrolytes.¹³⁵

The charge density of strong PE can be manipulated by modifying the chemical structure,¹³⁶ while for weak polyelectrolytes, an intermediate charge density is favourable to generate a PEM system.¹³⁴ Additionally, the charge density of weak polyelectrolytes was pH-tunable based on the theory of dissociation equilibrium, which would definitely influence the absorption of multilayers.¹¹¹ Moreover, except for the average charge density of PEs, the distribution of PEs will also significantly influence the formation of PEM. For instance, a short strongly charged block of block-copolymers can be assembled into PEM even if the average charge density have not reached the minimum charge density threshold.¹³⁷

Besides, the ionic strength of the PE solution was related to the concentration of the addition of salts, which would also influence the interactions between polyelectrolytes and other interfaces, thus controlling the thickness of the total multilayers due to the screening of the charges.¹³⁸ Basically, the charged groups of polyelectrolyte chains would repulse each other in a salt-free environment, which showed a stretched structure. While the chains would change their structure to coil conformation since the counterion from additional salts screens the electrostatic interactions.¹³⁹ The degree of thickness adjustment by ionic strength is dependent on the oppositely charged PE combinations. For example, at low ionic strength below 0.5 mol/L NaCl, the dependence of multilayer thickness tends to change from linear to square root of ionic strength.¹⁴⁰ When the ionic strength rises above 1 mol/L, the thickness increases less significant. However, besides the intrachain repulsion forces, the attraction between the PEs or between the charged interface and the PEs can also be screened thus the absorbed amounts of PEs may decrease at high ionic strength.¹³⁸

In addition, Frank Caruso and co-workers found that both ionic strength and charge density would influence the adsorbed amounts and surface topography.¹³¹ With the increasing of the salt concentration, in other words, the ionic strength, there is a significant difference in the growth behaviours of polyelectrolytes whose charge density was lower and higher than the critical charge density. If the salt concentration were higher than critical charge density, higher the salt concentration of the solution can induce more coiled polymer chain structure, result in thicker and rougher absorbing layers. On the contrary, the thickness and roughness of the multilayers would not be affected if the salt concentration was lower than the critical charge density.¹³¹ Additionally, an increase of the ionic strength can also decrease the free energy of polyelectrolyte interactions, and further affect the permeability of PEM.¹³¹

Other forces of non-electrostatic interactions like hydrogen bonds, hydrophobic interactions as well as van der Waals' force may also contribute to the multilayer formation.

Additionally, various factors such as the type of solvents, counterions and polyelectrolytes and so forth, would affect the balance of the intermolecular interactions.

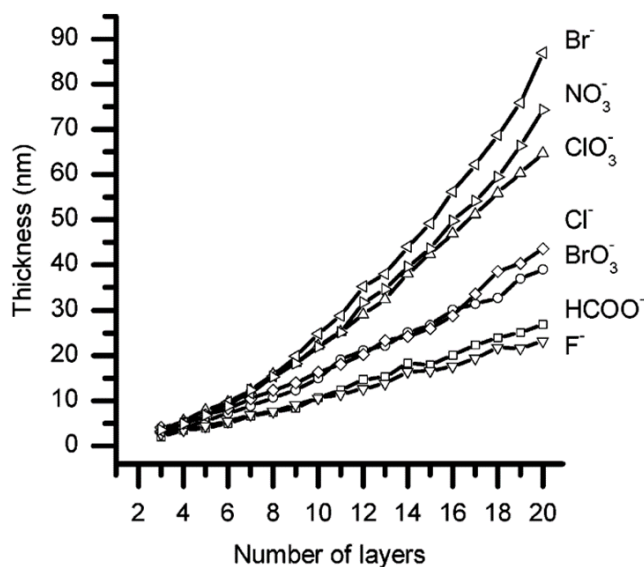


Figure 2.10 The thickness of PEM deposited under 0.1 M sodium salt of different anions.

Generally, the formation of PEM can be influenced by the type of counter ions while the effect of anions is greatly larger than the effect of cations.¹³⁸ When PE solutions are added with different salts, having various counter ions, the thickness of PEM would increase in the order: $\text{Li}^+ < \text{Na}^+ < \text{K}^+$ and $\text{F}^- < \text{Cl}^- < \text{Br}^-$, as shown in Figure 2.10.¹⁴¹ The PEM thickness is also affected by the type of PEs, specifically, by the balance between hydrophobic and hydrophilic properties of PEs, that a certain degree of hydrophobicity can result in a stronger thickness increase. Moreover, the solvent of the PE solution can affect the interaction between the polyelectrolyte chain and counter ions. For example, a stronger interaction occurs when the solvent is methanol and ethanol with a poor solvating effect on ions than water.¹³⁸ Further, hydrogen bonding can be served as an alternative driving force for PEM self-assembly. With the help of hydrogen bonding interactions, it is possible to form PEM on the surface with identically charged polyelectrolytes.¹⁴²

2.3.3. Biomedical Applications of PEM

PEM fabricated with LbL self-assembly method has been extensively researched and applied in the biomedical field, especially in the drug delivery area, since the simple and

versatile technique of LbL owns various distinctive advantages for preparing therapeutic delivery vehicles.¹⁴³ First, the PEM thin film can be absorbed in mild conditions on almost any substrates without considering the size and shape of substrates or the experimental conditions of extreme temperature, organic solvents, and surfactants and so forth. Second, the LbL technique can precisely prepare homogeneous coatings and materials with designable architecture. Third, the composition, permeability, stability, surface properties of the formed PEM can also be manipulated with the LbL method. Therefore, the bottom-up strategy of LbL enables the formation of multilayered structure on different geometries including planar films, microcapsules, microtubes, which owns the potential to deliver a variety of hydrophilic and hydrophobic cargos, ranging from small molecules, proteins to nucleic acid.

The PEM planar film as well as microcapsules prepared with LbL self-assembly technique can be applied for drug delivery based on biopolymers such with great biocompatibility, biodegradability and non-cytotoxicity nature, like polysaccharides, polypeptides, nucleic acids, and proteins etc., which are excellent drug loading vehicles for both reducing the doses and side effects of drugs, and prolonging the effective time of drugs under biological conditions, and further and targeted releasing drugs from the vehicles at designed site and time.¹⁴⁴ Besides, the therapeutic cargos can be loaded into LbL multilayered structure mainly in three ways. In the first method, the drug can be employed as polycations or polyanions that involved in the formation of PEM. Secondly, therapeutic agents can be aggregated into the template for subsequent PE absorption. Finally, the drug can be post-loaded into preformed microparticles or microcapsules by adjusting the permeability of the PEM shell.¹⁴⁵ It is noteworthy to mention that the delivery of multiple therapeutic cargos can be achieved as well thanks to the viability of LbL techniques of selecting the deposited materials and the number of absorbing layers.

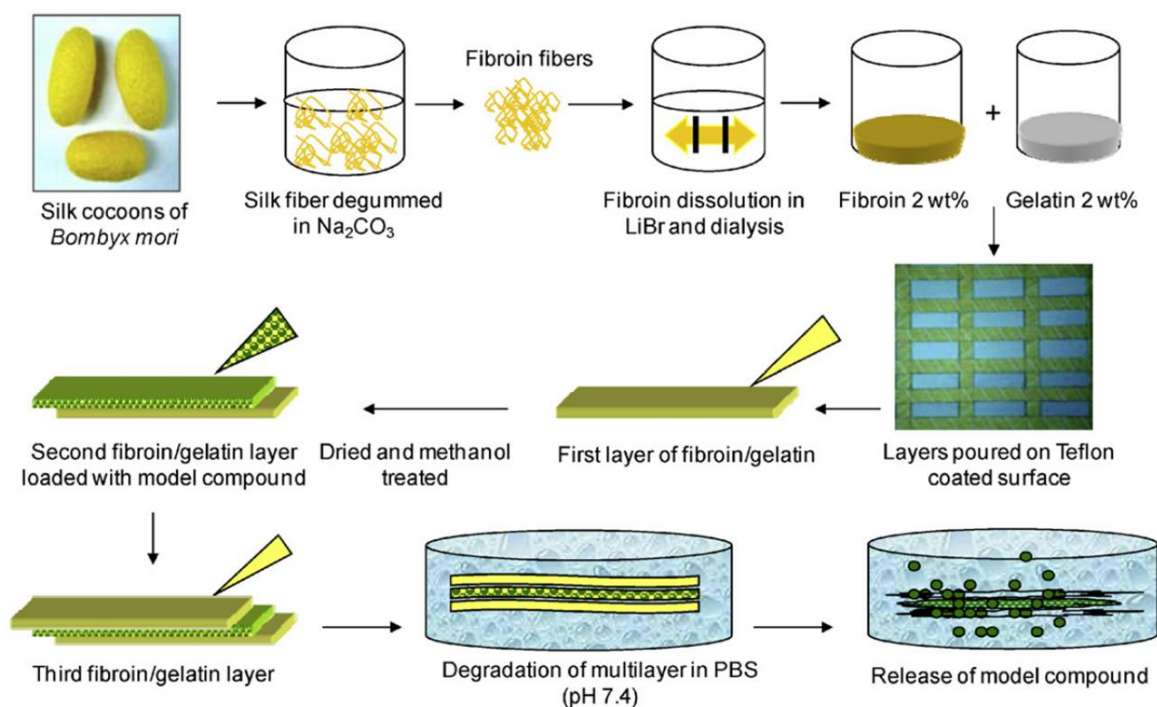


Figure 2.11 The fabrication process of model drug-loaded fibroin protein/gelatin PEM and its release.¹⁴⁶

The LbL PEM in the formation of films made of biopolymers has received great attentions for the delivery of therapeutic cargos. For example, silk fibroin protein and gelatin are employed as shell polymer and fabricated into biocompatible and biodegradable PEM films for the controlled release of model drugs of trypan blue, FITC-inulin, and FITC-BSA, as shown in Figure 2.11. In addition, PEM films of BSA and chitosan were fabricated as drug delivery vehicles to load and release hydrophobic drug molecules due to the affinity of some of the water-insoluble drugs like curcumin towards BSA. Moreover, after 10 bilayers of pyrene conjugated PEM of BSA and chitosan, the PEM film structures can be equipped as dual-drug delivery carriers by post-loading DOX, showing pH-dependent release behaviours which are especially beneficial in treating cancers.¹⁴⁷ Moreover, negatively charged branched DNA molecule and positively charged natural peptide poly(L-lysine) were fabricated as PEM film, and DOX was incorporated into the structure by intercalation with DNA, which was further controlled released from PEM due to the DNA origami structure.¹⁴⁸ Table 2-2 further lists some other representative PEM film systems for drug delivery applications.

Table 2-2 Examples of biopolymer-based multilayered films for drug delivery. ¹⁴⁴

Biopolymer	Other components	Drug	Disease targeted
CH/ALG	PMMA	APP	Inflammatory bowel disease
CH/ALG	/	PFD	Excisional wound healing
CH/dextran	GO	DOX	Breast cancer
CH/HA	Etafilcon A contact lens	Norfloxacin, timolol	Ophthalmic infection, glaucoma
Dextran/HA	PAH	Ibuprofen	Wound healing
PLL/HA	PSSA and PAH	PTX	Colon adenocarcinoma

ALG: alginate; APP: 4-amino-2-(2-hydroxy-1-decyl) pyrazole-[3,4-d] pyrimidine; CH: chitosan; DOX: doxorubicin; GO: graphene oxide; HA: hyaluronic acid; PAH: Poly (allylamine hydrochloride); PFD: pifrenidone; PLL: poly(L-lysine); PMMA: poly (methyl methacrylate); PTX: paclitaxel.

When the LbL self-assembly occurs on the 3D spherical templates rather than 2D flat substrates, the PEM capsules are therefore fabricated. The most common templates for fabricating PEM capsules are nano- or micro-sized solid particles including colloids, silica particles, calcium carbonate, liposomes and so forth, which are further removed if necessary to form PEM capsules with hollow structures.¹⁴⁹ For instance, By absorbing biopolymer of protamine sulfate and dextran sulfate or alginate on the sacrificial template of calcium carbonate nanoparticles with LbL technique, hollow PEM nanocapsules were successfully fabricated for delivering cisplatin, an anticancer drug but with a severe toxic side effect. The nanocapsules with a high drug loading efficiency can achieve sustained drug release during 48 h, with the release rate can be adjusted by the number of absorbed polyelectrolyte layers.¹⁵⁰

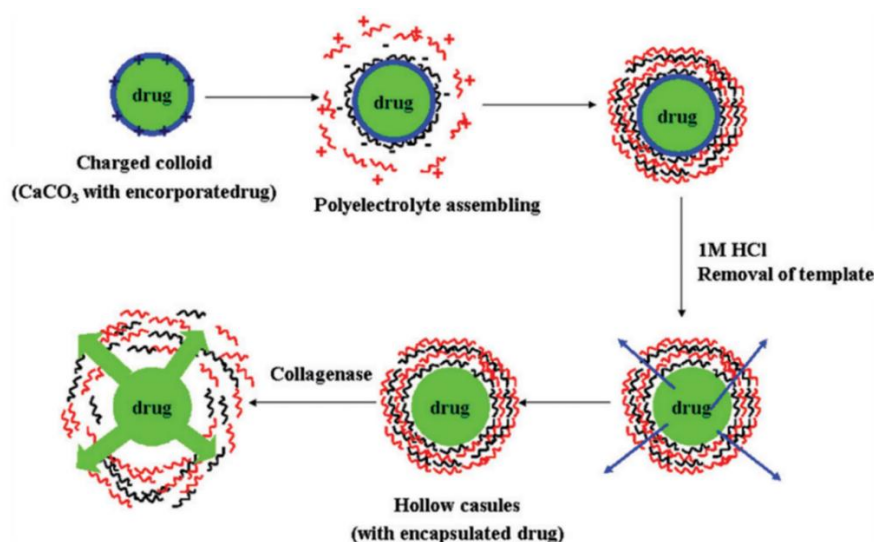


Figure 2.12 The process of producing drug-loaded hollow capsules and the enzymatic release. ¹⁵¹

In addition, hyaluronic acid and collagen were absorbed on BSA incorporated calcium carbonate template, resulting in the formation of PEM microcapsules as shown in Figure 2.12. The release of the model drug BSA was released by the enzymatic degradation of the biopolymer shell with collagenase, whose release rate can be manipulated by increasing the shell thickness of the microcapsules or by collagen crosslinking during the formation of microcapsules. More representative examples relating to the drug delivery applications of LbL assembled PEM capsules are listed in Table 2-3.

Table 2-3 Examples of biopolymer-based multilayered capsules for drug delivery. ¹⁴⁴

Biopolymer	Other components	Drug	Disease targeted
CH/ALG	PMMA	DTX	Breast cancer
CH/dextran	Silica particles	Ciprofloxacin Ceftriaxone	<i>Salmonella</i> infections
CH/dextran	Silica particles	Rifampicin	Tuberculosis
CH/heparin	SLNs Dextran	DOX	Breast cancer, Lung cancer
Dextran/HA	CaCO ₃ particles	DOX	Lung cancer
PRM/dextran	CaCO ₃ particles	α 1-Antitrypsin	Chronic inflammation
PRM/heparin	/	DOX	Breast cancer

ALG: alginate; CH: chitosan; DOX: doxorubicin; DTX: docetaxel; HA: hyaluronic acid; PFD: pirfenidone; PLL: poly(L-lysine);

PMMA: poly (methyl methacrylate); PRM: protamine sulfate; SLN: PTX: paclitaxel; SLN: solid lipid nanoparticles.

The formation of multilayered structures of planar films, nano/microcapsules and their biomedical application has been extensively studied for many years. The promising PEM structure combined with LbL technology is indeed a suitable candidate as a smart delivery system with controllable, targeted drug release behaviours and low side effects.¹⁴⁴ It is strongly believed that the simple, affordable, and versatile PEM system will undoubtedly pave new directions in various domains in the future.

2.4. Polycaprolactone

Polycaprolactone (PCL) is a polymer composed of hexanoate repeat units (Figure 2.13), included in the class of aliphatic polyesters, and is used as a common biodegradable polyester with a low melting point around 60°C and a glass transition temperature of about -60°C, which has been widely accepted as biomedical materials because of its great

biocompatibility, miscibility, slow degradability and good mechanical and thermoplastic characteristics.^{65,66}

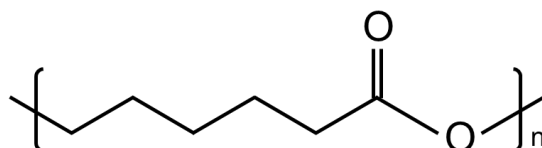


Figure 2.13 The chemical structure of polycaprolactone.

2.4.1. The Production Methods of Polycaprolactone

In 1934, the Carothers group reported the first preparation of polycaprolactone by ring-opening polymerization of the cyclic monomer ϵ -caprolactone which is polymerized into high molecular weight polyesters.¹⁵² Generally, there are two main pathways for the synthesis of polycaprolactone. One is by polycondensation of 6-hydroxyhexanoic acid, and the other is the ring-opening polymerisation (ROP) of ϵ -caprolactone.¹⁵³

Braud et al.¹⁵⁴ managed to synthesis polycaprolactone using 6-hydroxyhexanoic acid for condensation polymerization without adding extra catalyst. The equilibrium was moved towards the formation of PCL by vacuuming the system thus removing the generated water (Figure 2.14). Moreover, the molecular weight and distribution of polymerized 6-hydroxyhexanoic acid can be controlled by the addition of enzyme. For example, using lipase from *Candida Antarctica* under vacuum led to an average molecular weight of around 91 kDa of PCL and a polydispersity under 1.5 within 48h at 90°C with a monomer conversion rate of 82%.¹⁵⁵ While using lipase from *Pseudomonas sp.* at 45 °C to catalyse polycondensation resulted in polymers with an average molecular weight of 5.4 kDa and a polydispersity under 2.26 after 20 days.¹⁵⁶ However, the method of polycondensation of 6-hydroxyhexanoic acid can hardly reach a higher molecular weight. Therefore, in order to acquire a higher molecular weight and narrow distribution, the method of ROP is a preferred way to synthesis PCL.

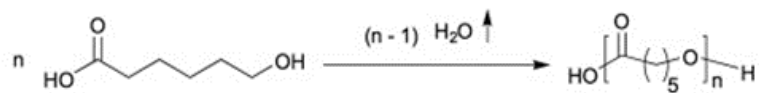


Figure 2.14 Synthesis of polycaprolactone by the polycondensation of 6-hydroxyhexanoic acid.¹⁵⁷

ROP is a form of chain-growth polymerization as a versatile method for synthesising biopolymers.¹⁵⁸ In the PCL case, ϵ -caprolactone is the monomer for chain-growth polymerization. Generally, there are four main mechanisms for the ROP of lactone based on the catalyst: anionic, cationic, monomer-activated, coordination-insertion ROP whose mechanical scheme is shown in Figure 2.15

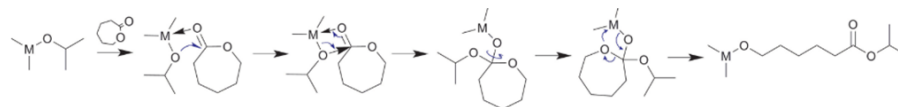
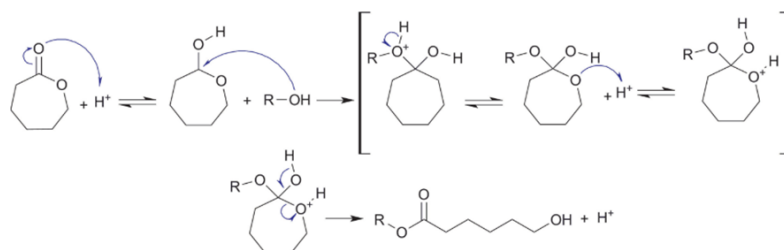
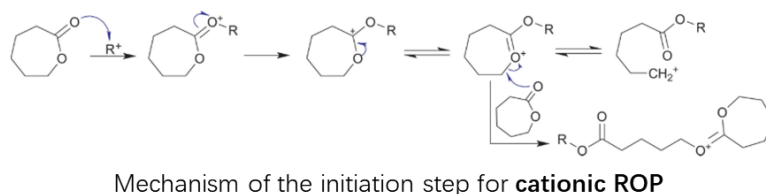
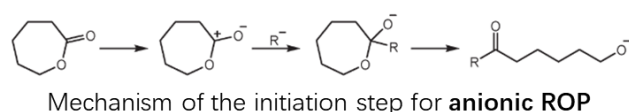


Figure 2.15 Schematic illustration of ROP mechanisms for the ROP of lactone based on different catalysts.¹⁵³

Following the above four mechanisms, a multitude of compounds can catalyse ROP of ϵ -caprolactone, including metal-based, organic and enzymatic systems.¹⁵³ However, different catalysts required different reaction conditions e.g. high temperature, vacuuming or mild conditions, thus the chosen catalysts need to consider the desired conditions and specific applications.

2.4.2. Physicochemical and Biodegradability of Polycaprolactone

Generally, polycaprolactone can easily be dissolved in a variety of solvents such as chloroform, dichloromethane, carbon tetrachloride, benzene, toluene, cyclohexanone and 2-nitropropane; slightly dissolved in acetone, ethyl acetate, dimethylformamide 2-butanone, and acetonitrile; but insoluble in alcohols, petroleum ether, diethyl ether and water at room temperature.¹⁵⁹

Besides, PCL housing great miscibility that it is often employed as blend constitute mixing with other polymers in order to enhance the stress crack resistance, adhesion and even control the drug release rate from microcapsules.¹⁶⁰ Therefore, the blending of different polymers in varied ratios enabling the manipulation of the permeability of different delivery vehicles. Moreover, a variety of monomers can be copolymerized with PCL forming either block or random copolymers such as polyethylene glycol, polystyrene, polyvinylchloride and etc., which has been comprehensively sorted out by Okada.¹⁶¹ Furthermore, physiochemical properties are the most important factors that need to be explored when considering the application, and some of the PCL properties are listed in Table 2-4.¹⁵³

Table 2-4 Properties of polycaprolactone.

Properties	Unit	Range
Number average molecular weight	$\text{g}\cdot\text{mol}^{-1}$	530 - 630 000
Density	$\text{g}\cdot\text{cm}^{-3}$	1.071 - 1.200
Glass transition temperature	$^{\circ}\text{C}$	(-65) - (-60)
Melting temperature	$^{\circ}\text{C}$	56 - 65
Decomposition temperature	$^{\circ}\text{C}$	350
Inherent viscosity	$\text{cm}^3\cdot\text{g}^{-1}$	100 - 130
Intrinsic viscosity	$\text{cm}^3\cdot\text{g}^{-1}$	0.9
Tensile strength	MPa	4 - 785
Young modulus	GPa	0.21 - 0.44
Elongation at break	%	20 - 1000

Thus, PCL is recognized as common and versatile polymers in various areas due to its low melting point, wide solubility among many organic solvents as well as excellent miscibility with other polymers.

PCL is a biodegradable polyester that can be degraded by living organisms such as bacteria and fungi that are able to produce corresponding enzymes.¹⁶² Therefore, due to the absence of specific enzymes, PCL can hardly be biodegraded in animal as well as human bodies.¹⁶³ The in vivo test showed that more than it took more than 2 years for the PCL implant to break into low molecular weight wreckages without the catalyse function of enzymes.¹⁶⁴ Therefore, the degradation of suitable enzymes needs to and has been investigated. Liu *et.al* using *Pseudomonas* lipase, an esterase for cleaving ester bonds on hydrophobic substances, successfully catalysed the degradation behaviours of both amorphous and crystalline solution-cast PCL films performed at 37 °C in buffer solutions.¹⁶⁵ Besides, Gan and his co-workers¹⁶⁶ studied enzymatic degradation of PCL films by incubation in a phosphate buffer solution containing *pseudomonas* lipase with the results showing that it only took less than 4 days for PCL film of 10*10*0.2mm size to be fully degraded in *pseudomonas* lipase buffer solutions of 0.5 mg/ml (Figure 2.16). Apart from that, *Rhizopus delemer* lipase¹⁶⁷ and *Rhizopus arrhizus* lipase can significantly accelerate the degradation activity of PCL as well, while *porcine pancreatic* lipase and *Candida cylindracea* lipase having no performance of degradation on PCL⁶³ as shown in Figure 2.16.

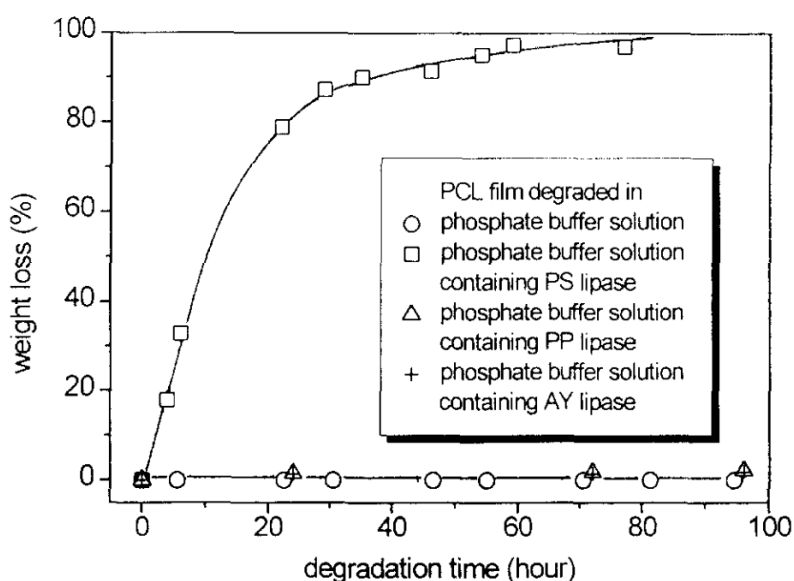


Figure 2.16 The enzymatic degradation of PCL film in PBS containing different lipases.⁶³

The fungal biodegradation of PCL in the presence of filamentous fungi have been researched by Huang and his co-workers, that enzymes of the fungi first attack the amorphous regions and ultimately the crystalline regions.¹⁶⁸ Additionally, the dominant factor determining degradability was either polymer molecular weight or crystallinity degree based on utilized the organism.¹⁶⁹ Same results and phenomenon were found when PCL was degraded with *Rhizopus arrhizus* lipase which preferred to attack amorphous instead of crystalline regions of PCL fibres.¹⁷⁰ The degradation procedures can be simply demonstrated as Figure 2.17 shows.

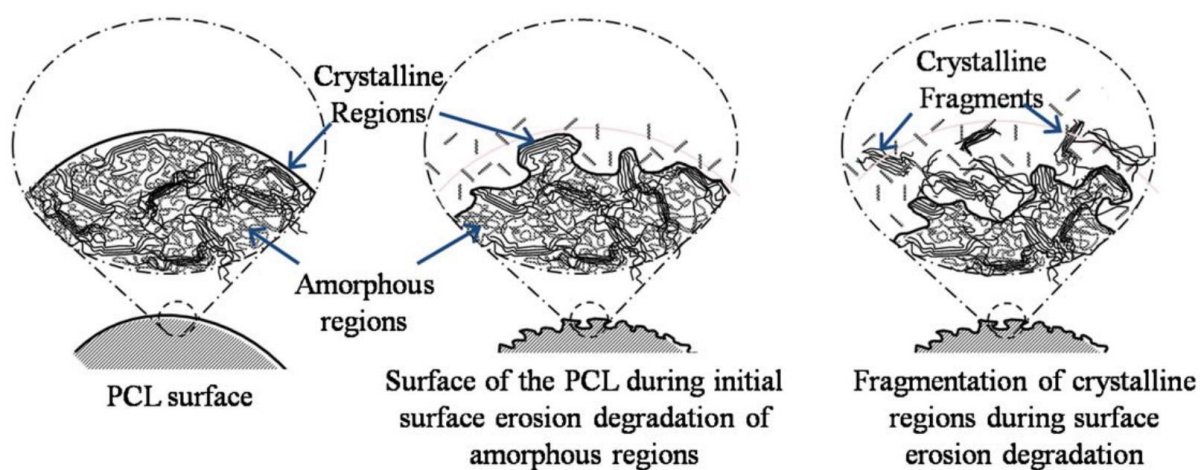


Figure 2.17 Accelerated degradation of PCL over 5 weeks in NaOH.¹⁷¹

Apart from studying the enzymatic degradation behaviours of neat PCL polymer, blending and copolymerization of PCL and other polymers also have been investigated. When being blend with other polymers, PCL can show different enzymatic degradation behaviours not only depending on the blend ratio of all the polymers, but also rely on the miscibility, crystallinity, and degradation mechanisms of the mixing components.¹⁷² Tokiwa and his co-worker prepared a variety of PCL mixtures by mechanical blending with other polymers, such as polyethylene, polypropylene, nylon 6, polystyrene, polyethylene terephthalate, and poly- ϵ -hydroxybutyrate, and found that the degradability of the mixtures changed differently, with the results indicated that the higher miscibility of PCL with other polymers, the harder the enzymatic degradation of PCL blends by the selected lipase.¹⁷³ Besides, Xing and his co-workers tested the enzymatic degradation of PCL and

poly(styrene-co-acrylonitrile) (SAN) blends under the catalyst of *Pseudomonas* lipase. They argued that the nondegradable content of SAN exposed on the surface of PCL/SAN film could block and prevent the lipase contacting with biodegradable PCL molecular chains, even only 1% of SAN was blended.¹⁷⁴ These experimental results showed that the composition, crystallinity and surface microstructure of the mixture can significantly influence the enzymatic degradation of PCL and their blends. Furthermore, in order to enhance the hydrophilicity, decrease crystallinity and shorten degradation time, Shen and his co-workers¹⁷⁵ copolymerized PCL and other components whose controlled enzymatic degradation behaviours in the presence of *porcine pancreatic* lipase are reported as well. Besides, electrospinning techniques are used to modify the surface of PCL-based copolymers. Moreover, their results also show that *porcine pancreatic* lipase can effectively catalyse PCL-based copolymers but have no obvious effect on PCL homopolymers. By modulating the materials' bulk structures and/or surface morphologies, both the enzymatic degradation rate and hydrophilicity of PCL-based polymers can be designed.

Since PCL polymer has such great biocompatibility, miscibility, slow degradability and good mechanical and thermoplastic characteristics and has been extensively studied on both PCL-based copolymers and blend polymers modifications, PCL and PCL-based device or systems has been further widely developed to a multitude of applications.

2.4.3. Biomedical Applications of Polycaprolactone

PCL is a biomaterial with excellent biocompatibility where one of the most important factors that distinguish biomaterials from other materials is that biomaterial can contact tissues without any harmful and unacceptable effect on that body. Therefore, great biocompatibility is essential for being applied in medical areas and has been of interests to many scientists. The definition of biocompatibility has been proposed¹⁷⁶ as quoted that "Biocompatibility refers to the ability of a biomaterial to perform its desired function with respect to a medical therapy, without eliciting any undesirable local or systemic effects in

the recipient or beneficiary of that therapy, but generating the most appropriate beneficial cellular or tissue response in that specific situation, and optimising the clinically relevant performance of that therapy.” Besides, PCL also owns the certificate from FDA⁷² (Food and Drug Administration, USA) and EC registered mark (European Conformity) which are essential for the commercialization of smart devices for different clinical uses as well as for packaging and composites applications, even though surprisingly few have been commercialized or widely translated to clinical studies.¹⁷⁷ For example, PCL has been widely used as a PVC solid plasticizer or for polyurethane applications. Different commercial grades are produced by Solvay (CAPA[®]), by Union Carbide (Tone[®]), and by Daicel (Celgreen[®]).¹⁷⁸ PCL can also be easily be functionalized, for instance, H. Jiang et al. use zwitterionic polymer brushes to functionalize PCL film surface to improve its blood compatibility.¹⁷⁹ Due to the above-mentioned advantages, PCL has been considered by scientists from many areas to be applied in the field of drug delivery, tissue engineering as well as medical devices.

2.4.3.1. PCL applications in drug delivery

The degradation rate of PCL is relatively low in the absence of suitable lipase for more than 2 years, enabling PCL the potential as long-term drug delivery carriers with high permeability to many drugs. Besides, because of the excellent biocompatibility and miscibility of PCL, the drug delivery behaviours can be tailored to fulfil the desired release. One of the most common methods for drug delivery is using free-flowing particles microspheres with drugs either entrapped or encapsulated inside. The loaded drugs can be released by the diffusion or the degradation of microspheres or matrix.¹⁸⁰ The selection of preparation methods, processing condition, polymer composition and organic solvents play important roles in altering the release kinetic and degradation behaviours. The methods for the preparation of PCL microspheres are demonstrated in Figure 2.18.¹⁸¹ For example, Benoit *et. al* prepared 5 to 10 μm size of PCL microparticles encapsulated with protein Bovine serum albumin (BSA) by the method of a double emulsion-solvent

evaporation technique, which is suitable for oral vaccine delivery.¹⁸² Besides, poly(D, L-lactide-co-glycolide) (PLGA) and poly(ϵ -caprolactone) (PCL) biodegradable microspheres were fabricated by water-in-oil–water (W/O/W) double emulsion technique as well in order to controlled delivery doxycycline (DXY) to periodontal pockets.¹⁸³

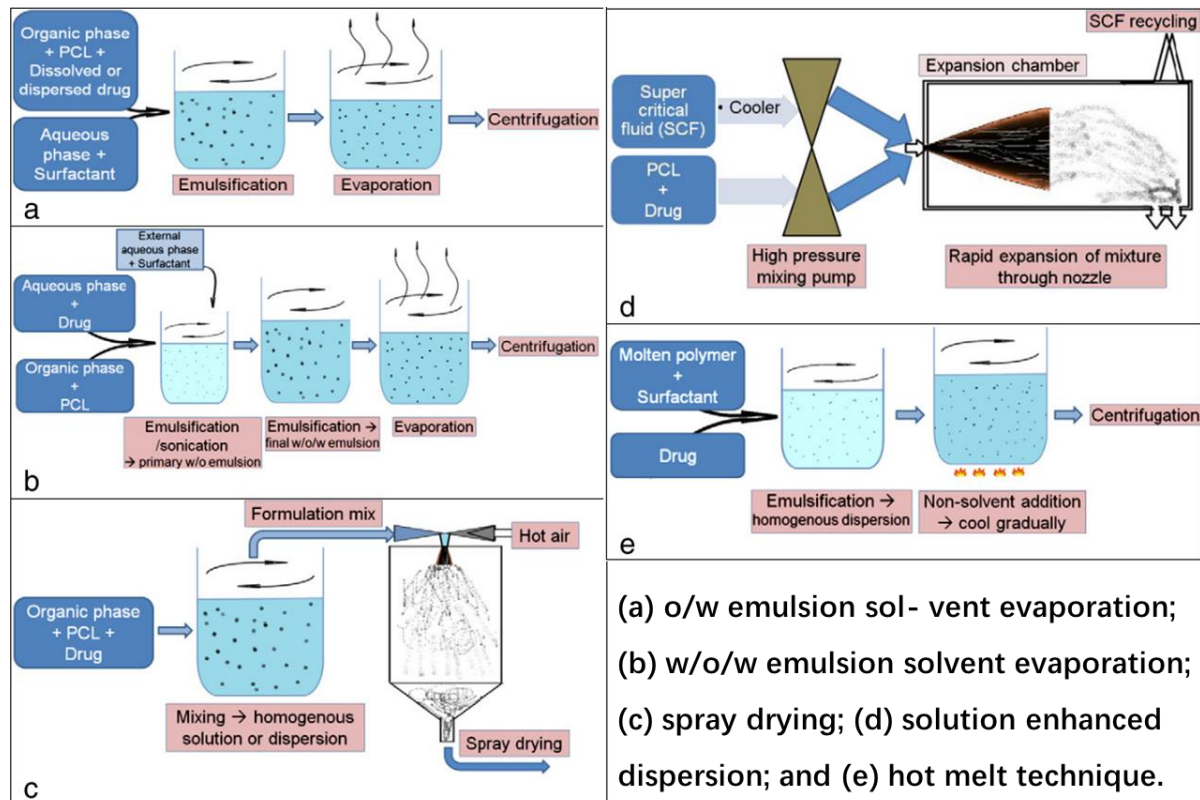


Figure 2.18 Schematic illustration of the preparation of PCL microspheres.¹⁸¹

Additionally, when the size of prepared particles decreased to less than 1 μm , the drug delivery systems become nanospheres where the drugs can be dispersed, absorbed or encapsulated as well. Similar to microspheres, the nanosphere can be termed as nanoparticles or nano-capsules based on the way the drug is loaded. The size, designed surface, enhanced solubility, multi-functionality allows the nanosphere applications in targeted drug delivery, drug stabilization.¹⁸⁴ The general concept for synthesising nanospheres are almost the same as described for microspheres, but the preparation parameters are changed to form nano-size droplets with a variety of techniques has been reported.^{185,186} Among various methods, the illustrations of preparing PCL nanospheres such as solvent evaporation, solvent displacement, interfacial polymer disposition, dialysis

and emulsion-solvent diffusion technique are shown here in Figure 2.19. Same for microspheres, preparing methods, processing conditions, polymer compositions and organic solvents used have strong influences on the physicochemical properties of PCL nanospheres.^{181,185} For instance, Zarghami and co-workers copolymerize PCL and poly(ethylene glycol) (PEG) producing nanoparticles to load Chrysin and deliver to breast cancer cells. The PCL-PEG nanoparticles with the antitumor effect can enhance cancer cell cytotoxicity.¹⁸⁷ Besides, a novel drug delivery system bovine serum albumin (BSA)-PCL conjugate nanoparticles have been proposed by Stenzel and co-workers, which can load curcumin for prostate carcinoma therapeutics. Their results show that the BSA-PCL conjugate nanoparticles can sufficiently release and deliver curcumin, thus limiting the growth of tumour spheroids.¹⁸⁸

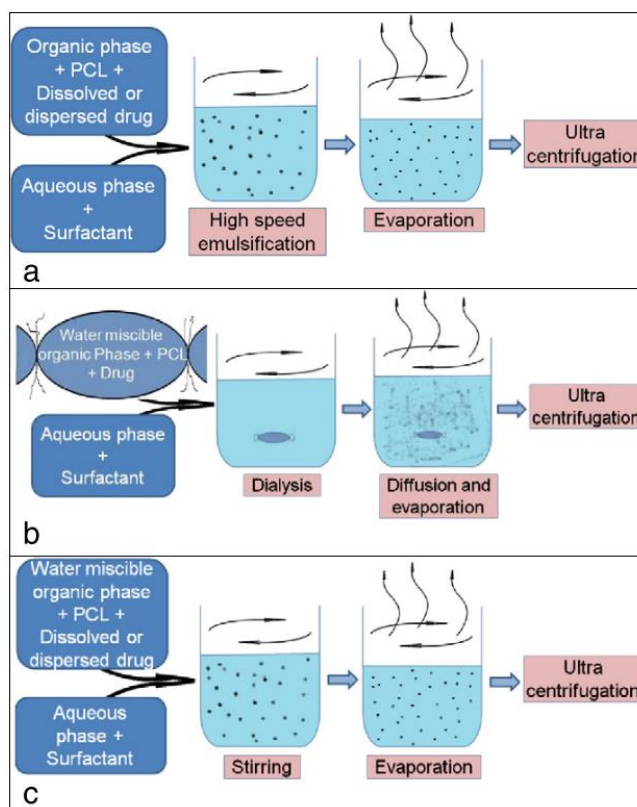


Figure 2.19 Schematic illustration of preparation of PCL NPs. (a) o/w emulsion solvent evaporation; (b) dialysis; and (c) diffusion solvent evaporation.¹⁸¹

Except for micro- and nanospheres, other PCL-based drug delivery systems can also deliver and release drugs.¹⁸¹ For example, PCL was also prepared as a thin-film matrix and

thin-film reservoir device for controlled drug delivery and release.¹⁸⁹ In addition, PCL film has also been served as scaffolds for the controlled release of complexed DNA.¹⁹⁰ Moreover, an implant of T-shape prototype of the intrauterine system can be prepared with PCL incorporated with drugs using 3-dimensional printing technique which can be used to deliver the drug as well.¹⁹¹ Therefore, the PCL-based drug delivery system is one of the most promising candidates with great biocompatibility, biodegradability, miscibility that can be manipulated as drug carriers for targeted or non-targeted delivery of many drugs ranging from small molecules to macromolecules such as proteins or nucleic acids,¹⁹² which owns the increasing potential to be used for a clinical drug delivery applications in humans.

2.4.3.2. PCL applications in tissue engineering

Tissue engineering is broadly accepted as followed definition, “an interdisciplinary field that applies the principles of engineering and life sciences to the development of biological substitutes that restore, maintain, or improve tissue function or a whole organ”¹⁹³. About tissue engineering, it is easy to think of the reparation or replacement of tissues such as bone, blood vessel, skin, nerve, cardiovascular, cartilage, tendon and ligament, as different portions require various mechanical and structural properties of materials. With the development of science and technology, engineered extracellular matrices also named scaffolds as artificial tissue replacement has attracted a large focus of researchers in the interdisciplinary field of cell culture, biomaterials, biomimetic environments. A typical scaffold is demonstrated in Figure 3.19 describing the main requirements of the scaffold. Basically, the scaffold should not only be able to attach, grow, migrate and differentiate *in vitro*, but also allow being implanted to *in vivo* injured part with attached differentiated cells and further guide the tissues to become or recover to a healthy state.¹⁸⁶

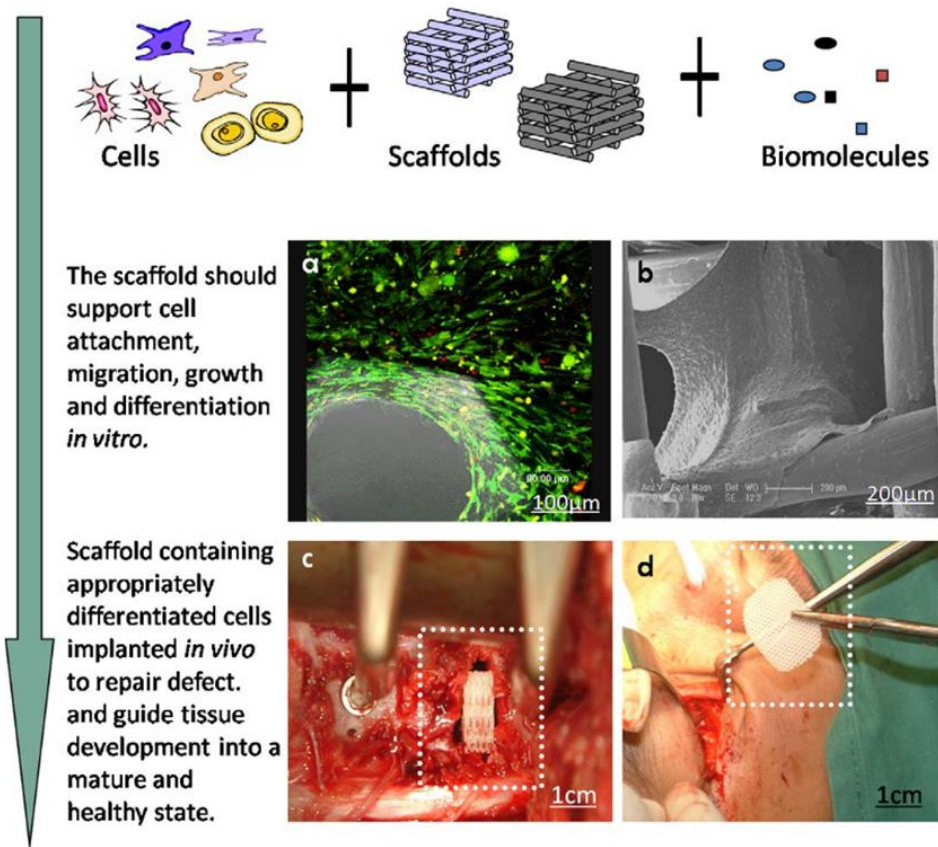


Figure 2.20 3D Scaffold-based system of tissue engineering aiming to incorporate cells and biomolecules *in vitro* until being implanted to specific tissues.¹⁸⁶

Various techniques have been proposed to prepare scaffolds for tissue engineering, and the mechanical properties of scaffold constitution materials play an important role in both the potential application area and the manufacturing methods. Apart from the above-mentioned requirements *in vitro* and *vivo*, the biocompatibility, biodegradability, processability of selected scaffold materials are of great importance and need to be taken into consideration as well.¹⁹⁴ Therefore, PCL as a versatile biodegradable polymer with appropriate physicochemical and biological properties is an excellent choice for fabricating tissue engineering scaffolds. The most common PCL-based scaffold preparing techniques have been summarised by Hutmacher and co-workers as shown in Figure 2.21 with the elaboration of the advantages and disadvantages of different routes.

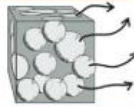
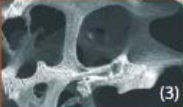
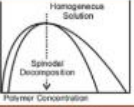

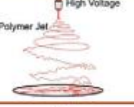

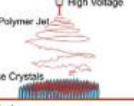

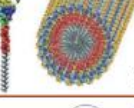

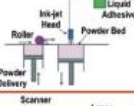

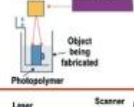
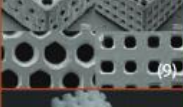
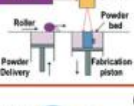
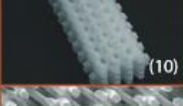
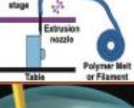
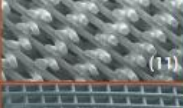


	Scaffold Name	Porosity & Size	Schematic	Advantage & Disadvantages	Image
Conventional Scaffold	Particulate leaching	Porosity < 90% Pore size 5-600µm		Adv: Simple and user friendly method, suitable with a range of biomaterials and no special equipment is needed. Disadv: Density differences result in non uniform pore size distribution. Difficult to achieve full interconnectivity and large pore interconnections. Skinning effect on outside surfaces of scaffolds. Organic solvents typically required.	 (3)
	Thermal Induced Phase Separation (TIPS)	Porosity < 90% Pore size 5-600µm		Adv: Simple method, suitable with a range of biomaterials and no special equipment is needed fully interconnecting pores and large pore interconnections can be fabricated if spinodal decomposition is achieved. Disadv: Skinning effect on outside surfaces of scaffolds. Organic solvents typically required.	 (4)
Nano-scale Scaffold	Electrospinning	Porosity < 90% Pore size <1-10µm		Adv: Inexpensive method to produce nano/micro fibers from a wide range of polymers. Excellent cell and tissue compatibility for mesenchymal cells. By using ice crystals as a collector, scaffolds with large pores and significant volume may be fabricated.	 (5)
	Electrospinning onto ice crystals	Porosity < 95% Pore Size 20-200µm		Disadv: Organic solvents often required, scaffolds with volume, and large pore size or thickness are difficult to manufacture except by using ice crystal technique which has the disadvantage that sublimation required that increases complexity of manufacture. Mechanical properties of electrospun fibers is generally poor.	 (6)
	Self-assembling Nanofibers	Porosity < 95% Pore Size 200-800µm		Adv: Self assembling system, typically in water and can be formed in the presence of cells, with bioactive functionality. Disadv: Relatively expensive to manufacture in significant quantities. Weak mechanical properties probably restrict this type of scaffold to soft tissues	 (7)
Solid Freeform Fabrication (SFF) Scaffolds	3 Dimensional Printing (3DP)	Porosity < 45-60% Pore Size 45-1600µm		Adv: SFF techniques have accurate control over pore size and interconnectivity over conventional/nanoscale approaches. The layer-by-layer process allows fabrication of complex and anatomically-shaped structures. Disadv: Expensive machinery required, resolution limitations at lower pore sizes. Biomaterials need to come in powder form with controlled particle size.	 (8)
	Stereolithography	Porosity < 90% Pore size 20-1000µm		Adv: Accurate control over pore size and interconnectivity. Layer-by-layer process allows fabrication of complex and anatomically-shaped structures. Disadv: Expensive machinery required. Polymers compatible with UV curing is required.	 (9)
	Selective Laser sintering (SLS)	Porosity < 40% Pore size 30-2500µm		Adv: Accurate control over pore size and interconnectivity. Layer-by-layer process allows fabrication of complex and anatomically-shaped structures. Disadv: Expensive machinery required. Resolution limitations at lower pore sizes. Biomaterials need to come in powder form with tight controlled particle size, mainly applicable to ceramic materials.	 (10)
	Fused deposition modelling	Porosity < 80% Pore size 100-2000µm		Adv: Accurate control over pore size and interconnectivity. Layer by layer process allows fabrication of complex pore architectures and anatomically-shaped structures with good resolution. Disadv: Since the technique uses polymer melts, it is limited to thermoplastics. Low pore sizes difficult to achieve while maintaining high porosity.	 (11)
	Direct Writing	Porosity < 90% Pore Size 5-100µm		Adv: Accurate control over pore size and interconnectivity. Layer-by-layer process allows fabrication of complex architectures with excellent resolution. Disadv: Expensive machinery required. Biomaterials used need to be able to form polyelectrolyte inks. Significant times are required to manufacture scaffolds with suitable thickness.	 (12)

Figure 2.21 Fabrication methods for PCL scaffolds in the tissue engineering area.¹⁹⁵

Based on these techniques, PCL scaffolds have been investigated and employed in a multitude of areas. For example, Vacanti and co-workers¹⁹⁶ using electrostatic fibre spinning techniques have achieved fabricating PCL scaffolds of nanofiber where mesenchymal stem cells derived from the bone marrow of neonatal rats were cultured, expanded and seeded. The results prove that the electrospun PCL scaffolds can provide an environment suitable for tissue mineralize, holding the potential for curing the bone defect. Besides, in the cartilage tissue engineering area, Cho and his co-workers¹⁹⁷ have successfully prepared a novel cell-printed bio-hybrid scaffold made of PCL-alginate using

three-dimensional bioprinting method with the results showing the negligible effects on the viability of the encapsulated chondrocytes which is beneficial for cartilage regeneration.

2.4.3.3. PCL applications in medical devices

Medical devices are clinically effective and well-designed device intended to be applied in the medical area that can provide safe and high-quality treatment for patients.¹⁹⁸ Except for the great permeability to many drugs, excellent biocompatibility to cells, PCL can find its application as medical devices owing to the special biodegradability where the degradation rate is slow compared with other biodegradable polymers and most importantly, the ability to be fully excreted when its biodegraded and absorbed in human body.¹⁹⁹

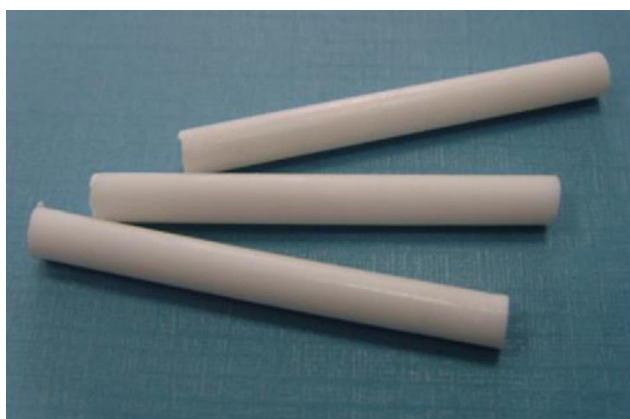


Figure 2.22 Praziquantel loaded implants made of PEG/PCL blends.²⁰⁰

Implants made of PCL and its blend polymers are one of the most common medical devices with a variety of applications. For example, subdermal contraceptive implants including Norplants[®], Jadelles[®] and Implanons[®] have been widely used among women.²⁰¹ However, nowadays the commercial subdermal contraceptive implants are made of non-biodegradable polymers to release the contained drugs. After that, the implants need to be removed surgically which exert another damage to patients. Therefore, PCL is an optimal candidate for achieving long-term implant drug delivery purpose. H. Sun et al. proposed a PCL-based implant as a model medical device and placed it in rats for 3 years. They proved that the implanted PCL could remain intact for 2 years and once it is degraded, it would not cumulate in body tissue and be fully excreted. Besides, implants with praziquantel loaded

made of PEG/PCL blends are also proposed (Figure 2.22), whose *in vitro* and *in vivo* drug release rate can be manipulated by simply varying the composition of the PCL.²⁰⁰

Sutures are also medical devices used for binding together tissues that have been separated because of the surgery or traumatic wound and PCL is one of the best candidates as biocompatible and biodegradable polymers. For instance, a controlled-release composite bioactive suture made of PCL is proposed with anti-inflammation drug Diclofenac loaded which is intercalated in a synthetic hydrotalcite as shown in Figure 2.23.²⁰² In addition, a self-knotting suture comprised out of polyurethane and PCL blended polymer are introduced which can show thermal shape memory behaviours when placed to 60°C water bath.²⁰³

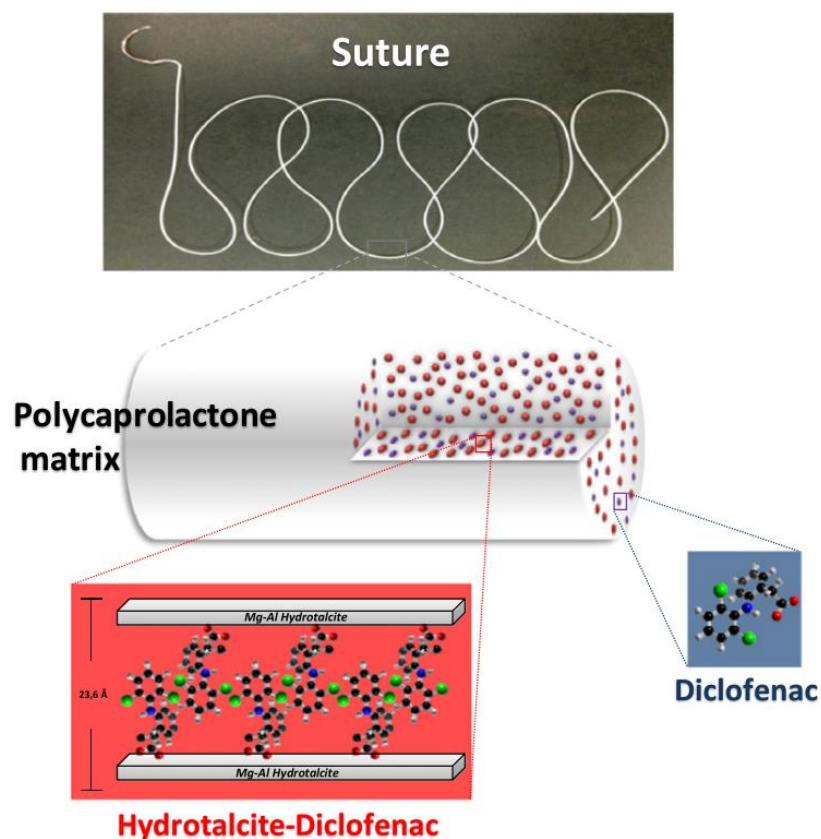


Figure 2.23 The concept of PCL suture loaded with anti-inflammation drug Diclofenac.²⁰²

Apart from implants and sutures, PCL can be employed in many other fields as medical devices. For instance, PCL nanofibers prepared by electrospinning method are coated with

polysaccharide via layer-by-layer techniques are developed as applied for wound dressing applications for healing.²⁰⁴ Besides, chitosan nanoparticles and the electrospun PCL nanofiber can also be prepared as a composite to achieve the function of both wound dressing and drug delivery.²⁰⁵ Moreover, applying electrospun PCL membranes incorporated with biosynthesized silver nanoparticles of various ratios as a wound dressing can add extra antibacterial property and prevent bacterial colonization in wounds when covered with this electrospun PCL membranes.²⁰⁶

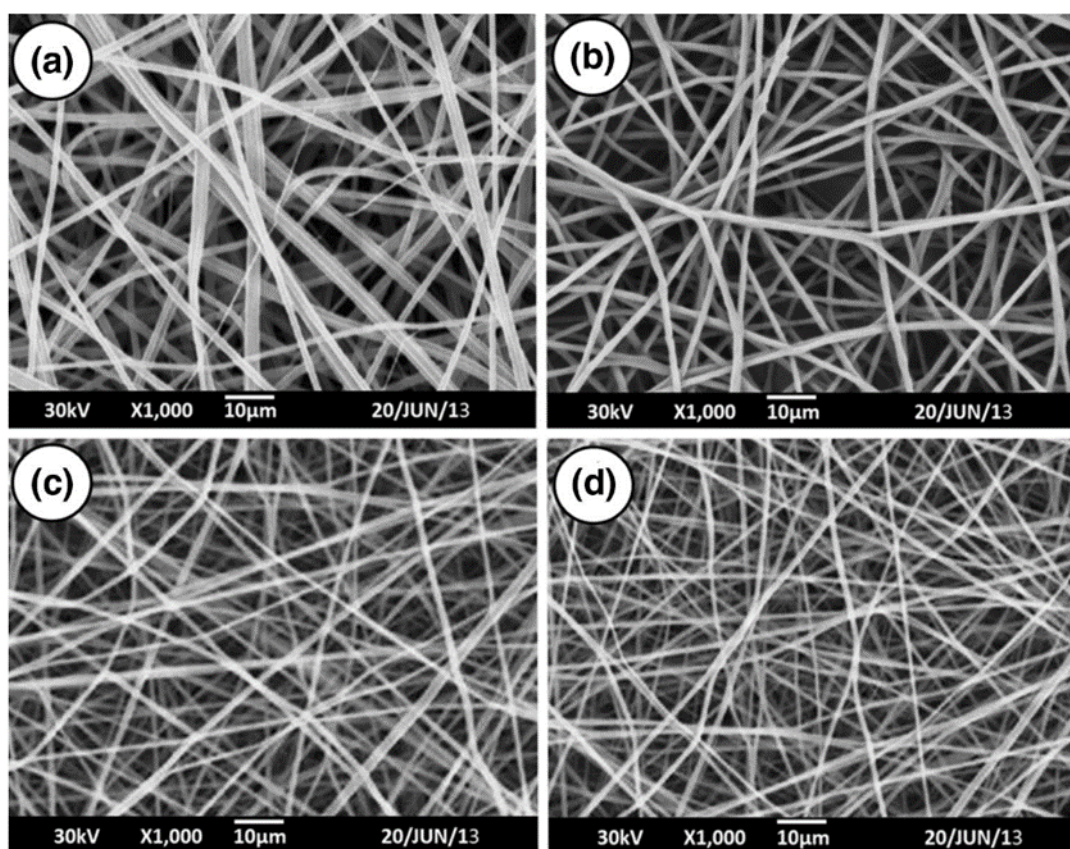


Figure 2.24 SEM morphology of fabricated PCL membranes. (a) and PCL/Ag nanocomposite membranes containing 0.05 wt% (b), 0.5 wt% (c) and 1 wt% (d) silver nanoparticles.²⁰⁶

The examples mentioned above are merely some of the applications, it is believed that PCL with all these excellent properties holds huge potentials to be applied in all kinds of fields and waiting for more researchers to find and benefit our lives.

2.5. Polylactic Acid

Poly(lactic acid) (PLA) or polylactide is one of the most well-known biocompatible and biodegradable aliphatic polyesters which has been intensively researched and applied in various areas.²⁰⁷ Lactic acid (2-hydroxypropionic acid, LA), as the raw materials and the constituent unit of PLA, is the most common carboxylic acid in nature whose molecular structure has chirality with two optical isomers (Figure 2.25): L-(+)-lactic acid as the natural and biologically major isomer, and D-(-)-lactic acid generated by microorganisms or by racemization. LA is derived from bacterial fermentation of renewable agriculture products such as cornstarch and corncobs.²⁰⁸ Currently, most of the commercial LA is produced by the bacterial fermentation of carbohydrates with a homolactic organism such as *Lactobacilli* and its modifications which exclusively produce LA,²⁰⁹ enabling PLA becomes a green eco-friendly product. Due to the above merits, PLA has been classified as generally recognized as safe (GRAS) approved by the United State Food and Drug Administration (FDA) and is believed to be safe in food contact applications.^{72,210} As the leading candidate of biomedical materials, PLA is commercially manufactured with a capacity of over 150,000 tons each year in Blair, NE,²¹¹ appealing interests from an increasing number of researchers from both academic and industrial areas.

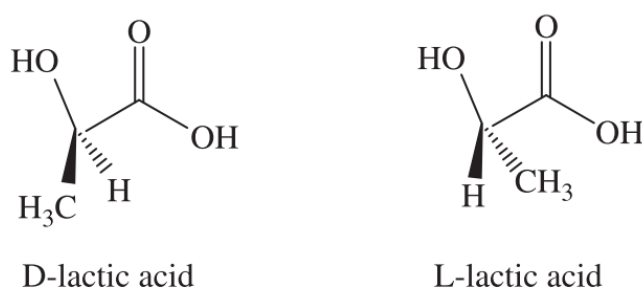


Figure 2.25 Stereoisomers of lactic acid.²¹²

2.5.1. The Production Methods of Polylactic Acid

The constituent unit of PLA, lactic acid, was first isolated from sour milk by Scheele from Swedish as early as 1780 and was first commercialized in 1881.²⁰⁹ While Carothers (at DuPont) was the first person who synthesis PLA in 1932 via the condensation

polymerization of lactic acid in vacuum conditions, resulting in a low molecular weight of PLA polymer.²¹³ Actually, both polylactide and polylactic acid are abbreviated as PLA since they are identical chemical. The only difference is the method used for producing the PLA. Generally, PLA can be produced via different methods such as polycondensation, ring-opening polymerization (ROP), azeotropic dehydration and enzymatic polymerization and so forth. Each method requires controlled react conditions such as pH, temperature, pressure, removal of the small molecules, the chemical used to catalyze the reaction, time duration of the polymerization.²¹⁴ Nowadays, among the above-mentioned techniques, two synthetic methods are mainly applied to yield PLA, one is direct condensation polymerization of the free lactic acid.²¹² The other way is the ring-opening polymerization of esters of the lactide monomer which is produced by polycondensation of lactic acid followed with depolymerization, as shown in Figure 2.26.²⁰⁷

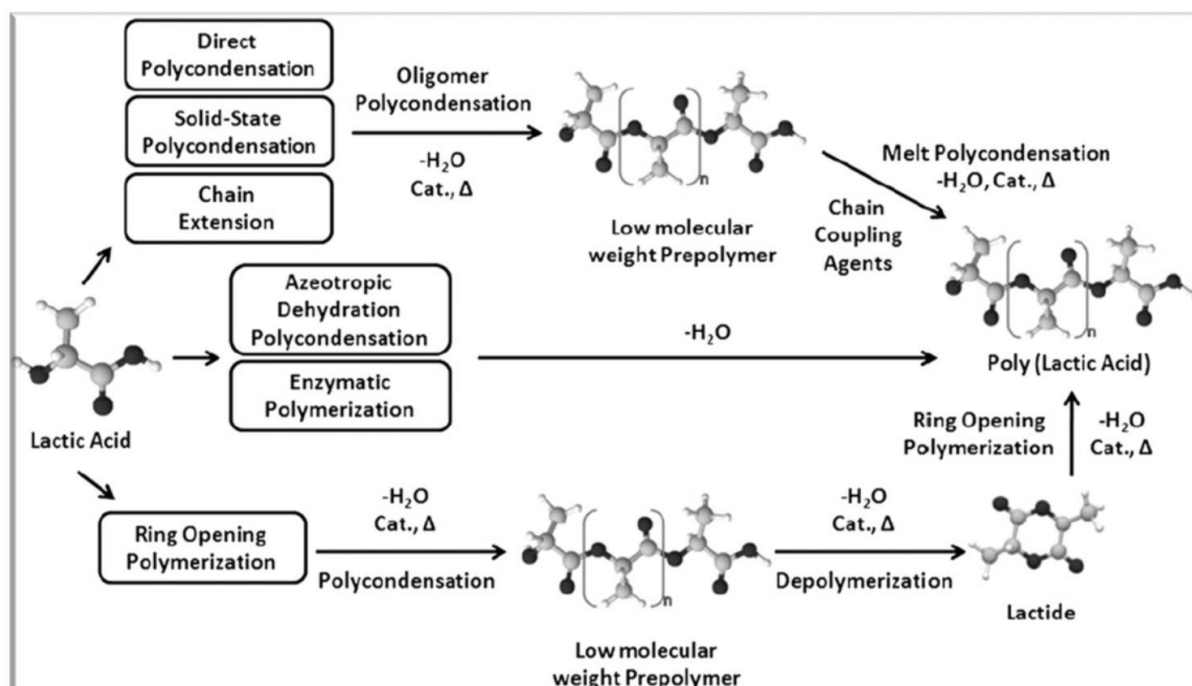


Figure 2.26 PLA synthesis methods from poly(lactic acid).²⁰⁷

Direct condensation polymerization can be further classified into solution polycondensation and melt polycondensation. Masanobu et al. achieved obtain PLA product with relatively high molecular weight in an organic solvent condition without

isolating intermediate and di-lactide. A molecular weight of up to 300,000 PLA can be synthesized at optimal conditions with the product owns enough mechanical properties.²¹⁵ Besides, with the melt condensation polymerization method, Sung et al. tested a variety of catalysts and found that with the catalyst of tin oxide and chloride, the molecular weight of PLA can be enhanced to about 100,000 in a comparatively short period.²¹⁶

Direct condensation polymerization is a simple and cost-effective method making it easy to commercially produce PLA. However, the equilibrium between the monomer, the oligomer as well as the small molecules produced in the condensation reaction puts limitations on the growth of the final PLA molecular weight.²¹⁷ Methods that avoid these limitations need to be developed to achieve higher molecular weight PLA polymer chains.

The ring-opening polymerization (ROP) method provides a solution to get PLA of high molecular weight, where the key point is that high purity lactides are used in the polymerization process avoiding the limitation of the reaction equilibrium. While the production of high purity lactides related to two equilibrium: dehydration equilibrium of esterification and ring-chain equilibrium involving the depolymerization of low molecular weight prepolymer into lactide,²¹⁶ thus the small water molecules equilibrium limitation is overcome. The ring-opening polymerization of lactides usually requires the addition of catalysts and PLA of high molecular weight is easily polymerized with the catalyze of tin, zinc, aluminium, and other heavy metal catalysts, with tin (II) and zinc producing polymers with high purity.²¹⁸ Table 2-5 demonstrates the applied catalysts, the solvent and the molecular weight of PLA polymer with different stereoisomer forms.

Table 2-5 Different catalysts used for the production of PLA.²¹⁹

Properties	Catalysts	Solvent	M_w
D, L-PLA/L-PLA	Aluminium Isopropoxide	Toluene	Mn. 90,000
D-L PLA	Stannous octoate	Alcohols	Mw < 3,50,000
L-PLA	Stannous octoate	Alcohols, carboxylate acid	Mn. 250,000

L-PLA	Stannous octoate and compounds of titanium and zirconium	Toluene	Mn = 40,000-100,000
D-PLA L-PLA D-L PLA	Stannous trifluoromethane sulfonate, scandium (III), trifluoromethane sulfonate	Ethanol	-
L-PLA	Mg, Al, Zn, Titanium alkoxides	Methylene chloride	-
L-PLA	Yttrium tris (2,6-di-tert butyl phenolate) (in toluene)	2-propanol, butanol, ethanol	Mn < 25,000
D-LPLA	Zn lactate	No solvent	Mn = 212,000
D-LPLA L-PLA	Butylmagnesium, Grignard reagent	Ethers	Mn < 300,000
L-PLA	Potassium naphthalenide	THF, toluene	Mn < 16,000
L-PLA	Complexes of iron with acetic, butyric, isobutyric and dichloroacetic acid	No solvent	Mw = 150,000

Though some of the heavy metal catalysts like tin octoate are approved by FDA,²²⁰ other heavy metal catalysts may contaminate the PLA product which limits the applications in food and medical areas. Therefore, many researchers are trying to find other non-toxic catalysts or special equipment and even design other polymerization methods such as enzymatic polymerization.²²¹ Anyway, the selection of the PLA synthesis route has to consider the reality such as the specific application, designed equipment, reaction conditions and so forth.

2.5.2. Physicochemical Properties and Biodegradability of Polylactic Acid

Properties of PLA play a significant role in industrial applications. In general, the component isomer, processing temperature, thermal history, average molecular weight, crystallinity percentage can directly influence the properties of PLA.²¹⁴ Among all the above factors, crystallinity is one of the most important parameters when selecting polymers for further applications. Generally, the crystallinity describes the percentage of the crystallized region in the polymer structure compared with amorphous regions, which closely related to the physicochemical properties of the polymer, such as density, heat capacity, melting point, mechanical and rheological properties.²¹⁰ The crystallinity of PLA varies with the component lactide isomers. Due to the chirality of the lactyl unit, lactide exists in three

stereoisomeric forms named L-lactide, D-lactide, and D, L-lactide whose structure were plotted in Figure 2.27.

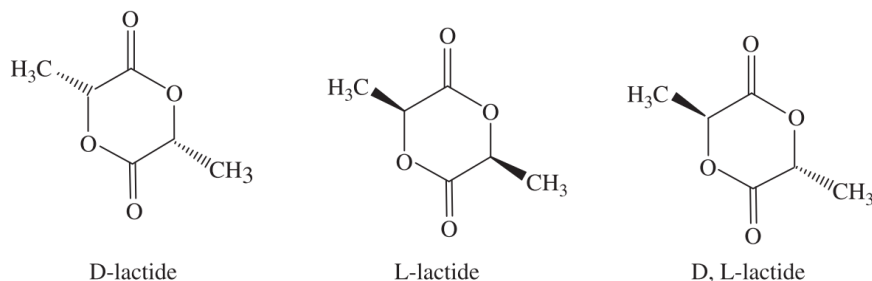


Figure 2.27 Three stereoisomeric forms of lactide.²¹²

Poly lactides produces with different lactide forms shows completely different properties that poly(L-lactide) (PLLA) and poly(D-lactide) (PDLA) are crystalline polymers with a melting point at around 180°C while poly(DL-lactide) is an amorphous polymer with a glass transition point at 50-57 °C.²²² Table 2-6 demonstrates the general properties of a commercial amorphous PLA (96: 4 L:D ratio content) as an example. The physical and mechanical properties of PLA vary to a large extent depending on the ratio and the distribution of the two isomers and the molecular weight of the polymer. The density of amorphous and crystalline PLLA has been reported as 1.248 g/ml and 1.290 g/ml, respectively. The density of solid PLA was reported as 1.36 g/cm³ for L-lactide, 1.33 g/cm³ for meso-lactide, 1.36 g/cm³ for crystalline and 1.25 g/cm³ for amorphous PLA.²²³ When the PLLA occupy over 90% of the content, the PLA polymer tend to be crystallized, while the lower optically pure is amorphous. It is noteworthy to mention that crystalline still owns an amorphous region since polymers cannot be completely organized into a 100% crystallized material.⁷² Besides, with the decreasing amount of PLLA content, both the melting point (T_m) and glass transition temperature (T_g) of PLA would decrease as well.²²⁴ It is also discovered that the blended polymer of PLLA and PDLA has a higher T_m of around 50°C than the pure enantiomeric polymers.²²⁵

Table 2-6 General properties of a commercial amorphous PLA (96: 4 L:D ratio content).²⁰⁷

Properties	Unit	Amount
Number average molecular weight	g.mol ⁻¹	66,000
Solid density	g.cm ⁻³	1.252
Melt density	g.cm ⁻³	1.073
Glass transition temperature	°C	55
Melting temperature	°C	165
Heat deflection temperature	°C	55
Vicat penetration	°C	59
Rockwell hardness	HR	88
Yield strength	MPa	70
Flexural strength	MPa	106
Tensile strength	MPa	59
Young modulus	MPa	1280
Ultimate tensile strength	MPa	73
Elongation at break	%	11.3

Generally, PLA can be easily dissolved in chloroform, dioxane, acetonitrile, methylene chloride, dichloroacetic acid and 1,1,2-trichloroethane and partially dissolved (unless heated to boiling temperature) in acetone, toluene, ethylbenzene and tetrahydrofuran. It is hard for PLA based polymer to be dissolved in water, alcohols like ethanol, methanol, propylene glycol and unsubstituted hydrocarbons such as hexane and heptane. Especially, crystalline polymer PLLA is insoluble in the solvent of acetone, ethyl acetate and tetrahydrofuran. A more detailed Table 2-7 below has been plotted showing the influence of the component stereoisomer forms of PLA polymer on the solubility, thermal and physical properties.

Table 2-7 Properties of lactide acid polymers.²¹⁹

PLA form	T_g (°C)	T_m (°C)	Density(g.cm⁻³)	Good solubility in solvents
PLLA	55-80	173-178	1.290	Chloroform, furan, dioxane and dioxolane
PDLLA	43-53	120-170	1.25	PLLA solvents and acetone
PDLA	40-50	120-150	1.248	Ethyl lactate, tetrahydrofuran, ethyl acetate, dimethyl sulfoxide, N, N xylene, and dimethylformamide.

It is valuable to address the rheological properties of the PLA as melt rheology plays an important role in the manufacture and procession. Many intrinsic factors can affect the rheological properties of PLA such as the branching type, the molecular weight distribution,

stereoisomer composition, optical block length distribution and melt stability.²¹² For example, semi crystallized PLA shows higher shear viscosity (3530 Pa.s) than amorphous PLA (3340 Pa.s).²²⁶ Above the melting temperature, PLA can behave like a typical flexible-chain polymer across all optical compositions, and the whole polymer chain mobility occurs with mechanical properties almost reduced to zero. Therefore, the processing temperature (ranging from 190°C-250°C) of PLA are usually significantly higher than the melting point since the viscosity of PLA at high temperature is drastically decreased, thus the polymer is easier to be processed into designed shape.²⁰⁷ For instance, PLA can be easily processed on standard plastic equipment to yield moulded parts, films for fibers.²⁰⁹

The degradation of a polymer usually occurs via the scission of the main chain or side chain of the polymer. Many factors can induce the degradation behaviours of polymer, such as hydrolysis, biological activity, oxidation, temperature activation, photolysis and radiolysis.²²⁴ Since the degradation process can be influenced by both physiochemical and biological factors, the overall mechanism of degradation behaviour can be referred as environmental degradation. Basically, the environmental factors such as pH, temperature, ions, humidity, oxygen and even nutrients will not only affect the degradation process of polymer, but also severely influencing the activity of involved microorganisms, thus a comprehensive condition need to be considered when applying biodegradability experiments of a polymer. Besides, the intrinsic properties of the polymer have to be thought over as well, such as thermal tolerance, mechanical strength, porosity, morphology, purity, crosslinking, chemical reactivity, and radiation resistance and so forth.²¹⁹

As one of the most important polyesters among medical-related industries, the degradation behaviours of PLA is a crucial property. PLA not only owns the complete biodegradability, but also not produces polluted chemicals during the biodegradation process. Generally, the degradation behaviours of PLA polymer are affected by multiple factors including molecular weight, crystallinity, purity, temperature, pH, terminal groups,

water permeability, added catalysts of enzymes, bacteria and inorganic filler.²²⁷ PLA of high molecular weight, as a stable polyester, can be fully resorbed after as much as 2 to 8 years and the long degradation time can lead to the occurrence of inflammation and infection in vivo.²²⁸ Therefore, it is of great importance to study the degradation behaviours of PLA in order to acquire desired PLA based medical devices. Figure 2.28 A) demonstrates a general mechanism of the hydrolysis degradation process of PLA and its degradation time upon different environment temperature.²⁰⁷ Basically, the molecular weight of PLA is reduced when the ester bond reacts with one absorbed water molecule, resulting in the hydrolysis process which is highly affected by temperature and humidity. With higher degradation temperature and high humidity, the degradation and disintegrate time can be extremely shortened within weeks to months.²²⁹ In addition, Figure 2.28 B) has shown two main steps of the PLA degradation mechanism.²³⁰ In the first step, high molecular weight polymer chains of PLA are hydrolysed into oligomers of low molecular weight. The second step begins when the average molecular weight of polymer chains reach around ~10,000 Da, the lactic acid and oligomers start to be metabolized by microorganisms into water and carbon dioxide.²³¹

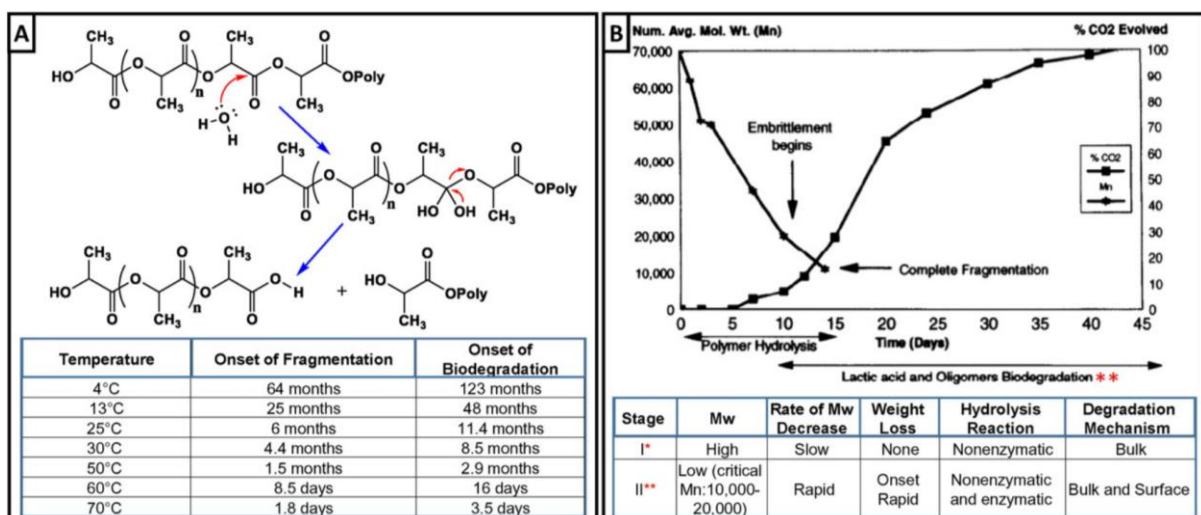


Figure 2.28 Biodegradation behaviours of PLA. (A) Hydrolysis of PLA and length of time taken to degrade to PLA in water. (B)

Biodegradation of polylactic acid in 60 °C compost.²⁰⁷

The biodegradation of PLA can be induced by bacteria, fungus, as well as enzymes. Common PLA-degrading bacteria include *Bacillus*, *Pseudomonas*, *Stenotrophomonas*, and so forth which are not widely distributed in nature.²³² The first isolated microorganism that can effectively degrade PLA is an actinomycete *Amycolatopsis* strain HT-32, which can degrade 60mg out of 100mg PLA film after 14 days.²³³ Further experiments showed that a variety of strains of *Amycolatopsis* can be served as PLA-degraders,²³⁴ and most of the PLA-degrading microorganisms were classified in the genus of *Amycolatopsis* in later researches.²³⁵ While *Bacillus brevis* was the first reported bacteria to efficiently degrade PLA, isolated from 144 soil samples with an enrichment culture medium.²³⁶

For PLA fungus degradation, only a few pieces of research were reported. Torres et al found that *Fusarium moniliforme* and *Penicillium roqueforti* were the only two filamentous fungal strains that can assimilate DL-lactic acid in a liquid medium.²³⁷ Besides, *Trichoderma viride* fungus was found owning the ability to biodegrade PLA and some of the plasticized PLA when cultured in a liquid medium and designed conditions.²³⁸ Fungi of *Tritirachium album* (ATCC 22563) was also found to be capable of degrading PLLA, which extra showed that the addition of gelatin can markedly increase the degradation rate of PLA in the base liquid medium.²³⁹ In addition, the degradation behaviours of PLA in soil and compost was researched found that the temperature was the dominated parameters of fungus degradation processes.²⁴⁰

Enzymes originated from microorganism also plays an important role in the biodegradation of PLA, most of which are proteases (serine proteases), and a few of which are lipase (esterase) and cutinase.²³² Serine proteases including proteinase K, a-chymotrypsin, subtilisin, trypsin and elastase, are the leading enzymes to degrade PLA. Proteinase K from *Tritirachium album* with a preference for the cleavage of the peptide bond was the first reported enzyme to hydrolyse PLLA in 1981.²⁴¹ Besides, the degradation behaviours of PLA catalysed by 56 commercial proteases was explored, indicating that only

alkaline proteases can lead to the formation of a large number of lactic acid from PLA while acid and neutral proteases show little effects. It is also reported that the type of the enzyme has relations toward the PLA constituted of different stereoisomers that protease with a preference toward PLLA (type I) while lipase/cutinase with preference to PDLA.^{242,243} Lipase originated from *porcine pancreas*, *Candida cylindracea* and *Rhizopus arrhizus* could hydrolyse the amorphous polymer, poly (DL-lactide).²⁴⁴ PLA of low molecular weight is more susceptible than high molecular weight PLA while amorphous can be degraded easier than crystalline. Additionally, the catalyse efficiency of enzymes can be influenced by the pH, temperature and PLA properties including stereochemistry and crystallinity as well.²³²

Moreover, the interaction between PLA and microorganisms during the PLA biodegradation processes were evaluated that the degradation behaviours showed significant differences when PLA films were degraded by *Kibdelosporangium aridum* in solid and liquid culturing environments. As shown in Figure 2.29, under the solid culture condition, a lot of small pits and holes were observed on the surface of the PLA film, while many grooves emerged on the PLA films surfaces when the PLA films were in the liquid culturing environment.²⁴⁵

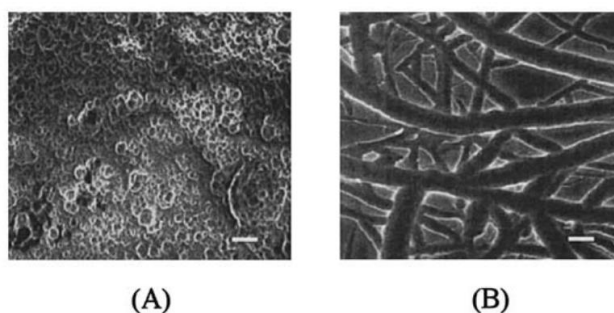


Figure 2.29 SEM images of PLA films after degradation by *Kibdelosporangium aridum* at 30°C. (A) in liquid culture, (B) in solid culture. Bar scale = 10 μm .²⁴⁴

All in all, the biodegradation activity of PLA is quite complicated in the real natural environment with a variety of parameters and conditions that need to be further comprehensively researched. Numerous researches have been applied to maximize the advantages of PLA of excellent properties and explore its applications in people's daily lives.

2.5.3. Biomedical Applications of Polylactic Acid

During the past several decades, the biodegradable polymer has gained focus and been extensively researched in medical applications due to the advantages of long-term compatibility and avoiding secondary surgery. In order to be applied in medical areas, the materials have to be biocompatible which is non-toxic, non-carcinogenic, non-mutagenic, non-allergenic, and free from contaminants and has no adverse immunological responses and harmless degradation products.²¹² Therefore, PLA with extraordinary properties of biodegradability, biocompatibility, processability and so forth, offers huge potentials as a bioresorbable polymer which is of great importance in biomedical applications owing to the unique ability to be completely resorbed *in vivo* in a designed time ranging from months to years.²⁴⁶ Besides, its great processability of PLA enables its versatile applications. For example, PLA thin films can be simply prepared with the solutions-casting method using organic solvents such as chloroform and methylene chloride, where the molecular weight and stereoisomer constitute of PLA as well as the solvent evaporation rate shows a huge impact on the crystallinity of the casted PLA films.²⁴⁷ Due to its excellent biodegradability, PLA can be employed as bioplastics such as loose-fill packaging, compost bags, food packaging and disposable tableware. When processed into fibres and non-woven textiles, PLA also owns the potential as disposable garments, upholstery, awning, feminine hygiene product and nappies.²⁴⁸

In the biomedical areas, due to the favourable characteristics of biocompatibility, biodegradability and processability, PLA has been widely applied as the materials of drug delivery system, surgical implant as well as porous scaffolds for the growth of tissues.^{249,250} Apart from the excellent properties of PLA, the low price is also one of the crucial factors that facilitate and accelerate its applications.²⁵¹

2.5.3.1. PLA applications in drug delivery

Back in the 1970s, the controlled drug delivery system has aroused increasing focuses for the purpose of releasing the drug with controlled, systematic, site-specific manners over an extended and prolonged period. This new delivery system shows numerous merits comparing with conventional therapeutic systems including a prolonged duration time, reduced side effect, retaining drug bioactivity, and ultimately the efficiency of the applied drugs is improved.²⁵² One of the commonly applied approaches for controlled drug delivery is to effectively incorporate the drug into biodegradable polymer nanoparticles or microparticles,²⁵³ which can display a controlled and sustained behaviour by the drug diffusion or the degradation (hydrolysis or enzymatic degradation) of the drug carrier.²⁵⁴ The advantages of this form of controlled drug delivery methods is that the nano and microparticle can be injected avoiding complicated surgical insertion and even comprised the potential for passive targeting when the size of the particles is in designed range.²⁵⁵ Besides, the large surface-to-volume ratios of nano- and microparticles also provide a significantly large number of reaction sites than macroparticles with fewer surface areas.²⁵⁶ While the shortcoming of the system is that the high initial burst release can cause toxic side effect and also the waste of drugs.²⁵³ Table 2-8 demonstrates more detailed advantages and limitations of PLA particles.

Table 2-8 Advantages and disadvantages of PLA micro- nanoparticles.²⁵³

Particle size	Advantages	Limitations
Microparticles	Subcutaneous injections Intramuscular injections Controlled release Reproducible processes	Unintended toxic side effect due to high initial burst Wasteful use of expensive drugs Reproducible processes due to initial burst release
Nanoparticles	Direct injection to the blood Potentially improved vaccine	Non-specific uptake by reticuloendothelial system (RES) systems Potential immunotoxicity responses

The preparation method of PLA particles has been intensively researched with a multitude of effective and valuable preparation techniques introduced. Figure 2.30

schematically illustrates the representative preparation method of PLA nano- and microcapsules in the way of classification, while the more detailed schematic descriptions of different methods for fabricating particles are introduced in Figure 2.31 and Figure 2.32.

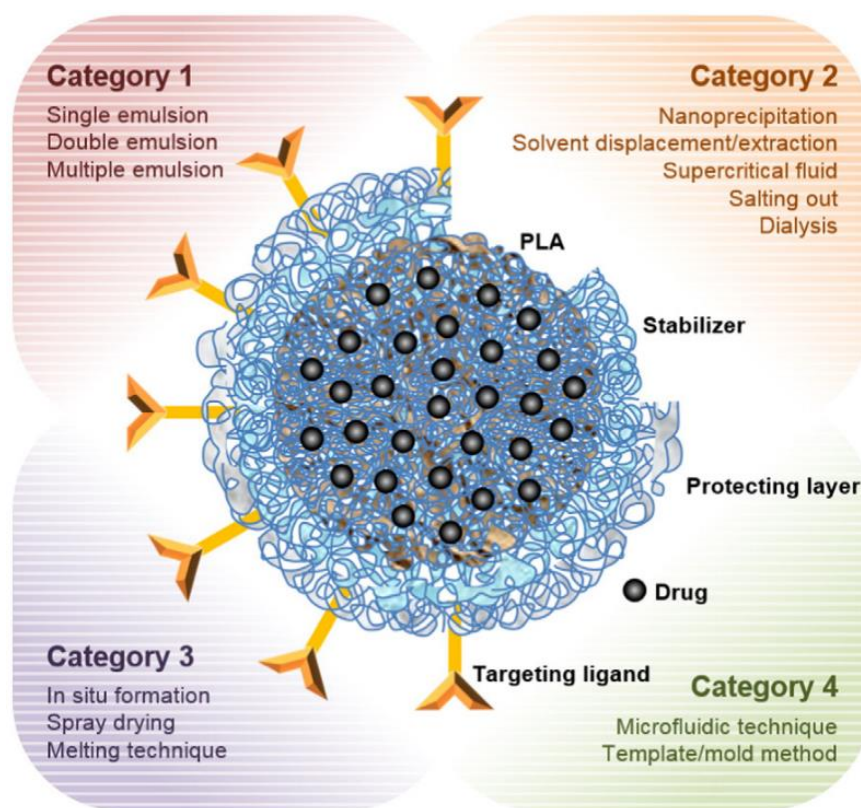


Figure 2.30 Schematic illustration of the preparation methods of PLA micro- and nanoparticle.²⁵⁷

No matter which methods is applied, the drug is either trapped and encapsulated inside of polymer shell-like capsules or dispersed and incorporated with polymer matrices.²⁵⁸ The selection of the specific preparation methods has to meet the requirement of the concrete applications and drug properties. For example, traditional emulsion related methods including single emulsion, double emulsion and multiple emulsion require specific solubility (either water or oil soluble) of the drug to form particles. Besides, since the size of the particles synthesis from emulsion methods can vary from nanometers to micrometres which are controlled by changing the agitation rate and other experimental conditions,²⁵⁹ the drug should not lose effect during agitation. Moreover, the salt out method does not have a heating procedure which is helpful in incorporating heat-sensitive drugs such as proteins, genes, vaccines and other bioactive drugs.²⁶⁰

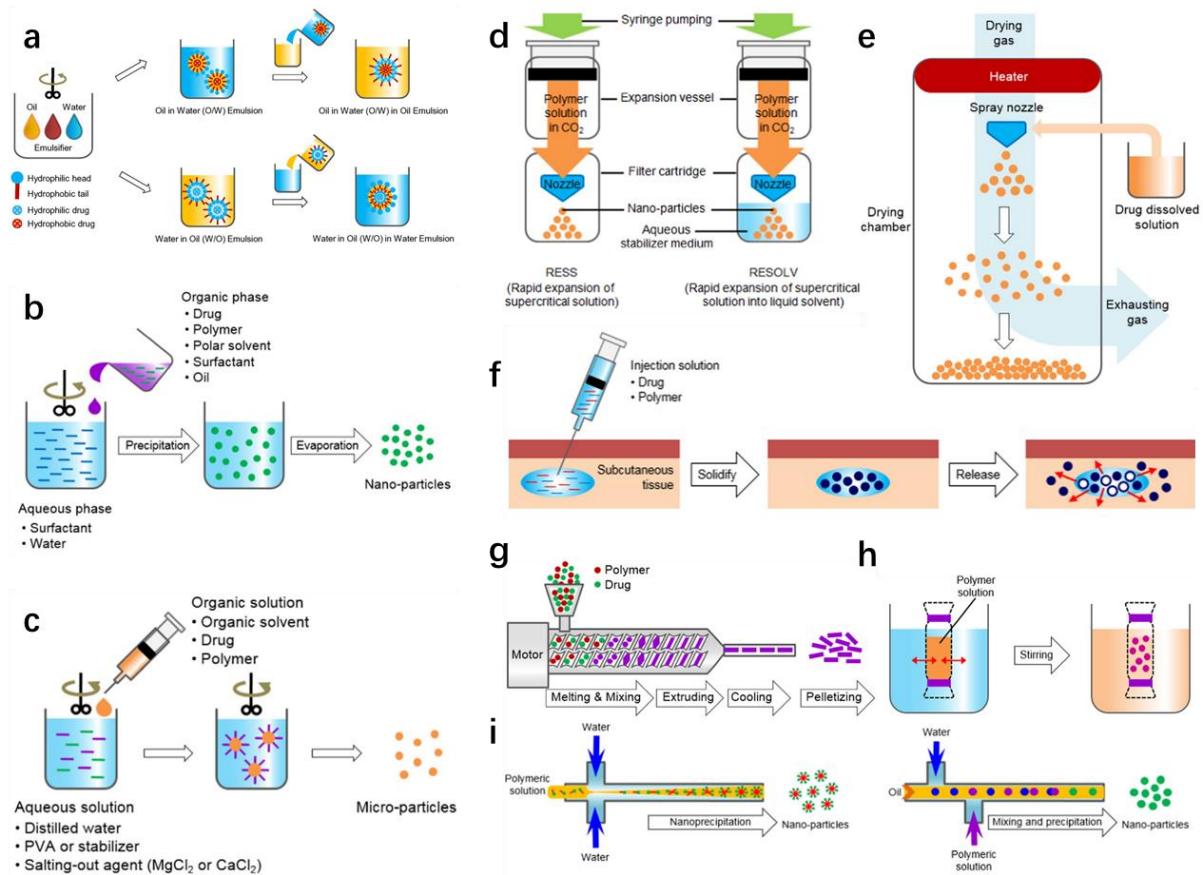


Figure 2.31 Schematic descriptions of different methods for fabricating polymer particles. a) emulsion-based methods. b) nanoprecipitation. c) salting-out method. d) supercritical fluids technique. e) spray drying. f) *in-situ* forming method. g) melting technique. h) dialysis technique. i) microfluidic technique.²⁵⁷

It is noteworthy to address the template-/mould-based technique due to the ability to produce particles in homogeneous sizes as schematically demonstrated in Figure 2.32. This moulding method requires a master template with a predesigned structure, which is produced via UV lithographic technique. First, hydrogel (e.g. gelatin) or poly(vinyl alcohol) (PVA) solutions are poured on the top of the master template, which is then solidified in low-temperature conditions in order to get the hydrogel or PVA sacrificial mould with reversed pattern structure compared with the master template. After peeling off the sacrificial mould, the drug with polymers, dissolved in a favourable solvent, is again poured on the surface of the sacrificial mould followed by evenly spreading to fill the empty structure. When the solvent was fully evaporated, the sacrificial template with microparticles was dissolved in water to harvest the drug-loaded particles which are ready for further purposes after several wash steps, centrifugation, or filtration.^{37,261} Apart from the merit of producing

monodispersed particles, this template-based technique also owns the advantages of selectable dimensions, easy scale-up and repeatable procedures. However, the size of the synthesized particles is limited in micro size due to the restriction of the UV lithography technique in producing patterns on silicon wafer master template. Other lithography methods are required to achieve nano-size particles.²⁵⁷

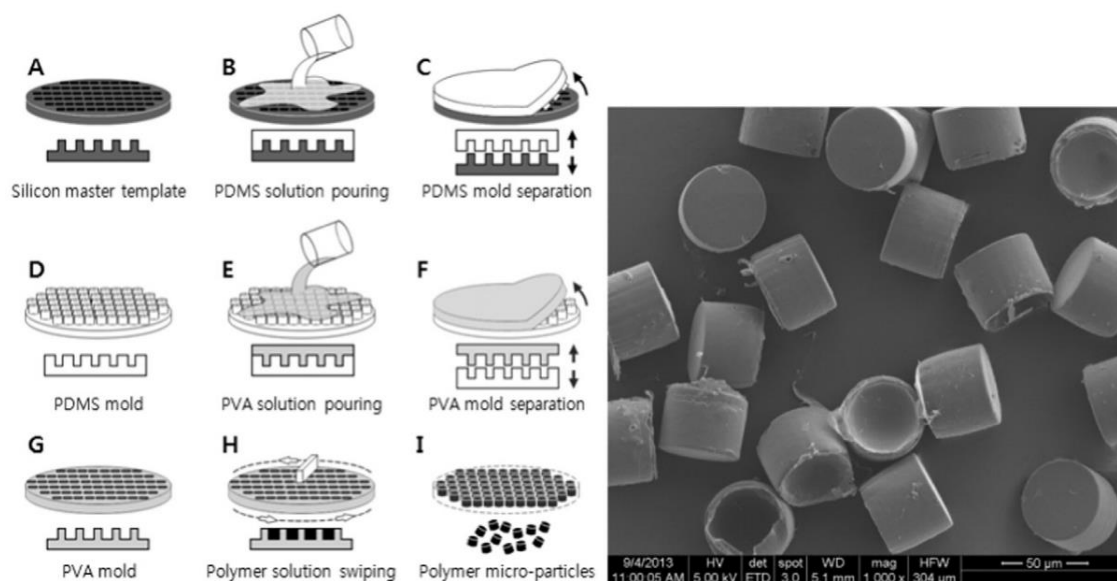


Figure 2.32 Schematic descriptions of template method process and fabricated PLA microparticles.²⁵⁷

Practically, PLA particles have been applied for continuous and controlled drug release among a variety of medical agent including contraceptives, narcotic antagonists, local anaesthetics, vaccines, peptides and proteins.²⁶² For instance, PLA microparticles has been widely applied in in vaccination area in order to prevent a large number of infectious diseases including AIDS, hepatitis B, anthrax, SARS, and MERS.²⁶³ Many research groups have proposed microparticle related single-shot vaccines with PLA-based polymer.^{264–266} However, there are many challenges of the PLA particles that inhibit the further application of the particles especially in drug delivery areas including the low drug encapsulation efficiency and capacity, high initial burst release and incomplete release of the drug, low producibility between batches and difficulties to scale up, the difficulties in characterizing the influences of the residual organic solvent, interaction between particles and immune system, also the terminal sterilization as so forth.²⁶⁷ Besides, the size of the particles also

plays a crucial role that due to the special mechanisms of the intestine, particles with a size smaller than 100 nm demonstrating a significantly higher chance to be absorbed compared with large particles.²⁶⁸

Manipulation and modification of both bulk polymer and the surface properties of the particles can be one of the feasible ways to improve the properties of PLA particles. The bulk polymers can be modified via the blending of different polymers, copolymerisation, plasticization and crosslinking, while the surface modification includes surface coating, entrapment and plasma treatment.²⁶⁹ For example, nanoparticles prepared from PLA-PEG copolymers can increase the blood circulation times and decrease clearance *in vivo* compared with nanoparticles made by PLA alone, since the hydrophilic PEG block owns the ability to repel proteins within an aqueous environment, inhibiting the absorption of proteins to the polymer surface and thus preventing the interaction between polymers and cells.²⁴⁸ PEG is also appropriate to be grafted on the surface of PLA particles enabling the particle to escape from the immune system when applying particles to the bloodstream thus prolong the blood circulation half-life of the particles.²⁷⁰ All in all, the purpose of the modification is to achieve high drug loading efficiency, controlled release rate and ultimately increase the effect of the drug and benefit the patients.

2.5.3.2. PLA applications in tissue engineering

When selecting the biomaterials for the applications in tissue engineering, biostability comes first which includes strength, elasticity, interface absorption as well as chemical degradation.²⁷¹ In other words, the scaffold should own sufficient mechanical properties and degradation rate in order to facilitate rather than hinder the regeneration of target tissues. It is of great importance to maintain the mechanical properties of the scaffold after being implanted for the reconstruction of hard, load-bearing tissues like bones and cartilage.²⁷² Generally, the scaffold should be designed to withstand the loads and stresses that target tissues can finally bear until it is no longer needed. Therefore, the mechanical

and rheological parameters such as elastic modulus, flexural modulus, tensile strength, maximum strain are required to be comprehensively considered.²⁰⁷ Besides, since the scaffold would finally be replaced by newly restored tissues from the adhere cells and different tissue requires various biodegradation activity, it is of great importance to consider and study the degradation behaviours of the scaffold in order to design and predetermine the degradation period of the scaffold.

Basically, the mechanical properties of the scaffold made of selected materials can be manipulated by altering the pore size, volume, shape, orientation, and connectivity. All these properties can change in the function of implantation time.²⁷³ A good understanding of the influences of the above factors can significantly facilitate the design of a medical device and predict the responses under practical conditions. For instance, scaffolds produced from polymers of PLA blended with PCL shows that the blending method (melting or solution casting) has significant influences on the surface roughness, cell adhesion and proliferation, and the PLA/PCL scaffold produced with the solution casting method presents a reduced pore size and enhanced cell proliferation.²⁷⁴

Because of the great mechanical properties of PLLA, it is possible to fabricate 3D structures such as trays, cages, meshes, fibres and scaffolds. In the area of guided bone regeneration, barrier membranes are required to prevent the growth of soft tissues and direct the recovery of new bone growth in the broken part, while still allow the permeation of the necessary nutrients.²⁷⁵ Kinoshita et al. employed a PLLA mesh tray and particulate cancellous bone and marrow for treating tumours, cysts, or alveolar atrophy of 62 patients as demonstrated in Figure 2.33. Besides, PLA-based porous scaffolds were also developed for the repair of articular cartilage defects.²⁷⁶ Moreover, since lactic polymers are able to stimulate isolated cells to grow into tissues and release drugs like painkillers, anti-inflammatories and antibiotics, cell transplantation become another area that the PLA-based scaffolds can play a part in.²⁷⁷

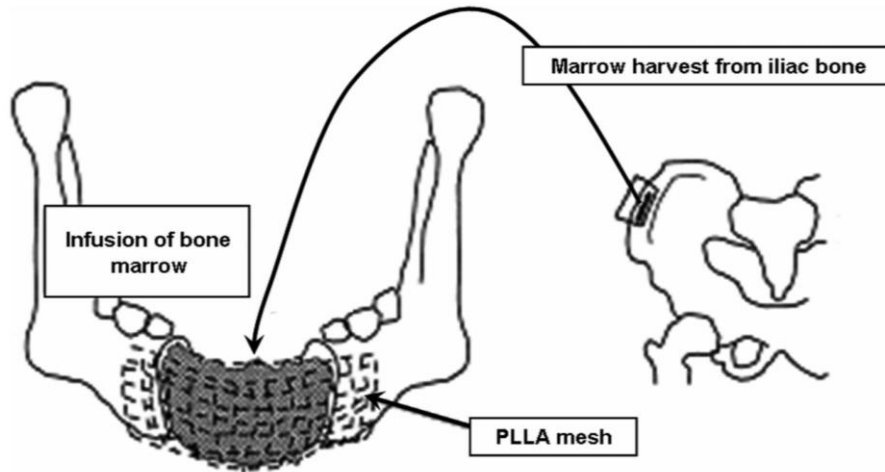


Figure 2.33 Diagram of mandibular reconstruction using a PLLA mesh and bone marrow.²⁷⁸

Nowadays, producing 3D scaffold with polymers has become one of the fundamental parts of tissue engineering.²⁷⁹ PLA with excellent biodegradability, biocompatibility becomes one of the most common polymers to produce high quality and resolution scaffold via 3D printing techniques.²⁸⁰ Moreover, the produced scaffold can be designed by computer based on the patient-specific anatomical data and many industrial and architectural applications.²⁸¹ In order to manipulate the physical and mechanical properties and improve the processing procedures of the scaffold, the combination between PLA and other materials including glass particles and PEG have been applied.²⁸² Some of the most representative application of PLA-based scaffolds produced via 3D printing techniques has been listed in Table 2-9.

Table 2-9 PLA-based scaffolds printed with a 3D system.²⁸³

Material	Experiment	Application
PLA/Polydopamine	<i>In vitro</i> - hADSCs	Craniofacial bone lesion repair
PLLA/PLGA	<i>In vitro</i> - Human skin fibroblast	Tissue engineering – skin fibroblast
HA/Collagen/PLA	<i>In vivo</i> - Rabbits	Bone scaffolds
PLA/PEG/G5 glass particles	<i>In vitro</i> - rMSC adhesion	Tissue engineering
PLA/ β -TCP	<i>In vivo</i> - Rabbits	Heterotopic bone formation
PDLA/rhBMP-2	<i>In vivo</i> - Rats	Mandibular bone repair

2.5.3.3. PLA applications in medical devices

Skin damages caused by injuries are unavoidable, depending on the severity of the injuries, some of the wound can self-healed, while the severe ones might require extra medical assistance, Therefore, it is of great importance to research wound dressings which can protect the damaged part from contaminations and infections and even remove exudations.²⁸⁴ The most attractive approach for producing wound dressings is electrospinning that fibres with diameters ranging from nanometers to micrometres can be extruded out. The electrospun wound dressing owns the excellent properties of high specific surface areas and small pores which can benefit the absorption of liquids as well as prevent the penetration of bacteria, thus facilitate wound healing.²⁸⁵

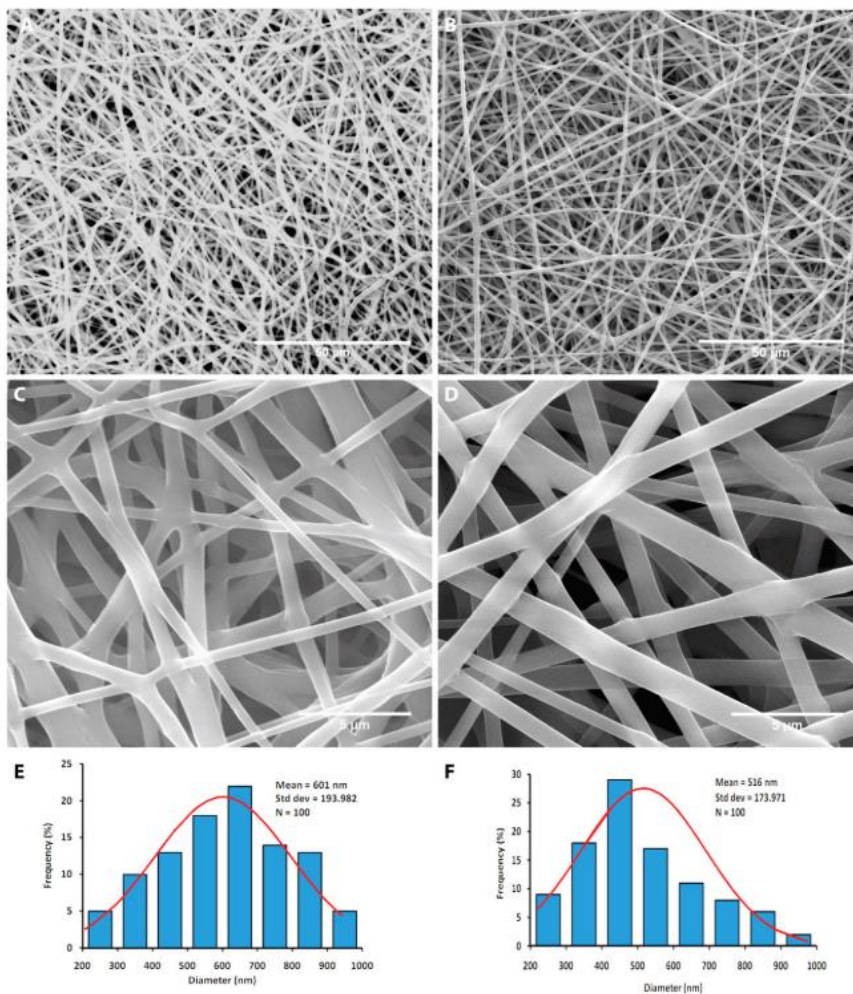


Figure 2.34 SEM images and the diameter distribution of electrospun fibres. A) PLA/Cur, B) PLA/HPG/Cur and C) PLA/Cur, D) PLA/HPG/Cur of SEM images with different magnification. E) and F) the diameter distribution of electrospun fibre PLA/Cur and PLA/HPG/ Cur respectively.²⁸⁶

As shown in Figure 2.34, PLA and hyperbranched polyglycerol (HPG) incorporated with curcumin (Cur) is prepared into nanofiber mats via electrospinning technique for wound heading applications. The properties of the wound dressing mats can be further improved via blending drugs during the formation of the mats. Basically, there are two well-developed methods for preparing nanofibrous electrospun mats that can be served in wound dressing applications. One method is to electrospinning polymer with intrinsic antibacterial and wound-healing properties,²⁸⁷ which is not appropriate for PLA. The other way is immobilizing drugs or antibacterial compounds in the electrospun polymers.²⁸⁸ For example, thymol as one of the components of a herb with anti-inflammatory and antibacterial effect is added into PLA/PCL nanofibrous mats via electrospinning technique, which demonstrates a remarkable performance in the wound-closure experiment.²⁸⁹

Except for medical devices of electrospun fibrous mats, the drug-loaded suture also possess the possibility to facilitate the healing of wounds. As a biodegradable and biocompatible polyester, PLA has been applied as surgical resorbable sutures and its tissue reaction has been investigated as early as 1971.²⁹⁰ Recent advances have enabled PLA surgical sutures the capability to release drug, inhibit bacteria growth and assist the wound healing.²⁹¹ For instance, microspheres incorporated with gentamycin sulfate (PM-Ds) was loaded on PLA suture, which can sustain release the drug while maintaining sufficient mechanical properties as shown in Figure 2.35.

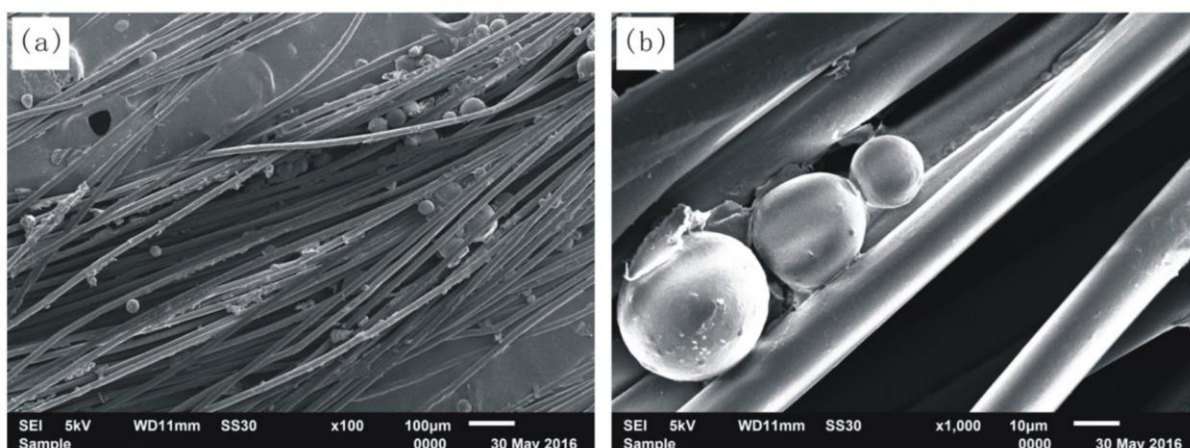


Figure 2.35 SEM images of PLA suture loaded with PM-Ds at different magnifications.²⁹²

Apart from wound dressing mats and surgical sutures, PLA has been applied as many other medical devices. For instance, Fangueiro et al. has introduced a method for manufacturing braided corrugated vascular prosthesis made of PLA and polyethylene terephthalate (PET), which can reconstruct the blood flow in the damaged blood vessel part (Figure 2.36 A)), enabling it huge potentials especially in vascular surgery. Apart from the medical device of the blood vessel, the group of Fangueiro also proposed the technology of preparing artificial ligaments made of PLA-based polymer that can mimic the function of natural ones as shown in Figure 2.36 B).

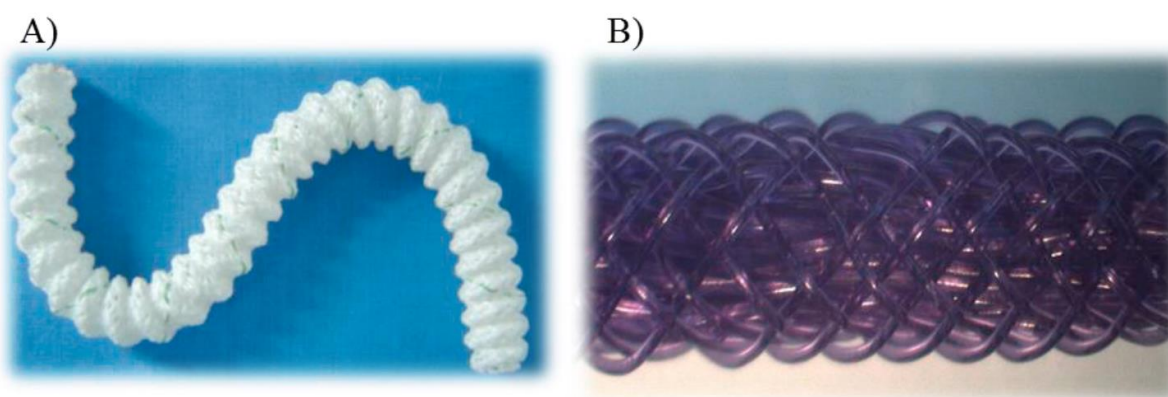


Figure 2.36 Implantable devices made by braiding. A) Braided vascular prosthesis as a medical device for blood vessel and B) PLA-based mimicking ligament.²⁹³

PLA has shown its potentials as versatile polymers and tools for drug delivery, tissue engineering as well as medical devices, and the further investigations of PLA can focus on combining with other polymers to leverage its strengths and mitigate its weaknesses thus further broaden its application area.²⁹⁴

2.6. Microarray Structure

Generally, a microarray structure is a periodical micropatterned surface with highly ordered surface features and well-defined dimensions fabricated on a proper substrate such as silicon or SiO₂ which can be further transferred to other materials. Some of the common structures that either periodical in one direction or two noncollinear directions are grooves,²⁹⁵ wells,² pillars³ or even chambers⁴ in microscale. These special structures of

microarray have attracted steadily growing interest due to their special morphology and properties and have been widely applied in a variety of fields ranging from lab-on-chip, sensing, electronics, optics, to microbiology biochemistry and biomedical areas and so forth, which will be further elaborated in 2.6.2. Therefore, a multitude of novel micro-nanolithography techniques has been proposed which are able to fabricate these special microarray structures.

2.6.1. The Production Method of Microarray Structure

Micro- and nanolithography can fabricate designed patterns with a feature size ranging from a few nanometers up to tens of millimetres. By combining lithography with other fabrication processes such as deposition and etching, sometimes repeating several times, a high-resolution topography with complex micro/nanoscale structures can be successfully produced.⁵ Generally, the lithography techniques can be divided into two categories as masked lithography and mask-less lithography based on whether a mask or templated are implemented or not. Masked lithography including photolithography, soft lithography, and nanoimprint lithography, can transfer all the pattern information of a large area from the mask to the substrate simultaneously, enabling a high-throughput fabrication up to several tens of wafers per hour. While the mask-less lithography, such as electron beam lithography, focused ion beam lithography and scanning probe lithography, can produce arbitrary patterns by serial writing without templates and can reach an ultrahigh-resolution with minimum feature size as small as a few nanometers.⁵ However, its serial point-by-point writing modality results in a long manufacturing time which severely limits the wide application of this technology in the large-area nanoscale image.²⁹⁶ The major lithography techniques along with their specifications of minimum feature size and throughput are summarized in Table 2-10.

Table 2-10 Specifications of the major lithography techniques.⁵

Lithography Technique	Minimum Feature Size	Throughput
Photolithography (contact & proximity printings)	2-3 μm	very high
Photolithography (projection printing)	a few tens of nano-meters	high - very high (60-80 wafers/hr)
Electron beam lithography	< 5 nm	very low
Focused ion beam lithography	~ 20 nm with a minimal lateral dimension of 5 nm	very low
Soft lithography	a few tens of nano- to micro-meters	high
Nanoimprint lithography	6-40 nm	high (> 5 wafers/hr)
Dip-pen lithography	a few tens of nano-meters	very low – low, possibly medium

Optical lithography, also known as photolithography, is one of the most common and well-established fabricating methods for semiconductor integrated circuit related industries that the nanoscale with ~65 nm gate lengths in large-volume manufacturing production can be achieved.²⁹⁶ Generally, optical lithography has three forms contact printing, proximity printing and projection²⁹⁷ which are schematically demonstrated in Figure 2.37. However, unless using the sophisticated optical-lens system, the optical lithography can hardly produce high-resolution patterns as small as a few tens of nanometers.²⁹⁸ Thus, immersion lithography,²⁹⁹ resolution enhancement technology³⁰⁰ and extreme-UV lithography³⁰¹ have been developed to overcome these lithography resolution limitations.

Though other methods like electron beam lithography³⁰² and focused ion beam lithography³⁰³ can produce smaller structures than optical lithography and with an almost complete structure flexibility thanks to the ultra-short wavelengths of electron/ion beams in the order of a few nanometers, its serial point-by-point writing modality results in a long manufacturing time which severely limits the wide application of this technology in the large-area nanoscale image. While optical lithography is a parallel writing technique that can save much more time.²⁹⁶

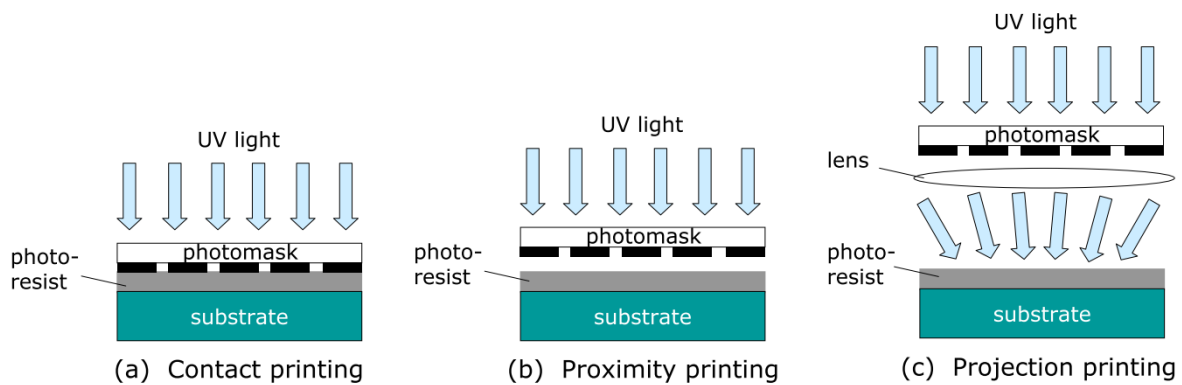


Figure 2.37 Schematic demonstration of three forms of photolithography.

(a) contact printing; (b) proximity printing; and (c) projection printing.²⁹⁶

A traditional optical lithography is a mask-based approach combined with an optical reduction technique that can ameliorate the demands on both the mask fabrication and the optical system. With the fabricated mask, the desired wafer can be simply microstructured by transferring all the designed information on the mask by the lithography step. However, in order to commercialize the optical lithography technique, special lithography tools and equipment are necessary, which are extremely expensive both in initial and in operating costs. Obviously only when the products are scaled up in a high number can the price be acceptable, which does not fit the reality in the research area.²⁹⁶

Fortunately, most of the applications do not require complicated structure but merely some periodic or quasi-periodic patterns, such as microarray structures, that can be achieved with other methods. Interference lithography, a simple laboratory-scale technology, is emerging as one of the most powerful yet relatively inexpensive techniques to fabricate patterns of large areas and volume with micro- or submicron-sized periodicities.³⁰⁴ With this unique technique, N-dimensional periodic structures (N is or less than 3) can be fabricated by interfering with (N+1) non-coplanar beams onto the photoresist. By varying the intensities, geometries, polarizations, and phases of the beams, both the symmetry and the shape of the periodic structure can be conveniently manipulated as shown in Figure 2.38. The specification of the lithographed structure can reach sub-50nm dimensions with shorter wavelength lasers and/or liquid immersion lithography technique.

Moreover, the two-dimensional structures with synonyms such as bi-gratings or crossed gratings can be fabricated with interference lithography technique as well.³⁰⁵ The technique of interference lithography also holds the potential to fabricate large-area, defect-free 3D micro- and nanostructure 3D structures in a rapid and cost-effective way.³⁰⁶ Basically, the available range of structures can be dramatically expanded by combining the multiple interferometric exposures with lower resolution, laboratory-scale optical lithography and further use of higher resolution electron beam lithography at special and limited areas.

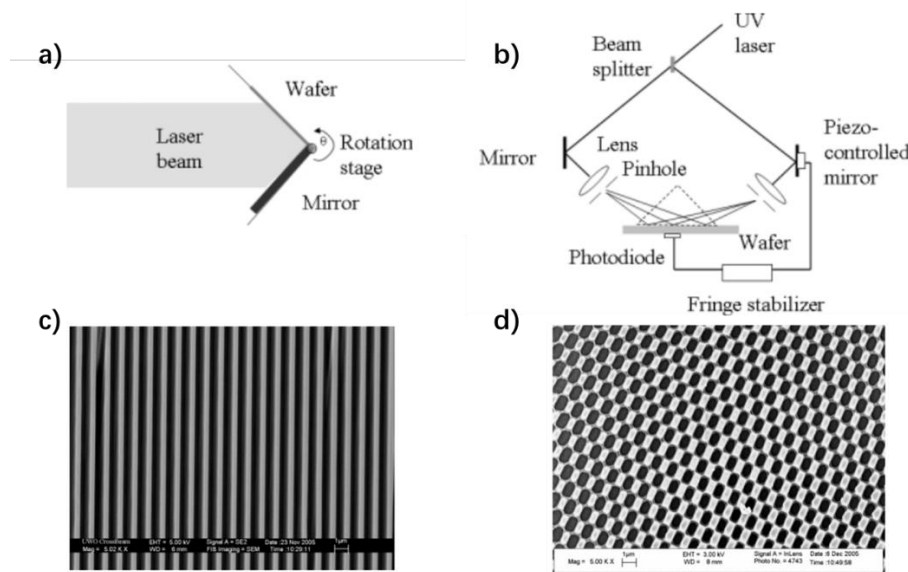


Figure 2.38 Interference lithography setups and representative microstructures. a) A Lloyd's mirror configuration of two-beam interference lithography setups. The angle of rotation indicated is about an axis normal to the page; b) A two-beam configuration created by a beam splitter where one mirror is piezo-electrically controlled for phase stabilization. The dotted triangle represents the prism used in liquid immersion lithography. c) A SEM image of 1D interference pattern having a 1 μm periodicity recorded in the negative photoresist SU-8. d) A SEM image of a hexagonal structure created by double exposure IL where the substrate was rotated 60 degrees about its normal between exposures.³⁰⁵

With micro- nanostructure being fabricated with various lithography methods, a replication toolbox is therefore needed to transfer the pattern onto a substrate made of other materials. Nanoimprint lithography is one of the optimal candidates as the replication toolbox where the surface structures of a template are transferred and replicated into substrates made of designed material by mechanical contact and three-dimensional material displacement. The transferring process can be achieved by shaping a liquid

followed by curing and hardening processes, by variation of the thermomechanical properties of a film by heating and cooling, or by any other kind of shaping process using the difference in hardness of a mould and a mouldable material.³⁰⁷ The nanoimprint lithography technique with the merits of low cost, high throughput and high resolution³⁰⁸ first introduced by S.Y. Chou as a “hot embossing technique” that can manage to achieve the definition of features with lateral sizes down to sub-10 nm.³⁰⁹ Basically, a standard nanoimprint lithography process can be categorized as origination, replication and pattern transfer³¹⁰ which is sometimes not complete if process cycles are iterated or combined with other processes as schematically demonstrated in Figure 2.39.

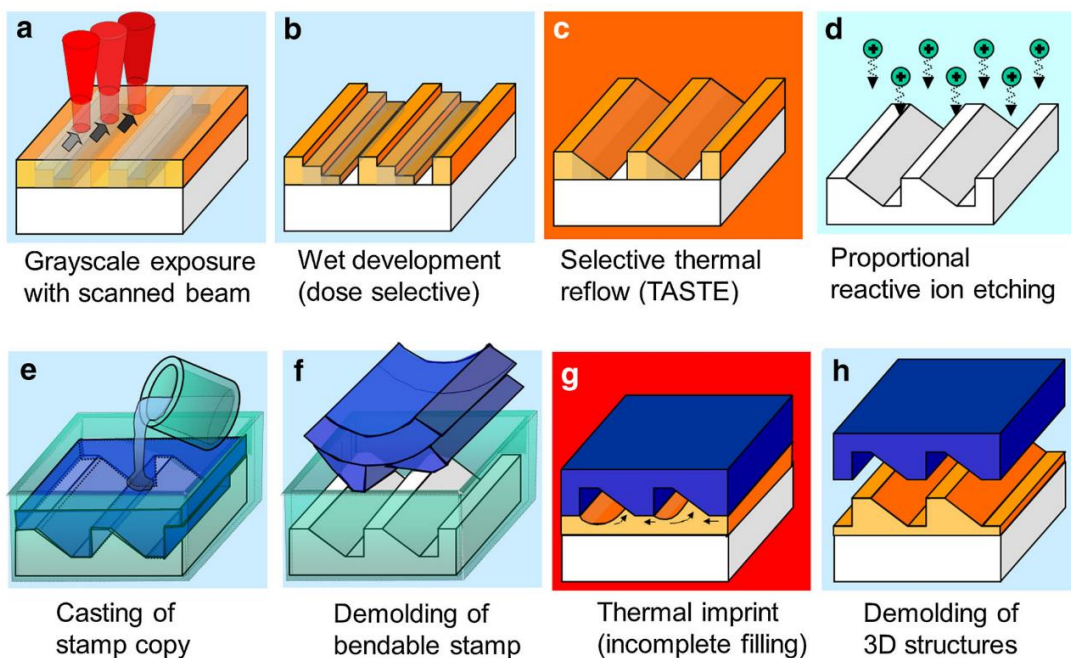


Figure 2.39 Schematics with different processes. a) origination by dose- modulated EBL, b) multilevel structures after development. Post-processing by c) sloped structures after selective thermal reflow, d) hard stamp by proportional etching and e) casting of a soft stamp, f) peel demoulding, g) imprint with hard or soft stamp f) and h) demoulding.³¹¹

Nanoimprint lithography (NIL) is not only a planar high-end technology that can structure the surface of wafer-like substrates like in photon- and electron-based traditional lithography, but also a 3D process as it can transfer various stamp topographies thanks to the 3D displacement of material and the soft and bendable of stamps while the mould empty structures are well filled as shown in Figure 2.40. It is believed that the nanoimprint

lithography technique is able to fabricate almost arbitrary sloped, convex and concave profiles in the same polymer film with dimensions in micro- and nanometer scale.³¹¹

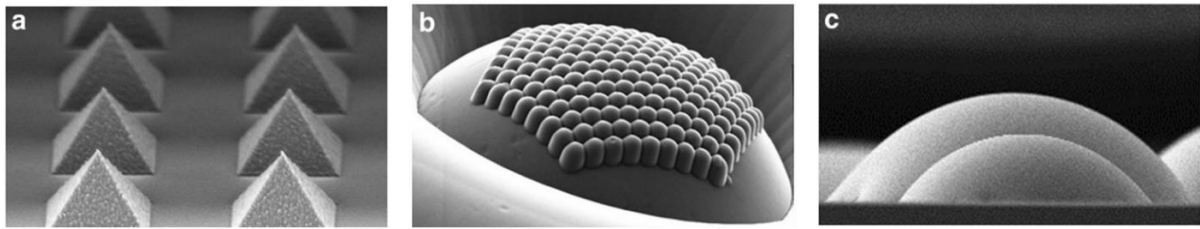


Figure 2.40 SEM micrographs of 3D shapes. a) pyramids (2 μm footprint) by moulding of a 100 silicon stamp after anisotropic etching. b) Convex lenses by moulding concave cavities in a silicon oxide wafer after isotropic etching. c) Convex spherical shapes by thermal reflow of PMMA granules at high temperatures (180 $^{\circ}\text{C}$).³¹¹

2.6.2. Rigorous Coupled Wave Analysis

Thanks to the rapidly developed fabrication techniques such as electro-beam lithography or holographic exposure, the grating structures with deep grooves and small period of high quality and definition are available to be constructed, thus, intensive attentions have been attracted to study the grating diffraction activity of electromagnetic waves.³¹² Since the periodical structure can be applied in various important and precise fields like acoustic-optics, integrated optics, holography, and spectroscopy,³¹³ the electromagnetic analysis of the grating structure should be rigorous without any approximations.

In general, the rigorous methods of analyzing grating diffraction can be classified into two main categories named integral methods and differential methods.³¹⁴ Integral methods are suitable for analyzing continuous gratings profiles, while differential methods are more appropriate for analyzing discrete grating profiles. Besides, numerical implementation of differential methods is less involved compared with the integral methods.³¹⁵ Generally, Differential methods can be divided into two types based on the way to represent the transition in permittivity. One type is to treat the permittivity transitions in the grating region explicitly like the exact eigenvalue (or classic model) method of Botten et al.³¹⁶ which is quite accurate but have limitation on the grating structure. The other type is to employ a

Fourier expansion of the permittivity and the most representative and widely applied model of this type is rigorous coupled-wave analysis (RCWA).³¹⁷

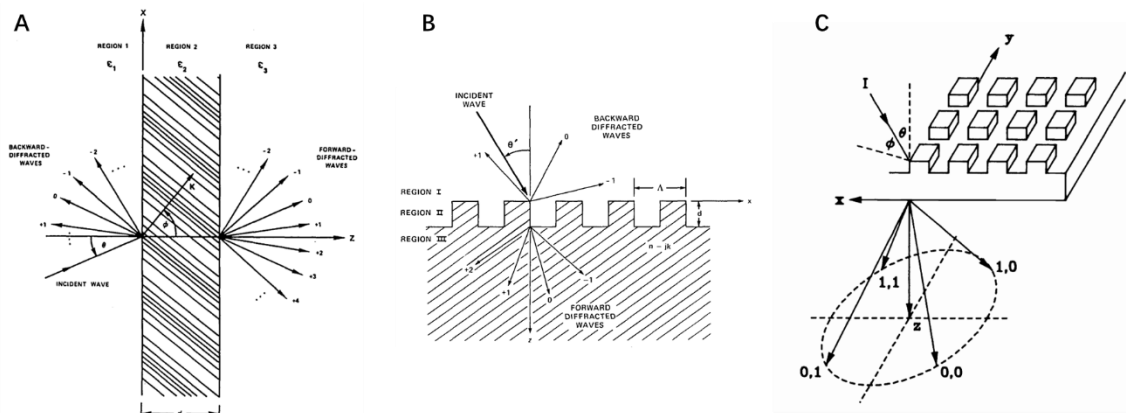


Figure 2.41 Geometry of different analysed grating structure. A) the planar-grating diffraction, B) the metallic rectangular-groove surface-relief grating diffraction, C) the two-dimensional grating diffraction.

The rigorous coupled-wave analysis (RCWA), as a semi-analytical method to solve scattering from periodic dielectric structures first introduced by Moharam and Gaylord for planar grating,^{313,318} and further extended to surface-relief grating,^{312,319} and crossed-grating structure,³²⁰ (Figure 2.41) has currently been widely applied in order to the analysis and the design of diffractive structures.³²¹ When implementing the RWCA technique, the permittivity of the grating region need to be expanded into a series of Fourier harmonics, followed by the electromagnetic field expressed as Fourier expansion with a corresponding order of harmonics.³²² In this way, it is possible to treat different gratings (planar or surface relief, lossy or lossless, single-groove or multi-groove) in a unified way. However, a common shortcoming of the RWCA technique is that, when a conducting grating is shot with a transverse magnetic (TM) polarized wave, it is difficult to get the convergence of the accurate solution since a large amount of spatial harmonics (orders) are required during the analysis and computation.³¹⁵

The same problem of the requirement of retaining a large number of orders also exists in the analysis of crossed-grating structure, which is a grating that periodical in two noncollinear directions with synonyms such as bi-gratings and the two-dimensional (2D)

grating.³²³ The crossed grating structure plays an important role in many applications such as laser beam fan-out elements, solar energy absorbers, antireflection surfaces, artificial graded-index materials, artificial anisotropic materials.³²³ Generally, complicated programs and comprehensive electromagnetic theory is required for analyzing the above elements. However, the crossed grating meshes of special harmonics leads to so many orders that even few orders are retained in each direction, the methods still tend to be memory hungry and time-consuming.³¹⁵ Thus, it is of great importance to reduce memory consumption and to increase the speed of convergence. Li managed to achieve a faster convergence rate of RCWA under TM polarization by implementing the inverse rule in the case of complementary jump discontinuities.³²⁴ Based on this, Lalanne increased the convergence rate of the 2D gratings via introducing coefficient involving structural parameters.³²⁵ After all the improvements and contributions from researches, the rigorous coupled-wave analysis has become a well-establish method for electromagnetic wave analysis.³²⁶

2.6.3. Applications of Microarray Structure

Here, microarray structures are generally classified as microchamber arrays and micropillar array structures based on whether there is empty space inside each micropillar. Microchamber arrays with hollow chamber structure can provide isolated space and prevent contaminations, thus tend to be intensively applied in biochemistry and biomedical related areas. For example, a silicon-based PCR microchamber array system with a small heat capacity was fabricated for the rapid polymerase chain reaction (PCR). The combined method of the constant temperature control avoiding large heating/cooling block can significantly increase the rate of thermal cycling, thus overcome the primary limitation of the rapid PCR technique.³²⁷ Besides, with the help of microchamber arrays structure, a picolitre scale PCR can be achieved.³²⁸

Moreover, it is reported that microfluidic cell culture chips can be fabricated via a simple micropatterning process to create a closed microchamber array with an extracellular matrix in order to rapidly and reproducibly finish small-volume sample assays avoiding labour-intensive procedures or expensive robotics.³²⁹ In addition, a flexible agarose-microchamber array was developed for on-chip cultivation of neural cells via the photothermal etching method, which showed the possibility for single-cell cultivation and measurement of nerve cells (Figure 2.43).³³⁰ Moreover, a cell culture chip with a structure of microchamber arrays, though in a relatively large scale produced by multilayer photolithography and replica moulding, enables pressure-driven perfusion cell culture and parallel cytotoxicity assay.³³¹

In addition, the combination of layer-by-layer (LBL) self-assembly techniques with the microwell array structures enables the fabrication of microchamber arrays films for the drug encapsulation and controlled release, especially for the site-specific release of chemical compounds in small and precisely defined quantities.²² For instance, Kiryukhin and co-workers successfully fabricated microchamber array films made of polyelectrolyte multilayers of (PSS-PAH)₄₀ with melamine formaldehyde colloidal particles encapsulated in

each microchambers, whose walls were incorporated with gold nanoparticles. By introducing focused laser radiations, a selected individual microchamber can be opened, result in the site-specific controlled release of encapsulated melamine formaldehyde colloidal particles, as shown in Figure 2.42. The release trigger of gold nanoparticles between the multilayered film can be further replaced with graphene oxide thin layers, which can cause microchamber opening with the radiation of near-infrared laser beam.³³² However, one of the limitations of microchamber array films made of polyelectrolyte multilayers is the difficulties of encapsulating small and hydrophilic molecules due to the semi-permeability of the chamber walls. This was overcome by Sukhorukov and co-workers who managed to encapsulate sodium chloride salt crystals, bioactive antibiotic doxycycline and fluorescent small molecular dye rhodamine B into microchamber array films by coating a thin layer of hydrophobic polylactic acid film on the top of polyelectrolyte multilayer microchamber array films. Moreover, the encapsulated cargos can be trigger released with low-frequency ultrasound exposure.³³³

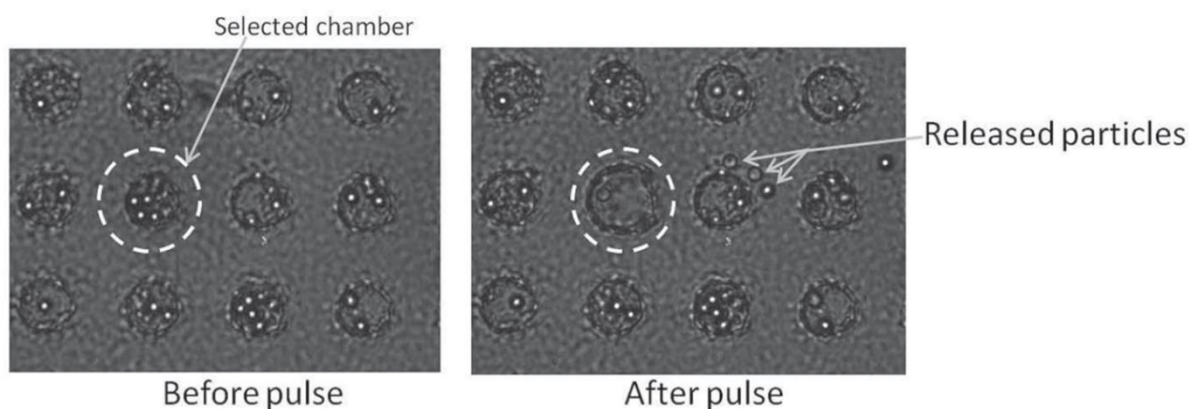


Figure 2.42 Optical microscope images showing the triggered release of MF particles into water. ²⁶

While the micropillar arrays, whose surface morphology and special structures are often focused, have been widely studied in the field ranging from lab-on-chip,³³⁴ sensing, electronics,³³⁵ optics,³³⁶ and microbiology. For instance, a silicon wafer with subwavelength sized micropillar arrays on the surface was fabricated by holographically recording a crossed-grating in a photoresist mask followed by reactive-ion etching to transfer the

primary mask onto the silicon substrate, which could display antireflection properties among visible light wavelength.³³⁷

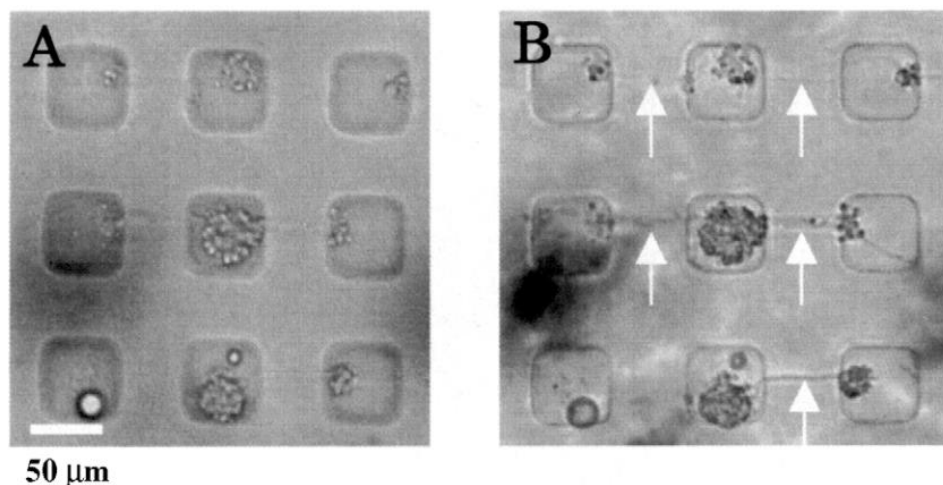


Figure 2.43 SEM images of the microchamber array for culturing nerve cells. (A)Phase-contrast micrograph images of cultured nerve cells in microchamber array at the beginning, (B) and after 48 hours.³³⁰

Micropillar arrays also own the possibility to perform molecular immunodiagnosis as the microarray structure can mimic highly diluted gel and maintain electrolyte within the micropillar zone with capillary effect (Figure 2.44).³³⁸ Besides, a lidless micropillar array electrospray ionization chip was prepared with deep reactive ion etching which results in accurate dimensional control. By combining the micropillar array chip with mass spectrometry, a novel method for direct analysis of biomolecules was achieved.³³⁹

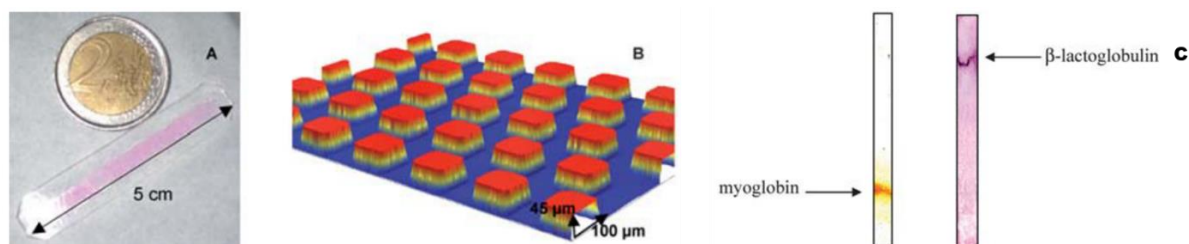


Figure 2.44 Micropillar arrays for molecular immunodiagnosis. (A) Picture of micropillar array filled by a coloured solution. (B) Profilometer picture of micropillar array. (C) Isoelectric focusing of a mixture of b-lactoglobulin and myoglobin on PDMS micropillar array coated by PDMA-AGE (left) immunoblotting with 10 ml of serum of allergic patient sensitized to b-lactoglobulin (right).³³⁸

Due to the inverse relationship between electrode impedance and surface area, electrodes with micropillar array structures are able to improve their electrochemical

performance as a high effective surface area can be achieved without modifying the geometrical parameters of electrodes.³⁴⁰ For instance, a polydimethylsiloxane (PDMS) elastomer substrate were first surface-patterned with micropillars fabricated by micro-working robot-made mould inserts and a replica moulding technique, followed with metal thin film coatings. The electrical impedance test results indicated that the micropillar structure caused statistically significant reductions in electrode contact impedance modulus and phase for each coating candidate.³⁴¹

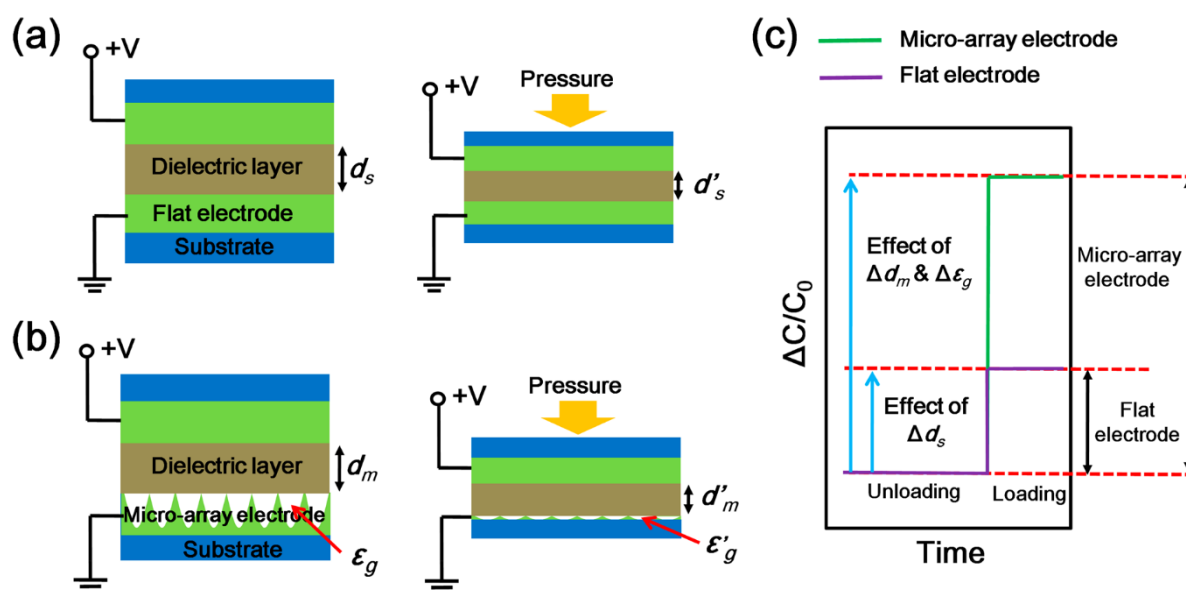


Figure 2.45 Sensing mechanisms of the sensors based on a flat electrode and microarray electrode. (a and b) Graphical explanation of capacitive pressure sensor based on a flat electrode and microarray electrode, and their corresponding geometrical change during the process of loading pressure, respectively. (c) Relative capacitance variations of pressure sensors based on a flat electrode and microarray electrode induced by identical levels of external pressure.³⁴²

Moreover, based on the micropillar structure and the silver nanowires coated elastomeric electrodes, a flexible pressure sensor can be achieved as illustrated in Figure 2.45. Such sensor owns the advantages of high sensitivity, low detection limitation, fast response, excellent flexibility and long-term cycle stability, enabling it the promising potentials as electronic skins and wearable healthcare monitors and even detecting noncontact pressure like voice vibration and air flows.³⁴² Besides, a micropillar array, fabricated with photolithography and electroplating techniques, was designed to facilitate the formation of stable and uniform liquid crystal (LCs) thin film, aiming at sensing the liquid

and vapour phase analytes based on the variations in the intensity of the transmitted light through the LCs.³⁴³

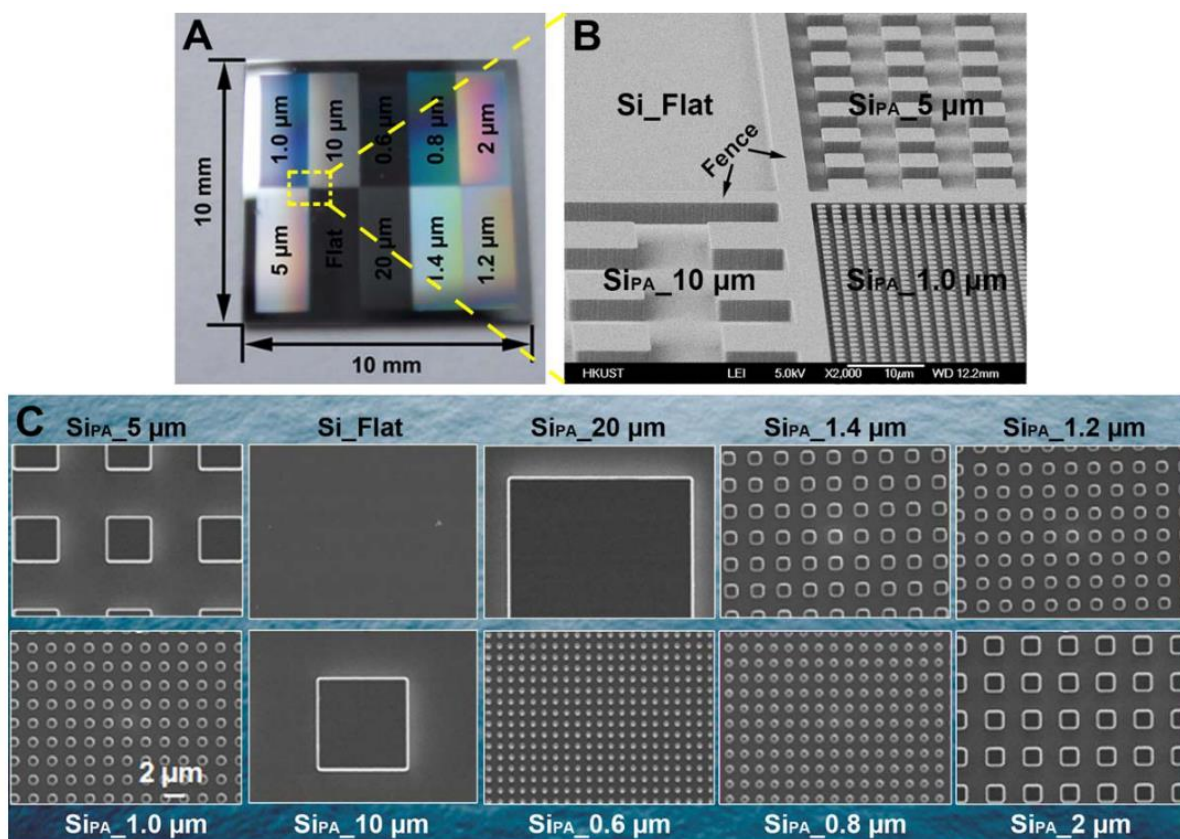


Figure 2.46 The specification of a silicon substrate for bacteria retention study. (A) A single sample of a silicon chip consists of 10 areas including one flat area and nine patterned areas; (B) every two areas are separated by a fence whose width is 4 mm and height is the same as that of the pillar (3 mm); (C) SEM images of silicon chip's top views.³⁴⁴

The special surface topography of micropillar arrays can also exhibit significant effects on bacterial responses. Ge et al. fabricated a silicon substrate with nine different feature size of micropillar arrays by photolithography and dry etching methods as shown in Figure 2.46, which is used to study bacterial retention, growth, proliferation as well as viability. The results showed that when the micropillar dimension is decreased to sub-micrometre size, the bacterial retention, growth, and proliferation would significant reduced, while the micropillar arrays structure has no obvious effect on the bacteria viability within 24 h.³⁴⁴ Similar research can also be found in microbial cell related work that the dimensions of microarray surface features may enhance or impede cell retention.²⁹⁵

In this literature review chapter, the background information of the main materials adopted in this work are introduced, including the properties and application of polyelectrolytes in complexed and multilayered forms, biodegradable polyesters polycaprolactone and polylactide acid. In addition, as the basic concept runs through all the works, the microarray structure of either micropillar or microwell geometries are introduced mainly about the production techniques, simulation methods as well as applications. The provided background information can undoubtedly facilitate the understanding of the aims, principles and importance of the whole work.

3. Materials and Methods

3.1. Materials

Poly (sodium 4-styrenesulfonate) (PSS, Sigma 243051, molecular weight ~70 kDa), Poly (allylamine hydrochloride) (PAH, Sigma 283223, molecular weight ~56 kDa) Poly (acrylic acid) (PAA, Sigma 181285, molecular weight ~450 kDa), poly-dimethyl diammonium chloride (PDDA, Sigma 409022, molecular weight 200 – 350 kDa), poly(ethylenimine) (PEI, Sigma MW ~ 750 kDa), polycaprolactone (PCL, Sigma 704105, molecular weight ~45 kDa). Polylactic acid biopolymer (PLA, GoodFellow 346310, 3mm nominal granule size, weight 100g), Lipase from *Pseudomonas cepacia* (Lipase PS, Sigma 62309, powder, ≥30U/mg). Poly (allylamine hydrochloride) (PAH, Sigma 283223, average M_w 50,000), Poly (acrylic acid) (PAA, Sigma 523925, average M_w ~100,000, 35 wt. % in H_2O), Polycaprolactone (PCL, Sigma 704105, average M_n 45,000), Calcium chloride ($CaCl_2$, Sigma C5670), Potassium chloride (KCl, Sigma P5405), Magnesium chloride ($MgCl_2$, Sigma M8266), Iron (II) chloride tetrahydrate ($FeCl_2 \cdot 4H_2O$, Sigma 220299), Sodium chloride (NaCl, Sigma S7653), Rhodamine B isothiocyanate (RITC, Sigma 283924), Nile red (Sigma 72485), 5(6)-carboxyfluorescein (5(6)-CF, Sigma 21877), Dexamethasone (DEX, Sigma PHR1526). All the chemicals above were used as received without further purification.

Poly (dimethylsiloxane) (PDMS) kit (Sylgard 184) was purchased from Dow-Corning, Midland, USA. In addition, PDMS (Elastosil, RT 602) from Wacker AG, München, Germany was used. Moreover, the temperature of enzymatic degradation was maintained at 37°C in a climate chamber (Memmert, HPP 110). Chloroform was purchased from VWR, Darmstadt, Germany. The ionic strength and pH of incubation solutions were maintained by phosphate-buffered saline (PBS tablets Sigma P4417). And the pH of polyelectrolyte solutions was adjusted by NaOH and HCl solutions. Deionised (DI) water from a Milli-Q (Millipore) water purification system, with an 18.2 M Ω -cm resistance, was used to prepare all the solutions.

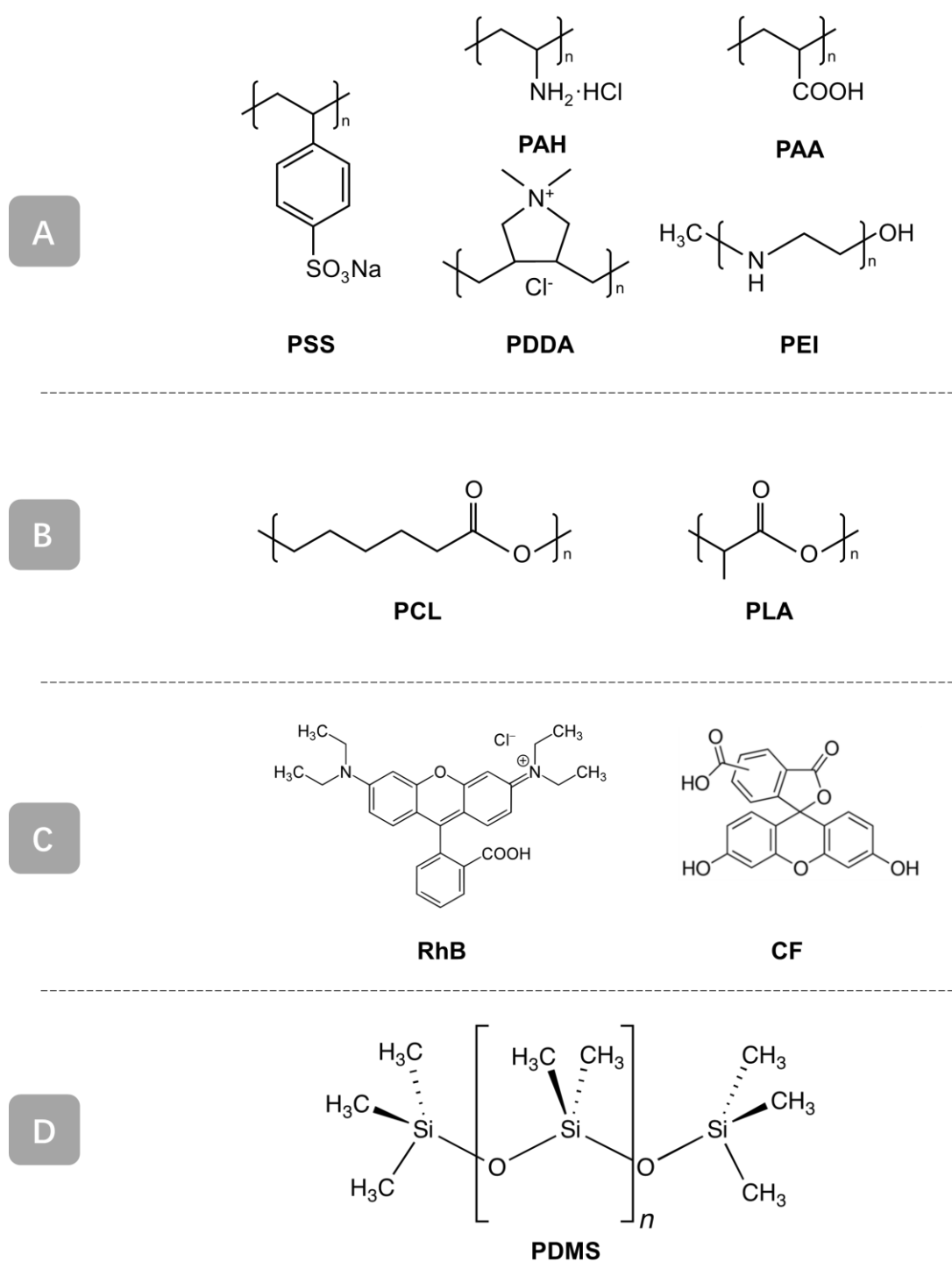


Figure 3.1 Structural formulas of materials used in the experiment. A) Polyelectrolytes for preparing polyelectrolyte complexes, B) Biodegradable polyesters for preparing microchamber arrays, C) Dye molecules as model drugs and labels, D) Poly(dimethyl siloxane)(PDMS) used for preparing patterned stamp with the reversed structure of patterned silicon master.

The template/mould with the microarray structure used to fabricate the PDMS stamp has various surface features and dimensions. The silicon masters with cylindrical micropillar arrays structures of different size (Figure 3.2 A) - C) were produced via standard

photolithography at Shenzhen semiconductor (Shenzhen, China), while the PMMA (poly methyl methacrylate) master of cubic microwell array structure is generously provided by Dr Kiryukhin (ASTAR, Singapore). Besides, copper master with rectangular structures (produced by V.E. Zuev Institute of Atmospheric Optics in Russia) was fabricated by photolithography and electroplating of nickel combination technique. Another type of silicon master with pyramid array structures was produced by Thales.

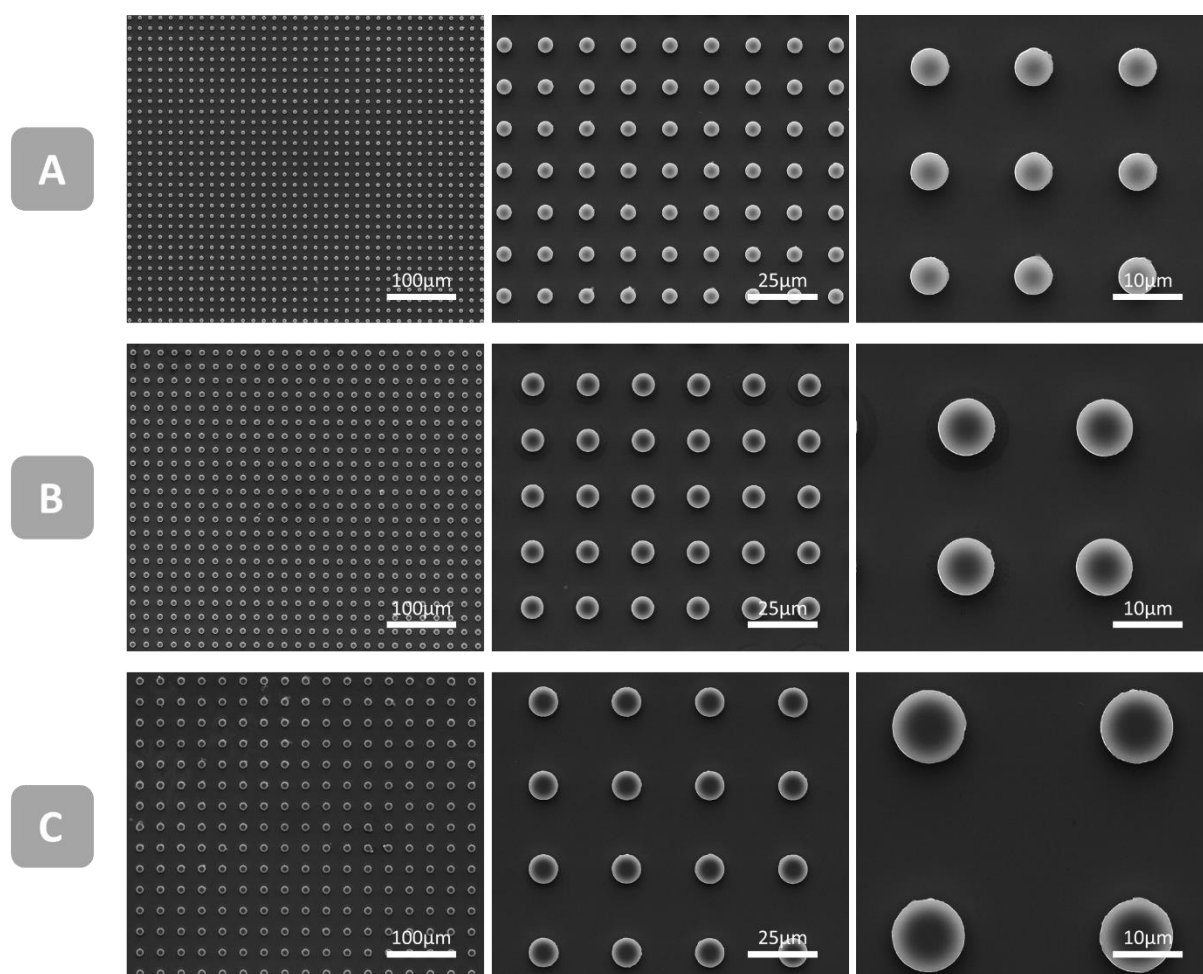


Figure 3.2 SEM images of silicon master of different specifications. A) Cylinder micropillar arrays with a diameter of 5 μm , height of 4 μm and period of 15 μm , B) Cylinder micropillar arrays with a diameter of 8 μm , the height of 4 μm and period of 20 μm , C) Cylinder micropillar arrays with a diameter of 10 μm , height 4 μm and period 30 μm .

3.2. Methods

3.2.1. Fabrication of Patterned PDMS Stamp

In order to get the reversed structure from the patterned template as well as transfer the microstructure into polyelectrolyte complexes or other polymer films with a high quality,

a patterned substrate made of low surface energy materials is of great importance to enable the smooth detachment of the resulted film or stamp after the printing procedures.³⁴⁵ Therefore, PDMS polymer of surface energy as low as $180 \mu\text{N}$ ³⁴⁶ is used to get the reverse structure of microarray template and print PEC and other polymer films.

Generally, to produce the PDMS patterned stamp, the PDMS mixture was firstly produced by mixing PDMS prepolymer and curing agent with the ratio of 10:1 followed by vacuuming for 30 minutes to remove the air between micropillars. Then, the patterned PDMS stamps with reversed microstructure were fabricated by casting PDMS mixture onto template substrates (e.g. silicon, copper, PMMA) with microarrays. The mixture, as well as the patterned template, were incubated and cured at 70°C in the incubator for 3 hours. Finally, the patterned PDMS stamps were finished by being lifted from the template and cut into the desired shape and size with a sharp surgery knife³⁴⁷ (i.e., the size of the PDMS stamps in the experiment is 1 cm^2 and 4 cm^2 of square shape). The flow chart of the process is shown in Figure 3.3 A) and B) which set silicon micropillar array master and PMMA microwell array master as the example, respectively. The process is the same when printing from the micropillar structured silicon master and from PMMA film with microwell arrays.

However, the above method can only fabricate the PDMS stamp with the reversed structure of the applied template. When the preparation of a PDMS stamp with identical surface features of the template is necessary, another printing and transferring procedure are required. Specifically, the targeted PDMS stamp can be fabricated by getting the reverse structure of the PDMS stamp with the reversed structure of the template. To achieve that, the generally PDMS stamp fabrication process is the same but one extra step is required that before casting PDMS prepolymer and curing agent mixtures onto PDMS template, a layer of gold is coated onto the PDMS template to avoid the adhesion between PDMS interfaces as schematically demonstrated in Figure 3.3 C).

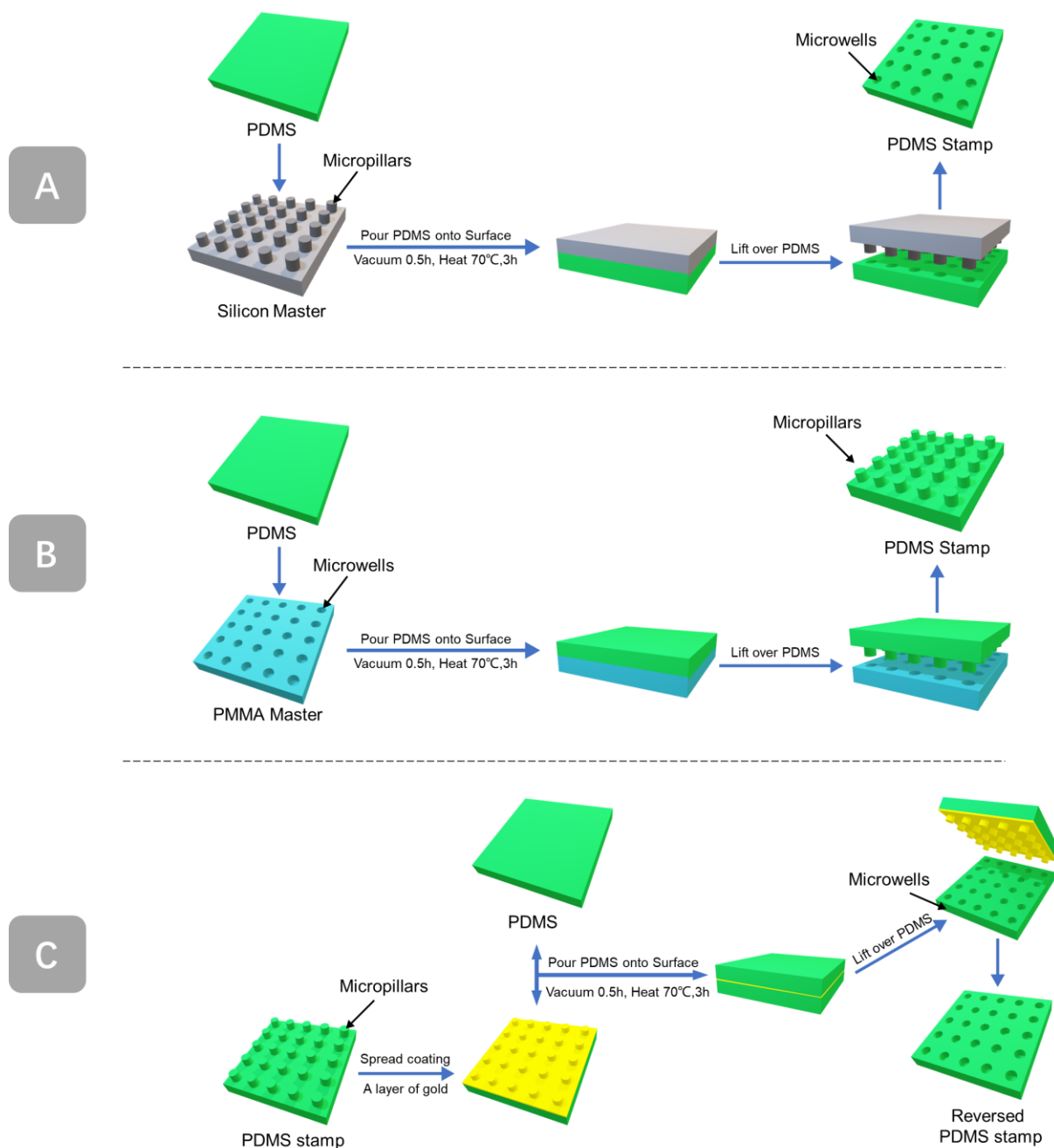


Figure 3.3 Schematic illustration of the preparation of patterned PDMS stamp from various templates. A) Preparing PDMS stamp from silicon master with micropillar arrays. B) Preparing PDMS stamp from PMMA film with microwell arrays. C) Preparing reversed PDMS stamp from PDMS stamp with micropillar arrays that obtained from B).

3.2.2. Preparation of Fluorescently Labelled PAH

PAH is labelled with the fluorescent dye rhodamine B isothiocyanate (RITC) for tracing purpose following the steps in reference.³⁴⁸ First, PAH of 100 mg was dissolved in 25 ml water forming 4 mg/ml solution followed with pH-adjusting to pH 8.5 with (1mol/L) NaOH solution, where the pH is confirmed with a pH meter. Then, 5 ml RITC methanol solution of

1 mg/ml concentration was added and mixed with the PAH solutions which were stirred in an ice bath for at least half an hour at the speed of 1000 rpm. In order to remove the unbonded dye molecules, the dialysis process is necessary that a dialysis bag (Carl Roth GmbH & Co. KG, Germany) with a cut-off weight of 8 - 14 kDa is selected. After removing the protection oil by incubating the dialysis bag at boiled deionized water for 15 minutes, the PAH and RITC solution mixtures were filled into the treated bag (less than 2/3 of the volume) and dialysed against deionized water (resistivity 18.2 MΩ·cm) for 3 days. During the dialysis process, the setup was always kept in the dark environment and deionized water was replaced twice a day. Finally, the resulted PAH-RITC solutions were kept in a well-sealed tube and stored in a 4°C fridge for further experiment.

3.2.3. Polyelectrolyte Multilayers Preparation by Dip-coating Robot



Figure 3.4 Images of homemade Layer-by-layer dip-coating machine. a) the general view of the dipping robot. b) the rotating plate and dipping pole while running. c) the polyelectrolyte solution and the DI water beaker positions on the dipping robot rotating plate.

For the preparation of polyelectrolyte multilayer films, a homemade dip-coating robot as shown in Figure 3.4 a), is applied for automatic assembling of polyelectrolyte multilayers on different growing substrates, including glass slides and PDMS stamp with microwell arrays surface structure. The dip-coating robot includes a dipping pole as well as a rotating plate, where the dipping and rotating are programmed and controlled by the software. The program enables the plate rotate clockwise as well as the pole dip vertically to the top position of the plate for predesigned time (Figure 3.4 b)).

Before the application of dipping robot, the substrate was sonicated for 5 minutes to remove the contamination as well as the trapped air bubble inside PDMS stamp microwells. Then, the substrates were incubated in 2 mg/ml branched PEI solutions for 15 minutes so as to form a positively charged anchoring layer of high charge density, thus assisting and facilitating the absorption of the following polyelectrolytes on the hydrophobic surfaces. Beakers with the oppositely charged polyelectrolyte solutions as well as the DI water were put onto the rotating plate following the order showing in Figure 3.4 c). The applied polyelectrolyte solutions were all at the concentration of 2 mg/ml with ionic strength provided by NaCl solutions with the concentration varying from 0.5 to 2 M/L depending on the desired film thickness. It is noteworthy to address that the charge density of the polyelectrolyte chains can be varied by the ionic strength of the polymer solution. The polyelectrolytes should reach a minimum charge density threshold to form multilayers, otherwise, the absorbed polyelectrolyte monolayer cannot overcompensate and reverse the surface charges of the multilayer films. Finally, the growing substrates were attached to the dipping pole of the robot and ready for the robotic operations.

In the robotic dipping steps, the dipping pole was programmed to dip substrates into PE solutions for 15 minutes, followed by washing steps by rotating the plate and dipping the substrate into DI water for 30 seconds in order to remove the non-electrostatically absorbed PE molecules as well as avoid the salt crystals formed between multilayers ultimately. After three-time washes in three DI water beakers, the growing substrate was then dipped into oppositely charged PE solutions for 15 minutes and followed with three times washing steps. The polyelectrolyte bilayer was formed after the cycle of two alternating dips in oppositely charged PE solutions and two three-time washes in DI water. The program of the robot can automatically control the dipping and washing steps for designed numbers of bilayer or cycle and after repeating layer-by-layer multilayer assembly, the PEM was successfully formed on the desired growing surface.

3.2.4. Printing of Polyelectrolyte Multilayer Microchamber Arrays

All the polyelectrolytes multilayer films in the experiment are conducted by a homemade layer by layer dip-coating robot as shown in Figure 3.4. Besides, the polyelectrolyte solutions are all at a concentration of 2 mg/ml with an ionic strength of 1 M/L adjusted by NaCl. Generally, in order to produce polyelectrolyte multilayer microchamber arrays, a patterns PDMS stamp with surface structures of microwell arrays are used. Prior to dip-coating procedures, the PDMS need to be sonicated in water for 5 mins to remove the air bubbles trapped inside microwell arrays, and further incubated in PEI solutions generating first anchor layers with a high density of positive charges due to the hydrophobic surface of the PDMS stamp. After that, the PDMS is set up on the dip-coating machine for designed multilayer films absorption. The program of the dip-coating robot is set as arbitrary cycles with one cycle that stands for a bilayer absorption. Specifically, one cycle includes 600 seconds in positively / negatively charged PE solutions followed with 3 times 30 seconds washes in DI water, and then using the same time and procedures for oppositely charged PE solution. The DI water washes were aiming to remove the polyelectrolyte molecules that were not electrostatically absorbed as well as avoid the crystallization of salt inside the multilayer films upon final drying.

The process of printing polyelectrolyte multilayer films is schematically shown in Figure 3.5. When the dip-coating of designed PEM on the PDMS stamp was finished, the formed multilayer films would be transferred onto glass slides which were precoated with 19.5 bilayers of polyelectrolyte multilayers since the charges of polyelectrolyte in the outer layer on the glass slide has to be opposite to the ending layer of polyelectrolyte films on PDMS stamp. It is noteworthy to point out that the glass slide also initially coated with PEI anchor layers like the step coating on the PDMS stamp which is not included in 19.5 bilayers. After putting a drop of water on the precoated glass slide, the Patterned PDMS stamp with multilayer films were pressed and printed onto the glass slide for 10 hours. Finally, the PEM microchamber arrays were achieved after separating the stamp from the glass slide.

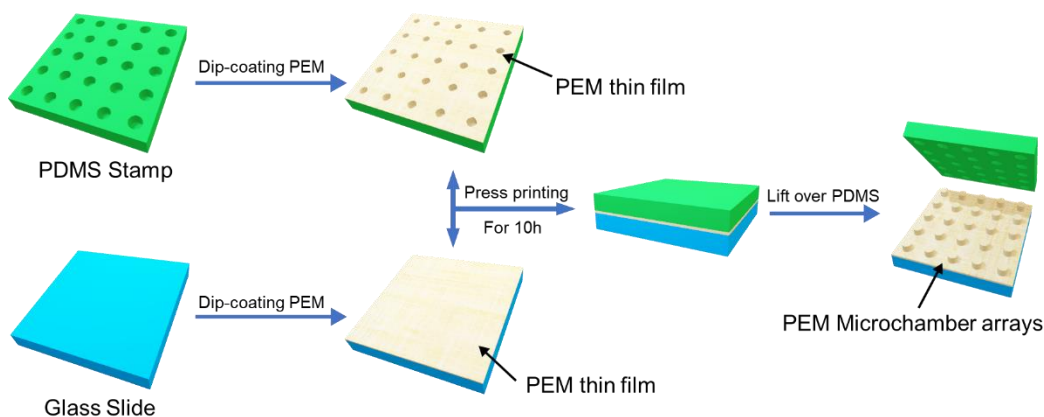


Figure 3.5 The process of preparing PEM microchamber arrays.

3.2.5. Preparation of Polyelectrolyte Complex Micropillar Array Films

Polyelectrolyte complexes (PEC) were simply fabricated by blending two oppositely charged polyelectrolyte solution with together into the beaker and mixed by a magnetic stirrer (Ika, C-MAG-HS10, Staufen, Germany) at the speed of 800 rpm for 10 minutes. The polyelectrolyte solutions were prepared at a concentration of 2 mg/ml and added with various concentration of NaCl to adjust the charge density (PAA/PAH PEC has 1M NaCl charge density). The PEC was harvested either by collecting with tweezers when the PEC was aggregated together or by waiting for it to precipitate and remove the supernatant water, then knead kneading the complexes from the beaker and magnet stirrer together. Before micro-structuring, the PEC was incubated into aqueous solutions to inhibit dehydration.

The preparation of PEC micropillar arrays, as schematically demonstrated in Figure 3.6, was first conducted by preheating a flat glass slide for 3 seconds on a heating plate at a temperature of 75°C. After that, the prepared PEC was spread onto the preheated glass slide and then pressed by a patterned PDMS stamp on the heating plate at 75°C for 5 minutes, while the time is variable depending on the amount of PEC employed. It is noteworthy to address that this sandwiched structure should be pressed vertically otherwise the micropillars might be tilted. After drying, the PEC micropillar arrays are successfully

fabricated on the glass slide by detaching it from the patterned PDMS stamp and cooling it down to room temperature.

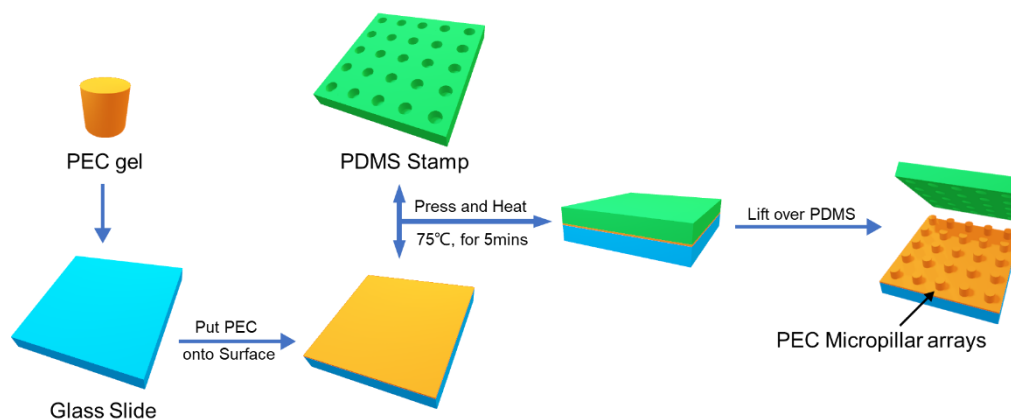


Figure 3.6 The process of preparing PEC micropillar arrays.

3.2.6. One-dip Method for Preparing PCL/PLA Microchamber Array Films

First, the PCL polymer solution was prepared by dissolving 0.5g PCL into 49.5 g chloroform, resulting in 1 % (weight percentage) solutions. While the PCL-PLA polymer solution was obtained by adding 0.3 g PCL and 0.6 g PLA into 74.1 g chloroform to get a 1:2 weight ratio of PCL and PLA. A glass slide, as well as a patterned PDMS stamp, was dipped into the polymer solution for 5 seconds. Following this, thorough drying of the polymer solution was conducted by leaving the components in ambient conditions for 5 minutes. If applicable, loading dyes or drugs into precoated individual microchambers occurred at this stage. Afterwards, the PDMS stamp was manually pressed onto a precoated glass slide, which was preheated so as to obtain an elevated degree of adhesion to facilitate the printing procedure. Finally, after thorough cooling of the glass slide, the microchambers were obtained simply by detaching the stamp from the glass slide carefully to guarantee the completion of the film.

Firstly, dip glass slide into the solution of hydrophobic polymers for five seconds which were dissolved in chloroform of designed concentration and wait for the polymer solution fully dried on to glass slide for about 3 to 5 minutes. Furthermore, a patterned PDMS stamp

was dipped in the solution and went on the same procedure. Finally, print microchambers simply by pressing patterned PDMS stamp onto a precoated glass slide for 30 seconds and detaching the stamp from the glass slide carefully to guarantee the completion of the film. The flow diagram Figure 3.7 shows the procedures.

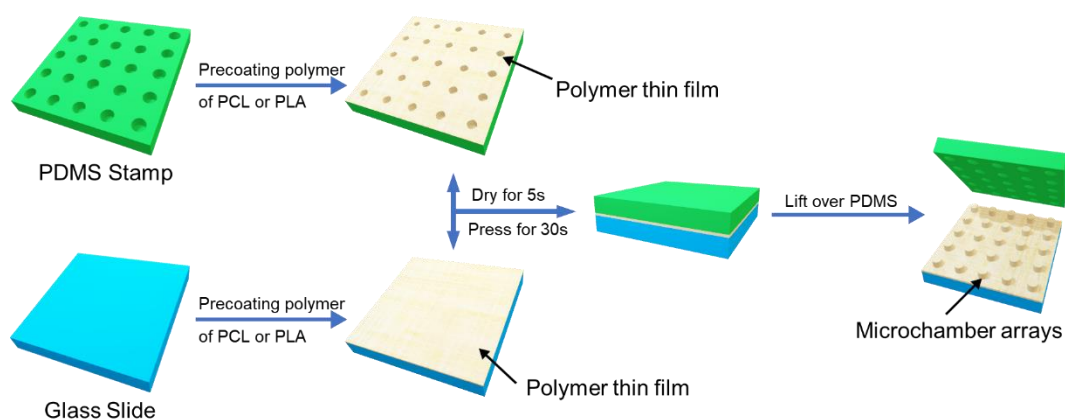


Figure 3.7 The process of preparing PCL or PLA microchambers.

3.2.7. Treatments for Microarray Films

3.2.7.1. Heat Treatment of Microchamber Arrays

Microchamber array films made of PCL were fabricated and incubated in an oven to maintain the heating temperature for thermal sensing. After designated times, the samples were rapidly taken out for diffraction pattern imaging. In addition, in order to acquire the optical micrographs of the melting state of PCL microchamber arrays, a water bath was used to maintain a constant temperature.

3.2.7.2. pH Treatment of PEC Micropillar Arrays

The pH treatment was conducted by full immersion of the PAA/PAH PEC micropillar arrays. Before the pH sensing experiment, the PEC films samples have to be triggered into the swollen state by submerging the new prepared film into pH 13 solutions for 10 mins. After the PEC films enter the swelling state, the prepared film will be detached from the glass slide and floating in triggered solutions. The pH sensing is applied by replacing the

submerging solutions of different pH values. The solution was, except stated otherwise 15 ml in a petri dish, whose pH value was adjusted by HCl and NaOH. Each incubation time in each pH solutions was maintained for at least 10 minutes to guarantee the swelling and shrinking procedures were balanced and stable (tested by observation in the bright-field microscope). Besides, when conducting the next pH value point measurement, the PEC micropillar arrays were washed twice with new pH solutions in order to eliminate the effects of the former pH solutions.

3.2.7.3. Ions Treatment of PEC Micropillar Arrays

PEC micropillar array samples were first exposed to pH 13 solutions to achieve a swollen state and detaching these films from the glass slide floating in the solutions, followed by washing the sample with DI water three times. After this conditioning treatment, the PEC micropillars were immersed in 15 ml calcium chloride solutions for responsiveness observation. The optical micrographs were measured after at least 1-hour incubation until the microstructure remains stable. Diffraction pattern images are captured at designed time points. Moreover, the samples exposed to calcium ions were recovered by adding pH 13 solutions to remove calcium ions, followed by rinsing with deionised water. After several washing steps, the PEC micropillar arrays are restored to the ions-untreated swelling state and were ready for another sensing step.

3.2.8. Generating Fraunhofer Laser Diffraction Patterns

The Fraunhofer diffraction patterns were acquired on homemade equipment which is shown in Figure 3.8. The samples were positioned at a constant height of 364mm above a plain surface in a parallel fashion, which was used to facilitate the comparison of patterns in each condition. Following this, a 532 nm wavelength green laser light was arranged vertically above the microchamber arrays, generating a Fraunhofer diffraction pattern beneath. The images were acquired from a constant height to maintain comparability.

Furthermore, the optical images were taken in a darkened room to optimise the clarity of the generated diffraction patterns.

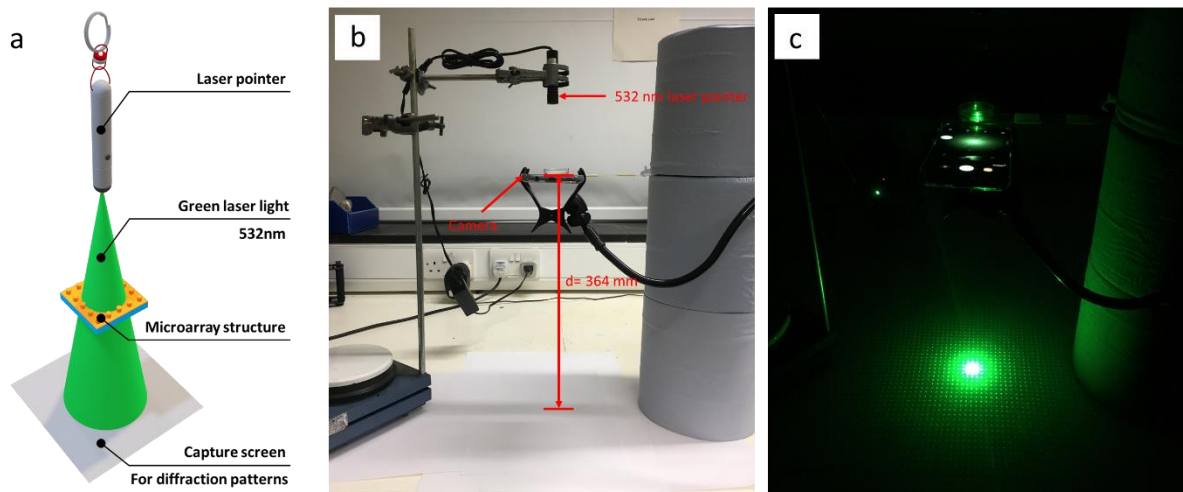


Figure 3.8 The Fraunhofer diffraction pattern imaging equipment. a) General cartoon illustration of the imaging equipment. b) The specification of imaging equipment. The distance between the sample and the flat surface is 364 mm. The wavelength of laser light is 532 nm. The phone camera is fixed at the same position during all the imaging process. c) Images of acquiring diffraction patterns at darkened conditions.

3.3. Instruments

3.3.1. Scanning Electron Microscopy (SEM)

Due to the limitation of conventional optical microscopy whose magnification is about 1000x, the microscope of higher resolution and magnification is highly demanded. Therefore, G.E. Palade, M.D. first published their research about electron microscopy in 1952.³⁴⁹ Scanning electron microscope is one of the electron microscopes that could image and analyse the topography, elements, electrical properties and crystal structures of different samples by using a focused electron beam to scan the surface of the specimens which could achieve high resolution better than 1 nanometre. The images of FEI Inspect F SEM are shown in Figure 3.9.



Figure 3.9 Images of FEI Inspect F scanning electron microscope. a) microscope general view, b) vacuum chamber with specimens fitted, c) sample holder with specimen close-up.

If the sample is an ultrathin section less than 100 nm thick or a suspension on a grid, the electrons can transmit through it without being fully absorbed and a transmission electron microscopy (TEM) would be captured. On the other hand, the electrons cannot get through the specimen if the sample is thick enough, therefore, SEM images can be taken based on the particles emitted from the sample surface, such as electrons, X-rays quanta, which are the information used in conventional SEM.³⁵⁰ The principle of a conventional scanning electron microscope is shown in the Figure 3.10.³⁵¹

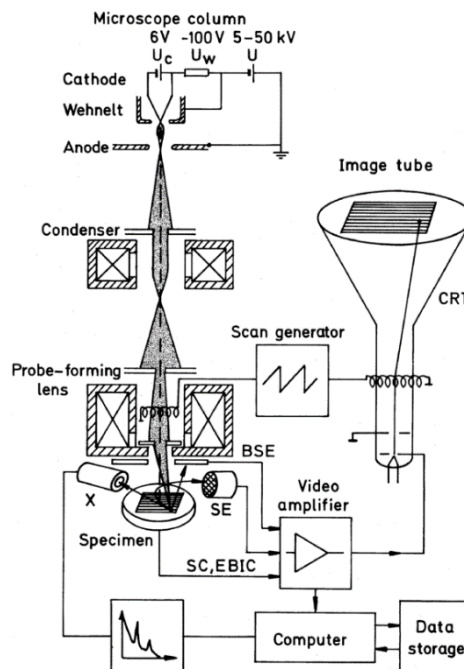


Figure 3.10 Principle of the scanning electron microscope. (BSE = back scattered electrons, SE = secondary electrons, SC = specimen current, EBIC = electron-beam-induced current, X = X-rays, CRT = cathode-ray tube)³⁵¹

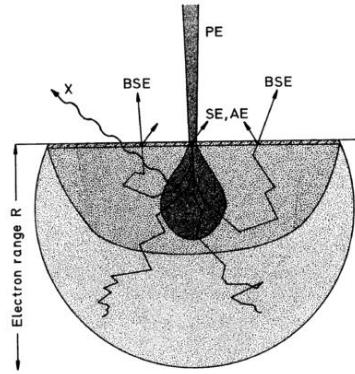


Figure 3.11 Origin and information depth of different electrons. (secondary electrons (SE), backscattered electrons (BSE), Auger electrons (AE) and x-ray quanta (X) in the diffusion cloud of electron range R for normal incidence of the primary electrons (PE)).³⁵¹

Typically, in an SEM, the incident electrons (primary electron) are usually accelerated through a voltage difference between cathode and anode ranging from 0.1 keV to 50 keV. Then, the electron beam was focused and minified by electromagnetic condenser lenses and probe-forming lenses into a small and narrow probe that would scan across the select area of the specimen surface. The electrons interact with the sample surface in a teardrop-shape volume from which all kinds of particles emerged (Figure 3.11).³⁵¹ The energy of the electron beam, the atomic masses of elements of the sample and the angle that the electron beam hits the specimen would have an impact on the volume of the specimen-beam interaction area. Higher the incident angle and the energy of the electron beam and lighter of the atomic mass, deeper of the specimen-beam interaction area.³⁵⁰

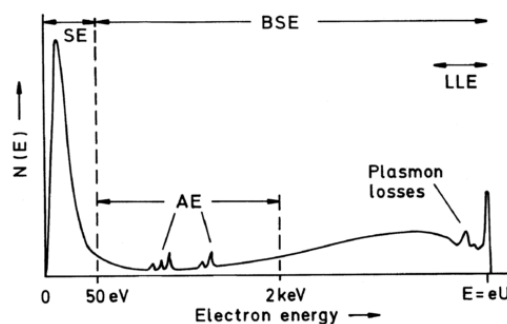


Figure 3.12 Schematic energy spectrum of electrons emitted consisting of secondary electrons (SE) with $E_{SE} < 50$ eV, low-loss electrons (LLE) with energy losses of a few hundreds of eV, backscattered electrons (BSE) with $E_{BSE} > 50$ eV and peaks of Auger electrons (AE)³⁵¹

Secondary electrons (SE) are those being hit out of the atomic orbits of the specimen by primary electrons (PE) whose energy is lower than 50 eV (see Figure 3.12). SE give the highest resolution of the image and provide mainly topography information since they leave the specimen from only the shallow surface layer of several nanometers thick. Besides, back scattered electrons (BSE) are those PE that gets close enough to the nuclear and emerge back to the surface because of the large angle scattering whose energy is higher than 50 eV. The number of BSE is smaller than SE, while the energy is higher. Most importantly, they can provide elemental information. In addition, Auger electrons (AE) are those PE that emitted from the orbits of surface atoms of specimens which could provide precious information about the surface chemistry. Due to the small number of Auger electrons, advanced and professional equipment is required to measure the precise energy of AE.

The electron may interact with atoms of the sample in different ways which are demonstrated in Figure 3.13³⁵⁰. The interaction between the electron beam and the specimen produces secondary electrons (SE), backscattered electrons (BSE), Auger electrons (AE), as well as X-rays probably lights, which are captured by a variety of detectors in the specimen chamber. The information from each detector would be sent to the video amplifier to amplify the signal. Afterwards, with the help of the scan generator, the picture is formed on the image tube which could be seen on the computer screen.

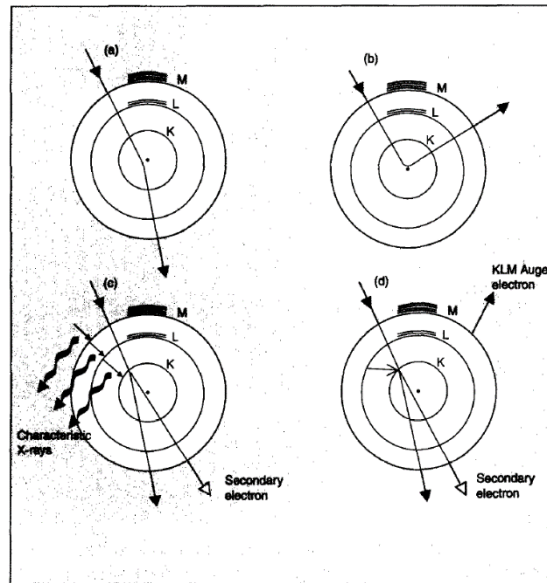


Figure 3.13 Some atom-high energy electron interactions. The inner electron shells of atoms are labelled according to standard notation (the innermost states are K, L etc). The incident particle is arrowed. (a) Low-angle scattering - electrons scattered in this way pass to the next layer of atoms with very little loss of energy (b) Back (or high-angle) scattering; (c) Emission of a secondary electron and characteristic x-rays; (d) Emission of a secondary electron and an Auger electron.³⁵¹

X-ray is produced by atoms when the high energy PE knocks out the electrons of the inner orbit of atoms and the electrons of the outer orbit move into the empty position. All the electron jumps from higher energy state to lower energy state until the entire system remains at lowest energy state, and atoms would emit X-ray to conserve energy because of the electron jumps.

The chemical composition of the specimen can be investigated by analysing the energy or calculating the wavelength of the X-ray using either an energy dispersive or a wavelength dispersive spectrometer to detect the signals. Energy dispersive x-ray spectroscopy (EDS or EDX) is a very common attachment of SEM which could give a rapid qualitative analysis of the sample. While an “Electron Microprobe” is an SEM fitted with wavelength dispersive x-ray spectrometers as well as analysis software and is dedicated to quantitative chemical analysis.³⁵²

If the sample is an ultrathin section less than 100 nm thick or a suspension on a grid, the electrons can transmit through it without being fully absorbed and a transmission

electron microscopy (TEM) would be captured. On the other hand, the electrons cannot get through the specimen if the sample is thick enough, therefore, SEM images can be taken based on the particles emitted from the sample surface, such as electrons, X-rays quanta, which are the information used in conventional SEM.³⁵⁰

The requirement of high vacuum in SEM has the weak point that only dried or dehydrate specimens could be scanned. Then, S. Vol *et al*³⁵³ found a new way to investigate wet specimens in nearly natural conditions by increasing the local pressure of water vapour a few millimetres above the sample named ESEM (environment scanning electron microscopy).

In this work, the scanning electron microscope (SEM, FEI inspect-F, Hillsboro, USA) is employed for all the sample morphology observations, including the microchamber array films, microcages, inorganic microarray film, loading of cargos and so forth. All the samples are coated with a thin layer of gold using a sputter coating system (SC 7620, Quorum, Laughton, UK) for 45 seconds at 20 mA. The SEM evaluations were performed at 5 kV with a spot size of 3.0.

3.3.2. Focused Ion Beam Scanning Electron Microscopy (FIB-SEM)

The focused ion beam technique is first developed by Levi-setti³⁵⁴ from the University of Chicago based on field emission technology and also by Orloff and Swanson³⁵⁵ using a gas field ionization source in 1975. Later in 1978, Seliger *et al.*³⁵⁶ from Hughes Research Laboratories proposed the first liquid metal ion sources (LMIS) -based FIB system. The first application of the FIB technique was in the semiconductor fields that a microstructure was milled from integrated circuits (IC) exerting a high current density focused ion beam from a liquid metal ions source of gallium.³⁵⁷ The FIB technique has been commercialized for decades mainly in the semiconductor industries including quality control, wafer repair, and microelectronic failure analysis.³⁵⁸

The focused ion beam system performs similarly to the scanning electron microscopy, but the electron beams are replaced by the ion beams. A FIB device is basically operated by using accelerated heavy ions to hit the target material where the atoms would be sputtered. Several requirements of the ion source need to be satisfied so that the efficiency of the sputtering process can be guaranteed. One is the momentum transfer at a given acceleration voltage should be maximized by using heavy ions. The other is the source of the material should have a low melting point and a low vapour pressure.³⁵⁸ Therefore, gallium (Ga) is selected as a perfect ion source that meets both requirements with the melting temperature at 29.8°C. In the FIB setups, a Ga liquid metal ion source is comprised out of a small Ga reservoir which is connected to a tungsten needle. The operation procedure starts with heating solid Ga above its melting point, thus liquid Ga would flow and wet to the tip of the needle due to the surface tension. After that, a strong electron field (10^8 V / cm) is applied to the tip of the needle leading to the formation of a point source of about 2 – 5 nm in diameter and extracts ions from the needle tips with energy up to 30 keV. With the continuous heating, liquid Ga would keep flowing to the needle tip and replace the extracted ions forming a constant ion current, indicating the formation of an automated sputtering process.³⁵⁸

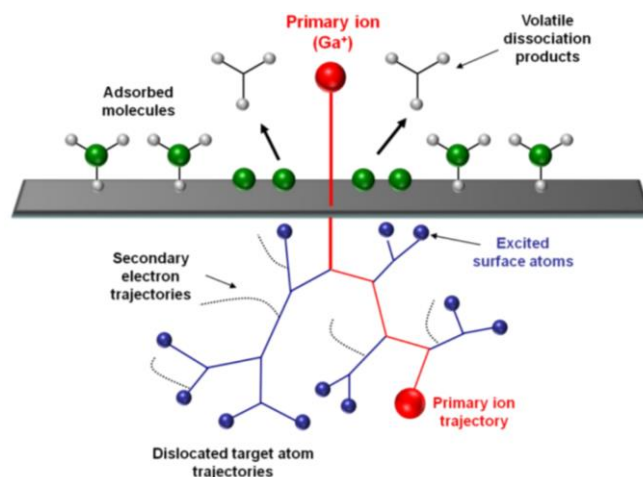


Figure 3.14 Primary ion beams generating secondary electrons and the collision cascade.³⁵⁹

In practice, the functions of FIB systems can vary with the ion currents. For example, when applying low ion beam current, little material would be sputtered on the target surface

leaving the surface with secondary ions, neutral atoms or even secondary electrons (Figure 3.14), collecting which can form images of the targeted area with the accuracy achieving 5 nm resolution.^{360,361} At a higher ion beam current, the materials of the targeted area would be significantly removed by sputtering, enabling the milling of the specimen with high resolution about sub micrometre or even a nano scale. Nowadays, the latest FIB system with high resolution can in-situ observe the FIB sectioned specimen without using a separate SEM instrument. However, the incident ion beam would damage the surface of the specimen, although can be reduced to a certain extent by covering metallic barrier layers (e.g. platinum) on the surface followed by cleaning and polishing the surface.³⁶² Thus, the SEM is still essential and necessary when imaging specimen with the highest resolution and preventing the damage of sensitive and fragile samples. The assembly of FIB and SEM columns into the same chamber is therefore needed to benefit the characterization.

The combination of an ion column with an electron column into one system results in an instrument that owns the capability of both FIB and SEM, allowing the same feature to be evaluated by either of the beams.³⁵⁸ In combination, the electron beam is used for scanning imaging without considering the sputter of the targeted surface and further facilitate the ion milling procedure by offering precise material surface information.³⁵⁸ Such system named as focused ion beam scanning electron microscopy, also referred to as dual-beam instrument, are versatile and multifunctional, widely employed not only in the single-beam FIB system-related applications such as TEM foil preparation, micromachining, metal deposition, and orientation contrast imaging, but also in 3D electron backscatter diffraction (3D EBSD), 3D cross sectioning, 3D imaging, and 3D EDX analysis as combined systems (Figure 3.16), and nowadays is also expanded to the fields of material science, life science, geology and so forth.

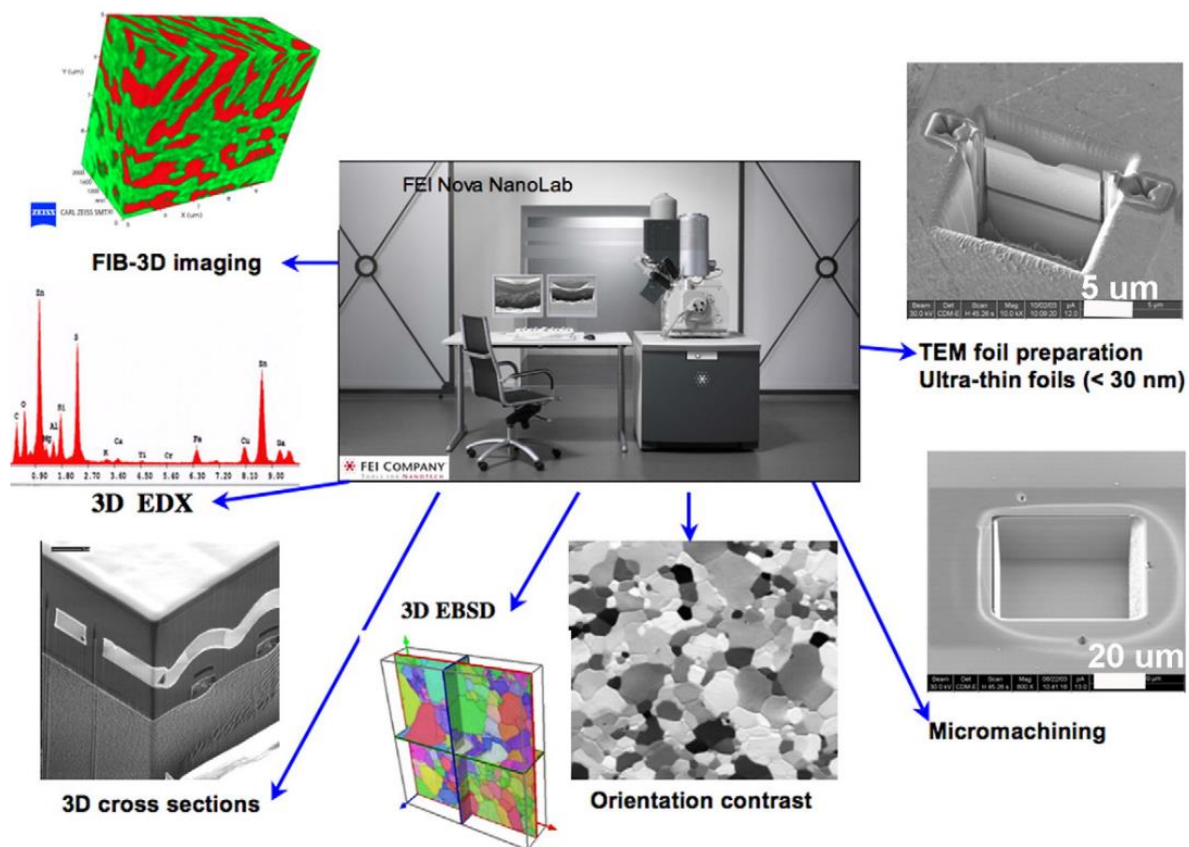


Figure 3.15 The image visualizes applications of a FIB-SEM combined system.³⁵⁸

In this work, the FIB-SEM (FEI Quanta 3D ESEM) is employed to cross-section the PCL and PCL-PLA microchamber arrays in order to confirm the empty structure as well as to measure the wall thickness of the microchambers. The working current was 5 nanoamperes with a working distance of around 10 mm. The specimen was sputtered coating with a layer of gold for 60 seconds in dry condition. A platinum protecting layer is applied when cutting the microchambers.

3.3.3. Fluorescence Spectrometer

A fluorescence spectrometer (also known as fluorimeter) is a kind of device that can measure the intensity and wavelength distribution of emission and excitation spectrum after the fluorophore molecules have been excited by a certain reference spectrum whose quantum yield is already known.³⁶³ Besides, when the type of measured compound is already known, the concentration of the fluorescent solution can be analysed quantitatively in a fast and inexpensive way as well.³⁶⁴ Therefore, the fluorescence spectrometer has

generally been equipped as a basic and primary research tool used by scientists from many disciplines, such as biochemistry³⁶⁵, medical diagnostics³⁶⁶, genetic analysis³⁶⁷ and so forth.

In order to know the principle of the fluorescence spectrometer, the theory of fluorescence needs to be explained. Generally, when the atoms or molecules of the analytes are excited to a higher state and absorb energy, very shortly the atoms will emit light which is the luminescence effect. Typically, luminescence is divided into two types, fluorescence and phosphorescence based on the nature of the excited state.³⁶⁸ The properties of the excited state and their relaxation process is demonstrated by a typical Jablonski diagram as presented in Figure 3.16.

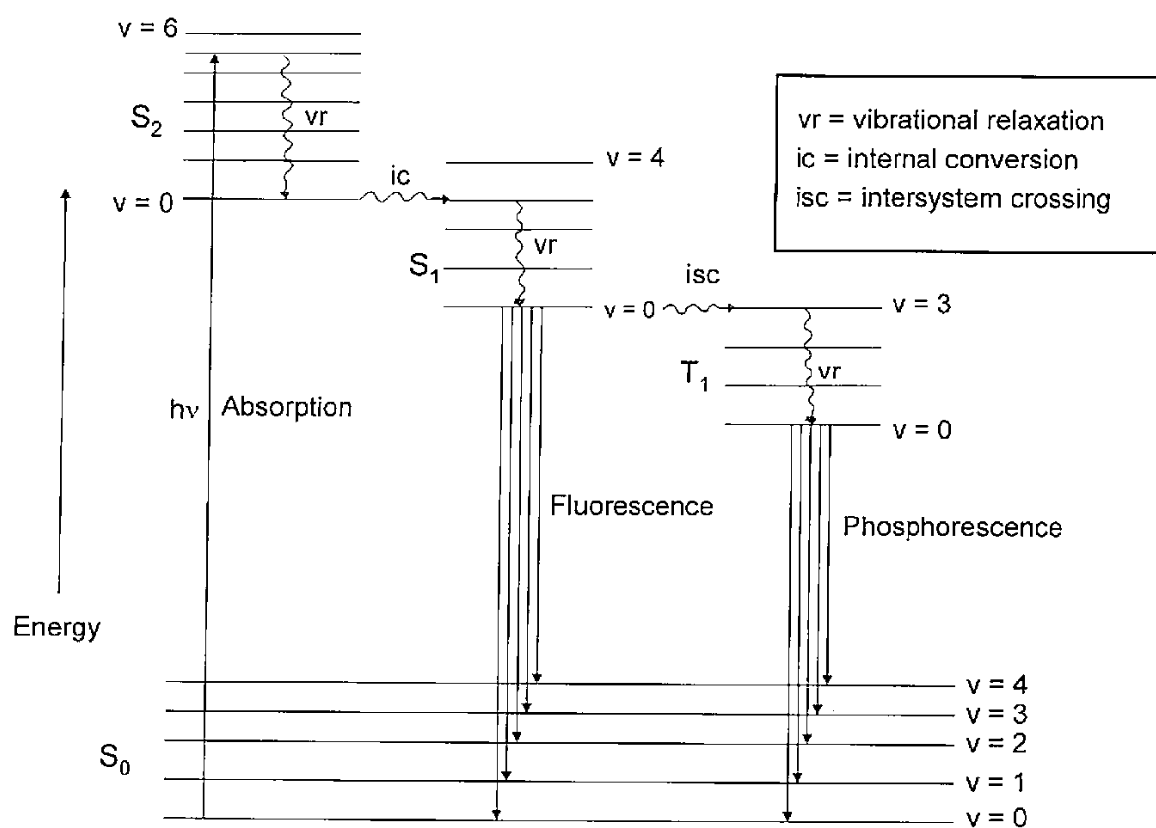


Figure 3.16 One form of Jablonski diagram for an organic molecule, illustrating excited state photophysical processes.³⁶³

Fluorescence is generated by the emission light from the excited singlet states where the electron in the excited orbital has the opposite spin orientation with the second one in-ground state orbital. As a result, it is allowed and frequently for the electrons of excited orbital to transit to ground state orbital by emitting a photon with the rate of about 10^8 s^{-1} .

Therefore, the lifetime of a typical fluorescence is around 10 ns. Here, the lifetime represents the average time between its excitation and return to the ground state. It is noteworthy to mention that the emitted photons with the speed of light can travel about 30 cm within the lifetime of fluorescence. The distance can be shorter with some other fluorophores. Besides, compared with absorbed radiation, the emitted light has a longer wavelength and lower energy in most situations.

Phosphorescence is the “glow in the dark” phenomenon that is commonly seen in daily lives. It is the emission of light when the substances are excited into a triplet state, where the electron in the excited orbital has the same spin orientation as the ground state electron. Therefore, the transition from the excited state to the ground state is forbidden, leading to slow emission rates (10^3 to 10^0 s⁻¹) and long lifetimes of about milliseconds to seconds. Here in the function of fluorescence spectrometer, only fluorescence rather than phosphorescence is considered.

Only a fraction number of chemicals have fluorescence and most of which have one or more aromatic rings in the molecular structure. These fluorescent chemicals are usually employed for labelling the non-fluorescent compounds for further analysis so that the application area of fluorescent chemicals can be expanded. Some of the commonly used fluorescent compounds are shown in Figure 3.17.

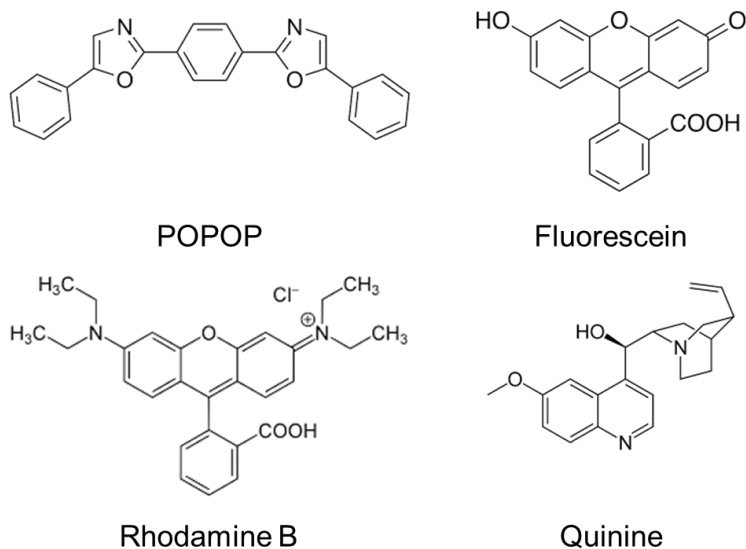


Figure 3.17 Chemical structure of typical fluorescent compounds.

The different fluorescent compound should be selected based on the practical experiment since the spectral properties of the selected fluorophores play the key roles in getting the available information of the experiment. As mentioned before, most of the fluorescence spectrometers are able to measure both excitation and emission spectra of a certain fluorescent substance. Figure 3.18 displays a schematic diagram of a fluorescence spectrometer.

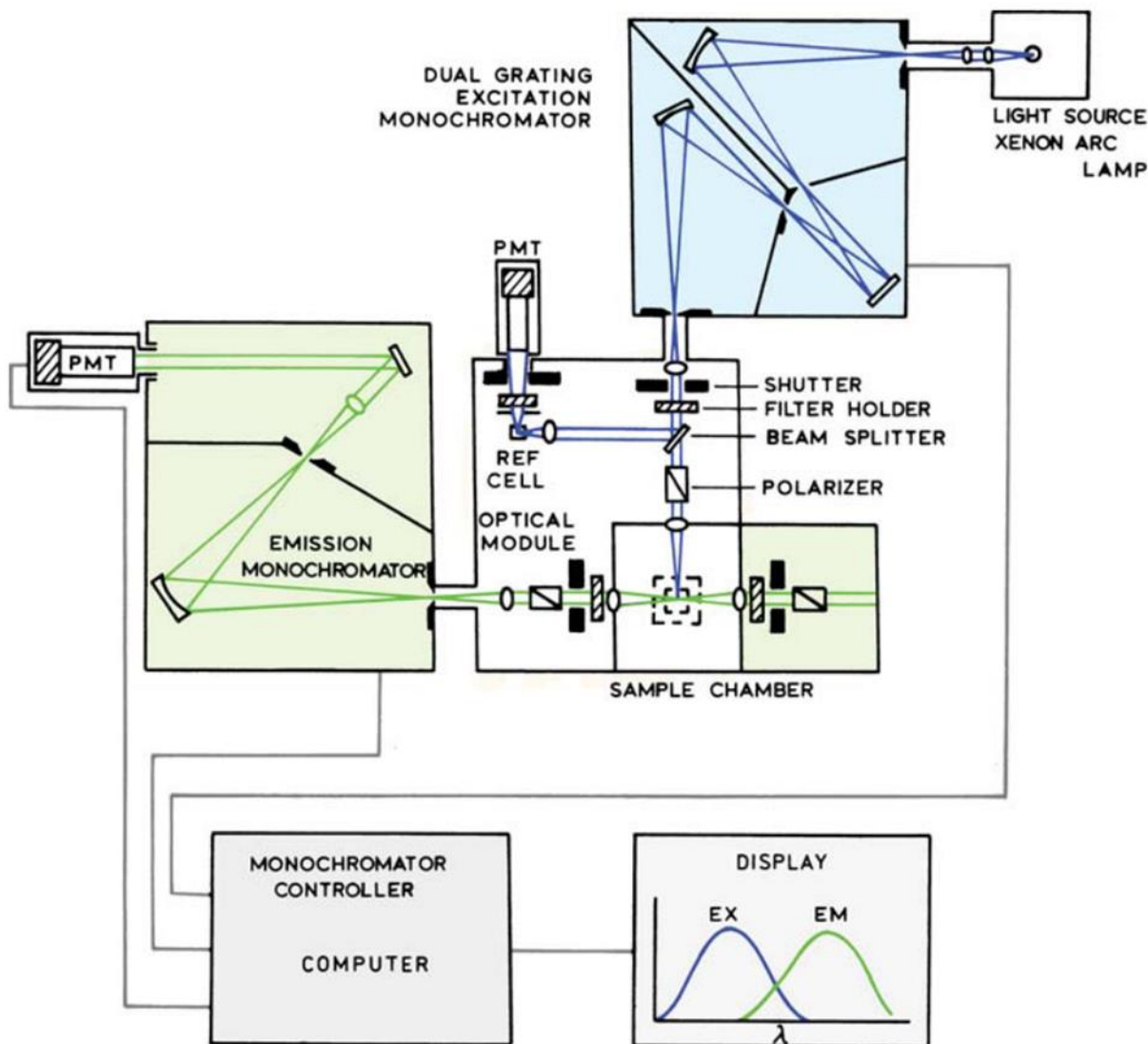


Figure 3.18 Schematic illustration of fluorescence spectrometer.³⁶⁸

In common fluorescence spectroscopy, a Xenon arc lamp is used as an exciting light source, which can generate light of all wavelengths ranging upward from 250 nm with high intensity. After that, the exciting light will pass through a dual grating excitation monochromator consisted of two gratings, which can decrease the light whose wavelength is different from the desired one. The monochromator is movable in order to automatically scan the wavelength of all available range. Then, the exciting light with the selected wavelength will pass through the sample solution in a cuvette and excites the electrons of sample molecules, which can shortly emit fluorescence light as explained before. The emitted fluorescence light, which occurs in all directions, is directed towards the detector

module and pass through the emission monochromator for decreasing the stray light. Finally, the emission light signals are detected by photomultiplier tubes (PMT), calculated by the computer and displayed in graphical forms.

Many advantages facilitate the wide application of fluorescence spectrometer. For example, if a chemical compound has fluorescence or is labelled with fluorescent probes, it is possible to quantitatively measure the amount of these compounds because the concentration of the fluorescent substances is directly proportional with the intensity of the emission light, which enables the versatile application of fluorescence.³⁶⁹ Besides, compared with steady-state measurement, more information can be acquired from the data captured with fluorescence spectrometer since the molecular changes in the quantum field can be analysed too.³⁶⁸ Moreover, a fluorescence spectrometer can work accurately when the concentrations of emitting fluorescence probes are quite low thanks to its spectral selectivity.³⁷⁰

However, it is difficult for a fluorescence spectrometer to perfectly measure the spectral properties of the fluorescence substance since many interferences and instrumental limitations can inhibit accurate detection. For instance, the weak fluorescence of background solutions when being magnified may influence the detection of samples.³⁷¹ The light leaked into sample chambers will also affect the intensity of the fluorophore spectrums. Besides, the fluorescent emission light intensities can be affected as well since the efficiency of gratings varies with the polarization of incident light.³⁶⁸ All these interferences need to be considered and avoided when performing a success of fluorescence experiments. Furthermore, since the lifetime of fluorescence is around 10 ns, complicated optical modules and electronics are required for the measurement of the time-resolved emission. And now, though it is easier to record the short time fluorescence emission due to the advances in science and technology, great efforts are still needed for more accurate measurements.³⁶⁸

In this work, quantitative measurement of fluorescent compounds (5,6-carboxyfluorescein (CF)) which is enzymatically degraded and released from PCL-PLA microchamber arrays was performed by a fluorescence spectrometer (Perkin Elmer LS 55, Waltham, M.A., USA). In this instrument, a high energy Xenon arc light is used as an exciting light source with the width of the grating slit of 10 nm. For measuring the amount of released CF dissolved in PBS, the excitation and emission wavelength is 494 nm and 525 nm.

3.3.4. Fluorescence Microscopy

Fluorescence microscopy is an optical microscope that can visualize the fluorescence of the specimen under a specific wavelength and generate fluorescent images of designed specimen positions. It is one of the most common methods for tracking and studying the dynamic behaviours of living cells. The biggest advantage is that different molecules can be stained or labelled with fluorescent probes of different colours, which enables the observation of multiple types of molecules at the same time when applying selected excited lights. Given the above advantages, fluorescence microscopy has become one of the crucial and versatile techniques in the field of cell and biology.³⁷²

The fluorescence phenomenon from a quinine solution under sunlight was first observed by Sir John Frederick William Herschel in 1845.³⁷³ Later in 1852, Sir George Gabriel Stokes published a report describing his observation that a blue colour near the surface was emitted when illuminated by sunlight which was filtered by a purple-stained-glass window. Then the emitted light was easily observed through a yellow glass filled with wine that blocks purple light.³⁷⁴ This way of observing fluorescence is similar to modern fluorescence microscopy, and so does the principles.

Nowadays, the most common and preferred fluorescent microscope is the epifluorescence microscope where the illuminating light and the excited fluorescent light pass through the same light path, in other words, the objective used by the illuminating light

is used by the excited fluorescent light as well.³⁷⁵ The schematic demonstration of the epifluorescence microscope is shown in Figure 3.19. Many reasons facilitate the wide application of epifluorescence microscope. First, most of the excitation light will penetrate the specimen which makes it easier to split excitation and emission light. In addition, the objective is also served as a condenser which avoids the procedure of focusing. Besides, the intensity of the fluorescent image increases with the numerical aperture of the objective lens. Furthermore, the loss of the fluorescent intensity is reduced since the excited fluorescent light does not have to pass through the specimen. Therefore, it is suitable for an epifluorescence microscope to observe and detect thick samples such as colonies or tissues.

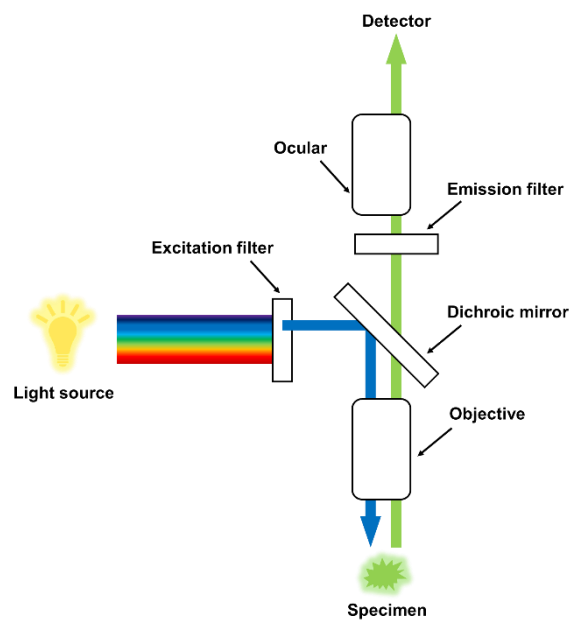


Figure 3.19 Demonstration of Epifluorescence microscope.

Generally, a light source of Xenon arc or mercury lamp or laser lights is applied to provide a relatively continuous light output of broad spectra. The provided light then passes through an excitation filter to acquire a designed wavelength of excitation illuminating light. After being reflected by a dichroic mirror and passing through an objective, the selected illuminating light will excite the specimen and enable the emit of emission fluorescent light of a longer wavelength as explained in 3.3.3. Here, one of the most essential parts of an

epifluorescence microscope is the dichroic mirror which can reflect light shorter than a certain wavelength but transmit longer wavelength light.³⁷⁶ Therefore, the generated fluorescent light of a longer wavelength can pass through the dichroic mirror. After that, the emitted light will be filtered by an emission filter to guarantee that only the emitted fluorescent light of the selected wavelength can get through the ocular and be received by the detector. Finally, the detected fluorescent light can be used to plot fluorescent images with the help of computer software. It is noteworthy to mention that the emission filter can be designed to transmit the emitted light of multiple wavelengths when the specimen is labelled with multiple fluorophores.

However, the shortcomings of fluorescence microscopy should be considered comprehensively as well for better application in various fields. First, as mentioned before, any structure that can be stained or labelled with fluorescence can be visualized by a fluorescence microscope. Thus, on the contrary, unlike some traditional transmitted or reflected light microscope, the fluorescence microscope cannot observe the structure without fluorescent probes. Besides, the phenomenon of photobleaching that fluorophores show a time-dependent decrease and finally lose the fluorescent signal permanently inhibit the detection of a fluorescent microscope. Though theoretically, the fluorophores can cycle between the ground state and excited state unlimited times, the working conditions of fluorophores such as chemical damage can put limitations on the cycle times.³⁷² This can sometimes be minimized by decreasing the excitation light intensity. And gentle stirring of the sample can also minimize photobleaching since the bleached solution can be replaced by the fresh one. Moreover, the high energy light of short wavelength owns the potential to damage the living tissues and cells.³⁶⁸ And some fluorescent probes can also generate reactive chemical compounds when being illuminated which will contribute to the phototoxic effect as well.

In this work, an epifluorescence microscope (Leica DMI4000B camera: LEICA DFC300 FX CCD, Germany) is used which has bright field (BF) mode, phase contrast (PH) mode and fluorescent mode with DAPI, FITC, TRITC, Texas Red and Y5 filters. Besides, the device is optimized for observing and imaging cell and tissue samples (<20 μm thickness). It was used for capturing ordinary optical images of microchamber, micropillar arrays and microcages under different conditions. Further, the fluorescent images of microchamber arrays were acquired by this microscope for confirming the encapsulation as well as the enzymatic release of fluorescent dyes 5,6-CF.

3.3.5. Confocal Laser Scanning Microscopy (CLSM)

A Confocal Laser Scanning Microscopy (CLSM) is one of the optical imaging methods that can improve micrograph contrast compared with a conventional microscope which would otherwise create blurred images of a specimen. This is achieved by excluding most of the out-of-focus light from the specimen in imaging formation.³⁷⁷ A laser beam would be used for scanning as the light source in the CLSM situation.

The principle of confocal imaging methods was pioneered by Marvin Minsky in 1955³⁷⁸ aiming to overcome the limitations of traditional wide-field fluorescence microscopy that the entire specimen is flooded evenly in light from a light source. Two crucial elements are supporting this idea. The first element is the point-to-point illumination of the specimen. The confocal images are captured by scanning a point of light sequentially across the specimen and receive the returning light. Since there is only one point of light illuminating, the specimen will not return the light at the same time, by this, avoiding the unwanted scattered light. The rejection of out-of-focus light is the second important element. The received light will pass through a second pinhole aperture (The first aperture is the one that generates the light point) which will block out the return light that is not from the focal point. After that, the passing light is collected, multiplied and finally reconstructed on a long-persistence screen.³⁷⁹ Since the focal plane and the pinhole plane are conjugated planes and the

focused point of the objective lens and the pinhole is conjugated points, the method is named “confocal”. A schematic diagram of the confocal microscopy principle is shown in Figure 3.20.

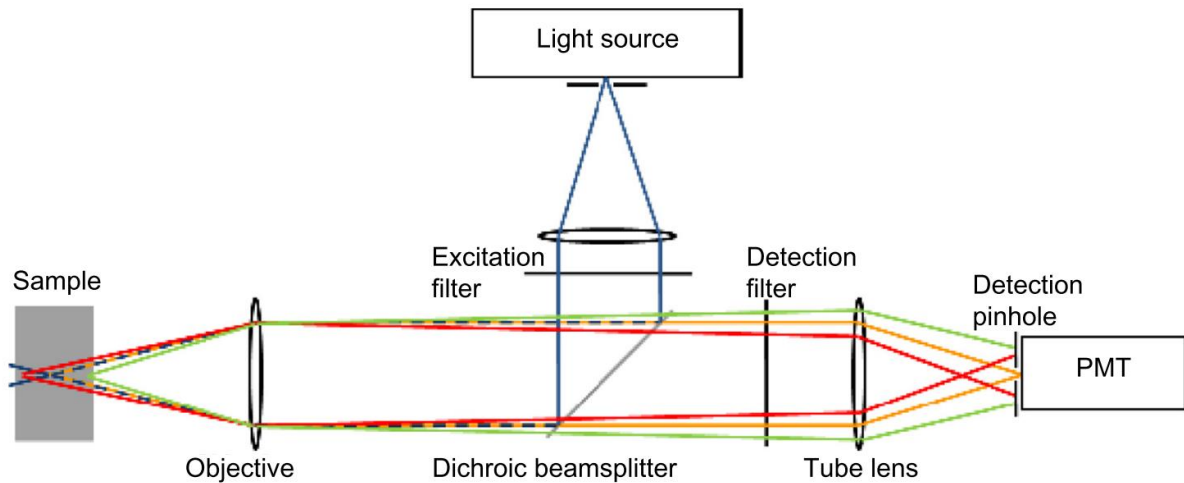


Figure 3.20 Schematic diagram of confocal microscopy principles.³⁸⁰

As demonstrated in Figure 3.20, the blue light indicates the illuminated point-light to the specimen which pass through an excitation filter and reflected on a dichroic beam splitter, finally focused on the specimen surface by the objective lens. The orange light represents the returning light from a sample section in focus which will pass through the pinhole and be detected. The dichroic beam splitter can reflect light shorter than a certain wavelength but transmit longer wavelength light. After that, the orange light can be the exciting light if the sample is a fluorescent substance or scattered/reflected light based on the imaging mode. While the out-of-focus light (red and green) will be rejected since the photons of these rays are blocked out. As a result, the acquired image has fewer noises and higher contrast. The passed light will be collected by a photomultiplier tube (PMT) and constructed into graphs with the help of the computer. Further sequentially scanning the whole specimen surface by moving the sample or the point-light can get a complete image of the focused plane.

The captured image is in two-dimensional (2D) which represents a thin cross-section of the specimen. Therefore, apart from allowing better resolution of sample details, the

three-dimensional (3D) reconstructions of a volume of the specimen can be achieved by means of taking a series of 2D micrographs at different focal depth along the vertical axis.³⁸¹ This 3D imaging nature of CLSM enables it to be widely applied biomedical research, e.g. cell biology³⁸² and living tissues³⁸³ observation. Usually, fluorescent substances or probes are labelled to facilitate the specimen visualizations and labels of multicolours³⁸⁴ could help the researcher to distinguish different selected parts.

However, CLSM, as with every instrument, also owns defects that limit its broad applications and compromises are required to optimize performance³⁸⁵. One of the most obvious shortcomings is that since the pinhole aperture plane can reject out-of-focus photons, the detected signal intensity of captured image will strongly depend on the size of the pinhole.³⁸⁶ If the pinhole size is reduced, the signal-to-noise ratio of the images would decrease as well due to the fewer photons received by PMT. Therefore, in order to improve the contrast and accuracy, the number of photons that reaches the PMT need to be increased. Practically, this is achieved by capturing and averaging many frames though the imaging frame rate is slowed down.³⁸⁷ Another way is to increase the incident light intensity, or the intensity of the fluorescent signal e.g. increase fluorescence. But this only effective to a certain degree, since the high-intensity light can damage the specimen and fluorescent substances³⁸⁸ and concentrated dye molecules can quench each other³⁸⁹. Therefore, the selection of intensity, fluorescent labels and other practical situations need to be comprehensively considered when using CLSM for imaging.

In this work, the CLSM images were captured by Leica TS confocal scanning system (Leica, Heidelberg, Germany). Polyelectrolyte PAH is labelled with RITC for measuring the height of micropillar arrays with CLSM. In addition, microchamber array films that loaded with model drug CF were also observed with CLSM for confirming the encapsulation of the drug. Moreover, the PLA shell of fabricated microcages was labelled with Nile red for confirming the encapsulation of model drugs as well.

3.3.6. Differentiated Scanning Calorimetry (DSC)

Differential scanning calorimetry (DSC) is a thermal analytical technique that can provide qualitative and quantitative information as a function of time and temperature regarding transitions in materials that involves endothermic or exothermic processes, or changes in heat capacity. Owing to the merits of simple preparation and efficient analysis process of both solids and liquids samples over a wide temperature range, DSC has been widely applied for the measurement of various materials ranging from polymers, pharmaceuticals, foods and inorganics.³⁹⁰

Generally, the sample and reference crucibles are placed in two thermally insulated chambers in the same furnace, where the temperature is controlled by the designed program to maintain the temperature of both the sample and reference always presents the same and increases linearly as the function of time. The underlying principle of DSC is that when physical transformation merges, the sample would experience an endothermic or exothermic process so that for maintaining the same temperature between the sample and reference, more or less heat is required to flow to the sample. By recording the difference of heat flow to the sample and reference, the amount of heat absorbed or released from the sample during the transition as the function of time and temperature is recorded by the program, which would result in a curve of heat flux versus temperature or versus time. The positive and negative peaks on the curve represent the properties of the sample transitions. Some of the typical transitions that can be analyzed with DSC including crystallization, glass transition, chemical reaction, melting, phase transition and so forth.

In this work, a differentiated scanning calorimeter (DSC 25, TS instrument, New Castle, UK) was used to measure the melting point of PLA, PCL and their polymer blends.

3.3.7. UV-vis Spectroscopy (UV-vis)

Ultraviolet-visible spectroscopy (UV-vis) is one of the most common a non-invasive quantitative measurement frequently employed in analytical chemistry, which can examine the absorption and reflection of electromagnetic radiation ranging from ultraviolet to visible spectra region. Based on wavelengths, the ultraviolet (UV) region are divided into UVC (180 - 280 nm), UVB (280 - 320 nm) and UVA (320 -400 nm) while the visible (vis) region covers the 400 – 800 nm spectral range.³⁹¹ The spectroscopy in the above UV-vis region involves the observation of the excitation of outermost electrons of the atoms, in other words, the spectroscopy of the electron states.³⁹²

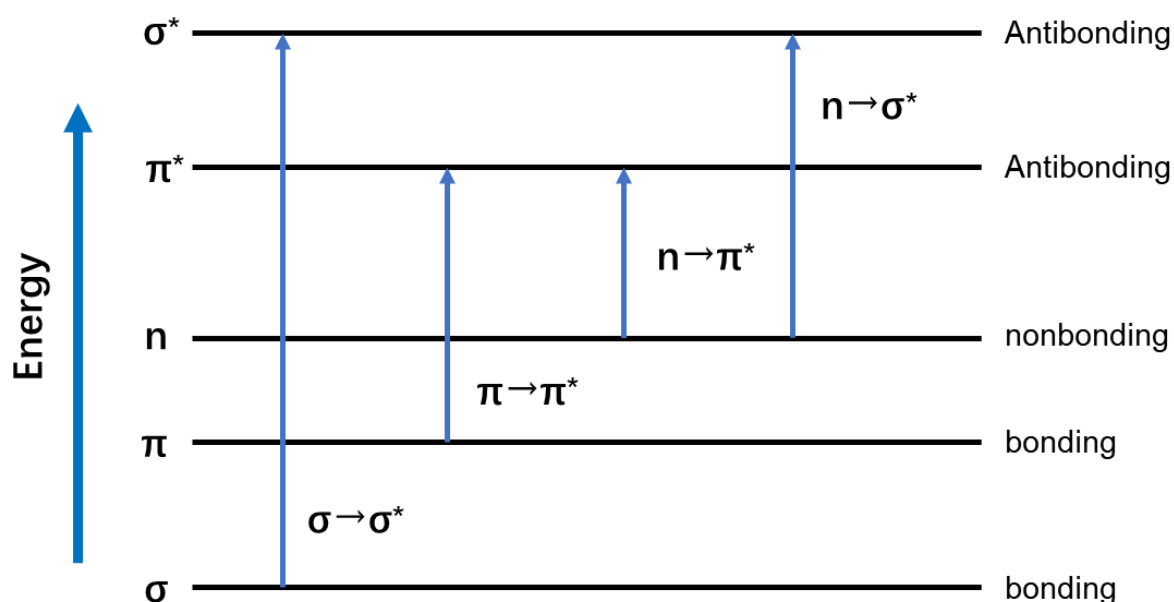


Figure 3.21 Different transitions between various electronic states in UV-Vis spectroscopy.

Basically, the excitation of an electron is induced when the frequency of the incident electromagnetic wave matches the energy difference between two electronic states of the atoms. Though the difference in two states energy varies with the electronic structure of the molecule type and the surrounding environment,³⁹² the electronic states are generally classified as single bond (σ), multiple bonding (π) as well as lone pairs (n) as shown in Figure 3.21. After the photon absorption, electrons on binding orbitals (σ and π electrons) and nonbinding orbitals (n -electrons) of the molecules would be excited to higher anti-

bonding orbitals as σ^* and π^* electrons, thus, four possible types of electron transitions may emerge: $\sigma\text{-}\sigma^*$, $\pi\text{-}\pi^*$, $n\text{-}\pi^*$, $n\text{-}\sigma^*$. However, the most intensive absorption range of 200 – 700 nm is contributed by n and π electrons to π^* transition.³⁹² As a result, for experimental convenience, it is more recommended to measure samples with unsaturated groups, which can provide π electrons.

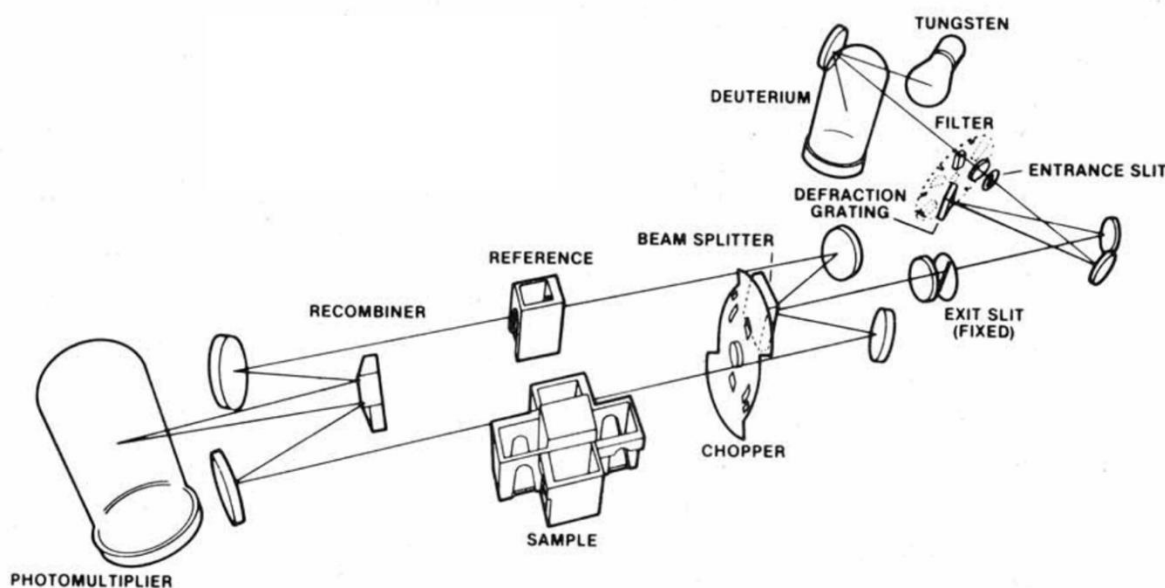


Figure 3.22 Optical illustration a typical of double-beam UV-vis instrument.³⁹³

The optical illustration of a typical double-beam UV-vis spectrometer is shown in Figure 3.22. Generally, electromagnetic radiation is provided by two different light sources, one is a tungsten-halogen lamp for generating light in the visible range with the advantages of long life and more energy, while the other one is a deuterium lamp for producing continuing, convenient and high-energy light in UV region with long life expectancy.³⁹³ The light beams are reflected from a mirror and hit a monochromator which can eliminate all but one required wavelength (as close to one wavelength as possible) with the assistance of a dispersing device (diffraction grating here) so that a parallel and highly monochromatic light is successfully produced and passed through the exit slit. The monochromatic lights are then hit the split-beam optics where lights are separated into two beams: one for sample measurement, the other is applied as the reference beam. It is noteworthy to address that modern beam-splitter has significant improvements in energy level that only 8% of the

incident lights are reflected for referencing, enabling high energy and excellent resolving capabilities.³⁹³ After splitting, one test beam would pass through a transparent cuvette with test samples while the other reference beam passes through the reference cuvette. In the end, the above two light beams would hit the recombiner and fall on the detector. The generated signals are proportionally amplified by a photomultiplier tube for comparing the intensity differences between sample and reference channels.³⁹³

Since the absorption intensity of the samples has a correlation with its concentration, the amount of sample chemical in solutions can be calculated based on the calibration data, which is captured by measuring a series of standard chemical solutions with known concentrations. In this work, a UV-Vis spectrophotometer (LAMBDA 950, Perkin Elmer, M.A., USA) was employed for measuring the amount of drug encapsulated in PLA microcages after dissolving the microcages in chloroform solvent.

4. Microarray Films for Real-time Sensing via Diffraction Patterns

4.1. Introduction

Stimuli-responsive polymers reacting to the chemical and physical changes of the surrounding environment such as pH value, chemical ions, media, temperature etc. have attracted significant attention over the years as smart materials in the field of drug delivery,⁵³ biochemical,⁵⁴ and sensing^{55,56} areas. These environmental changes in nature usually cannot be visualized and perceived, therefore sensors are employed to convert external chemical or physical stimuli into testable signals or changes of sensing material itself.⁵⁷ Thus, stimuli-responsive polymers become one of the best candidates for sensing applications.⁵⁸ Besides, laser light, as a kind of precisely collimated, coherent and monochromatic electromagnetic wave invented in 1958,³⁹⁴ has been widely applied in many fields especially in the sensing area.³⁹⁵ Typically, diffraction of laser light has been extensively used to magnify minor differences, thus enhance the sensitivity and accuracy of sensors.¹⁰ However, though numerous diffraction-based sensors have been proposed to measure refractive-index changes,^{11,12} particle parameters,¹³ and identify chemical compounds,^{14,15} viruses,¹⁶ etc., there are limited diffraction-based sensors for detecting thermal, ionic or pH changes.

Traditional sensors such as pH meter or mercury thermometer have already enabled common people to detect and measure normal physiochemical changes, but these traditional sensors can only be used in limited range and conditions.^{17,18} Therefore, many other cutting-edge sensors were proposed, which have broadened the application area of sensors.³⁹⁶ For instance, a high sensitivity optical sensor is proposed for sensing organic vapour via polymeric swelling-induced variation of fluorescent intensity.^{397,398} A pH-sensitive copolymer is used in conjunction with a magnetoelastic ribbon to remotely sense the surrounding pH.³⁹⁹ Many cutting edge sensors however measure the signals via specific equipment, which are either used by specialized companies and universities only, or the

high cost and non-portability (due to large optical readout systems) limit the applications of those sensors.^{19,20} For example, large equipment systems based on microscopic sensing units, like microscope-based temperature sensors able to determine the temperature of small areas require extensive data analysis, size and costs which severely limit the range of applications.⁴⁰⁰ An inexpensive and portable sensing platform to expand the sensing ability as well as the application area of traditional sensors is therefore needed.

Aiming at improving the efficiency and the reduction of cost to observe and visualize chemical and physical environmental changes, this chapter focus on presenting an inexpensive, convenient and portable multi-sensing platform to detect these variations in macroscopic and microscopic environments. Here, stimuli-responsive polymers including polyelectrolytes or biodegradable polymers are fabricated into microarray thin films that cause upon illumination of monochromatic laser light regular scattering patterns, which can be detected in far-field by the naked eye. The introduction and combination of microarray structures and diffraction patterns provide a novel angle and dimension to well-known stimuli-responsive polymers that expand their ways to sense and visualize the surrounding for the naked eye invisible parameters. The stimuli-responsiveness can change the feature-length of the microarray structures and therefore the scattering patterns or in extreme cases complete loss of diffraction properties. This allows for novel future applications in the field of sensing, including local changes around the sensor units which are real-time detected based on laser diffraction effects. The utilized polymeric films significantly change their microstructure upon changes in surrounding media, pH, temperature as well as the presence of metal ions.

4.2. Sensing of Different Environmental Stimuli

A microarray film that is able to change its microscopic structure must respond to an external stimulus, which is translated into either swelling or shrinking of its microstructure and even the loss of microstructures. The fundamental principles of swelling, shrinking, and

the loss of microstructures based on external stimuli are demonstrated by the sensing of several different external stimuli in this subchapter.

4.2.1. Media Sensing

One possible stimulus to cause the films to change their microstructures is hydration-based swelling. This stimulus can be induced by changes in surrounding media which are important for determining the flood of buildings or raising water levels in dams. Also, liquid filling levels in tanks are potential applications for this kind of sensor which are also called environmental sensors or liquid level sensors.⁴⁰¹ Such sensors can be read out in the far-field via light scattering. Here, one of the most widely applied polyelectrolyte couples, poly (acrylic acid) (PAA) and poly (allylamine hydrochloride) (PAH) as oppositely charged weak polyelectrolytes interacting by electrostatic force, were selected to fabricate PEC. This PEC was then further engineered into periodical repeating microstructures named micropillar arrays.⁴⁰² When the PAA/PAH PEC micropillar arrays are illuminated by laser light, a diffraction pattern emerges, due to the light diffraction effect. Any external stimuli that affect the randomly distributed competition between attractive and repulsive interactions of polymer chains give rise to the swelling and shrinking behaviours of PEC.⁴⁰³ In the presented system weak polyelectrolyte complexes, which are highly hydrophilic and swell in contact with water, increase the distance between micropillars, as well as the micropillar diameter. This diameter and micropillar distance changes are causing a convergence of scattering peaks, as demonstrated in the scattering pattern difference between ambient conditions (Figure 4.1 a) and pH 13 (Figure 4.1 b) as well as pH 7 (Figure 4.1 c). SEM micrographs of these PEC changes can be observed in Figure 4.2.

4.2.2. pH Sensing

Another example of inducing swelling-shrinking effects in ionic materials is to induce changes in the material's internal charge density. This can be induced by changing the pH surrounding the sensor if it is submerged in aquatic media. These properties are useful for

real-time and far-field based sensing applications of pH values in environmental sciences,⁴⁰⁴ food industry,⁴⁰⁵ biology⁴⁰⁶ and related applications. For decades, the stimuli-responsive behaviour of weak polyelectrolytes (PEs) has caused extensive interests in the area of microsensors^{407–409} for uses as e.g. pH sensors.⁴¹⁰ Weak PEs, as one of the most essential stimuli-responsive polymers, can react to pH changes since the protonation and deprotonation (and thereby the charge density) of monomeric groups can be influenced by pH changes.⁴¹¹ For these reasons this kind of polyelectrolytes were fabricated into stimuli-responsive polyelectrolyte multilayer (PEM) films²³ as well as capsules⁴¹² via Layer-by-layer self-assembly techniques.⁴⁰ A bulk polyelectrolyte complex (PEC) can be synthesized by pouring two solutions^{402,413} containing oppositely charged polyelectrolytes together. This causes aggregation of polycations and polyanions due to electrostatic interactions, hydrogen bonds, the entropic release of water molecules and hydrophobic effects.^{22,138}

4.2.2.1. pH Sensing via PEC Micropillar Arrays

In the case of weak polyelectrolyte complex systems, the repulsive force between ionised charged groups of the same weak polyelectrolytes can be adjusted by pH values.⁴¹⁴ Any variation of pH values in both acidic and alkaline environment contributes therefore directly to the swelling or shrinking of the PEC microstructure, resulting directly in the changes of laser diffraction patterns. Generally, after preparing PAA/PAH PEC micropillar arrays, the sample was exposed to solutions with a pH value lower than pH 3 or higher than pH 11 in order to shield charges of one type of polyelectrolyte. This causes the PEC to enter a swollen state and enable carboxylic groups or amine groups to be ionised faster compared to a shrunken PEC state. In this experiment, PEC film enters a fully swollen state after 45 minutes of conditioning time in pH 12, or alternatively 10 minutes of conditioning time in pH 13 solution. The treatment pH values only affect the time it takes for the structured PEC film to enter the swollen state and is not influencing the sensing behaviour of PEC films as shown in Figure 4.3. The pre-conditioned PAA/PAH PEC micropillar arrays

were then exposed to solutions of different pH values resulting in swelling or shrinking behaviour, as Figure 4.1 and Figure 4.2 shows.

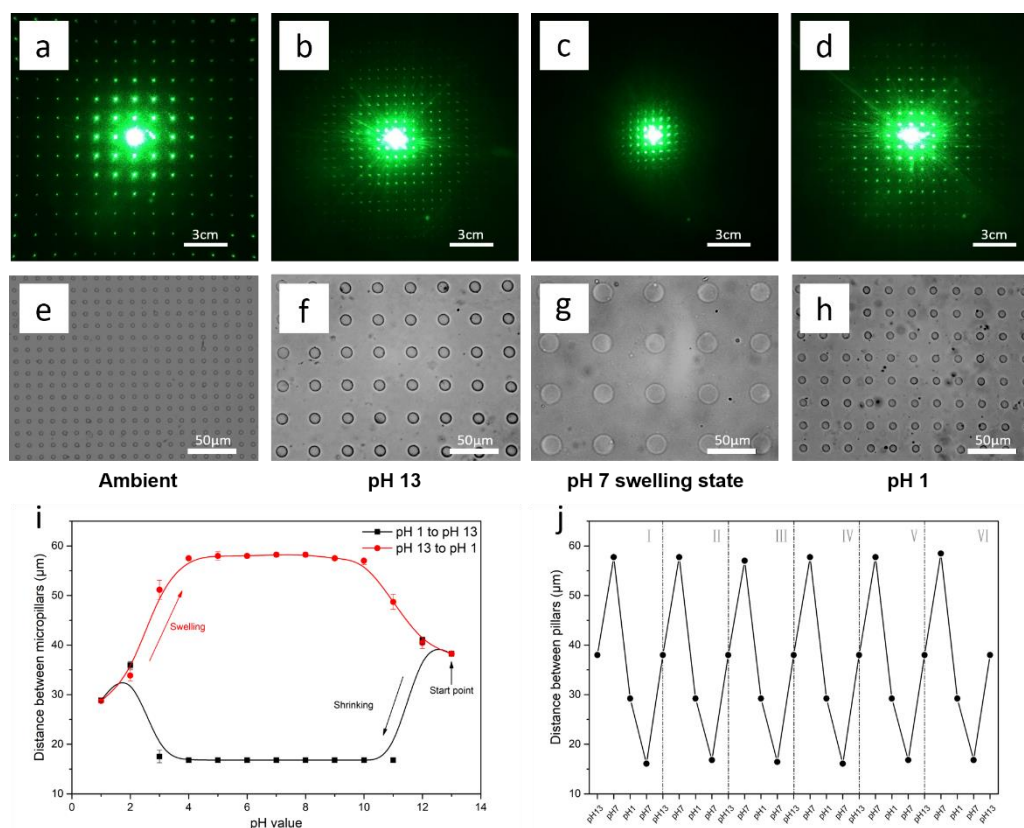


Figure 4.1 Diffraction patterns (a-d), optical micrographs (e-h) of PAA/PAH PEC micropillar arrays as a function of immersion media and solution pH. (a, e) micropillar arrays in ambient condition, (b, f) micropillar arrays in pH 13 solution, (c, g) micropillar arrays in pH 7 solution swollen state, (d, h) micropillar arrays in pH 1 solution. a pH treatment cycle of PAA/PAH PEC micropillar arrays; i) real space values for distance between chambers; Red curve refers to the responsiveness of the sample from pH 13 to pH 1 while the black curve represents the swelling/shrinking behaviours from pH 1 to pH 13. The immersion time of each pH value is 10 minutes at room temperature. j) reversibility of PAA/PAH micropillars of pH sensing. The immersion time of each pH value is 10 minutes at room temperature. Dry film thickness is around 60 μm.

Figure 4.1 a, e) displays the structure and diffraction patterns of PAA/PAH PEC micropillar arrays as prepared without any pH treatment in the air. Optical micrographs in Figure 4.1 allow confirming the integrity of the micropillar array morphology after exposure to different pH values. Photographs of laser diffraction patterns were acquired while the samples were still incubated in aqueous conditions. SEM micrographs of each condition can be found in Figure 4.2, however, SEM micrographs are in a shrunken state with acid

partly evaporated, due to vacuum conditions, thus causing the difference between the SEM and optical micrographs in Figure 4.1 and Figure 4.2.

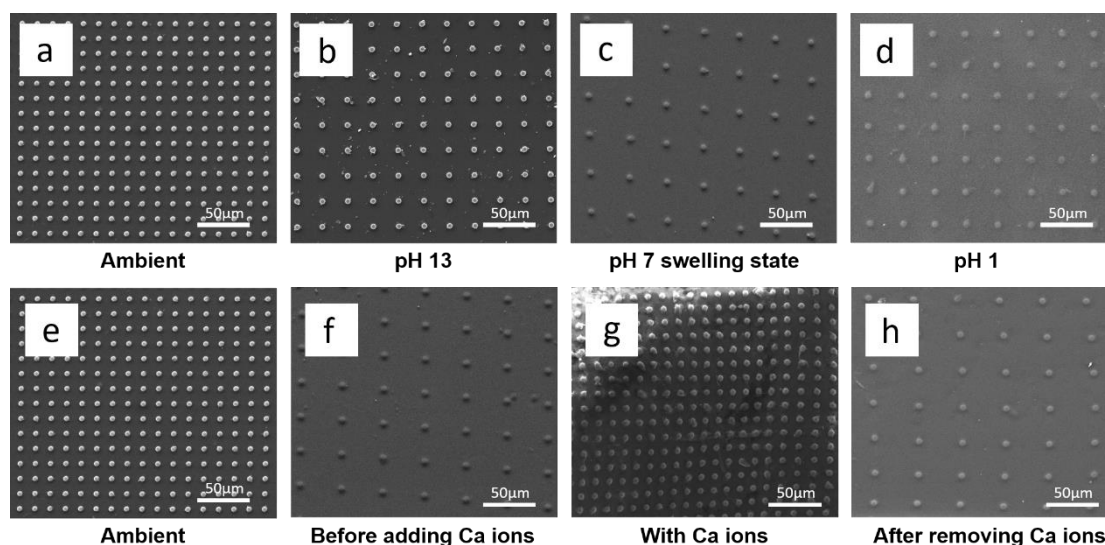


Figure 4.2 SEM images of PAA/PAH PEC micropillar arrays under different conditions. a) Ambient micropillar array structures before pH treatment. b) Micropillar array structures after treated with pH 13. c) Micropillar array structures of pH 7 after treated from b). d) Micropillar array structures after treated with pH 1. e) Ambient micropillar array structures before entering the swelling state. f) Micropillar array structures in swelling state at pH 7 before ions treatment. g) Micropillar array structures in swelling state after Ca ions treatment. h) Micropillar array structures in swelling state after removing Ca ions and back to pH 7.

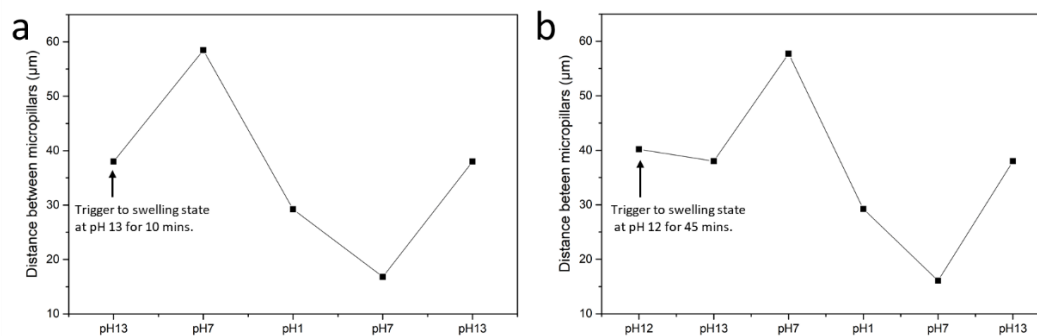


Figure 4.3 pH sensing behaviours of PAA/PAH PEC micropillar films triggered at different pH values. a) PEC films fully enter a swelling state after being treated at pH 13 for 10 minutes. b) PEC films fully enter a swelling state after being treated at pH 12 for 45 minutes.

As can be seen in optical micrographs, the PEC in ambient conditions owned a perfectly periodic structure, and the corresponding laser diffraction patterns were also clear and periodical with each diffraction order clearly distinguishable (Figure 4.1 a, e)). In order to apply PAA/PAH PEC micropillar array films to sensing pH, the sample has to be

submerged in pH 13 solution for 10 mins so that the micropillar arrays entered a swollen state, resulting in the whole polymer film being swollen, which then detached from the glass slide and floated in the pH solution. All the pH sensing treatments are based on the swollen and floating PEC micropillar array film by changing the pH value of the solutions. In the general diffraction equations, the distances between maxima of the laser diffraction patterns are inversely proportional to the period of physical structural size. Therefore, the laser diffraction pattern of PAA/PAH PEC micropillar arrays at pH 13 shows a decreased distance between the intensity maxima, as shown in Figure 4.1 b, f). Moreover, a similar phenomenon was detected by the micropillar arrays in pH 1 as well, as demonstrated in Figure 4.1 d, h), in which the distance between micropillars increased as well and the laser diffraction pattern shrank, but to a different extent. It is worthy of note that the mechanisms of swelling in pH 1 and pH 13 differ due to hydration, and dehydration of oppositely charged ionic groups.

The functional groups of PAA and PAH are at pH 7 only weakly ionised. This effect along with a strong hydrophilic character of the chains causes high hydration and therefore from pH 13 to pH 7, significant swelling of the pillars is observed as presented in Figure 4.1 c, g). In acidic conditions above pH 3, the pillars are compared to the state in pH 13 still swollen which is mainly attributed to the electrostatic repulsion forces of protonated ammonium groups of PAH.⁴¹⁵ The shielding of negatively charged PAA groups below pH 3 increases the hydrophobic effect which leads to shrinking of the micropillars (Figure 4.1 i)).

A complete pH cycle curve of diffraction patterns is gained by immersing PAA/PAH PEC micropillar arrays for each pH value from pH 13 to pH 1 and back to pH 13 (Figure 4.1 i)). It is worth noting that the swelling and shrinking behaviours of PAA/PAH micropillars are reversible, and the pH treatment cycle can be reproducibly repeated multiple times being detected from the same prepared PAA/PAH PEC micropillar arrays sheet (Figure 4.1 j)).

Detection of a stable scattering angle was possible within 10 minutes of exposure time in each respective pH solution.

Changes in pH from alkaline (pH 13) to acidic conditions cause the PEC micropillar arrays to swell to a larger size (Figure 4.1 i)). This swelling results from a balance between electrostatic forces and hydrogen bonding.⁴¹⁶ As the pH value decreases, the degree of charged monomer groups in PAH increases.⁴¹⁷ Therefore, the electrostatic force is the dominating interaction in this pH range. Based on titration curves of PAA/PAH complexes,⁴¹⁸ the protonation degree of PAA/PAH complexes stays nearly constant from pH 10 to pH 4. Consequently, the PAA/PAH PEC micropillar arrays remain in this pH range without significant size changes. Upon further decreasing the pH value from pH 4 to pH 1, the PEC micropillar arrays gradually perform a shrinking behaviour. This refers to the increase of the protonation degree of PAA and PAH that leads to the increase of hydrogen bonding, a decrease of PAA charge and an increase in hydrophobic effects.

pH-responsive behaviours of PAA/PAH PEC micropillar arrays exposed to a pH change from acidic to alkaline environment display a significantly different behaviour proving a hysteretic effect (Figure 4.1 i)). With the increase of pH values from pH 1 to pH 2, PAA/PAH PEC micropillar arrays were swelling as expectedly the hydrogen bonding and hydrophobic effect was weakened.⁴¹⁹ When pH 3 was reached, the micropillar arrays gradually shrunk within 5 minutes into a collapsed state with the size almost the same as the untreated samples in ambient condition. With further increase of the pH value, the collapsed PECs microstructure remained unchanged. Only when the pH value was raised above pH 11, the micropillar arrays re-entered the swollen state due to full deprotonation of the PAH groups. Finally, the PAA/PAH micropillar arrays shrank, as expected, from pH 12 to pH 13, which was the same size as started from pH 13 to pH 1. This phenomenon can be repeated many times on identically prepared samples.

This hysteretic effect is intimately associated with the limitation of the number of hydrophobic interactions of PAH, which is influenced by the ionisation degree changes of PAH driven by pH.^{420,421} Additionally, the electrostatic interactions between PAA and PAH are not negligible as well. Therefore, the differences between polyelectrolyte complex structure in acidic and alkaline condition need to be compared.

In an acidic environment like pH 1 and pH 2, the swelling is dominated by the repulsion of highly ionised PAH polymer chains⁴²². Therefore, PAH cannot form hydrophobic regions at this state because of the repulsion between ammonium groups.⁴²² When the ionization and charge density of dominant PAH chains decreases, driven by the increase of pH value, the PAH chains established a hydrophobic region avoiding pH solutions get inside due to the hydrophobic interactions as well as the weakening of repulsive force, leading to the shrinkage of the PAA/PAH PEC micropillar arrays. This domination of hydrophobic effects is not eliminated until pH is increased above 11 at which most of the carboxylic groups are ionized into carboxylate group whose repulsion interactions are strong enough to overcome the minima energy barriers of hydrophobic regions.⁴²³

However, in the basic environment of pH 12 to 13, the swollen state is mainly contributed by the repulsive interactions between hydrophilic carboxylate groups of PAA with extended conformations.⁴²² Therefore, when the pH value is decreased, though the electrostatic force caused by the carboxylate group were slightly weakened, the hydrophobic region of PAH chains still cannot form because of the frustrate effects of dominant PAA segments.⁴²² As a consequence, the complexes cannot establish a perfect microstructure with minimised interaction energy, so instead, they formed locally minimised structures with barriers between them^{423,424}. Therefore, when the pH value decreased from pH 10 to pH 4, both PAH and PAA were ionised, resulting in the highly swollen state of micropillar arrays.

The utilised PEC is interesting when only a pH range between 1 and 7 is used showing no hysteresis, upon exposure again to lower pH than 7. The same is true for pH changes between 13 and 7 and back to 13. Only when pH changes were surpassing the neutral range, a hysteresis effect was observed. This property makes the utilised PEC ideal for investigating pH changes in a small but defined range, like for bio-analytical and biotechnological applications, where enzymes like pepsin operate in a small pH window (± 1 pH unit) in defined conditions are performing defined actions.⁴²⁵ This reversible swelling shrinking effect in defined ranges is demonstrated in Figure 4.1.

4.2.2.2. pH Sensing via PEM Microchamber Arrays

PAA and PAH are applied to form polyelectrolyte multilayer films via layer-by-layer techniques which are further transferred and printed into PEM microchamber array films following the fabrication methods in 3.2.3. Generally, the sealing layer of PEM coated on a flat glass slide is 20 bilayers with the first PEI anchor layer and the ending layer whose charges are opposite to the last layer on the PDMS stamp. While the number of bilayers coated on the PDMS stamp is adjustable which determines the wall thickness of the microchambers. In order to get an optimal layer thickness of PEM microchamber arrays, different numbers of bilayers were coated on PDMS stamp and further transferred and sealed with a precoated glass slide to form PEM microchamber arrays, whose morphology was evaluated with SEM with results shown in Figure 4.7.

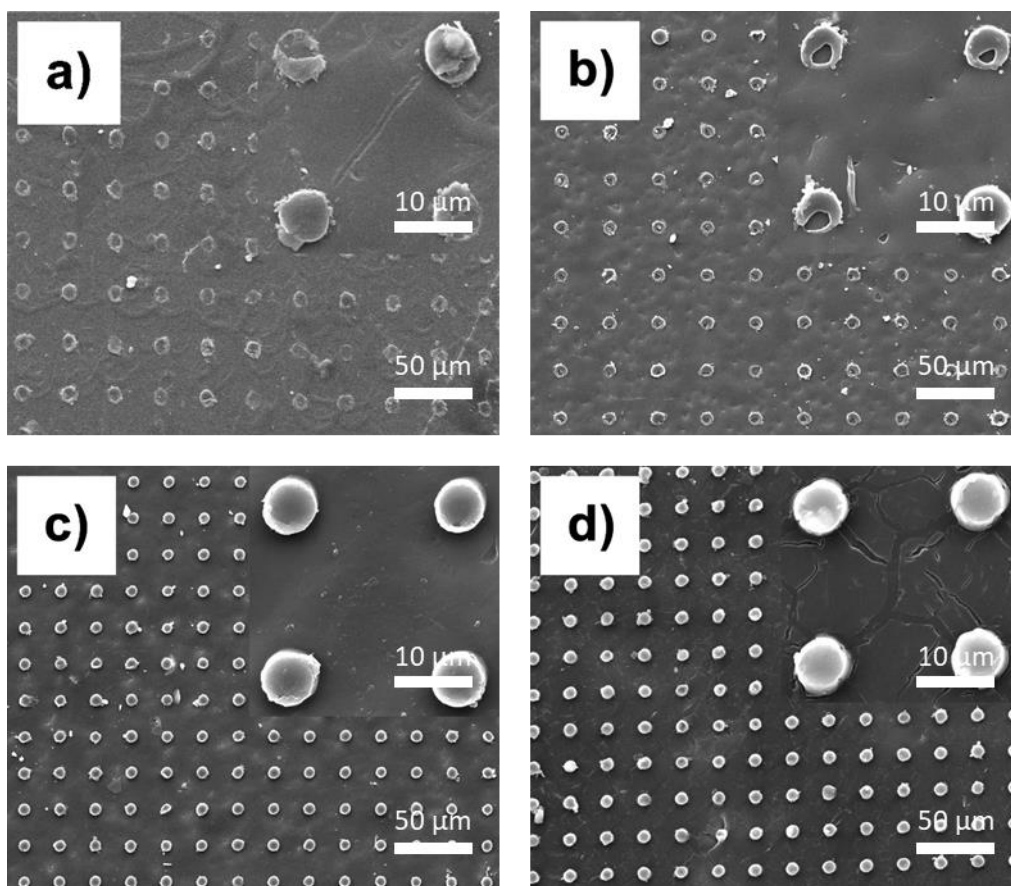


Figure 4.4 The SEM images of PAA/PAH PEM microchambers of different bilayers. a) 15 bilayers of PAA/PAH, b) 20 bilayers of PAA/PAH, c) 25 bilayers of PAA/PAH, d) 30 bilayers of PAA/PAH coated on PDMS stamp

The PEM microchamber array films of different bilayers showed the extinct difference. The microchambers of 15 bilayers of PAA and PAH (Figure 4.7 a)) showed a flattened array structure since the walls were so thin and weak that cannot support the formation of the microchamber or even pillar structure. When the number of bilayers increased to 20 bilayers, as shown in Figure 4.7 b), a microchamber-like structure was almost built but caps were not well-sealed. Complete and well-sealed microchamber arrays were prepared when the number of bilayers of PAA and PAH reached 25 which can be found in Figure 4.7 c). Further increasing the bilayer numbers to 30 (Figure 4.7 d)) can result in thicker and more complete microchamber arrays. However, with the increase of the film thickness, the surface of the multilayer become rougher which would increase the energy of reflected and scattered light and decrease the transmission and diffracted light energy, resulting in less readable diffraction patterns. Besides, the fabrication time was significantly prolonged with more

assembled layers. Thus, the number of PAA/PAH bilayers for fabricating PEM microchamber array films was selected as 25 in the following experiment.

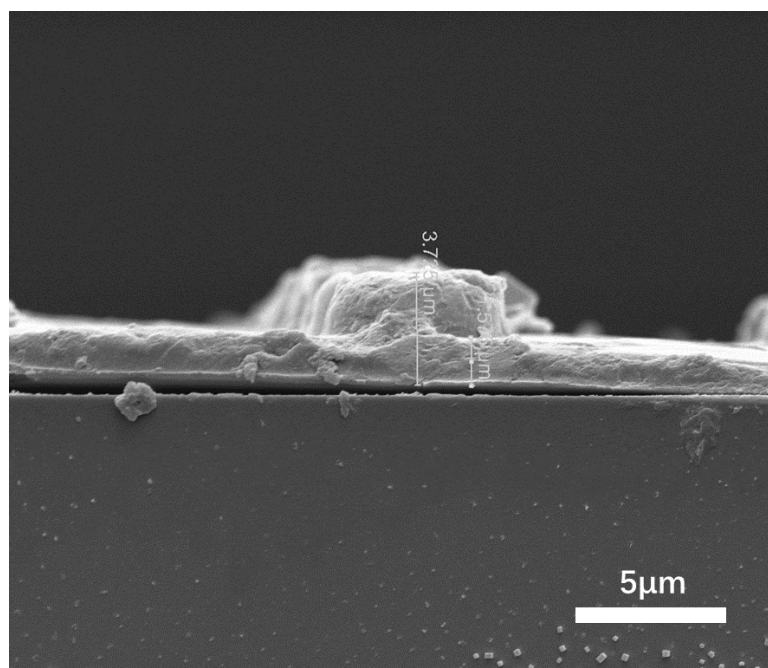


Figure 4.5 The SEM images of the cross-section of PAA/PAH PEM microchambers.

The film thickness of PAA/PAH polyelectrolyte multilayer film was measured using SEM, with the result shown in Figure 4.5. For (PAA/PAH)₃₀ PEM microchamber array film transferred on (PAA/PAH)₂₀ PEM flat film has the film thickness of 1.575 μm as well as 2.15 μm microchamber height, therefore, the overall thickness of the microchamber array films around 3.725 μm. It is calculated that a bilayer of PAA/PAH was 31.5 nm, thus 15.75 nm for each polyelectrolyte layer in average.

Both PAA and PAH are weak polyelectrolytes whose ionization would vary with the pH values of the surrounding environment and further influence the interactions between the oppositely charged polyelectrolyte pairs. Figure 4.6 demonstrated the morphology of prepared PAA/PAH PEM microchamber array films of 25 bilayers after treated with solutions of different pH values by putting a drop of pH solutions on the sample corner.

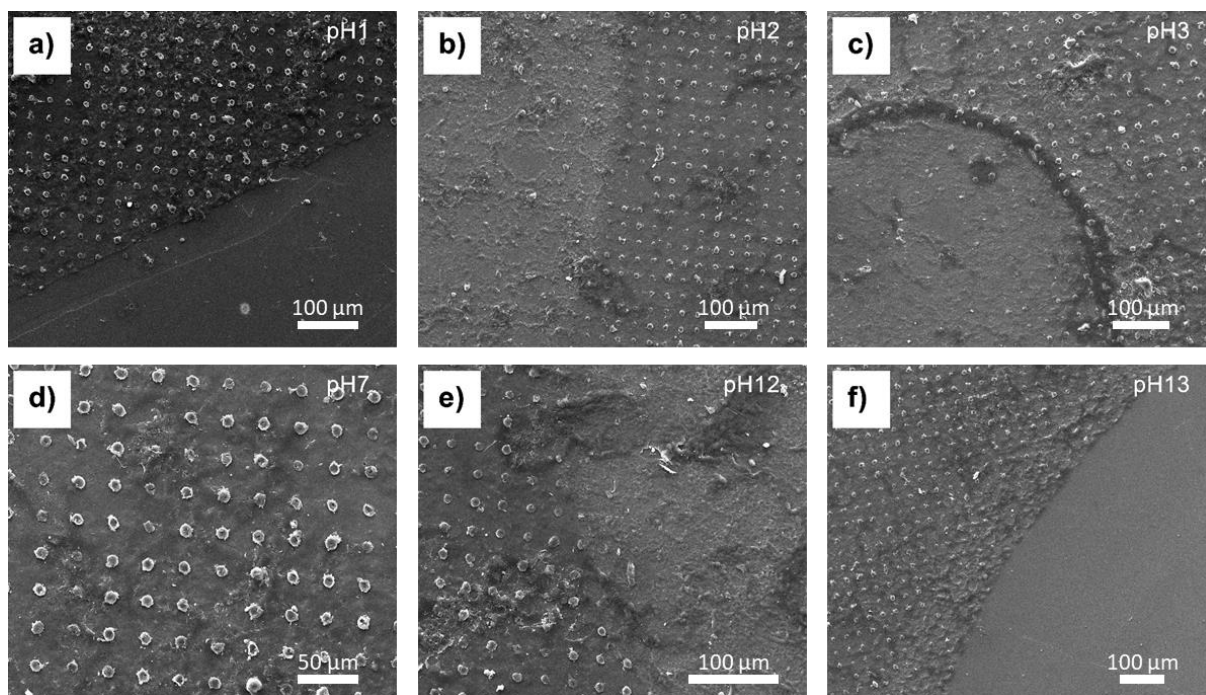


Figure 4.6 The SEM images of PAA/PAH 25 bilayers PEM microchamber array film treated at different pH values.

Significant changes emerged when comparing the morphology of PEM microchamber array films before and after the pH treatment. For the sample treated with a solution of pH 1 and pH 13, the PEM was thoroughly dissolved after the pH treatment due to the strong ionic strength, leaving a clear and distinct border. While pH 2, pH 3 and pH 12, the multilayers still exist, but the microchamber array structures were disappear resulting in the disappearance of the laser diffraction patterns.

4.2.3. Ions Sensing

Another potential stimulus to induce structural changes in micropillar arrays is the interaction of the material to ionic species. Polyacrylic acid (PAA), as a weak anionic polyelectrolyte with numerous carboxylic groups along the molecular chains, can interact with a variety of divalent metal ions.⁴²⁶ Here, calcium ions were selected as model ions to observe ion responsiveness behaviours since they play crucial roles in ecosystems⁴²⁷ and the human corpus.⁴²⁸ Previous studies demonstrated that calcium ions can efficiently

destroy polyelectrolyte networks by simultaneously chelating with the carboxylic group through an intra/inter-chain O-Ca-O linkage^{429,430} resulting in crosslinking of PAA chains.⁴³¹

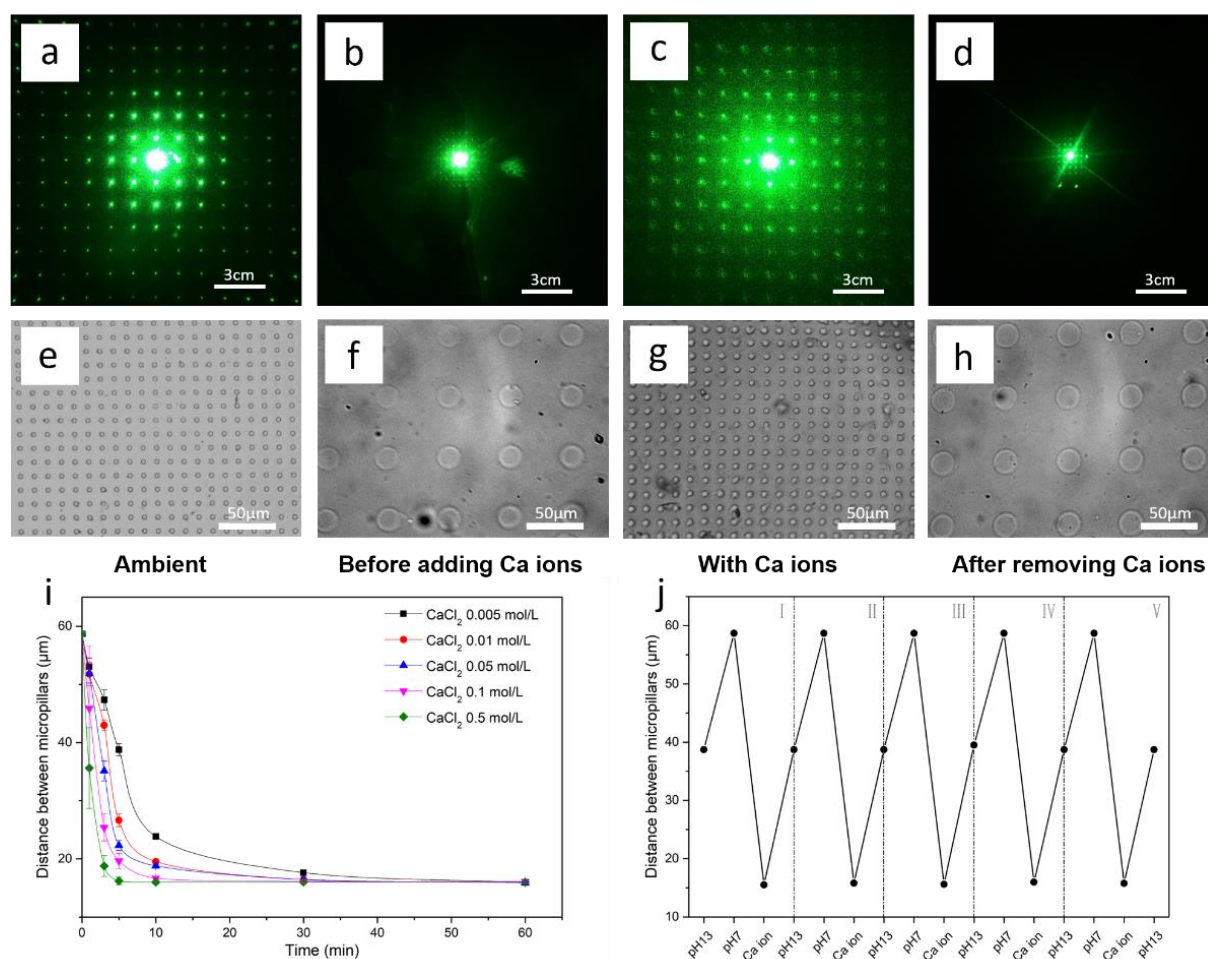


Figure 4.7 Diffraction patterns and optical micrographs of PAA/PAH PEC micropillar arrays before, during and after the exposure to calcium ions. (a, e) Ambient conditions. (b, f) PEC exposed to aqueous conditions. (c, g) PEC exposed to calcium ions. (d, h) PEC after removal of calcium ions. i) The distance between micropillars under different calcium ion concentrations.

j) Reversibility of PAA/PAH micropillar arrays of calcium ions sensing at the concentration of 0.01 mol/L.

As a result, not only the polyelectrolyte complex structure does shrink, but also the distance between individual micropillars can decrease because of the shrinkage of the whole PEC film including the area between the micropillars (Figure 4.7). Since the diffraction equation is inversely proportional to distance, the changes in the structure can be detected by diffraction patterns (Figure 2) and be visualized by naked eyes.

Optical micrographs are applied to visualize the structure of micropillar arrays in a wet state, which shows a different periodicity compared to SEM images (Figure 4.2), due to the hydration induced swelling of PEC. Moreover, the periodical structure variations of PEC micropillar arrays are accurately and real-time reflected by diffraction patterns in each state. By comparing the pattern before and after calcium exposure, the presence of calcium ions can be easily determined.

Before sensing Calcium ions, the ambient PAA/PAH PEC micropillar film (Figure 4.7 a, e)) had to be triggered and enter the swollen state where PEC films detach from the glass slide and float in solutions. After adjusting the solution pH value to 7, the floating PEC film was ready for calcium solution treatment (Figure 4.7 b, f)). A noticeable decrease in microstructure diameter took place when the swollen PEC micropillar arrays were incubated in calcium solutions as shown in Figure 4.7 c, g). From the optical micrographs, it is evident, that the distance between individual micropillars was additionally shortened, indicating a significant shrinkage of the whole PEC micropillar structure, due to the chelation of calcium ions with carboxylate groups of PAA as explained before.

Moreover, it is necessary to state that the PEC micropillar arrays were incubated in an excessive amount of calcium ions, while the number of carboxylate groups of PAA is constant. Therefore, the PEC micropillar arrays will shrink to the same degree where all the Ca-O binding positions are fully occupied. However, the rate that the occupation of the binding positions occurs, varies with the concentration of calcium ion solutions (Figure 4.7 i). For this reason, the presented PAA/PAH PEC micropillar arrays are considered a demonstrator that can determine the concentration of calcium ion solution. As illustrated in Figure 4.7 i), with a higher concentration of calcium ions, the time to reach the final shrunken degree is shorter. For example, it takes as short as 5 minutes for PEC micropillar array films to shrink to the final degree with the chelation with 0.5 mol/L calcium chloride solutions, while it takes an hour for the PEC film to shrink to the smallest size under the chelation with

0.005 mol/L calcium ions. However, due to the fast chelation binding at a higher concentration of calcium ions, the PEC film will shrink rapidly leading to bending and folding of the film structure which could increase the difficulties to gather diffraction pattern. It is suggested to operate and apply PAA/PAH PEC micropillar array film for sensing the concentration of calcium ions lower than 0.05 mol/L.

Figure 4.7 d) shows a regular periodic structure of PAA/PAH PEC micropillar arrays after one calcium ion exposure and washing out cycle whose laser diffraction patterns Figure 4.7 h) can be observed and distinguished, though the diffraction area is small. This can be interpreted in a way that the PEC micropillar arrays are highly swollen, and after washing out calcium ions at pH 13, the PEC film is restored to the same state as before exposed to calcium ions and ready for another exposure. Therefore, it is noted that the chelation between calcium ions and the carboxylate group of PAA is reversible. By removing the calcium ions at basic conditions, the PEC swells again and regains the ability to retrigger this effect, as demonstrated in Figure 4.7 j), PAA/PAH PEC micropillar arrays structure can be reproducibly restored and therefore sense calcium ions several times.

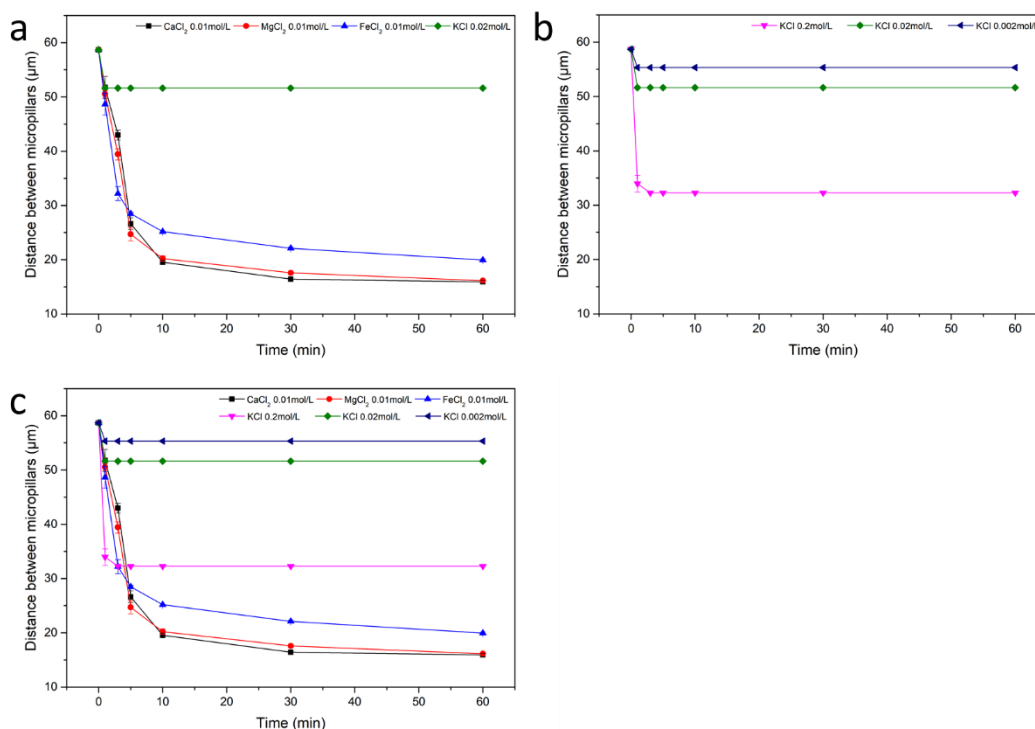


Figure 4.8 Line charts of PAA/PAH PEC micropillar arrays sensing different ion of various compositions and concentrations. a) The distance between PAA/PAH PEC micropillar arrays exposed to different ions. b) The distance between PAA/PAH PEC micropillar arrays exposed to different concentration of KCl ions. c) The comparison of a) and b) showing the different shrinking behaviours upon different ions.

Besides, except calcium ions, other divalent ions also have an impact on PEC micropillar arrays as shown in Figure 4.8 a). The PEC films were exposed to the same concentration of CaCl_2 , MgCl_2 and FeCl_2 of solutions. The results show that both samples treated with calcium ions and magnesium ions are shrunk to the same degree and their shrinking curves are similar. While the samples treated with iron (II) chloride shrink faster but not as small as the other two ions. In comparison image of Figure 4.8 c), where PEC micropillar array films are submerged in KCl solutions of different concentrations(Figure 4.8 b)), the PEC films do shrink but only to a certain extend and become stable within 3 minutes which proves that potassium ions do not chelate with a carboxylate group. It is believed that the minor shrinking is due to the osmotic pressure which increases with the concentration of KCl solutions, resulting in the PEC films shrinking to a higher degree. It is worthy of note, that not only the period of arrays is influenced, but also the pillar height and diameter are affected by the swelling and shrinking processes. To measure the height and diameter of micropillars of the PEC film, fluorescent dye RITC was labelled onto PAH (as demonstrated in 3.2.2) which was then employed to form PEC and fabricate micropillar arrays. The RITC labelled PEC micropillar array films were characterized with confocal laser scanning microscopy after being treated at different environment, with the results shown in Figure 4.9 and the pillar height and diameters were measured and sorted out in Table 4-1.

Table 4-1 The height and diameter change of micropillar arrays under different stimuli.

	Ambient	pH1	pH7 swell	pH7 shrink	pH13	With Ca ions
Diameter (μm)	4.75	13.69	28.03	6.55	14.70	5.72
Height (μm)	3.03	5.22	7.19	4.10	9.91	1.78

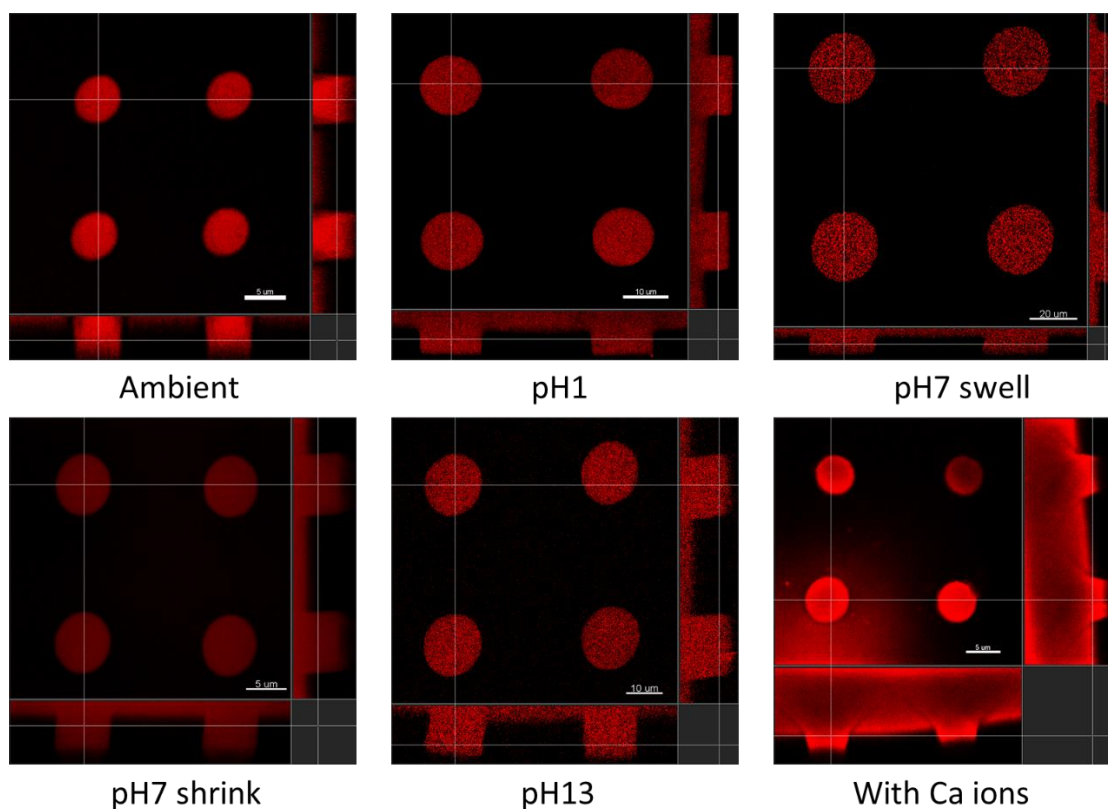


Figure 4.9 Confocal images of PAA/PAH PEC micropillar array films under various conditions. The PAH is labelled with RITC for tracing purpose.

Therefore, PAA/PAH PEC micropillar arrays are able to perform as a reversible, real-time and reproducible sensor platform to determine not only the existence but also the concentration of divalent metal ions based on the generated laser diffraction patterns.

4.2.4. Temperature Sensing

For inducing stimuli-responsive structural changes in microarray structures, thermal effects are also suitable. Sensing the temperature has always been a critical activity, especially in food processing and storage.^{432,433} Inappropriate storage temperature during transportation and handling will decrease food quality, nutrition, and may even lead to food poisoning and food losses.⁴³⁴ Therefore, it is of great importance to find an inexpensive and easy-to-operate device to monitor the temperature of food, especially for individual food packages. Nowadays, many advanced thermal sensors have been proposed with many advantages, such as wide temperature sensing range,⁴³⁵ high sensitivity⁴³⁶ and even dual-sensing ability,⁴³⁷ the high cost and requirement of complicated and expensive equipment

prohibit the application of these devices for ordinary people. While for the traditional thermometer, although it is simple to operate and has been widely applied in people's daily life, is too expensive for equipping every food package with a thermometer, able to irreversibly record a threshold temperature.

In order to sense the temperature of individual food packages, a simple design, easy fabrication and extreme cost-effective thermal sensors is hereby proposed, which is made of polycaprolactone (PCL). PCL is an aliphatic and hydrophobic polymer composed of hexanoate repeat units with a low melting point ($\sim 60^{\circ}\text{C}$) and a glass transition temperature of about -60°C .⁶² PCL has been approved by the US Food and Drug Administration (FDA)⁷² for preparing commercial products in the field of medicine and drug delivery because of its excellent biocompatibility, slow degradability and good mechanical and thermoplastic characteristics.^{65,66}

PCL microchamber arrays were prepared with a one-step-dip coating method followed by microcontact printing (see Figure 3.7 for details)⁴³⁸ causing regular microchamber array arrangements as optical and SEM micrographs in Figure 4.11 demonstrate. PCL moulded into microchamber array films exhibits the same structure and photonic properties as PECs films described afore. The only difference is that the micropillars are filled pillars but the microchambers are empty inside. Confocal laser scanning microscopy was applied to specifically presenting the difference as shown in Figure 4.10. The ability to perform light diffraction scattering is demonstrated in Figure 4.11 as well.

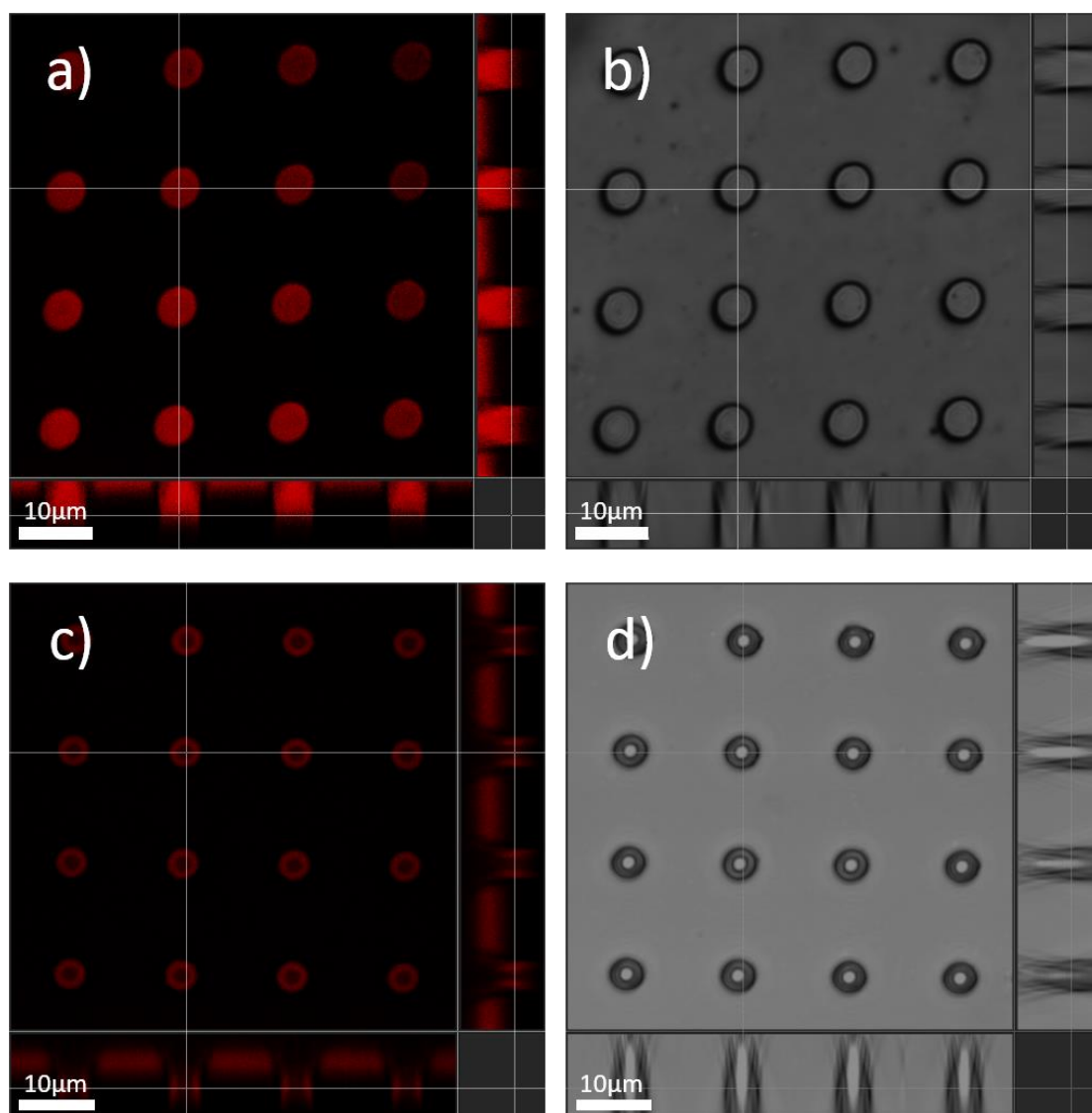


Figure 4.10 Confocal microscope images of PAA/PAH PEC micropillar arrays and PCL microchamber arrays. a,b) Confocal microscope fluorescent image and grey channel image of PAA/PAH PEC micropillar arrays with filled pillar structures. c,d) Confocal microscope fluorescent image and grey channel image PCL micropillar arrays with empty structures.

When the microchamber arrays made of PCL were heated just above its melting point (T_m), both the individual microchambers and the periodical structures vanish, resulting in the disappearance of diffraction patterns. This structure loss can be in real-time observed under an optical microscope, with the result shown in Figure 4.11 b, f). It is inferred, that when the temperature surpasses the T_m , the PCL polymer enters a viscous flow state causing the surface to minimise its area to form a smooth surface and loss of scattering pattern.

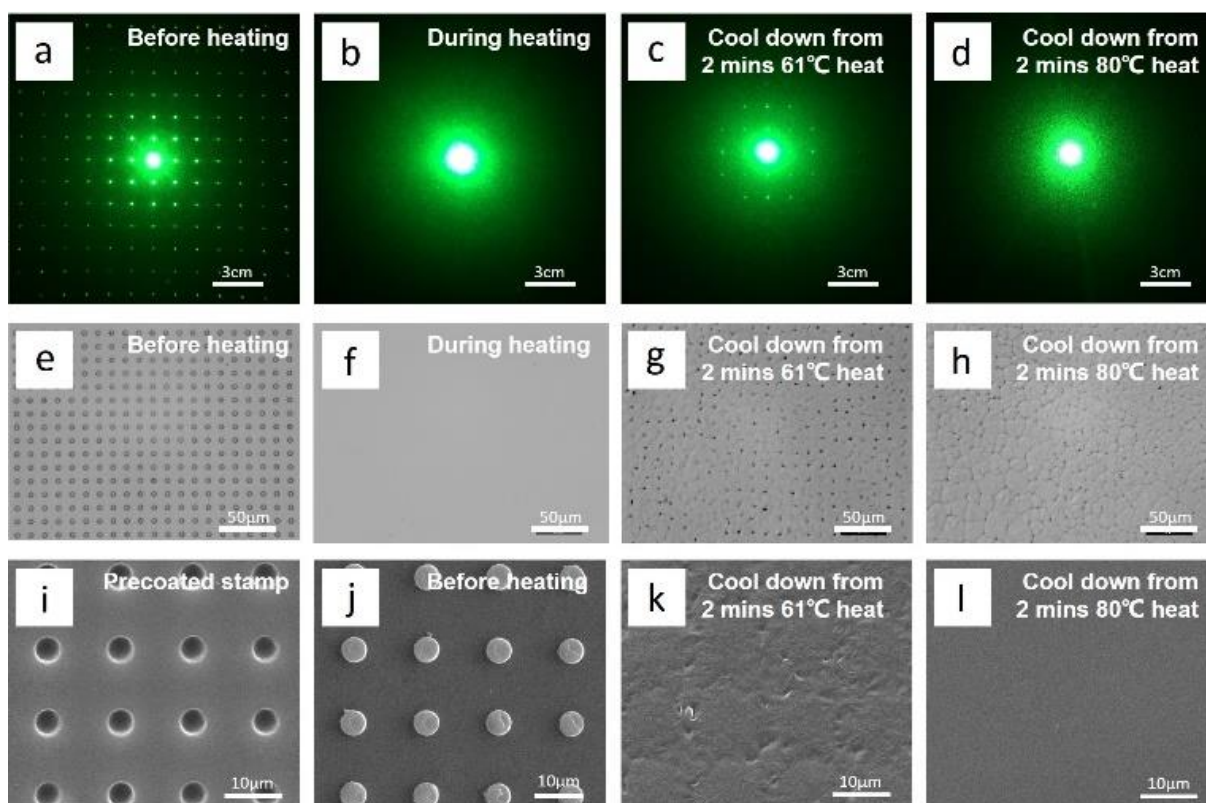


Figure 4.11 Laser diffraction patterns (a-d), optical micrographs (e-h) and SEM images (i-l) of PCL microchamber arrays during the thermal sensing process. (a, e, i) PCL microchamber arrays as prepared without any heat treatment, (b, f) PCL microchamber arrays maintained at 61°C for 2 minutes. (c, g, k) PCL microchamber arrays after cooling down from heating at 61°C for 2 minutes. (d, h, l) PCL microchamber arrays after cooling down from heating at 80°C for 2 minutes. (i) Precoated PDMS stamp with microwells.

After a 2-minute heating procedure, PCL microchamber arrays were cooled down to room temperature. The diffraction pattern reappeared only to a small portion, probably due to some “shape memory effect”⁴³⁹ owing to the short heating time, though not a complete restoration was achieved. The restored pattern was displaying weak diffraction patterns around a centre of diffusely scattered light, which proved a decrease in long-range order (Figure 4.11 c)). In order to determine the causes of the restored diffraction, an optical microscope and SEM were applied to observe the periodical structure and the surface morphology of PCL microchamber arrays respectively. The optical micrograph in Figure 4.11 g) shows that a large number of dark dots and grooves emerged surrounding the position where the original microchambers existed, forming an uneven repeating structure that led to the formation of laser diffraction patterns. Based on SEM micrographs of Figure

4.11 k), it is found that dark dots corresponded to the lower position which was located at the centre of 4 microchambers. Grooves were found between two microchambers' positions. These grooves stem most likely from two microchambers forming, upon melting on short timescales, small bumps on the ground causing the area between two chambers and four chambers respectively to be visualised as groves or dips.

In order to break the artificial created “groves” effect, a higher flow temperature (T_f) or more diffusion time needs to be applied. To confirm this hypothesis, the heating temperature of PCL microchamber arrays was increased to 80°C for 2 minutes. After cooling down from 80°C, the laser diffraction patterns disappear, leaving only transmitted direct laser beam and blurred light in the centre as shown in Figure 4.11 d). The previously mentioned periodical groove structure did not emerge upon cooling in the diffraction pattern. This finding was confirmed by optical microscope and SEM in Figure 4.11 h) and i) respectively proving our hypothesis.

PCL microchamber arrays as thermal sensors own loads of advantages. For example, 1 g of PCL polymer can be used to fabricate more than 4000 microchamber array samples, if each sample has an assumed area of 0.25 cm², which is enough for forming diffraction patterns. Besides, an ordinary laser pointer, an easily obtained and operated device, is the only equipment required to measure the thermal changes, which is inexpensive and portable that can extensively facilitate practical applications.

In this part, PCL microchamber array films are proposed to serve as a thermal sensor based on the existence of diffraction patterns. The low costs and simple measurement procedures, excellent degradability and biocompatibility enable the broad applications of PCL microchamber arrays in food storage, biomedical and biology areas.

4.3. Numerical Simulations of Different Environmental Stimuli

To simulate and explain the experimentally observed laser diffraction pattern, Rigorous Coupled Wave Analysis (RCWA) is applied.⁴⁴⁰ This method is also known as the Fourier modal method in the scattering matrix form. In order to improve the convergence of this method, Li's factorisation rules³²⁴ are implemented. In this formalism, the electromagnetic field is represented as a set of planar waves with wavevectors $\vec{k}_{n,m} = [k_{x,n}, k_{y,m}]$ where

$$k_{x,n} = k_{x,0} + n \frac{2\pi}{a} \quad (\text{S1})$$

$$k_{y,m} = k_{y,0} + m \frac{2\pi}{a} \quad (\text{S2})$$

where a is the grating period in real space, n and m are integers, $k_{x,0}$ and $k_{y,0}$ are the x and y -projections of wave vector of incident light:

$$k_{x,0} = \frac{\omega}{c} \sin \theta \cos \varphi \quad (\text{S3})$$

$$k_{y,0} = \frac{\omega}{c} \sin \theta \sin \varphi \quad (\text{S4})$$

where θ and φ are the polar and azimuthal angle of the incident light. If $|\vec{k}_{n,m}| < \frac{\omega}{c}$, then n and m correspond to an open diffraction channel in a vacuum. For open diffraction channels, we can construct a small scattering matrix S , which, by definition, connects the amplitude reflection and transmission coefficients at different open diffraction orders:

$$S = \begin{pmatrix} r_{tt}^{pp} & r_{tt}^{ps} & t_{tb}^{pp} & t_{tb}^{ps} \\ r_{tt}^{sp} & r_{tt}^{ss} & t_{tb}^{sp} & t_{tb}^{ss} \\ t_{bt}^{pp} & t_{bt}^{ps} & r_{bb}^{pp} & r_{bb}^{ps} \\ t_{bt}^{sp} & t_{bt}^{ss} & r_{bb}^{sp} & r_{bb}^{ss} \end{pmatrix} \quad (\text{S5})$$

where symbols r or t denote reflection or transmission, s or p denote the polarisation state of incident, transmitted or reflected waves, t or b refer to top or bottom semi-infinite space, where the light is incident (first symbol in pair) or reflected/transmitted (second symbol in pair). Each of the sixteen elements of block matrix S is a matrix that consists of the corresponding coefficients at different diffraction orders. In our system, the period-to-

wavelength ratio is about 27-70. Therefore, there are many open diffraction channels in the far-field zone.

To describe the diffraction properties of gratings, we consider a diffraction form-factor, F , i.e. diffraction efficiencies at different diffraction orders. We calculate the form-factor as a polarization averaged transmission coefficient vs the number of diffraction channel (n, m). In the RCWA formalism, these transmission coefficients correspond to the square's absolute values of the elements of the small scattering matrix:

$$F(m, n) = \frac{1}{4} \left(|t_{tb}^{pp}|^2 + |t_{tb}^{ps}|^2 + |t_{tb}^{sp}|^2 + |t_{tb}^{ss}|^2 \right) \quad (S6)$$

In our calculations of the scattering matrix, we assume that the action of external stimuli such as drying, pH solution or ions comes down to the geometrical squeeze of the diffraction grating in the grating plane. In a simplified assumption, the thickness of the grating as well as the heights of cylinders are considered as not affected by the external stimuli. Besides that, we consider that after the action of pH solution, the dielectric constants of PEC remain the same.

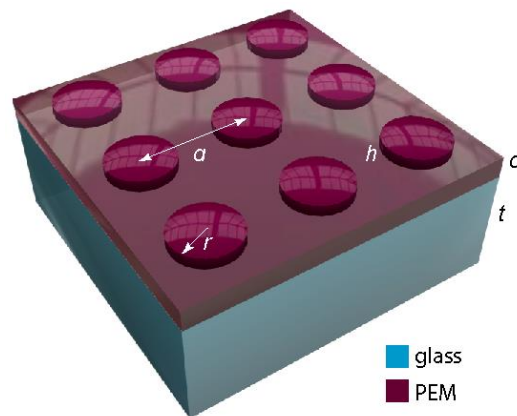


Figure 4.12 Sketch of the diffraction grating. In the calculation of diffraction patterns, the following parameters have been used. For ambient conditions structure $a = 14.63 \mu\text{m}$, $r = 4.60 \mu\text{m}$, $h = 2.24 \mu\text{m}$, $d = 60.00 \mu\text{m}$, $t = 1500.00 \mu\text{m}$, for pH 13 as well as calcium presence, only $a = 37.72 \mu\text{m}$, $r = 14.63 \mu\text{m}$, $d = 191.00 \mu\text{m}$ were considered changed.

Further, we calculate the diffraction pattern in real space by equation (S3) and (S4) accounting for the geometry of the experimental setup. The simulated model is

demonstrated in Figure 4.12 with applied parameters of original PEC structures and pH 13 exposed PEC structure. Besides, the comparison of experimental and simulated PAA/PAH PEC micropillar array diffraction patterns of ambient state and pH 13 presence in 3D view is shown in Figure 4.13

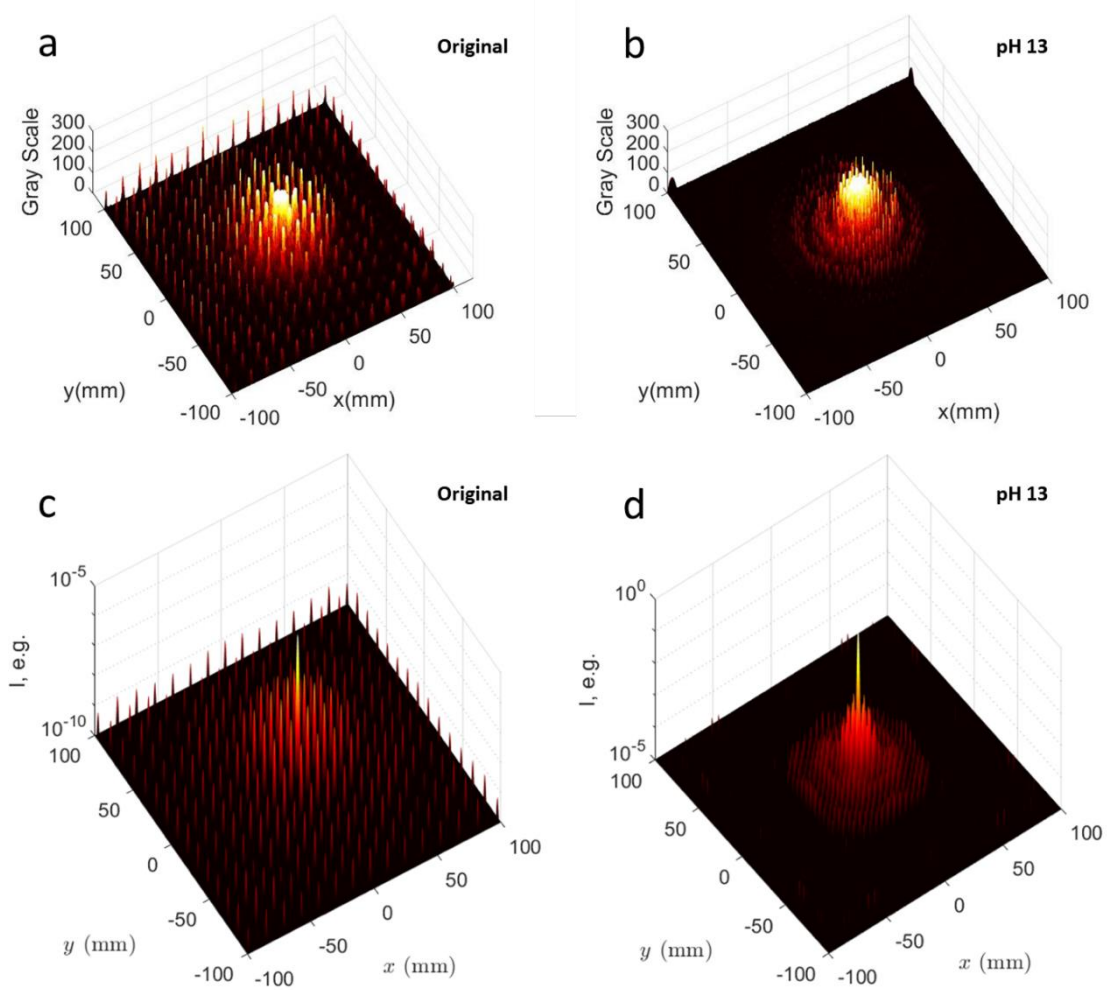


Figure 4.13 Comparison of experimental and simulated PAA/PAH PEC micropillar array diffraction patterns of ambient state and pH 13 presence in 3D view. a) Experimental results of original PEC micropillar arrays. b) Experimental results of pH 13 presence PEC micropillar arrays. c) Simulated results of PEC micropillar arrays in ambient conditions. d) Simulated results of pH 13 presence PEC micropillar arrays.

It is noted, that this model is oversimplified, as at pH 13 also other parameters change like the height ($h = 7.13 \mu\text{m}$) (which changes also in aqueous and ionic conditions), the height of micropillars, however the change in a, r and d is significant enough so that the

simplification of the h parameter is not significant. It is noted, that due to similar size change degrees' pH 13 and calcium simulation were performed with similar values.

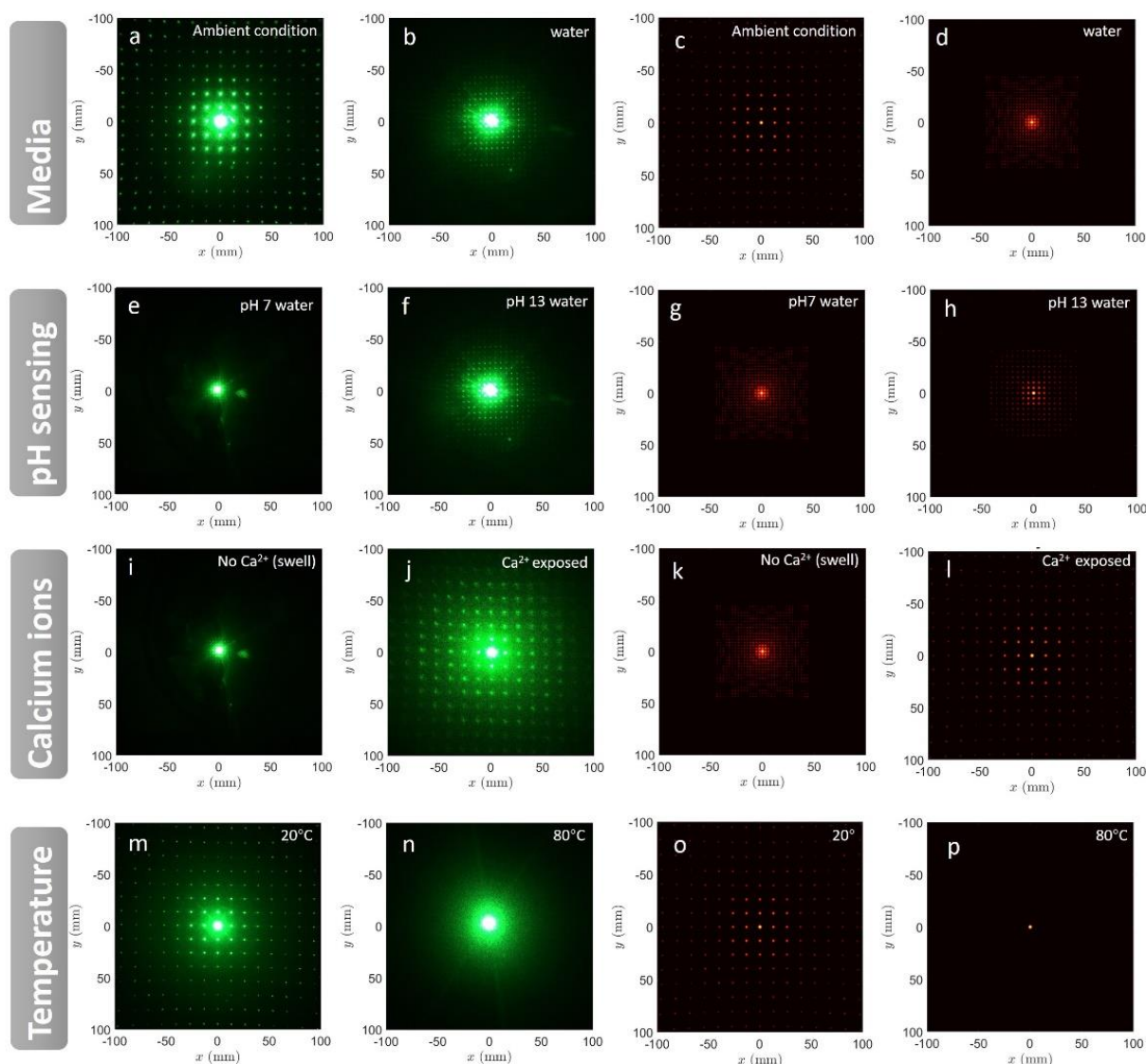


Figure 4.14 Comparison between experimental and simulated laser diffraction patterns of microstructured PEC and PCL at varying stimuli. (a) experimental diffraction pattern in ambient condition, (b) experimental diffraction pattern during exposure of aqueous solution; (c) simulated diffraction pattern of PEC in air, (d) in aqueous solution; (e) experimental diffraction pattern of PEC in pH 7 solution, (f) in pH 13 solution; (g) simulation of PEC in pH 7 in solution, (h) simulation of PEC in pH 13 solution; (i) experimental diffraction pattern of PEC during exposure to deionized water, (j) experimental diffraction pattern of PEC during exposure to calcium ion-containing solution; (k) simulated scattering pattern of PEC ion free water, (l) simulated diffraction pattern of PEC in calcium ion-containing PEC; (m) experimental PCL diffraction pattern at 20°C, (n) experimental diffraction pattern of PCL at 80°C; (o) simulated diffraction pattern of 20°C, (p) simulated diffraction pattern at 80°C.

The calculated diffraction patterns in the far-field zone of the PEC structure in ambient conditions and aqueous conditions of neutral pH show a significant change in the diffraction

pattern width, which significantly correlates with experimental diffraction patterns (Figure 4.14 a) – d)). Water uptake induced swelling of the PEC, which was assumed to cause swelling in PEC causes an increase in real space structures, which in return causes a significant decrease in scattering angles, explaining the experimental observation.

Changes in pH from pH 7 and 13 cause in the simulated scattering pattern a significant change in scattering pattern width which agrees with experimental observations (Figure 4.14 e) – h)). From pH 7 to pH 13 a significant microstructure shrinking was observed experimentally, which results in a significant increase in the simulated scattering angle. Furthermore, the cross-sections of diffraction patterns from Figure 4.14 g) and h) at y-coordinates corresponding to $m=0$ were plotted in order to further compare the diffraction intensity of experimental and simulated data, with the results being demonstrated in Figure 4.15. It is noteworthy to mention that the high energy central zone was oversaturated when capturing the images because of the limitation of the camera and the necessity to adjust the exposure time to a value that the diffraction peaks are still visible. Therefore, in Figure 4.15 a) and b), when being transferred and plotted into charts, the greyscale (Y-axis) referring to intensity was capped at 256. Besides, the experimental diffraction images were asymmetric since the laser light was not perfectly vertical to the PEC micropillar arrays, and the prepared PEC film was not perfectly flat.

By comparing the simulated diffraction efficiency with experimental greyscale, it is clear to notice that the simulated results (Figure 4.15 c, d) agree with experimental diffraction results (Figure 4.15 a, b) on diffraction intensity trend. Besides, one can see that at $m=0$ the grating form factor is almost not affected by the pH 13 solution, while the peak position changed significantly. Generally, this effect can even destroy the diffraction pattern if the geometry perturbation due to the action of alkaline or acidic solution are strong enough. By inspecting Figure 4.14 and Figure 4.15, the good agreement between theoretical and experimental diffraction patterns is evident. This simulation-based agreement proves, that

stimuli induced geometrical changes are the cause of the changes in diffraction patterns and not changes in surrounding or PEC dielectric constants.

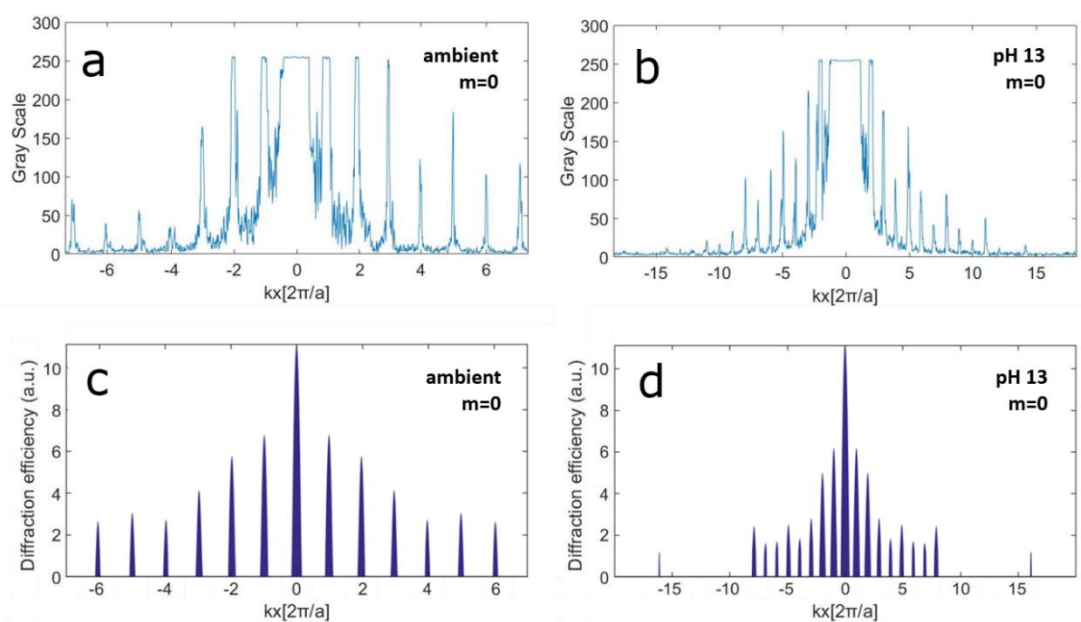


Figure 4.15 Horizontal diffraction pattern intensity comparison between experimental and simulated data of PEC micropillar arrays in different conditions. Experimental results of PEC diffraction patterns in ambient conditions (a) and aqueous pH 13 (b) at $m=0$ (a, b). The simulated diffraction patterns of PEC in ambient conditions (c) and aqueous pH 13 (d) PEC structures at $m=0$ (c, d).

The sensitivity of the PEC sensor towards ionic species (calcium ions) was also compared in regard to simulation and experiment, whereby a qualitative agreement between simulated and experimental values were determined (Figure 4.14 i) – l)). The calcium-induced pattern shrinking causes in the simulation an increase in scattering angle, which is in agreement with microscopic and diffraction evaluation. For this reason, the calcium-induced pattern shrinking is covered by the utilised theory.

The loss of microscopic patterns upon heating the PCL pattern to 80°C leads in the simulation to a loss of diffraction patterns, whereby only the direct beam remains. This simulation is strongly supported by the experimental scattering pattern, which had after heating to 80°C only the direct beam and surrounding roughness induced light scattering

remaining (Figure 4.14 m – p). Therefore, the utilised simulation and theory is able to explain the loss of light scattering.

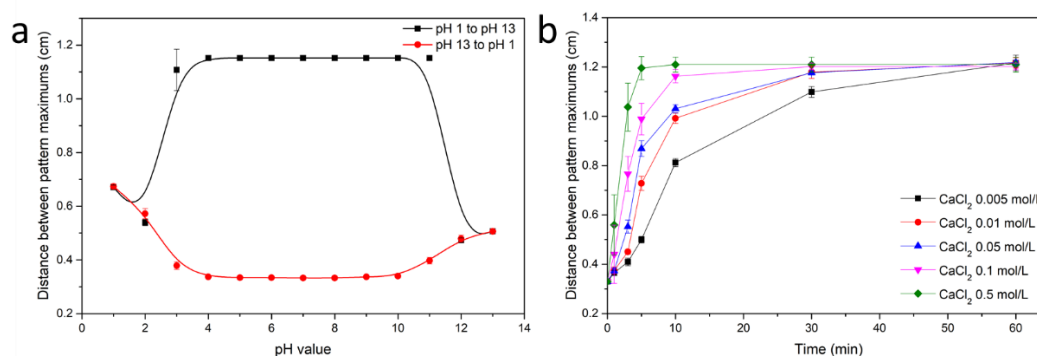


Figure 4.16 Distance changes between pattern maximums of laser diffraction patterns. a) pH of different values diffraction pattern changes. b) Calcium ions of different concentration diffraction pattern change.

In this sub-section, a numeric model to simulate the laser diffraction patterns of PEC micropillar/microchamber arrays with the RCWA method is proposed. This model implements Li's factorisation rules whereby the RCWA simulations are in agreement with experimental results on media, pH, ion and thermal sensing. In the case of real experiments, the total swelling and shrinking processes are visible for the naked eye in all cases by notable convergence and divergence in the scattering patterns which is in our setup in the range of centimetres (Figure 4.16).

The RCWA numeric model established in current work, though in early stage due to limited stimuli-responsive sensing data used and simulated, however, can still give general guidance to the practical experiments. One of the largest advantages of RCWA simulating model is that given current combination of polyelectrolyte complexes, when the microarray structures were changed to different specifications, the model can quickly simulate and provide reliable diffraction patterns without repeating the same work on the new structure. At the same time, the experimental diffraction patterns can be used to confirm and improve the simulation model. In addition, current microarray sensing system finds it difficult to directly distinguish multiple environmental factors due to the overlapping structural deformation. Ideally, with sufficient experimental results and special algorithms, the

simulation model can help to distinguish multiple influencing factors and expand the application areas of the proposed sensing system.

4.4. Conclusions

In summary, we have proposed an inexpensive and portable multi-sensing platform based on structured microarray films. The proposed films are comprised out of stimuli-responsive polymers which are fabricated into repeating structures of microchamber and micropillar arrays. When illuminated by normal laser light, the microarrays give rise to the formation of diffraction patterns. Any external stimuli that can contribute to the structural deformation of the stimuli-responsive materials will be accurately and efficiently reflected in form of laser diffraction patterns. Thus, minor or for the human eye invisible external environmental changes are real-time magnified and transformed into diffraction patterns that can be perceived and visualised even with the naked eyes on the laser scattering patterns. In other words, by introducing and combining with microarray structures and diffraction patterns, well-known stimuli-responsive polymers are provided with a novel angle and dimension to convert external invisible physicochemical parameters into visible and testable light signals.

Based on this diffraction property, stimuli-responsive polymers like PAA/PAH PEC can be fabricated into hydrophilic micropillar arrays which were successfully used for visualising media changes. The media caused a hydration driven swelling-shrinking behaviour of the microstructure, which in turn affects the diffraction pattern in experiment and simulation. However, this swelling behaviour is not sensitive and rapid responsive enough as the micropillar array film has to be submerged into the media and will not response to water drops, and the film also require more than 10 hours to be fully swelled.

The second application example of the presented fundamental microarray structure-based sensing principle utilised pH sensing. The utilised PEC polymers are weak polyelectrolytes PAA and PAH, whose ionisations are intimately associated with pH, are

able to shrink and swell depending on the utilised pH changes. It is shown that the pH solution variations induce variations in the PEC microstructure and by this, alter the resulting diffraction patterns. These processes are relatively stable and reproducible, showing similar structural deformation degree even after six times recycles. While the response time of the change usually takes 1 to 3 minutes, which is not fast but still acceptable on special occasions. The sensitivity and range of the microarray pH sensing ability varies with the selected polyelectrolytes. With proposed PAA and PAH PEC, the system can only show significant structural change below 4 and above 10. RCWA simulations prove that all the changes of the diffraction pattern are attributed to the induced changes of microarray geometry rather than optical constants of PEC, with simulations agreeing well with experimental results. The small range, in which the utilised PEC shows an intense swelling and shrinking range is ideal for investigating e.g. maximum effectivity ranges of enzymes like pepsin.⁴²⁵

Besides, the same PEC is also utilised to confirm the presence of calcium ions since the chelation between PAA and divalent metal ions can lead to the shrinkage of PEC microarray structures due to reduction of charge repulsion, causing an increase in the diffraction pattern angles. This effect was found to be reversible, allowing multiple detections with the same sensor sheet and were confirmed by RCWA simulations. The response time of PEC toward divalent ions can be significant influenced by the concentration of the ions. Higher the concentration, shorter the response time. In addition, this ion sensing system is still in early stage and can only measure one ions at a time, which may also influenced by other environmental factors like pH and temperature. These challenges are expected to be solved later by introducing multiple PEC micropillar array films made of different polyelectrolyte combinations.

Moreover, thermal-responsive polymer PCL is micro-structured into microchamber array films to serve as a thermal sensor due to the viscous flow-induced microstructure

elimination when the temperature surpasses the melting point of PCL. This microstructure elimination causes loss of light scattering properties which is consistent with RCWA simulations. The thermal sensing system is reproducible but irreversible, whose principle enables a high sensitivity with fast responding time. In addition, the sensing range of the system depends on the selected polymer, which brings flexibility to the design of the system.

It is noteworthy to address that the above selected environmental changes are merely some examples of what the sensing platform of microarray structure can achieve, as the goal of this study is to present a fundamental principle and illustrate how microarray structure combining with diffraction patterns works. A multitude of other reversible and irreversible external stimuli sensing properties can be realized by changing the types and/or compositions of polymers being structured into microarrays. For example, the crosslinked polyelectrolytes PMMA can be fabricated into microarray structures for sensing pH value ranging from pH 4 to pH 8.⁴⁴¹ Besides, biodegradable polymer-based microarray films can be enzymatically degraded by the catalysis of corresponding enzymes leading to the irreversible disappearance of both the repeating structure and the diffraction patterns, thus indicating the existence of the specific enzymes.⁶³ In the future enzymes might be introduced into these polymers to enable sensing chemical species.⁴⁴² Theoretically also sensing mechanical properties by the use of flexible polymers is possible.⁴⁴³ Also the local pH can be determined by microscopic observation of micropillar swelling and shrinking or alternatively by focused light scattering of low amounts of pillars or chambers.⁴⁴⁴ Moreover, the microarray structure reveals a unique chance to further incorporate different functional and responsive polymers into one entity. Since there are empty spaces in microchambers, the microchamber arrays also own the potential to encapsulate cargos^{333,445} which can be released by temperature and other stimuli.^{35,36} Most importantly, the generated diffraction patterns can be observed in real-time to monitor the release behaviours remotely.

Ultimately, an inexpensive, convenient and portable multi-sensing platform fabricated in structured film arrays can be presented by combining the stimuli-responsive properties of different materials which provides the opportunities to determine multiple external stimuli in real-time. Therefore, we believe the outstanding versatility of the microchamber/pillar arrays will undoubtedly attract the attention of researchers and engineers to explore many fascinating and promising applications in the fields of biosensors, drug delivery, catalysts and even electronics. Also, sensor arrays might be utilized in the future in combination with multivariate data analysis to increase sensitivity towards isolated species and for quantification of the number of single species.

Though the multi-sensing platform of microarray structures are promising way for stimuli-responsive sensing, the idea is still in early stage with multiple challenges to be solved. In this chapter, the sensing parameters were all considered individually, while in practical sensing environment, multiple parameters would be presented simultaneously so that exert an overlapped shrinking or swelling behaviours on the microarray films, making it way more difficult to sense and distinguish the influencing factors. Other than multiple parameters sensing problems, single parameter sensing systems were not optimal as well. Current pH sensing ability can only show significant changes for pH value below 4 or above 10, which put huge limitation on the practical applications. Other polyelectrolyte complexes combinations that response to pH range of 4 to 10 should be developed. Similar problem also exist in thermal sensing system, where only when temperature above selected points can the microarray structure changes be detected. More stimuli-responsive polymer with different melting points should be structured to maximize the capability of the system. Moreover, the simulation model presented in this work was still not complex and updated to solve practical problems, as it can just prove that the experimental results fit well with the simulation results.

Based on above discussion, in order to further develop the proposed sensing platform, the most straightforward route is to expand the sensing database of various stimuli-response polymers, finding the principle and mathematical correlations between microarray films made of different materials and the single or multiple sensing parameters. Only after the collection of sufficient experimental data can we find the optimal stimuli-responsive materials for practical applications as well as the simulation model training and predictions.

5. Microchamber Array Films for Cargo Encapsulation and Release

5.1. Introduction

For decades, the development of micropackaging and delivery platform technologies such as housing the potential for chemical compound encapsulation and release through external stimulation has become a significantly prevalent concept, most notably in the fields of drug delivery^{446,447}, therapeutics⁴⁴⁸, biosensor⁴⁴⁹, lab-on-chip⁴⁵⁰, and tissue engineering⁴⁵¹. A common strategy employed to achieve the encapsulation is loading chemical cargos into microcapsules made of functional constituents in capsule wall what is often produced by layer-by-layer(LbL) self-assembly techniques^{23–25}. Later, this strategy has broadened to microchamber arrays^{21,22}, a newly developed micropackaging platform, which enables multilayer microchambers to encapsulate microparticles and hydrophobic cargos for site-specific controlled release via laser radiation²⁶. However, the micropackaging platform above produced by LbL techniques could only manage to encapsulate cargos with high molecular weight²⁷ or small but hydrophobic molecules²⁸ due to the semi-permeability of multilayer films^{29,30}. Since the molecular weight of most biologically active is under 500 Da³¹, the successful encapsulation and biologically stimulated release of small hydrophilic molecules remain a significant challenge to the scientific community.

Apart from encapsulation, a large number of trigger release methods have been extensively studied for both microcapsules and microchamber arrays, such as pH⁴⁵², temperature^{453,454}, magnetic field⁴⁵⁵, sonication⁴⁵⁶ and laser light^{332,457}, in order to facilitate the drug release by either enhance the permeability of the carrier shell or break and destroy the carrier. When compared to conventional methods of drug administration, carrier systems would minimise systemic toxicity⁴⁵⁸, protect sensitive drugs from undesired degradation⁴⁵⁹ and prolong the active duration of drugs^{460,461}. Conversely, the inappropriate application of external triggers may cause inefficiency, with the potential to induce

deleterious side effects in living systems - prohibiting their applications in biological and medical fields. For example, physical stimuli such as laser offer a low penetration depth into tissue⁴⁶² ultimately limiting the application to the superficial skin, while altering pH and temperature of in vivo biophysical environment might lead to undesirable damage to biological tissues⁴⁶³. Moreover, although sonication of low intensity has been widely applied as diagnostic and therapeutic methods for clinical trial⁴⁶⁴, the thermal injury still might occur because of the high intensity focuses ultrasound (HIFU) treatment⁴⁶⁵. In contrast, exploiting enzymes as a trigger has a multitude of merits since most of the enzyme degradations are under a mild condition with neutral pH, stable ionic strength and low temperature⁴⁶⁶, while the strong selectivity of enzyme enables the carriers to be degraded at the specific defined position to controlled release^{467,468}. Particularly, comparing with the traditional physical triggered release, external stimuli are not required for carriers made of enzyme-degradable polymers⁶⁰, empowering enzyme-degradable platforms to become one of the most promising systems for controlled drug delivery⁶¹.

One approach to solving the problem of encapsulation and enzymatic release of hydrophilic cargos involves the use of both biodegradable and hydrophobic polymers, through the exploitation of the characteristic low water permeability that hydrophobic polymers possess⁵⁹. Therefore, the fabrication and enzymatic degradation of polycaprolactone (PCL) microchamber films are presented in this work. Polycaprolactone (PCL), an aliphatic and hydrophobic polymer composed of hexanoate repeat units, has excellent processabilities with a low melting point ($\sim 60\text{ }^{\circ}\text{C}$) and a glass transition temperature of about $-60\text{ }^{\circ}\text{C}$ ⁶². Furthermore, PCL has been approved by the US Food and Drug Administration (FDA) for preparing commercial products in the field of medicine and drug delivery⁷². Moreover, owing to the numerous advantages including variable biodegradability, biocompatibility^{65,66}, great miscibility⁶⁷, excellent mechanical properties⁶⁸, PCL has been broadly selected as scaffolds for drug delivery and sustained release⁶⁹⁻⁷¹. The hydrophobic nature of pure PCL, alongside its high crystallinity, yields a slow rate of

degradation in the absence of enzymes – up to 2 years^{72,469}. Generally, lipases are lipolytic enzymes that hold the potential to catalyse the hydrolysis of polymers with ester bonds¹⁶⁵. Here, the selected corresponding enzyme for PCL is the lipase from *Pseudomonas Cepacia* (lipase PS) – a specific lipase that significantly catalyses the degradation process of PCL compared to samples incubated in buffer alone^{63,64}.

In this subchapter, free-standing PCL microchamber array films were designed and fabricated by solution casting⁴⁷⁰ and microcontact printing methods^{471–473}. The degradation behaviour of PCL microchamber films under different lipase concentration was studied. Further, in order to observe the encapsulation and enzymatic release behaviour of small hydrophilic molecules, 5(6)-carboxyfluorescein (CF, 376 g·mol⁻¹) was selected as a model drug for encapsulation into PCL microchamber arrays. Further to this, monitoring of microchambers degradation was achieved utilising laser light to illuminate microchambers arrays forming an observed Fraunhofer diffraction pattern. Since PCL film has permeability for water-based compounds, and hence impaired the ability for cargo retention⁴⁷⁴, we explored blending composition with PLA to reduce permeability and thus facilitate the encapsulation of small hydrophilic molecules. Here, the model drug CF was encapsulated into PCL and PCL/PLA blended microchamber array films and subsequent release was achieved under the catalysis of lipase. The surface morphology of microchamber arrays was observed via scanning electron microscopy (SEM). Fluorimeter and confocal laser scanning microscopy (CLSM) were used to confirm the encapsulation and enzymatic release of labelled cargos.

5.2. Preparation of PCL Microchamber Array Films

The polycaprolactone (PCL) microchamber arrays were prepared following the schematic illustration shown in Figure 5.1 (dye encapsulation is optional). Patterned rubber stamps made of polydimethylsiloxane (PDMS) were prepared by casting and curing PDMS on the top of silicon masters with micropillars whose specifications can be found in Figure

5.2. After lifting off the silicon master, the PDMS stamp with microwells was obtained for fabricating PCL microchambers. The patterned PDMS stamp and a glass slide were dipped into polymer solution for 5 seconds and dried in ambient conditions resulting in the formation of a thin polymer layer on both surfaces. Afterwards, if drug loading was needed, the ground submicron size drug particles were spread on the top of the precoated PDMS stamp. Further, in order to seal and transfer the polymer film from the patterned stamp, the drug-loaded precoated PDMS stamp was pressed with a pre-coated glass slide which is preheated at 75°C for 2 seconds until the films were thoroughly cooled down. Finally, after gently and carefully lifting off the PDMS stamp, the drug-loaded PCL microchamber arrays were fabricated and become ready for further enzymatic degradation experiments, whose SEM images were shown in Figure 5.3.

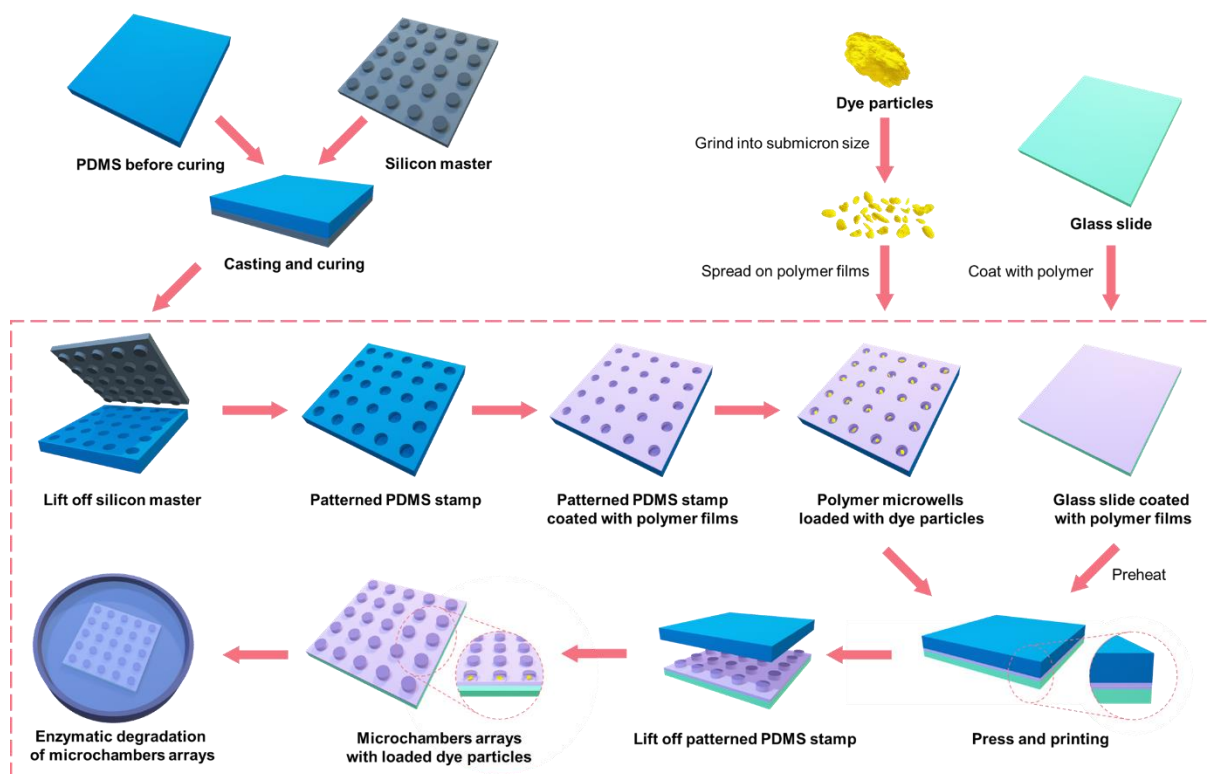


Figure 5.1 Schematic illustration of the fabrication of drug-loaded microchamber array films and enzymatic drug release.

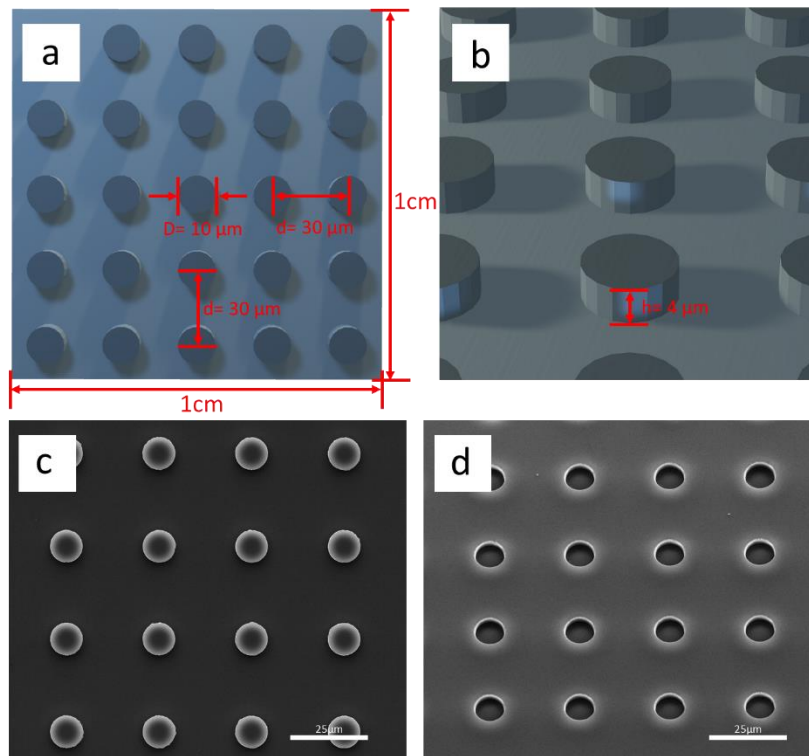


Figure 5.2 Schematic illustration and SEM images of patterned silicon master. a,b) Schematic illustration of patterned silicon master (size: 1 cm × 1 cm) with micropillars (10 μm diameter, 4 μm height and a centre-to-centre distance of 30 μm) used in this work. c) SEM images of patterned silicon master. d) SEM images of patterned PDMS stamp made from the patterned silicon master.

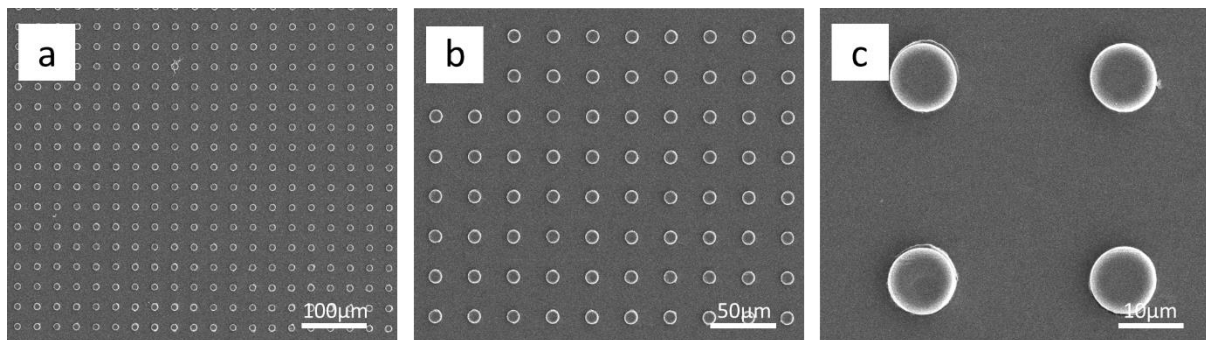


Figure 5.3 SEM images of PCL microchamber array films of different magnification. a) 500X, b) 1000X, c) 5000X

5.3. Enzymatic Degradation Behaviours of PCL Microchamber Array Films

In order to be applied in vivo work, the materials of drug delivery vehicles have to be biocompatible and non-toxic towards cells and tissues. If intended for the drug delivery applications, the materials of the vehicles have to be biodegradable with the degraded product can be metabolized by human body. Potential polyester can be polylactic acid and polycaprolactone, poly(lactic-co-glycolic acid). For polyelectrolytes for drug delivery can be polypeptides, polysaccharides, polyarginine and so forth.

The enzymatic degradation experiments were conducted simply via incubation of prepared PCL microchamber array films with lipase PS solutions of different concentration sequences at 37°C in a climate chamber for designated times. The results were shown in Figure 5.4. Notably, the full degradation is defined by the absence of any microchamber-shaped remnants on the SEM images and as confirmed by the full disappearance of the laser diffraction pattern.

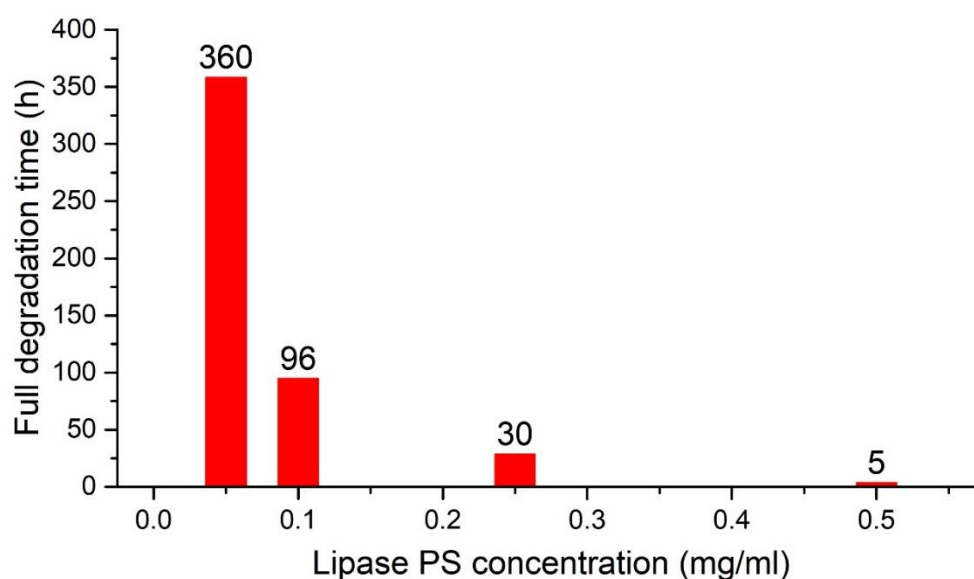


Figure 5.4 Full degradation time of PCL microchamber arrays in various lipase PS concentrations at 37°C.

The clear correlation demonstrates that elevated concentrations of lipase PS resulted in reduced times required for complete degradation. There would be 10% measurement error due to the checking time as well as the confirmation of the full degradation. The degradation processes were reproducible. For lipase concentrations of 0.05 mg/ml, the PCL microchamber arrays were degraded after as much as 360 hours. While for the lower concentration groups of 0.1 mg/ml as well as 0.25 mg/ml, the enzymatic degradation action took 96 hours and 30 hours respectively. Furthermore, complete degradation of PCL microchamber arrays at lipase concentration 0.5 mg/ml, occurred after just 5 hours of exposure. During the incubation procedure, the degradation process of PCL microchamber arrays could be real-time monitored via Fraunhofer laser diffraction patterns with the results found in Figure 5.5.

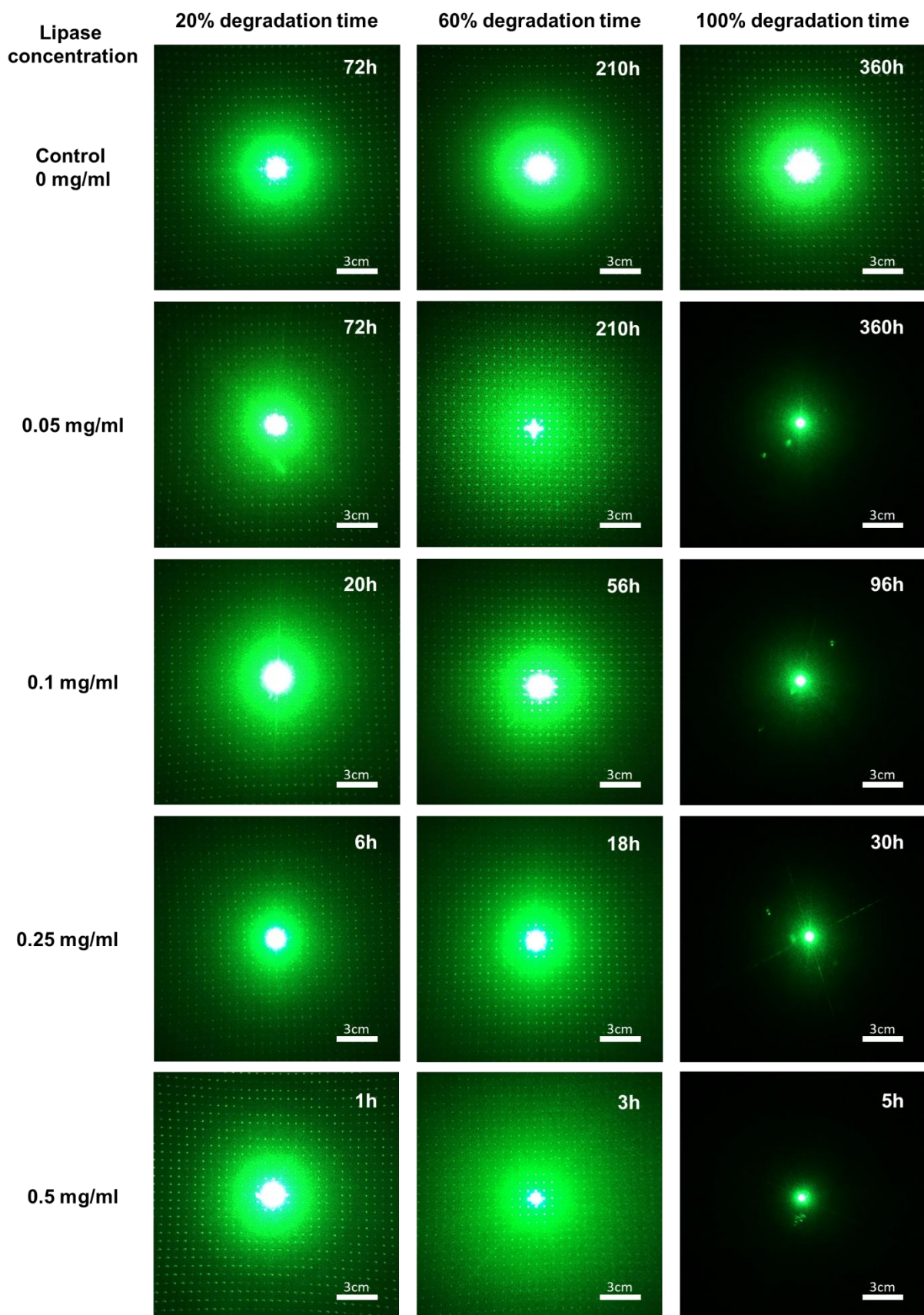


Figure 5.5 Diffraction patterns of PCL microchamber arrays in different lipase concentration during degradation procedures.

Here, the lipase PS concentration of 0.5 mg/ml was utilised as an example, with lipase concentrations mentioned later being 0.5 mg/ml as default. Within only 5 hours of lipase exposure, PCL microchamber array films were fully degraded without polymer remnants present as seen on the SEM image. In order to figure out the surface erosion mechanism of PCL, SEM was used to analyse and examine the changes in surface morphology of PCL microchamber array films after enzymatic degradation of different times. Some of the most representative stages of samples are selected and shown in Figure 5.6.

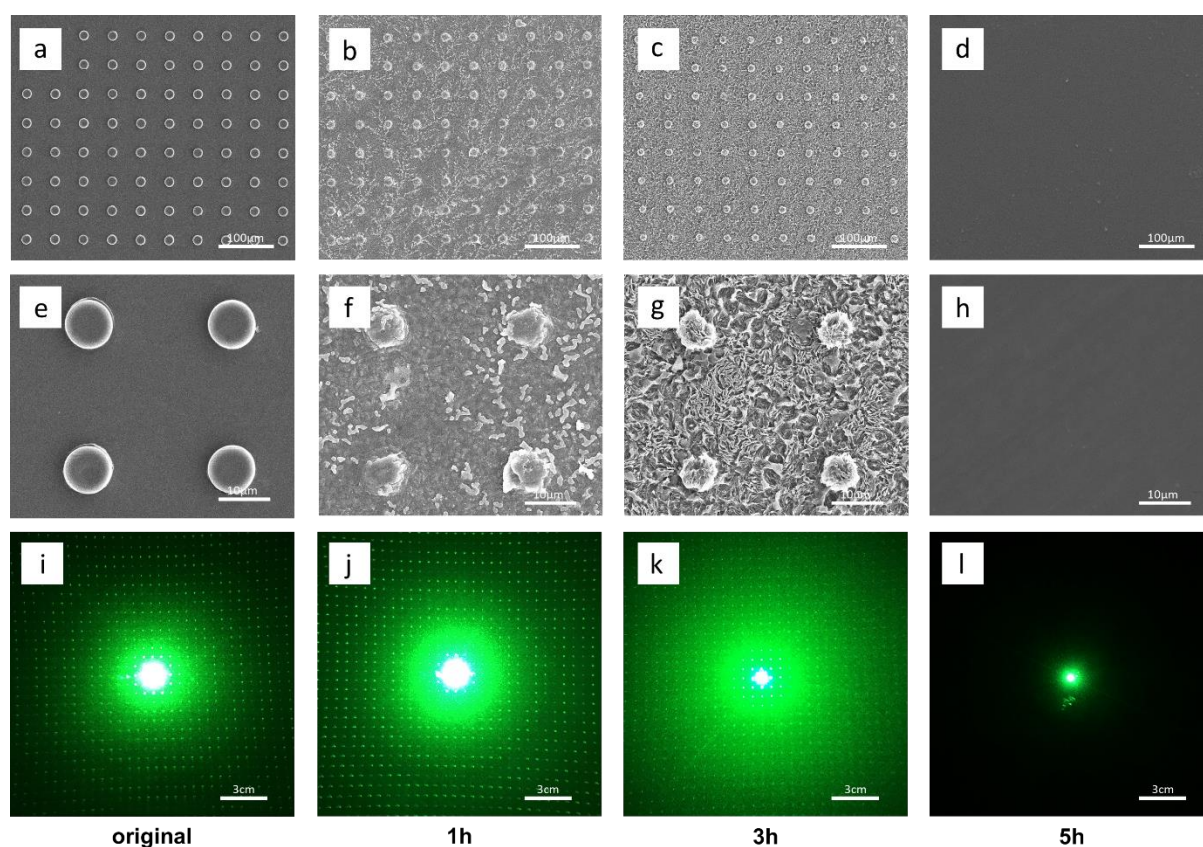


Figure 5.6 SEM images and Fraunhofer laser diffraction patterns of PCL microchambers with different enzymatic degradation times at the lipase PS concentration of 0.5mg/ml. a-c) the SEM and laser diffraction Enzymatic degradation of PCL microchambers. PCL microchambers a,b) After PBS incubation for 5h. c,d) After 1h lipase degradation. e,f) 3h lipase degradation. g,h) 5h lipase degradation.

The main aim of the surface morphology examinations was to observe and confirm the PCL degradation profiles through Lipase PS exposure over time until complete degradation occurred. Moreover, if PCL microchamber array films were illuminated by laser light when incubated with specific enzymes, the biodegradation behaviours of the film could be

monitored based on the variations of Fraunhofer diffraction patterns due to the changes of the periodical structure of microchamber arrays by enzymatic degradation. Since light is a highly sensitive parameter, the existence and variations of PCL microchamber arrays can be precisely detected by Fraunhofer diffraction patterns. Therefore, this system can be used as an “enzyme sensor” base on the existence of the laser scattering patterns.

Here, a control sample is chosen for incubation in PBS solutions only for 5 hours whose structure is shown in Figure 5.6 a, e, i). The morphology of the film is complete and smooth without any contaminations, and all the microchambers are arranged periodically with a regular, circular appearance, which led to a periodic and complete laser dot array with a broad range and distinguishable diffraction orders – therefore setting an excellent reference to compare with other lipase-treated samples. After 1-hour of incubation in lipase solution, as shown in Figure 5.6 b, f, j), a multitude of small and shallow fissures emerge on the surface of PCL microchambers which proves that the lipase could interact and degrade the surface PCL microchambers. It is noteworthy to mention that hydrophilic enzymes such as lipase PS are not able to diffuse within imprinted structures made of hydrophobic polymer⁴⁷⁵. Therefore, only the surface of PCL can be subjected to degradation caused by lipase PS. The laser diffraction pattern slightly changed at this stage, and while vaguely visible, the different diffraction orders began to blend and become less distinguished. The laser light was slightly scattered into a blurred area in the centre due to the fissures that appeared on the surface of the film. Further, in Figure 5.6 c, g, k), the specimen exhibits the presence of some small pores on the surface of the microchambers due to broader, deeper fissures forming following 2 hours of lipase degradation. Though the microchambers were not perfectly round and complete, with a rough, broken superficial appearance, the chambers were still arranged into periodical arrays that could form diffraction patterns by laser light. However, the pattern was extremely scattered and blurred because of the roughness of the film surface, leaving only pattern dots without diffraction orders. Finally, after 5 hours of enzymatic degradation process, shown in Figure 5.6 d, h, l), all the PCL microchambers

were hydrolysed and degraded by lipase without leaving any debris. The diffraction patterns were gone, resulting in one laser point at the centre of the image, which is an efficient signal to judge and examine the enzymatic degradation procedures.

5.4. Cargo Encapsulation in PCL and PLA Microchamber Array Films

A variety of cargos can be selected to be loaded into the empty space of the microwells, followed by a sealing process as cargo encapsulated microchamber array films. Based on the properties of the desired cargos, different drug loading methods can be employed. In this work, two different methods are applied: the solution loading method and the dry loading method. Both methods can load cargos into microwell arrays but have their unique pros and cons.

Typically, the solution loading method for microchamber arrays involves submerging a polymer-precoated PDMS stamp into drug water solutions followed by application of sonication bath for 30 seconds to remove the trapped air bubbles inside microwells,⁴⁷⁰ thus, the drug solution would be trapped inside microwells due to the capillary forces, avoiding the entrapment of air bubbles and facilitate the better encapsulation. Since the applied polymer surface is hydrophobic, the drug solution that was not trapped inside microwells would form water beads with can be easily wiped away with fuzz-free lab wipes after the dipping and sonication procedures. The drug particles or crystals would be successfully precipitated and loaded into microwells after the evaporation of drug solutions, as shown in Figure 5.7. Finally, the precoated film layers loaded with precipitates were sealed and transferred onto a precoated glass slide, forming microchamber arrays with cargo loaded. Before further characterization, the microchamber arrays film need to be incubated in water avoiding any non-trapped cargos. This method is applicable for cargos that are highly soluble in water solutions, otherwise, the loading efficiency would be extremely low as the trapped drug solution only contain minor drug content. In practice, however, some of the

drugs may have low water solubility or even insoluble in water solutions which place limitations on the application of such a method.

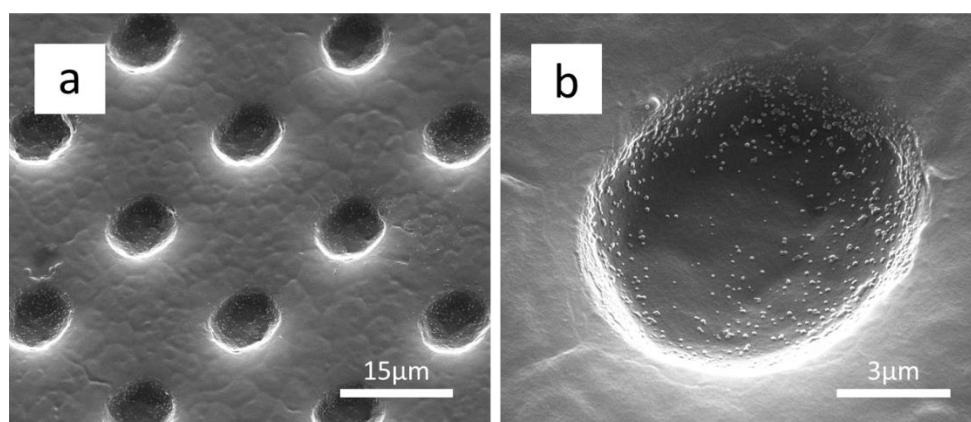


Figure 5.7 SEM of 5(6)-carboxyfluorescein dye precipitates loaded in microwells with solution method. a) CF precipitates on PDMS precoated with a layer of PLA film. b) Higher magnification of a).

Another facile method for loading drugs into microchamber array films was the dry loading method, demonstrated by spreading milled dry powders on the top of a precoated PDMS stamp which has been performed a single dip into polymer solutions. It is noteworthy to address that before the loading process, the drug powders had to be milled, crushed, and ground into particles of submicron size, as shown in Figure 5.8. After sweeping and removing the excess crystals from the surface with wet fuzz-free lab wipes, the drug particles would be physically trapped in microwells with a large amount. Since this special method that the overwhelming majority of non-trapped particles outside microwells are swept away and can be reused for next time, the drug loading efficiency is relatively high. After microcontact printing into microchamber films, the samples were incubated into 0.01M PBS solution at 37°C for 2 hours in order to rinse off the residue and non-encapsulated dyes. After that, the specimens were washed and cleaned with DI water, dried for further treatment and characterization. The primary limitation of such a method would be that only polymer films with smooth surfaces could be utilized, otherwise, the particles would be trapped on the polymer surface fissures making it difficult to sweep away as demonstrated in Figure 5.11. Nonetheless, it can expand the types of packageable drugs when combined with the solution loading method mentioned above.

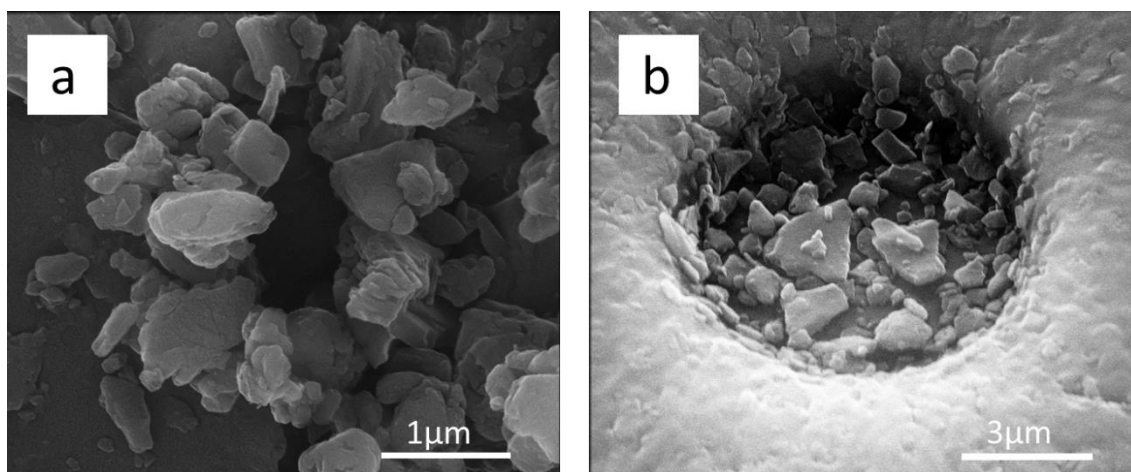


Figure 5.8 SEM of 5(6)-carboxyfluorescein dye particles loading into microwells in the dry method. a) Submicron size milled CF particles. b) Submicron size dye particles loaded into microwells of pre-coated PCL-PLA (1:2) patterned PDMS stamp. The diameter of each microwell is 10 μ m.

5.4.1. Encapsulation of BSA-FITC

BSA-FITC was selected as a model drug for enzymatic degradation release. Simply dipping PDMS stamp pre-coated with PCL film into BSA-FITC water solution and sonicating for 30 seconds. Then, wait for the water solution to dries in the air after cleaning the dye solution on the top of the film. The BSA-FITC solution would be trapped inside microwells due to the capillary effect leaving small precipitates there, as shown in Figure 5.9.

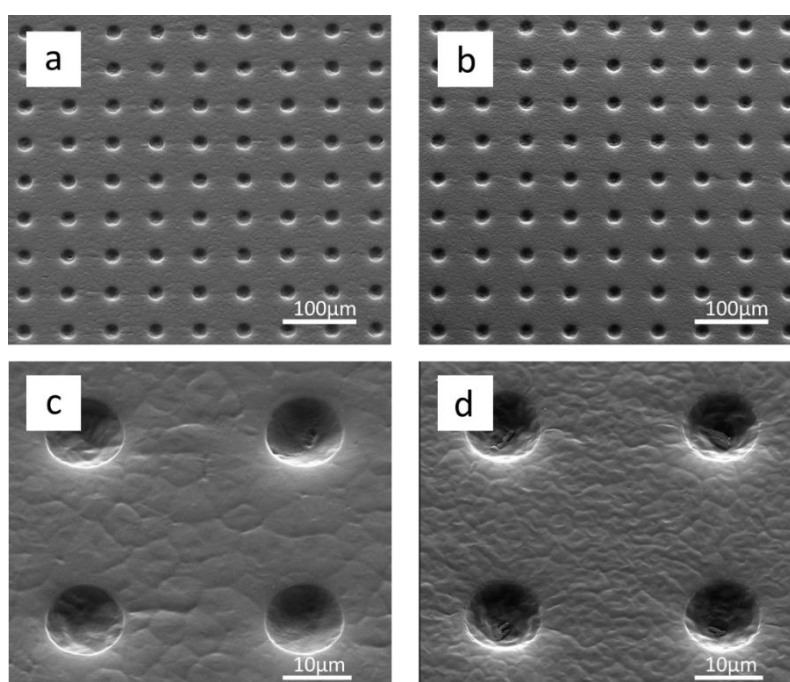


Figure 5.9 SEM images of trapped BSA-FITC in PCL microwells. a,d) SEM images of PCL pre-coated PDMS stamp before BSA-FITC loading. b,e) SEM images of PCL pre-coated PDMS stamp after loading BSA-FITC.

The success of encapsulation was checked with the confocal laser scanning microscope shown in Figure 5.10. Green colour emerged inside PCL microchambers and located in each microchamber position. Since the loading amount of BSA-FITC in each microchambers could not be controlled, the green colour distribution was inhomogeneous.

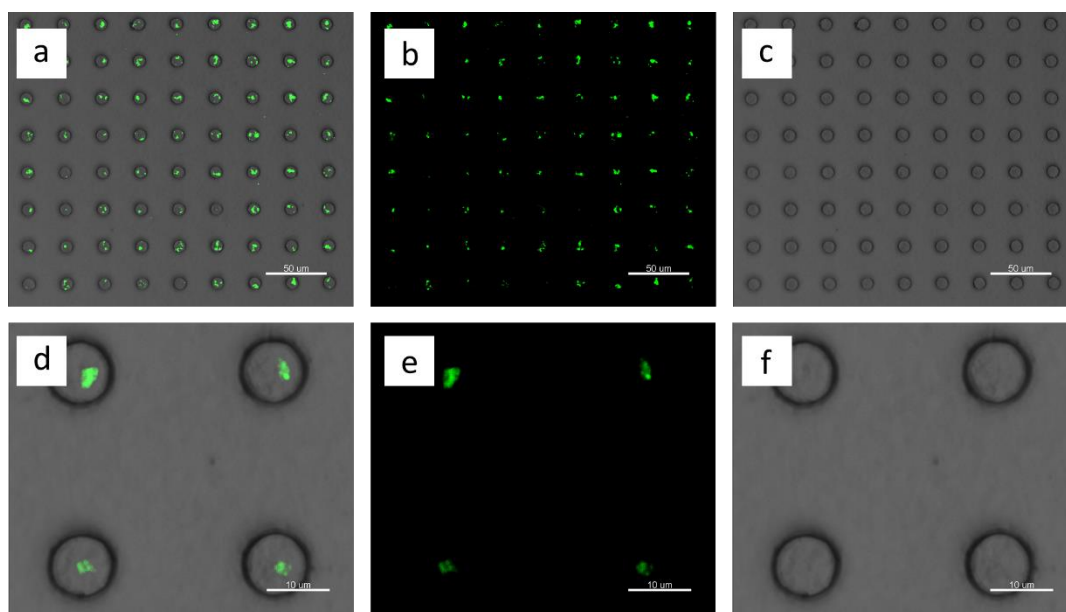


Figure 5.10 CLSM images of BSA-FITC encapsulated in PCL microchamber array films. a,d) Overlapping channel. b,e) Fluorescent channel. c,f) Bright field channel.

5.4.2. Encapsulation of CF

Typically, the drug loading method for microchamber arrays involves submerging a precoated PDMS stamp into drug water solutions followed by the application of sonication to remove air bubbles.⁴⁷⁰ In practice, however, some of the drugs may have low water solubility or even insoluble in water solutions which place limitations on the application of such a method.

Specifically, the solution loading method can be a preferable way to load highly water-soluble cargos whose properties would not change before and after the dissolution procedures and not react with water. If cargo is semi-soluble, only a small amount of can be precipitated leading to a low encapsulation efficiency. Also, the microwells should be deep enough to allow the capillary force to trap cargo solution. While the dry loading method

can overcome some of the drawbacks of solution loading methods as the encapsulated in conducted in dry state without considering the solubility. However, the spreading procedures of the dry method require a smooth polymer film surface to facilitate the removal of non-trapped particles. Besides, the dry method can hardly load cargos that cannot be milled into the desired size like branches structured proteins. In practice, the selection of the method to load cargos into microchamber arrays need to be considered in terms of the physicochemical properties of the drug.

Here, another facile method of dry powder loading method for loading drugs was introduced, demonstrating that by spreading milled dry powders on the top of a precoated PDMS stamp, after sweeping the surface, the microparticles would be trapped in microwells with a large amount. Because of this special method that the overwhelming majority of non-trapped particles outside microwells are swept away and can be reused for next time, it is inaccurate to calculate the loading efficiency. But ultimately, all the drug crystals can be used and loaded into microwells, indicating a fully used of drugs. One of the largest advantages of this technique is the ignorance of the solubility of drugs. Besides, the loading processes are also time-saving as the drug crystals were physically trapped into microwells without solvent evaporations. While the primary limitation of such a method would be that only polymer films with smooth surfaces could be utilized, otherwise, the particles would be difficult to sweep away as demonstrated in Figure 5.11. Nonetheless, it can expand the types of packageable drugs when combined with the solution loading method above.

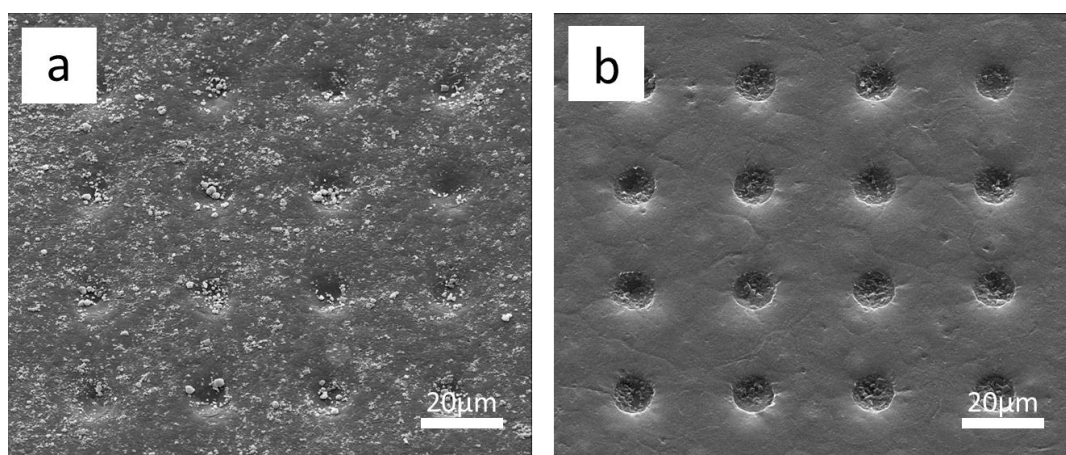


Figure 5.11 SEM images of a layer of PCL film of different surface roughness on PDMS stamp after loading CF particle with dry powder loading method. a) PCL polymer layer formed with acetone as solvent. The CF particles are distributed both inside microwells and film surface which are unlikely to be swept away due to the rough surface. b) PCL polymer layer formed with chloroform as solvent. The CF particles only trapped inside microwells since the surface is smoother.

CF, a small and hydrophilic fluorescent dye, was selected as a model drug to be encapsulated in microchamber arrays enabling a direct and simple tracing purpose. Although it is feasible to load CF with a solution loading method³³³, the encapsulation is inefficient due to the low solubility of CF. Therefore, the encapsulation of CF was achieved in the dry method by spreading submicron powder particles on the top of the PDMS stamp precoated with PCL polymer films.

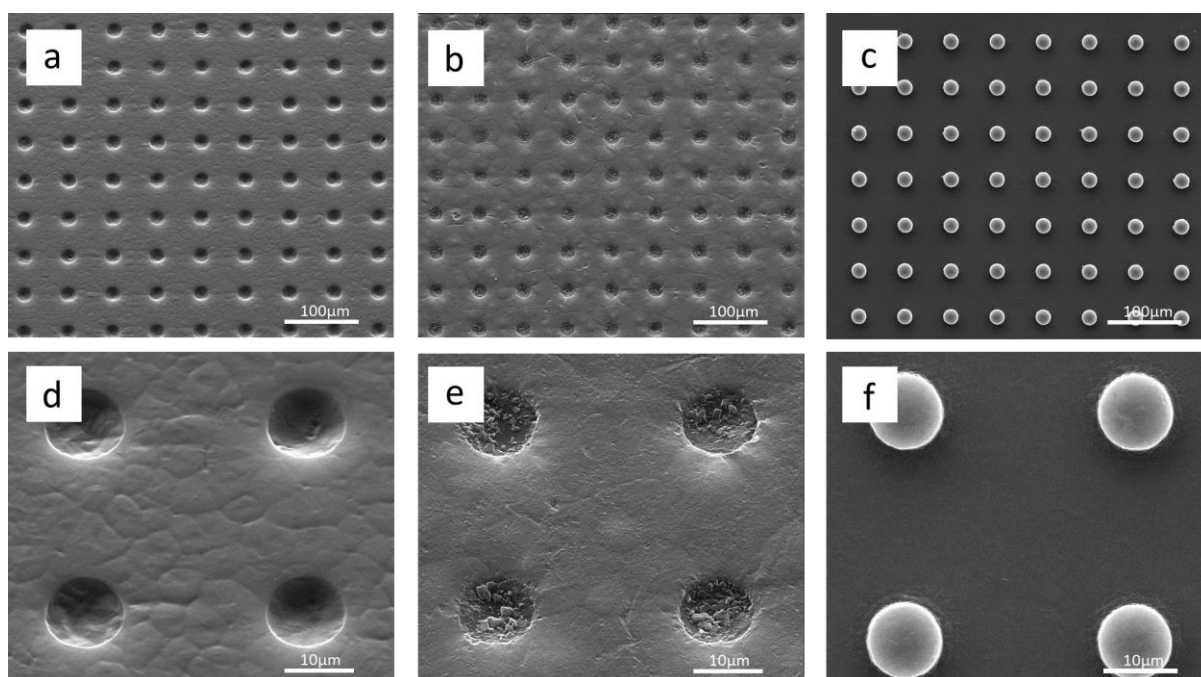


Figure 5.12 Encapsulation of 5(6)-CF in PCL microchamber arrays. a,d) SEM images of precoated PDMS stamp before loading. b,e) SEM images of precoated PDMS stamp after loading 5(6)-CF dye particles. c,f) SEM images of PCL microchamber arrays loaded with 5(6)-CF dye particles after sealing and printing.

SEM was used to observe the encapsulation procedures and the results were shown in Figure 5.12. By comparing microwells on the precoated PDMS stamp before and after spreading, it can be easily identified that the dye particles were loaded into microwells of high efficiency leaving a clean and smooth surface. Then, after sealing and printing was performed, the morphology of dye-loaded PCL microchamber arrays were observed

demonstrating perfectly round-shape microchambers arranged on the smooth and clean film surface. The cross-section of the PCL microchamber was characterized with FIB-SEM, whose results proved the empty structure inside the chamber with the wall thickness was around 2.3 μm as demonstrated in Figure 5.20. However, SEM was not able to view and prove the particles were encapsulated inside microchambers. In order to confirm the encapsulation of dye particles after fabricating PCL microchamber arrays, CLSM was used to view the dyes, with the results presented in Figure 5.13.

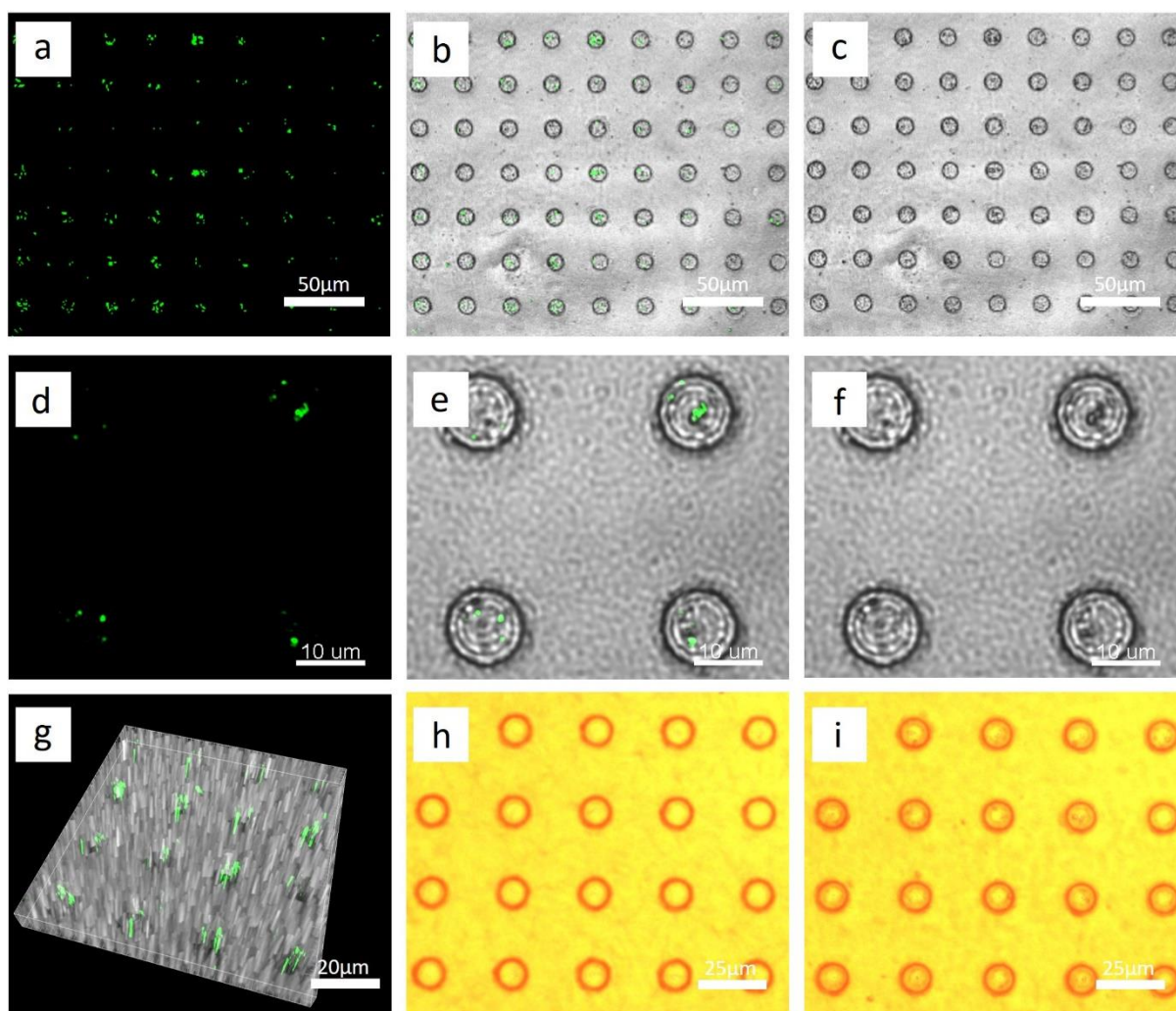


Figure 5.13 PCL microchamber arrays encapsulating 5,6-carboxyfluorescein inside microchambers. a-f) CLSM images of dye particles in PCL microchamber arrays. g) 3D view of dye distribution. h) optical microscope image of PCL microchamber arrays before dye loading. i) optical microscope image of PCL microchamber arrays after dye loading.

CLSM images in Figure 5.13 illustrates that dye particles were accommodated inside each microchambers. Here, the dark colour inside microchambers of the bright field

represents dye crystals as shown in Figure 5.13 c) and f). Moreover, as demonstrated in Figure 5.13 h) and i), the housed dye particles can also be observed as dark spots at the position of microchambers by comparing through optical microscopy analysis before and after encapsulation. Therefore, it has been confirmed that dye microparticles were successfully encapsulated inside microchamber arrays.

After confirming the encapsulation of dyes, the sample film was incubated in PBS solution to confirm whether microchamber arrays were leaky. As reported almost 75% of the encapsulated dyes were diffused out with a fast rate in the first 30 minutes (the diffusion curve is given in Figure 5.14). The overall amount of encapsulated dye amount may vary from 0.8 μ g to 1.2 μ g, but the general release kinetic was similar. There would be about 5% measurement error for determine the concentration. Therefore, the leakage of PCL microchamber arrays makes it problematic to retain CF inside the chambers at explored condition. This problem is crucial, and the leakage has to be reduced.

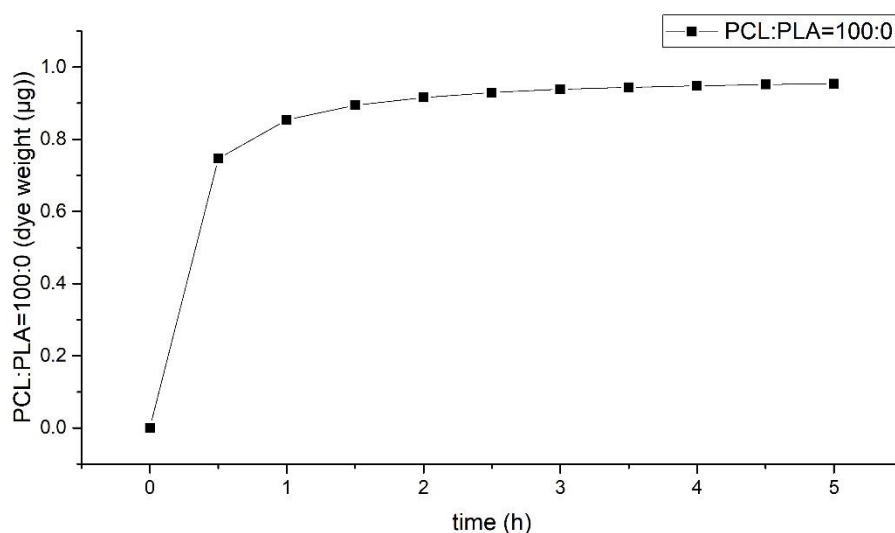


Figure 5.14 Dye diffusion curve of PCL microchamber arrays encapsulated with 5(6)-carboxyfluorescein. Almost 75% of loaded dyes were leaked in the first 30 mins, indicating that PCL film could not prevent the leakage of small molecule dyes.

5.4.3. Encapsulation of DEX

Dexamethasone (DEX) is one type of the glucocorticoids that can be used for anti-inflammatory and analgesic treatments in musculoskeletal diseases,⁴⁷⁶ and has been also widely delivered for the treatment of arthritis.⁴⁷⁷ DEX has a very low solubility in water, thus can hardly be loaded in drug delivery vehicles using common solution loaded methods. The dry loading techniques proposed can be one of the feasible ways to load DEX, with the results can be found in Figure 5.15.

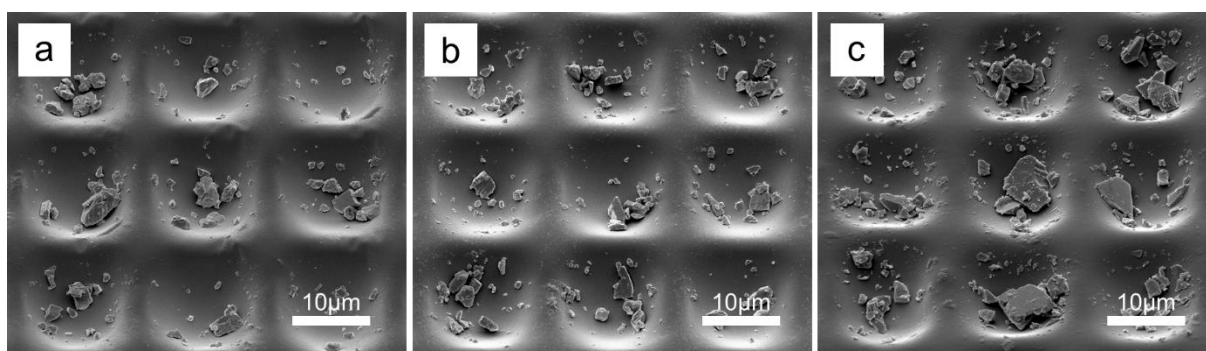


Figure 5.15 The SEM images of dexamethasone crystals loaded on PDMS stamp coated with PLA thin layers from different concentration of PLA chloroform solutions. a) 2%; b) 1.75%; c) 1.5%

As Figure 5.15 a) shows, DEX crystals can be successfully loaded onto PLA precoated PDMS stamp, though the loaded capacity was relatively low. Moreover, with the decrease of the concentration of PLA solutions (Figure 5.15 b) and c)), the thickness of PLA films layers coated on PDMS stamp tend to be thinner, leaving more space to be occupied by drug crystals. However, even in the lowest concentration of 1.5% PLA group, there were still many space left in the microwells. It is inferred that the crystals were too large to be loaded in microwells and would be removed in the last surface cleaning steps. Therefore, the DEX crystals were broken into smaller pieces with homogenizer (Bertin) for multiple times, with the results shown in Figure 5.16.

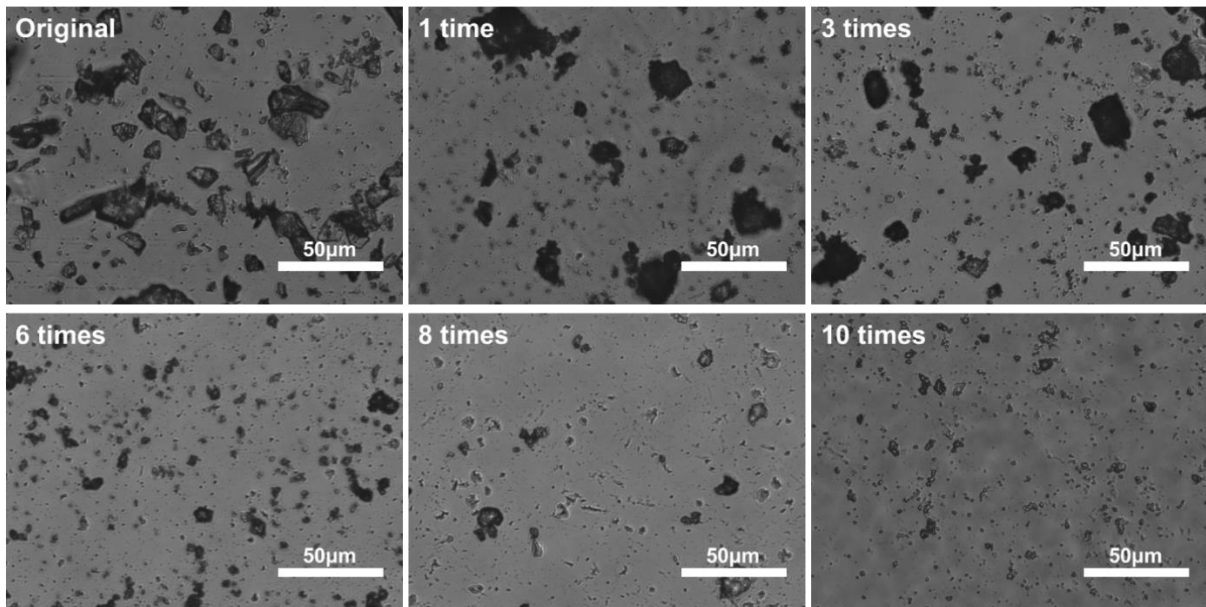


Figure 5.16 The optical images of dexamethasone crystals after homogenizing for different times. At each time, the drug crystals were homogenized at 5000 cycle/min for 30 seconds.

As expected, with the increased time of homogenizing, the smaller size drug crystals take more proportion as large blocks were smashed into smaller. Significant differences can be found when comparing the DEX crystals homogenized for 10 times with untreated DEX crystals (Figure 5.19). The homogenized DEX crystals were again loaded onto 1.5% PLA precoated PDMS stamp, with the SEM results shown in Figure 5.20.

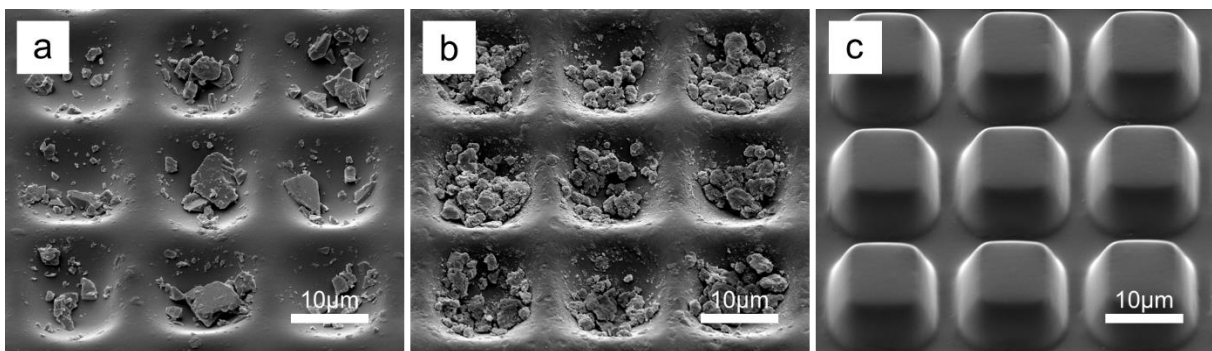


Figure 5.17 SEM images of dexamethasone loaded into microwells and after sealing and transferring as microchamber array films. a) DEX without homogenize loaded onto 1.5% PLA precoated PDMS stamp. b) DEX after 10 times homogenize loaded onto 1.5% PLA precoated PDMS stamp. c) homogenized DEX loaded and printed into microchamber array films.

Compared with loading with non-homogenized DEX crystals (Figure 5.17 a)), the PLA microwell arrays can load significant higher amount of homogenized DEX particles with less non-occupied space in microwells as demonstrated in Figure 5.17 b), though the DEX

amount in each microwell still varies. Besides, Figure 5.17 c) showed the morphology of Figure 5.17 b) after sealing and transferring into PLA microchamber array films can still remain complete and intact even loading higher amount of drugs. It is noteworthy to address that although the drug crystal amount varies a lot among individual microwells and it is of great importance to have a uniformed drug loading amount, these drug differences would be alleviated once considering the large number of microwell arrays.

5.5. Encapsulation of Small and Hydrophilic Cargos in PCL-PLA Microwell Arrays

Poly(lactic acid)(PLA)⁴⁷⁸, an FDA approved aliphatic polymer⁷², possesses a lower water vapour permeability than poly(caprolactone) (PCL), and thus was selected here to blend with PCL for encapsulation of small molecule weight hydrophilic cargos into microchamber films. In order to determine the optimal blend ratio for encapsulation, PCL-PLA samples with different blend ratios were prepared and incubated in PBS whose diffusion behaviours were demonstrated in Figure 5.18. The encapsulated amount of dye crystals may have 10% - 15% variation. And there would be about 5% measurement error for determine the concentration. However, the general trend that higher the PCL ratio, faster the release rate would still hold.

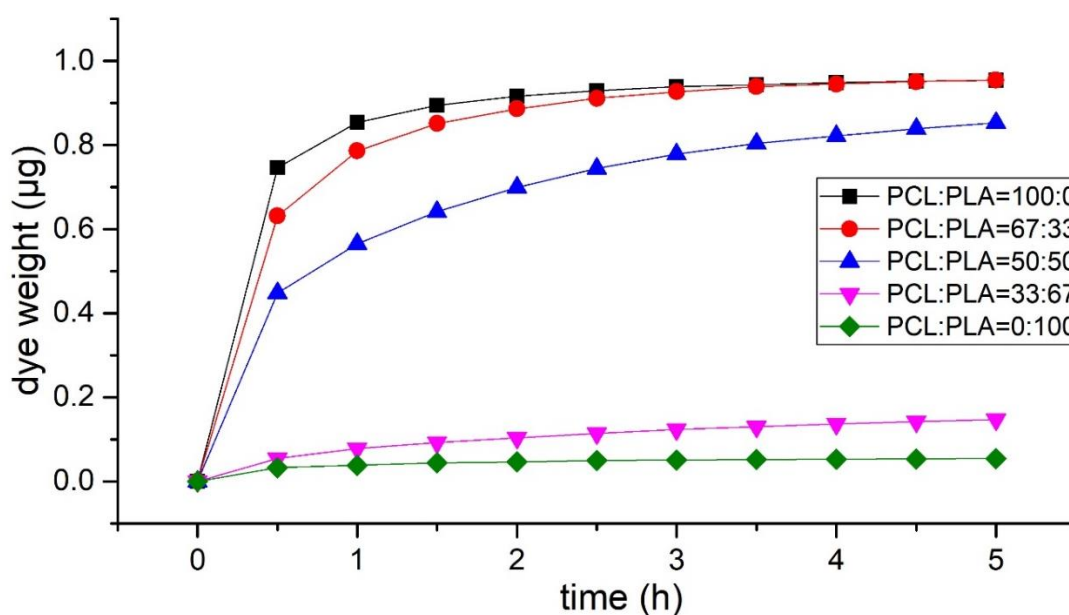


Figure 5.18 The diffusion curve of PCL blend with PLA in different ratios in PBS.

For PCL content ratio of 100% and 67%, most of the encapsulated dye molecules were diffused out in the initial 30 minutes of incubation in PBS. While the diffusion rate declined for 50% PCL that only around half of the loaded cargos were released in the first half an hour following by a steady release (Figure 6). Interestingly, increasing the PLA content to 67% with 33% PCL content, the diffusion rate drops significantly, demonstrating an excellent retention ability. Based on the diffusion curve, PLA was an excellent choice to prepare microchamber arrays for encapsulating small hydrophobic molecules. Therefore, it is evident that the diffusion rate of PCL decreased with the addition of PLA content, indicating that PLA is feasible to reduce the permeability of PCL film and PCL-PLA (1:2) is an excellent blend ratio for encapsulation and controlled release. With the same encapsulating method, the small molecular hydrophilic dye CF particles were successfully loaded into PCL-PLA (1:2) microchamber arrays in the form of crystals in a large proportion which has been confirmed by SEM, as demonstrated in Figure 5.19.

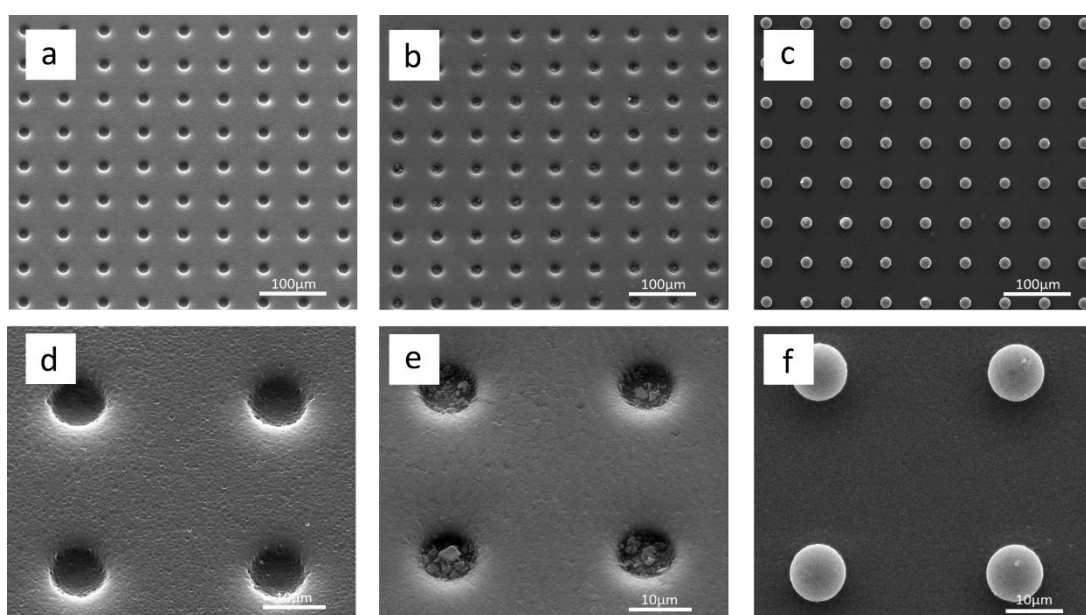


Figure 5.19 Encapsulation of 5(6)-CF in PCL-PLA (1:2) microchamber arrays. a,d) SEM images of pre-coated PDMS stamp before loading. b,e) SEM images of pre-coated PDMS stamp after loading 5(6)-CF dye particles. c,f) SEM images of PCL-PLA (1:2) microchamber arrays loaded with 5(6)-CF dye particles after sealing and printing.

Though both PCL and PCL-PLA blending polymer can form thin layer on the PDMS stamp, compared with PCL thin film coated on PDSM stamp in Figure 5.12, some

morphology differences can be observed for PCL-PLA(1:2) film. As PCL a semicrystalline polyester, the spherulite structure can be observed on the film surface. In addition, the microwells formed on the PDMS stamp demonstrate a shallow structure with less space for drug loading, thus having less loading capacity (Figure 5.12). After blending with PLA, not only the water permeability of the thin film was decreased, but also the crystalline region was decreased. Based on the SEM results of PCL-PLA(1:2), as shown in Figure 5.19, the spherulite crystalline structure of PCL can not be observed. Besides, more space was formed for each microwell of PCL-PLA thin layer, where more drug crystals can be loaded, leading to a high loading capacity.

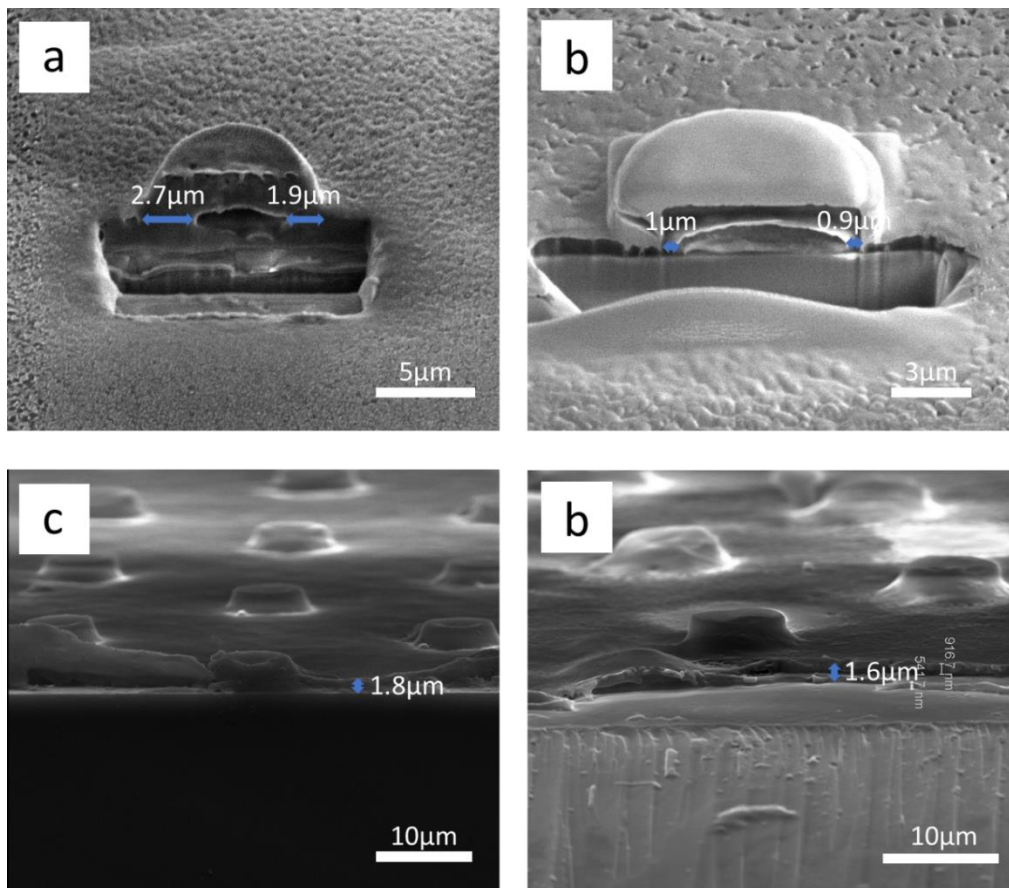


Figure 5.20 The wall thickness of microchambers and film thickness of microchamber array films of different polymers. a) FIB-SEM image of the wall thickness of PCL microchamber is about 2.3 μm . b) FIB-SEM image of the wall thickness of PCL-PLA (1:2) microchamber is about 1 μm . c) The thickness of the PCL microchamber array film is about 1.8 μm . d) The thickness of the PCL-PLA (1:2) microchamber array film is about 1.6 μm .

Besides, the wall thickness as well as the film thickness of microchamber array films made of both PCL and PCL-PLA (1:2) blended polymer was characterized by using FIB-SEM to conduct the cross-section measurement, and by using SEM to observe the cross-section part achieved by freezing cut the film in liquid nitrogen, respectively. Figure 5.20 a) and b) showed that the wall thickness was about 2.3 μm for PCL microchambers, 1 μm for PCL-PLA blended microchambers. While the film thickness of microchamber array films made of PCL and PCL-PLA blended polymer was 1.8 μm and 1.6 μm , respectively.

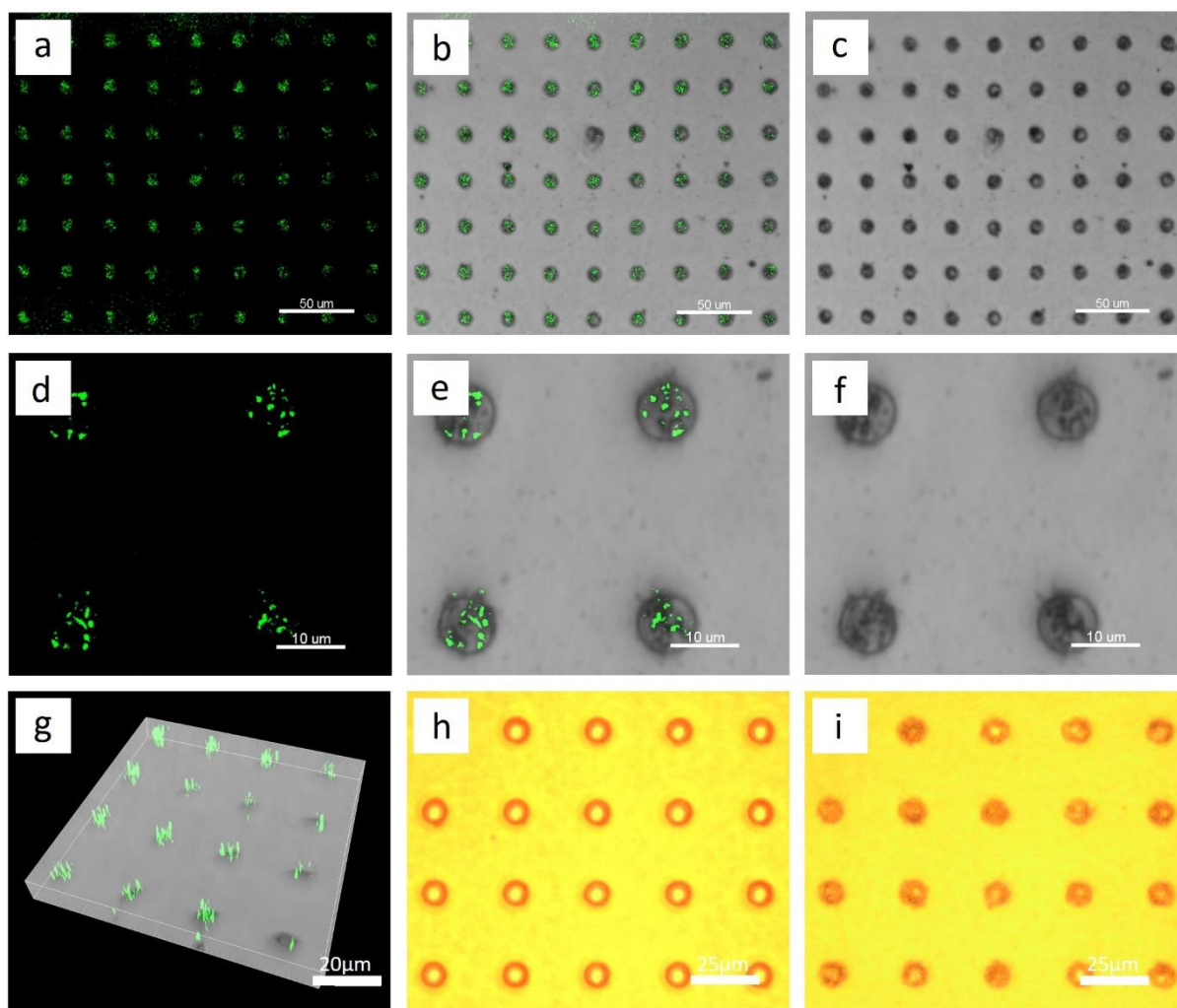


Figure 5.21 PCL-PLA (1:2) microchamber arrays encapsulating CF particles inside microchambers. a-f) CLSM images of dye particles in microchamber arrays. g) 3D view of dye distribution. h) optical microscope image of PCL-PLA (1:2) microchamber arrays before dye loading. i) optical microscope image of PCL-PLA (1:2) microchamber arrays after dye loading.

Figure 5.21 shows the CLSM images of printed PCL-PLA (1:2) microchambers with encapsulated fluorescent dyes, which had been submerged in PBS solutions for more than

2 hours what indicates that the CF dyes are not in contact with solutions. Otherwise, the CF crystals would dissolve immediately. Therefore, the PCL-PLA microchamber arrays can be used to retain small hydrophilic molecules.

5.6. Enzymatic Release Behaviours of PCL-PLA (1:2) Microchamber Arrays

The encapsulated PCL-PLA (1:2) microchamber arrays were used to conduct enzymatic degradation release experiments. In order to provide fixed and optimal pH, temperature and ionic strength conditions, all the enzymatic degradation procedures were processed in 0.01 M PBS solutions at 37°C. Both the PCL and PCL-PLA microchamber films with a size of 1 cm² were submerged into 3 ml PBS solutions containing lipase PS solutions of 0.05 mg/ml, 0.1 mg/ml, 0.25 mg/ml as well as 0.5 mg/ml, while a controlled group using PBS only was set for comparison. All the Petri dishes were maintained at 37°C in the climate chamber and took out for pattern imaging periodically without separating and drying microchamber films. The results of the enzymatic degradation release experiments were shown in Figure 5.22.

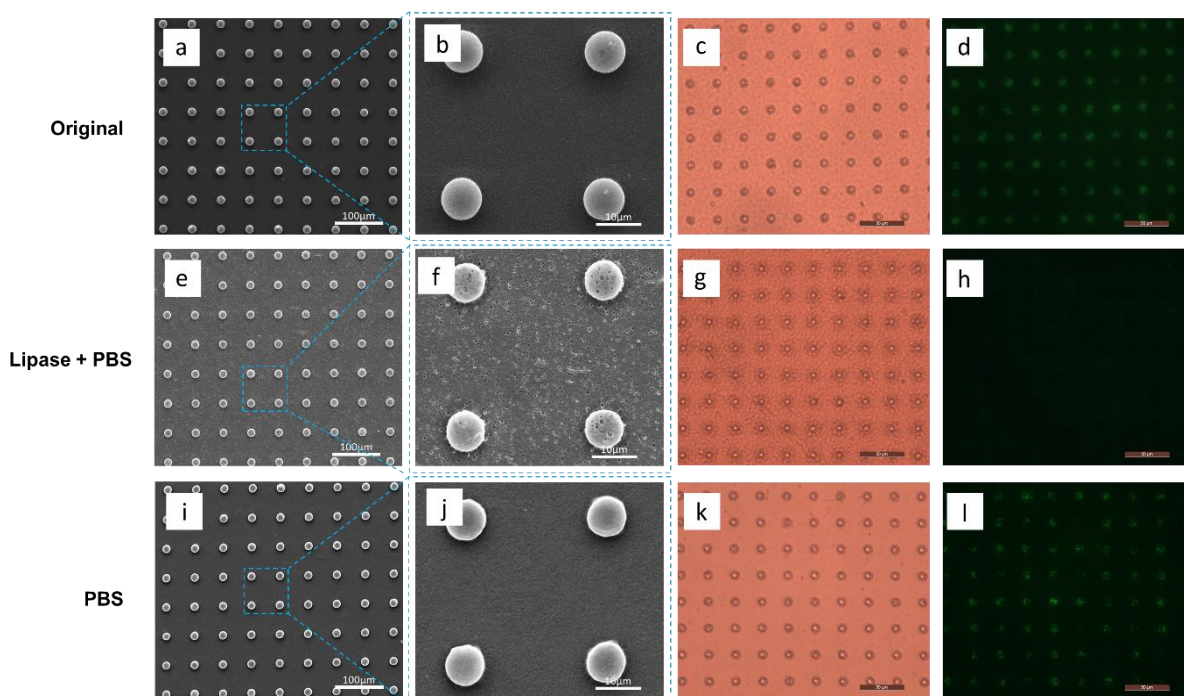


Figure 5.22 Enzymatic degradation of PCL-PLA (1:2) microchambers loaded with dyes. a-d) PCL-PLA (1:2) microchambers after encapsulating 5,6-CF. e-h) PCL-PLA (1:2) microchambers after 26h 0.5 mg/ml lipase solution incubation. i-l) PCL-PLA (1:2) microchambers after 26h incubation with PBS.

Here, SEM was used for observation and comparison of PCL-PLA (1:2) morphologies before and after enzymatic degradation. Also, fluorescent microscopy was applied to confirm the existence of CF dyes. As demonstrated in Figure 5.22 a-d), the surface of the as-prepared PCL-PLA (1:2) film was smooth and flat with periodic and perfectly circular microchambers which were fully loaded with dye particles. Figure 5.22 e) and f) shows 26 hours of incubation in lipase solution, where clear surface morphological changes are present with a significant appearance of holes both on the top of PCL-PLA (1:2) film and the microchambers. It is concluded that the microchambers were opened resulting in the release of the encapsulated CF dyes. The reason for the existence of holes might due to the different affinity of PCL and PLA to the solvent chloroform. As a result, the blended mixture produces a two-phase structure forming a macroscopically inhomogeneous system in which the PCL phase dispersed into PLA phase⁴⁷⁹ and had been fully degraded by lipase, leaving the hole-like structure distributed in previously filled regions of PCL (see Figure 7e,f).

Moreover, the corresponding fluorescent microscopy images (Figure 5.22 g) and h)) demonstrated that the CF dyes were all released leaving no green colour in the position of each microchamber. Nevertheless, for the control group shown in Figure 5.22 i-l), after 26 hours of incubation in PBS solution without lipase, the morphology of PCL-PLA (1:2) microchamber films was still as intact and complete as before incubation with most of the dye particles encapsulated inside microchambers.

Compared to the degradation of pure PCL microchambers (5 hours to fully degrade), the PCL content of PCL-PLA (1:2) microchamber arrays required more prolonged exposure to lipase for complete degradation and thus release of the encapsulated cargos (Figure 5.23 shown until 26 hours). Since the PCL was not homogeneously degraded and lipase can only interact with the surface of PCL polymer, not all of the microchambers were degraded and opened at the same time to allow for sustained cargo release. Here, the maximum rate of dye release was achieved during the second hour of lipase exposure. By

diluting the polymer solution, it is possible to obtain thinner microchamber wall thickness and accelerate the release rate, but the number of cargos encapsulated inside is unlikely to remain constant which would influence the further comparison. Therefore, the polymer solution concentration and microchamber wall thickness were fixed here to provide a representative enzymatic cargo release curve.

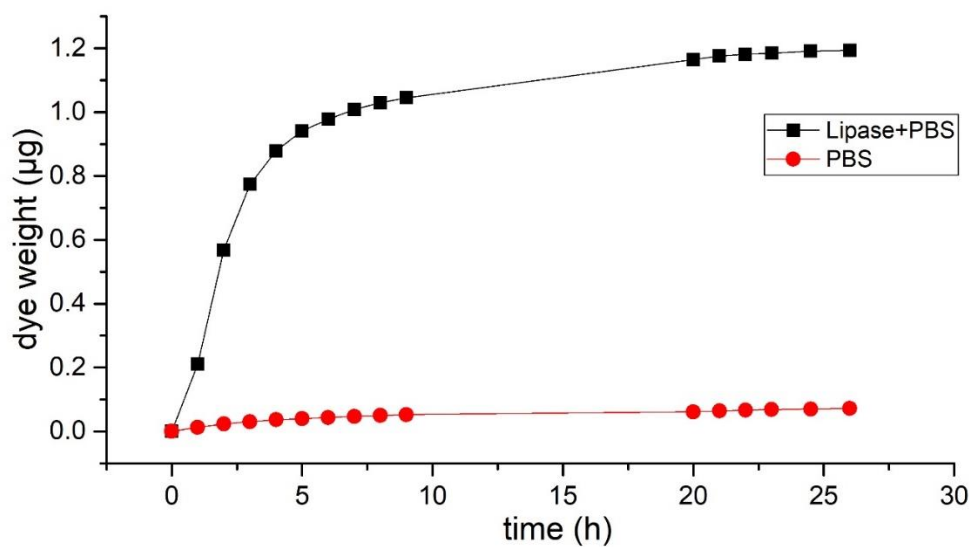


Figure 5.23 The enzymatic dye release curve of PCL-PLA (1:2) microchambers. The degradation is conducted at a lipase concentration of 0.5 mg/ml in PBS solutions at 37°C.

Based on the dye release curve presented in Figure 5.23, it is easily observed that overall approximately 1.2 µg CF dyes were encapsulated into microchambers of 1 cm² surface area. It is noteworthy to address that in the first 5 hours, almost 80% of encapsulated dyes were enzymatically released. However, the overall quantity of dye release can be attributed to both diffusion and degradation processes. Since the amount of dye released in the controlled group is about 0.07 µg, it is calculated that 5.8% of dyes were diffused out without degradation of lipase after 26 hours incubation, proving that the microchambers are well-sealed and protected. After several repetitions, it is calculated that the loading cargo variations in 1.2% PCL-PLA (1:2) microchamber array films are about 1.15 ± 0.3 µg per sample. Considering the period of microchamber arrays are 30 µm, and the size of the microchamber film sample is 1 cm², it can also be calculated that each

microchamber is able to incorporate 10.35 ± 0.27 pg dye particles or 1.15 ± 0.3 $\mu\text{g} / \text{cm}^2$ indicating that a great amount of cargos are encapsulated in microchamber array films. The release experiment may have 5% - 10% measurement error. However the phenomenon of slow release of PLA microchamber array films and enzymatically release of PLA microchamber films are stable and reproducible.

5.7. Conclusions

Microchamber array films made of blended biodegradable polymers (PCL and PLA in various ratios) can be designed and fabricated efficiently by dipping a patterned PDMS stamp into a polymer solution and sealing with polymer monolayer on glass via microcontact printing methods. Microchamber arrays made of pure PCL are enzymatically degradable by lipase PS at a concentration of 0.5 mg/ml within 5 hours of exposure. With the decrease in lipase concentration, the degradation time becomes prolonged. Furthermore, the alterations in the degradation procedure of PCL microchamber arrays can also be conveniently and real-time checked with directed laser light forming the Fraunhofer diffraction patterns. Thus, based on the time of full degradation time and the disappearance of laser diffraction patterns, the biodegradation of PCL microchamber film can be served as an “enzyme sensor” and not only can recognise the specific enzyme, but also react to the enzyme of various concentrations differently. While blending PLA with PCL helps to decrease the permeability of PCL film, microchamber arrays consisted of PCL-PLA (1:2 ratio correspondingly) blended polymers can retain encapsulated small hydrophilic molecules such as CF with a controlling release triggered through lipase catalysis. In addition, in terms of the results of the enzymatic degradation dye release curve, it is calculated that about 11 pg of CF dye crystals were loaded into individual microchambers of 1 cm^2 surface area, indicating that the microchamber array films can accommodate model bioactive compound in a highly efficient way. In conclusion, microchamber array films made of biodegradable polymers provide a novel approach to encapsulate and enzymatically driven the release of small hydrophilic drugs, enabling applications in

biochemically induced reaction and controlled drug delivery, such as implant coating and catalyst-controlled release.

It is noteworthy to mention that the size and period of microchamber arrays can vary in terms of the specification of PDMS whose resolution limit is in the range of 100 - 200 nm⁴⁷³. Therefore, the technology of microchamber arrays made of biodegradable polymers and their blends pave a way to broaden the perspectives in entrapping and sustain the release of biologically active molecules at specific locations, thus prolonging the release time and enhancing pharmacological efficiency. Through the alteration of the specific biodegradable polymer composition, the release of encapsulated cargos can be triggered under the catalysis of different enzymes. Moreover, should drug loading be unnecessary, the microchamber arrays can serve the purpose of enzyme sensing based on laser Fraunhofer diffraction patterns as a promising application that enables the possibility to sensitively detect the presence of different digestible enzymes.

Though the practical applications are still unclear, the biodegradable microchamber array films are still one of the promising two dimension drug delivery vehicles due to its excellent capabilities of loading drugs either in solution or directly in solid crystals and can be controlled release with enzymes. However, these promising properties are limited by its inherent two dimensional structure to be expanded in wider medical areas. Fortunately, this can be overcome by separating the microchamber arrays into individual microcapsules, which was further introduced in chapter 6. Another challenging problem is the encapsulation amount in each microwells. Although the empty space in microwells were almost the same, the amount of drug crystals loaded in can not be constant, as some empty space of the microwells were not fully occupied by the drug. This occasion can not be avoided, but can be alleviated by loading drug crystals multiple times to guarantee the microwells are occupied as much as possible. The quantitative analysis of this method needs to be further tested and analyzed.

6. Biodegradable Microcages for Dye/Drug Encapsulation and Release

6.1. Introduction

Microcapsules, as microscale particles possessing inner hollow structures, have received numerous interests in the field of drug delivery,⁴⁸⁰ sensing,⁴⁸¹ bioimaging,⁴⁸² microreactors,⁴⁸³ cosmetics⁴⁸⁴ and so forth. One of the most important applications of microcapsules is drug delivery vehicles which can provide a range of advantages including protecting the encapsulated cargos from unfavourable environmental conditions, controlling their release profiles on demand, improving drug stability and bioavailability and reducing the biological side-effects.^{57,485,486} Practically, the therapeutic efficacy is not only determined by the function of the drug itself, but also influenced by the involved methods and materials for delivering the drug.⁴⁸⁷ Therefore, compared with non-biodegradable polymers, biopolymers are more attractive candidates for preparing drug delivery vehicles since the side-effect as well as undesired toxicity in the living system can be significantly minimized thanks to their excellent biocompatibility and biodegradability.⁴⁸⁸

In order to achieve preparing biodegradable drug delivery vehicles for biomedical applications, a variety of novel micro-encapsulation techniques have been developed. For example, the layer-by-layer (LbL) self-assembly approach has been confirmed as one of the most powerful methods to synthesis drug delivery vehicles,^{40,41} where microcapsule shells were formed on various micro/nanoparticles through alternate deposition of oppositely charged materials driven by electrostatic interactions followed with the removal of sacrificial core template. Thus, it is feasible to design biodegradable microcapsules based on the versatile LbL technique.⁴⁸⁹ However, the assembled microcapsules can only manage to encapsulate cargos of high molecular weight²⁷ or small but hydrophobic molecules,²⁸ due to the semi-permeability of multilayer shell.^{30,44} Since the molecular weight

of most biologically active molecules is under 500 Da,³¹ it is of great importance to overcome the challenge of small and hydrophilic cargo encapsulation and release.

Another common method for preparing microcapsules is bulk emulsification techniques. Generally, an emulsion is a dispersion of droplets of one liquid, which exceeds the usual size limits of colloid, in another completely immiscible liquid.⁴² The droplets, stabilized by additional surfactant, can be further emulsified in other liquid phases, forming double and even multiple emulsions when combined with solvent evaporation techniques.²⁵⁷ By selecting the polymer dissolved in the external phase, biodegradable microcapsules can be achieved via the double emulsification method.⁴⁹⁰ Nevertheless, since the size of the emulsion droplets is significantly dependent on the emulsification device, introduced surfactant as well as the energy applied to the system, both the emulsion droplets and the later formed microcapsules would have poorly uniform size distributions when emulsified with standard batch high-shear mixing methodologies.⁴⁵ As the variation of size distribution and the mean diameter have impacts on the control of particle surface area, which, among other factors, can modulate the drug release behaviours,⁴⁶ a uniformed size distribution of prepared microcapsules is required to facilitate the applications in drug delivery area.

Microfluidic techniques, with the ability to manipulate a small amount of fluids (10^{-9} to 10^{-18} litres) using lithographed channels with dimensions of tens to hundreds of micrometres, have enabled the synthesis and fabrication of monodispersed microcapsules,^{491,492} including biodegradable ones.⁴³ Basically, immiscible liquids are driven through independent microchannels and mixed at the junction where droplets are harvested due to the high sheer forces generated between two immiscible liquid.⁴⁷ The size of the formed droplets are determined by a variety of parameters such as the relative flow rates of two immiscible fluids, the viscosities and interface tension of the fluids, and the dimensions of independent microchannels, which can be carefully adjusted in microfluidic devices.^{493,494} Although the microfluidic method can offer a promising and versatile route to

prepare highly monodispersed microcapsules, the drug-loaded liquid core of the synthesized microcapsules has to be immiscible to shell material phase which puts huge limitations on the selections of active compounds to be encapsulated.

An improved approach for fabricating biodegradable drug delivery vehicles that not only are capable of encapsulating small and hydrophilic molecules in a non-liquid fashion, but also have a uniformed size distribution is therefore of high demand. Basically, the solution for the encapsulation of small and hydrophilic cargos involves the use of both hydrophobic and biodegradable polymers as microcapsule shell, through the exploitation of the characteristic low water permeability that hydrophobic polymers possess.⁵⁹ While the size distribution control can be achieved with template-based methods that homogeneous microstructures are able to be lithographed on the template surfaces by various nanofabrication techniques,⁵ in which the polymers are filled, embedded and confined, resulting in identical particles of the same size and shape of the engraved microstructure.³⁸ Therefore, combining the above two solutions, a novel method of the preparation of a homogeneous biodegradable drug delivery vehicle from a microarray-structured template is presented in this work. Biodegradable polymer here is selected as polylactic acid (PLA) and polycaprolactone (PCL), both of which are aliphatic and hydrophobic polymers with numerous advantages including excellent biocompatibility,^{65,495} exceptional miscibility^{496,497} and great mechanical properties,^{207,498} have been approved by the US Food and Drug Administration (FDA) for preparing commercial products,⁷³ enabling the wide applications in the area of drug delivery,^{499,500} tissue engineering^{501,502} and so forth. In addition, the employed template is a polymethyl methacrylate (PMMA) film with surface structures of microwell arrays. Although homogeneous biodegradable microparticles have recently been successfully prepared on similar template structures,²⁶¹ the harvested microparticles was merely the blends of polymer and drugs rather than core-shell structure as microcapsules, which could result in a systematic waste and unprotection of loaded drugs near the interfaces.

Aiming at overcoming the limitations associated with conventional methods for synthesizing biodegradable microcapsules, in the present work, a novel, facile, scalable microprinting technique for the preparation of identical biodegradable microcages was first-time proposed. Besides, an original dry state drug loading method was introduced and applied,⁴⁴⁵ enabling a simple and quick encapsulation of any solid compounds without considering the solubility, the molecular weight and the interactions with the solvent. Moreover, the release behaviours of the printed microcages are manipulated by adjusting the composition of the shell polymer. Here, identical PLA microcages are fabricated by microprinting technique based on a microwell-patterned template with predesigned homogeneous size and shape. The controlled release behaviours of the printed microcages are further achieved by adjusting the blending ratios of PCL with PLA, thus manipulating the permeability of the microcage polymer shells. Furthermore, 5(6)-carboxyfluorescein (CF, 376 g/mol), as small and hydrophilic molecules, was selected as a model drug to be encapsulated into biodegradable microcages with dry loading method, thereby facilitate the observation and characterization of the encapsulation and release behaviours of the printed microcages. In general, the proposed microarray structure-based microprinting technique paves a novel way to synthesis identical biodegradable drug delivery vehicles with wide drug encapsulation availability, hence broaden the potential applicability of microcapsules, especially in biomedical related areas.

6.2. Preparing Drug-loaded Microcages from Microarray Structure

General schematic illustrations of the preparing of drug-loaded microcages from microarray structures via hot pressing method were demonstrated in Figure 6.1, Figure 6.2 for 3D view and cross-section view, respectively, to facilitate the principles of the fabrication method. First, a PDMS stamp with microwells array structure and a flat PDMS was precoated with a layer of polymer thin film via the one-step dip method (see 3.2.6). When the think film on the PDMS stamp was fully dried, drug particles that were milled into submicron size were spread and loaded into microwells. After that, the drug-loaded

precoated PDMS stamp was pressed with precoated flat PDMS forming a sandwich structure and heated at 160°C on the heating stage for 1 minute. Then the sandwich structure was removed from the heating stage and cooling down without release the pressure. After both the PDMS and the films were cooled down to room temperature, the flat PDMS was lifted over leaving microcages embedded inside microwells. To harvest the microcages, the PDMS stamp with microcages are pressed onto a glass slide pre-spread with gelatin and forming again another sandwich structure which was frozen in -20°C freezer for 10 minutes. When the gelatin was solidified, the PDMS stamp was lifted over, resulting in microcages on a glass slide with a layer of gelatin. Afterwards, the microcages are dispersed into water solutions by dipping the glass slide into the warm water of 37°C that melt the gelatin. After several washes with warm water, the microcage water suspension solutions were finally prepared and ready for further experiment.

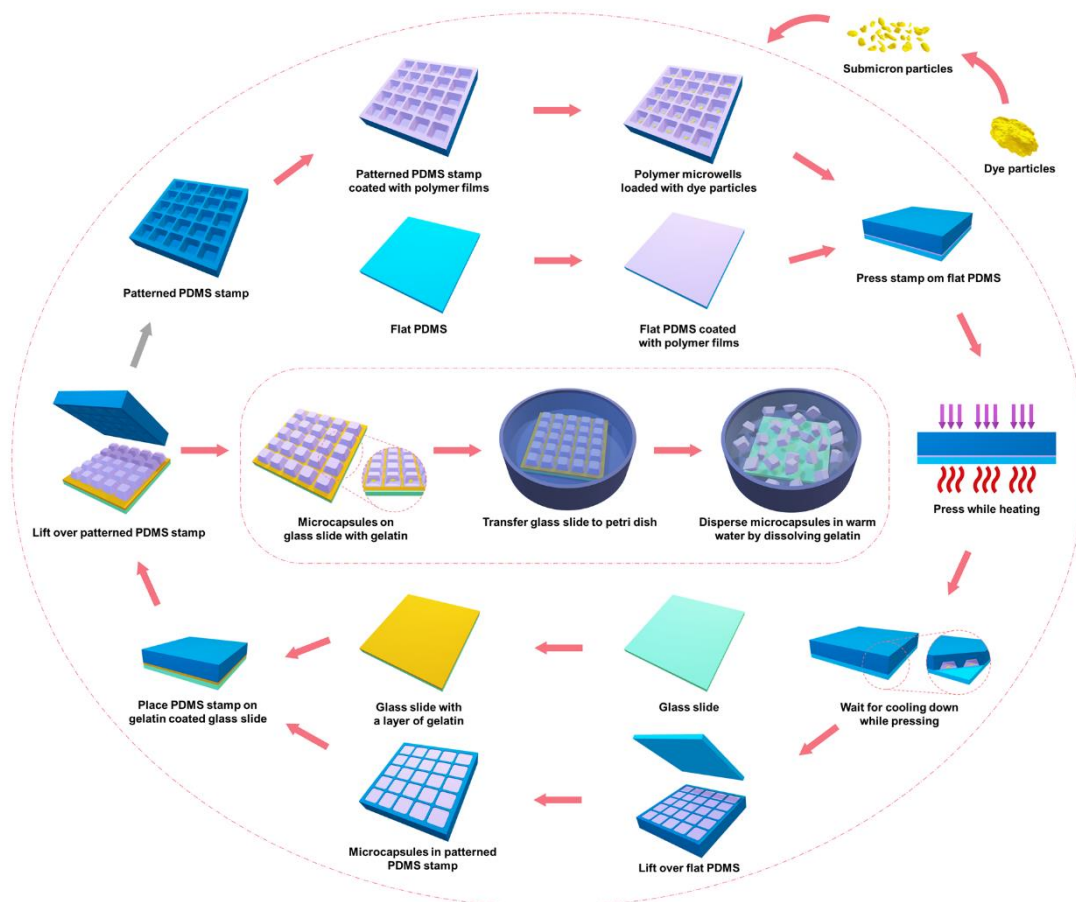


Figure 6.1 Schematically illustration in the 3D view of preparing drug-loaded microcages.

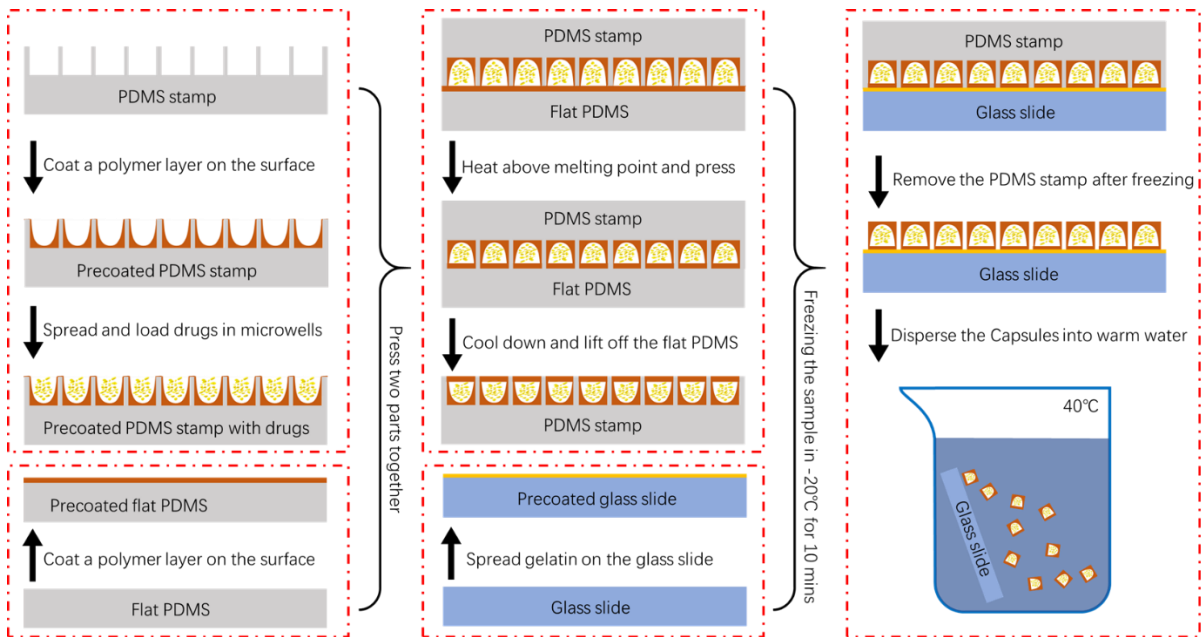


Figure 6.2 Schematic illustration in the cross-section view of preparing drug-loaded microcages.

6.3. Characterization of Printing Process and Resulted Drug-loaded Microcages

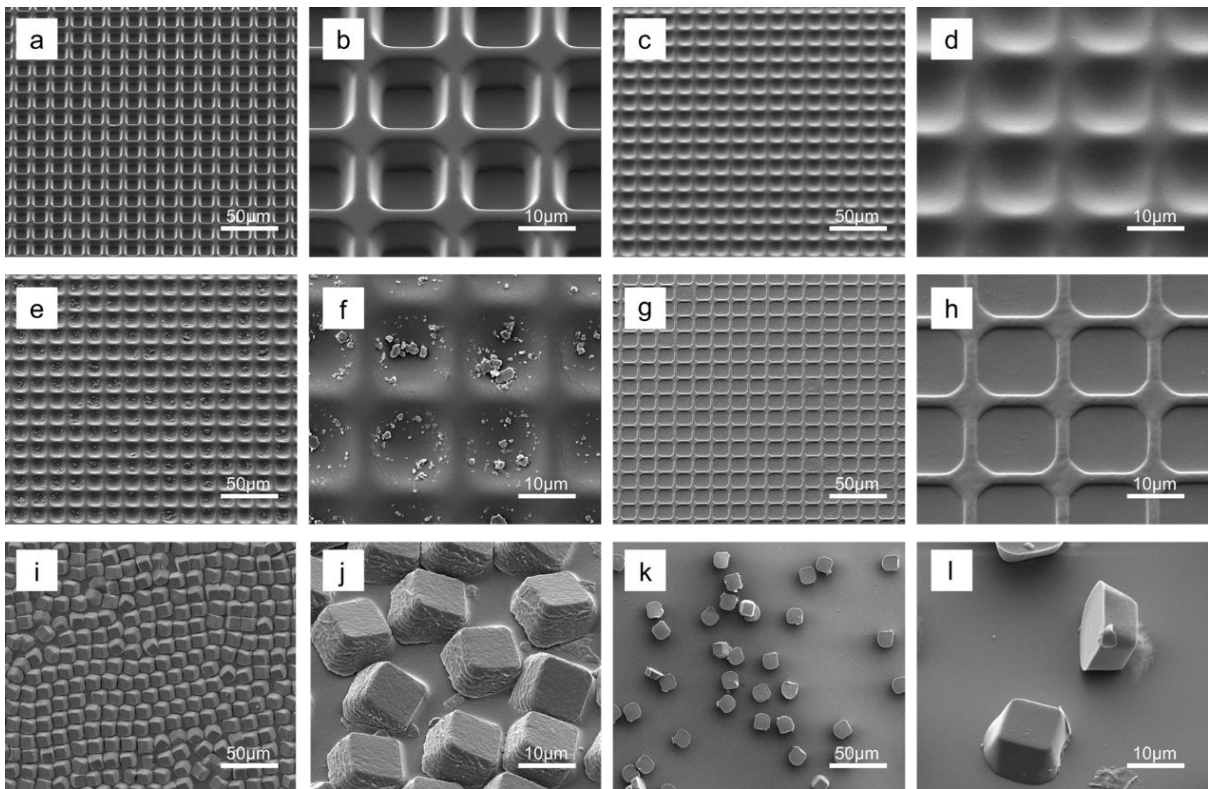


Figure 6.3 SEM images of key stages during the preparation of microcages. a, b) PDMS stamp with microwell array structure. c, d) a layer of pre-coated PLA film on the surface of the PDMS stamp. e, f) CF particles loaded into microwell arrays of PLA films on PDMS stamp. g, h) Microcages embedded inside microwell arrays after detaching the flat PDMS. i, j) Transferred PLA microcages on gelatin. k, l) printed PLA microcages after dispersing and wash steps.

In order to facilitate a better understanding of the printing procedures as well as figure out the mechanism of the microcage formation and drug encapsulation, scanning electron microscopy (SEM) was applied to check and observe the detailed surface morphology variations at key stages during the printing process of both the PDMS stamp as well as the final printed microcages. In this section, PLA was selected as an example of biodegradable polymers to be printed into PLA microcages, with the SEM results of the preparing process demonstrated in Figure 6.3.

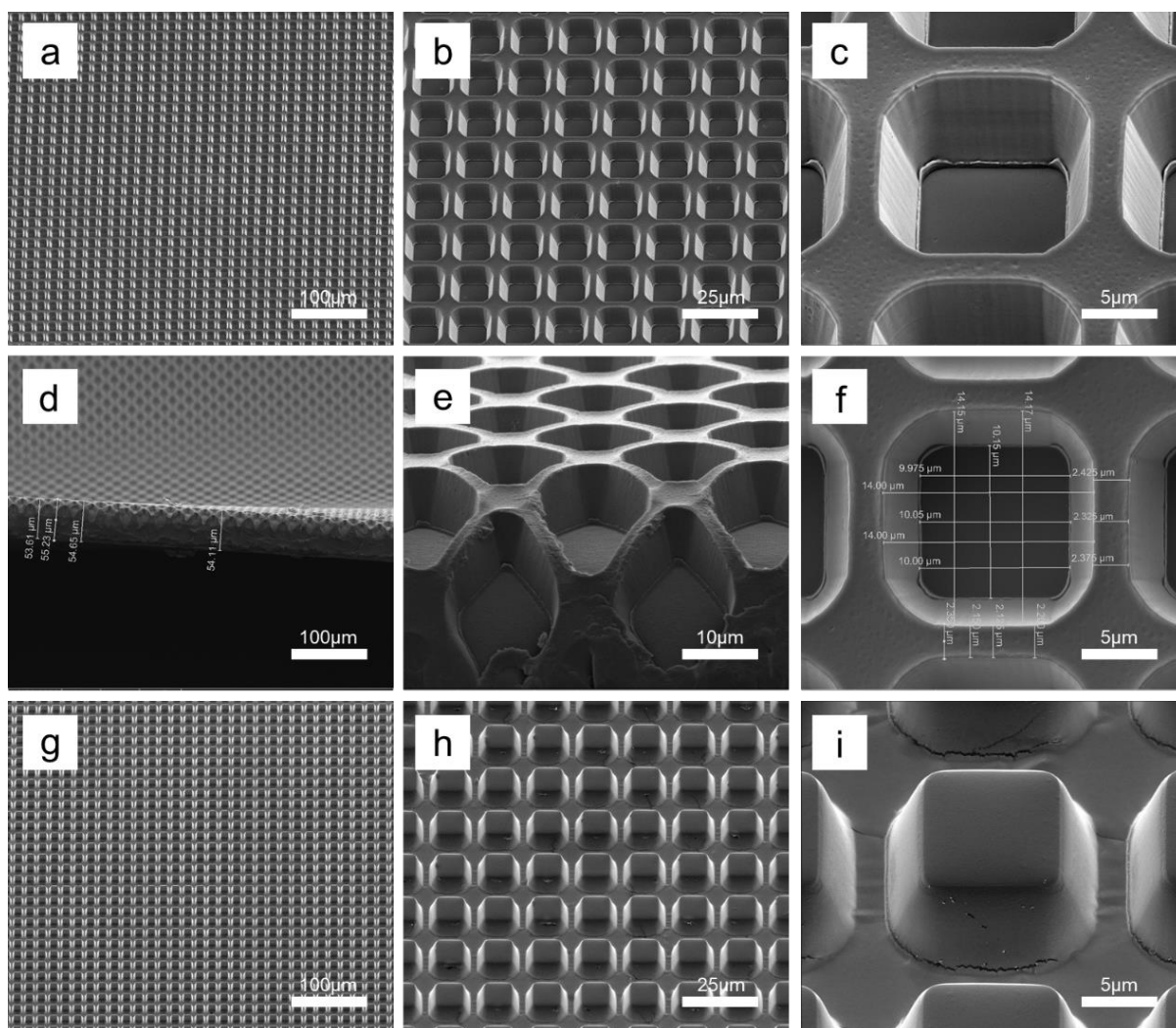


Figure 6.4 The specification of the PMMA template as well as the PDMS template for preparing patterned PDMS stamp. a-f) The SEM images of the PMMA template at various magnifications and angles. g-i) The SEM images of PDMS template of different magnifications. The period of microwell arrays is 16.35µm. The microwell is in the shape of a rounded quadrangular frustum pyramid, with the short side, long side, depth as 10µm, 14µm, 8µm respectively. The distance between microwells (wall thickness) is 2.35µm. Moreover, the thickness of PMMA template films is about 54µm including the 8µm depth of microwells.

Generally, a rubber stamp made of polydimethylsiloxane (PDMS) with microwell array surface structure was necessary for printing biodegradable microcages, which was prepared by a double casting and transferring procedures of PDMS based on a predefined PMMA template with microwell array structures on the surface whose specifications can be found in Figure 6.4. The schematical demonstration of the preparation process of the PDMS stamp is shown in Figure 6.5 with a detailed introduction to the fabrication procedures can be found in section 3.2.1. In addition, Figure 6.3 a, b) showed the morphology of as-prepared patterned PDMS stamp at different magnifications that the identical size and shape defined microwells with smooth morphology were periodically arranged in the form of arrays on the surface of the PDMS stamp.

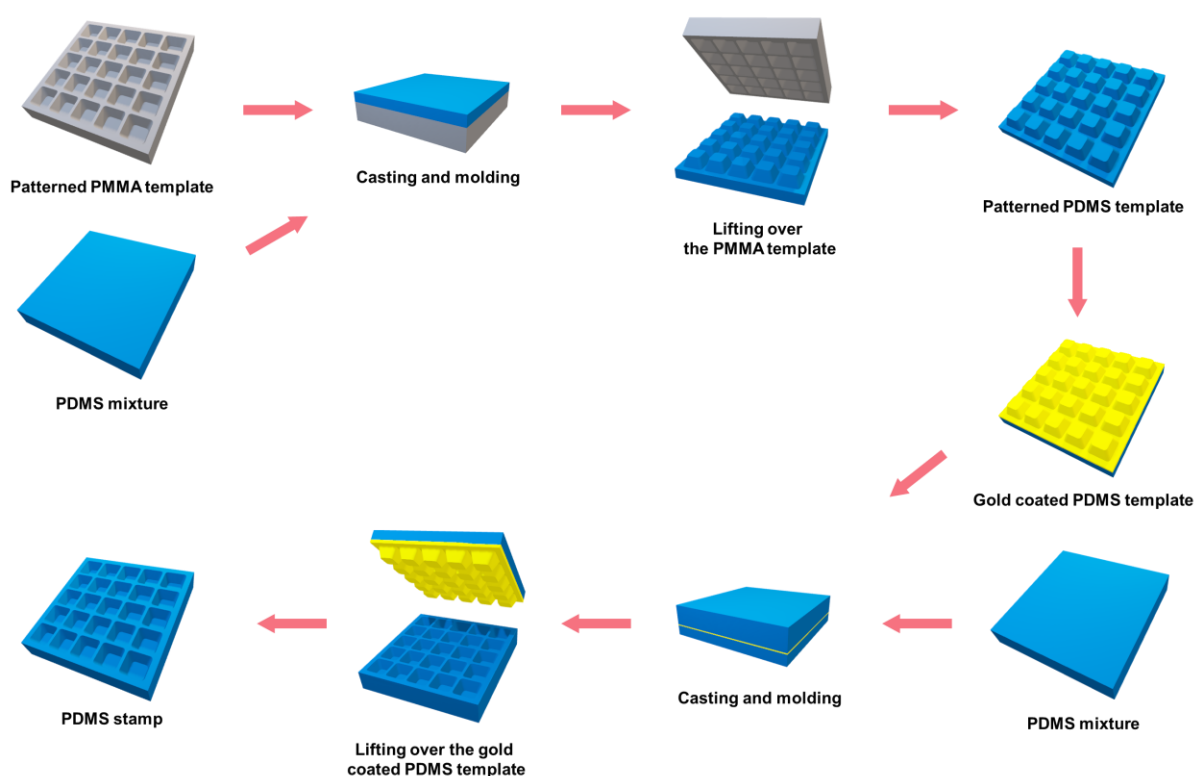


Figure 6.5 Schematically illustration of the procedures for preparing microwell-patterned PDMS stamp.

Typically, the microcage printing process started with dipping microwell-patterned PDMS stamp as well as a flat PDMS into PLA polymer solution for 5 seconds, followed with gently and slowly withdraw of both the PDMS stamp and the flat PDMS which were then dried in ambient conditions, leaving a thin layer of PLA film on the surface after the

evaporation of organic solvents. After dip-coating a thin layer of PLA polymer film, the surface structure of the precoated PDMS stamp was shown in Figure 6.3 c, d). The PLA thin film was completely and uniformly coated on the PDMS surface including the walls and microwells, forming a large number of periodical and shallow microwells where drugs can be loaded and stored.

Here, 5,6-carboxyfluorescein (CF), a small and hydrophilic fluorescent dye, was selected as the model drug to be encapsulated into these sunken areas. Although the CF model drug can be loaded with solution loading method, the loading efficiency was insufficient because of the low water solubility of CF, thus, a more simple and efficient powder loading method designed for this special microwell array structure was applied that the CF particles were directly spread on the surface of PLA film precoated PDMS stamp. However, due to space limitations, the large CF particles were required to be milled and ground into submicron-sized crystals. Considering the small molecular weight and hydrophilic properties of CF, the release rate would not be significantly affected by the grinding process as CF particles would dissolve instantly once they contact the water. Additionally, in practice, the drug particle size was usually given. After the spreading of the crushed CF particles, the surface of the precoated PDMS stamp was gently swiped with fuzz-free tissue to remove the excess amount of CF particles. Only those submicron-sized CF particles trapped in the sunken microwells can be left on the surface of the precoated PDMS stamp. Figure 6.3 e, f) proved that the submicron-sized CF particles had been successfully loaded into the periodical microwell array structure, with the particles only located in the sunken area without staying on the surface of walls in between.

Subsequently, this drug-loaded pre-coated PDMS stamp was covered and sealed by the afore dip-coated flat PDMS forming a sandwiched structure, while all the components were heated and pressed at 140°C for 90 seconds, aiming at stamping and separating the melted polymer films between the PDMS stamp and the flat PDMS into individual

microcages. The selected heating temperature of 140°C was just above the melting point of PLA, as the DSC result shown in Figure 6.6, aiming at facilitating the separation of PLA polymer films by the wall of microwells on the PDMS stamp. Next, when the whole system cooled down to room temperature at ambient conditions, the flat PDMS was lifted over, leaving PLA microcages embedded in microwell array structures on the surface of the PDMS stamp, whose surface morphology were displayed in Figure 6.3 g, h). Apparently, all the identical and uniform drug loaded PLA microcages were perfectly embedded and well-sealed with a smooth surface, located at the positions that used to be microwells. It is noteworthy to point out that the top of the PLA microcages was lower than the PDMS stamp surface plane owing to the elasticity of PDMS polymer, as the walls of the microwells would bend while pressing and heating the sandwiched structure.

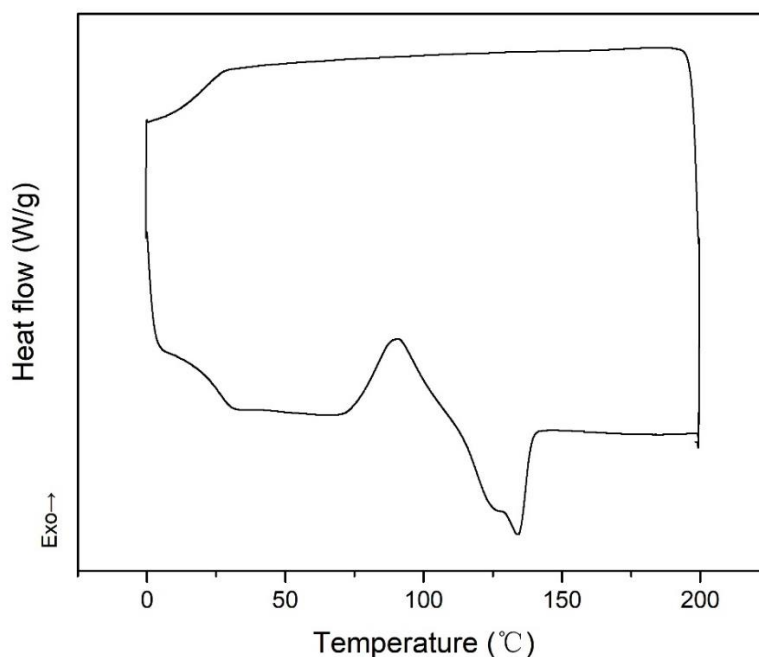


Figure 6.6 DSC results of polylactic acid (PLA). The curve is constituted by 5 minutes isothermal at 200°C, temperature decrease from 200°C to 0°C at the rate of 10°C/min, 5 minutes isothermal at 0°C and temperature increase from 0°C to 200°C.

Basically, at this point, the drug-loaded PLA microcages had been successfully prepared, however, printed microcages were stuck inside microwells which can hardly be directly dispersed in DI water by normal flushing or rinsing, as both PLA and PDMS were

hydrophobic polymer and they were tightly attached. Therefore, gelatin was used to stick and detach the microcages from the PDMS stamp. Generally, a layer of 10% gelatin DI water solution was spread on the top of a glass slide, on which the PLA microcages embedded PDMS stamp was placed. Afterwards, the gelatin-coated glass slide together with microcages embedded PDMS stamp were frozen at -20°C for 10 minutes so that the gelatin would be fully solidified. By lifting over the PDMS stamp while the gelatin was frozen, the PLA microcages would be stuck on the surface of gelatin, thus transferred onto a glass slide. Here, one of the fascinating advantages of this microcage printing method was that the detached PDMS stamp can be reused for another cycle of microcage printing numerous times after simple cleaning steps.

Figure 6.3 i, j) illustrated the surface morphology of PLA microcages after transferred by gelatin on a glass slide. It is worth noting that all the PLA microcages were periodically arranged on the surface of solidified gelatin right after detaching the PDMS stamp, while the prepared SEM sample were microcages fixed in melted and further dried solidified gelatin. Although Figure 6.3 i, j) can hardly represent the exact position and array order of microcages on frozen gelatin, the SEM micrograph did indicate that after the heating and pressing procedure, the evenly coated PLA film on the PDMS stamp had been separated by the walls of microwells, resulting in a large number of individual drug-loaded PLA microcages as expected. Finally, the printed PLA microcage water suspension was achieved by placing the microcage fixed gelatin-coated glass slide into a petri dish, rinsing the glass slide with 37°C DI water so that the gelatin would be dissolved and the PLA microcages would be dispersed into DI water, following with DI water washing for three times to remove the dissolved gelatin.

The final PLA microcage morphology after washing and drying steps was presented in Figure 6.3 k, l), that all the microcages were identical and uniform both in shape and size determined by the applied template without any aggregation behaviours. Additionally, it is

evident that a small “tail” was attached at the edge of the individual PLA microcage at a higher magnification view. The “tail” came from the crossing part of the walls on the PDMS stamp after heating and pressing, caused by the distortion of the PDMS while pressing.

Additionally, it is evident that a small “tail” was attached at the edge of the individual PLA microcage at a higher magnification view. It is assumed that the “tail” came from the crossing part of the walls on the PDMS stamp after heating and pressing. However, after several PLA microcage preparation repetitions, there was no regulation on the appearance of the “tail”. Thus, though the “tail” has little impact on the applications, its specific formation mechanism may need to be further investigated.

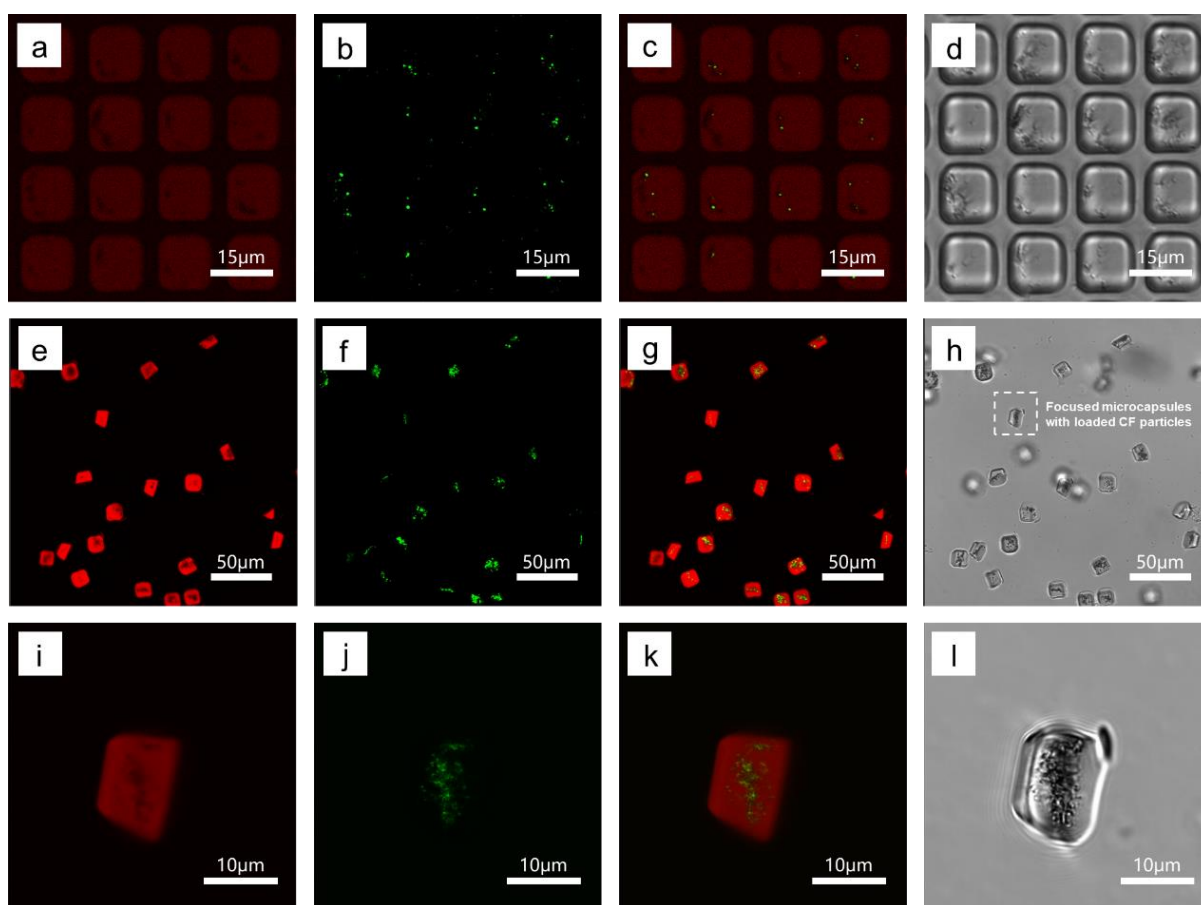


Figure 6.7 CLSM images of PLA microcages for confirming the encapsulation of CF model drugs. a-d) CF loaded PLA microcages printed and embedded inside the microwell arrays of patterned PDMS stamp. e-h) CF loaded printed PLA microcages dispersed in DI water. i-l) higher magnification of e-h) focusing on one single PLA microcage. PLA is labelled with red fluorescent dye Nile Red and the green colour represents the encapsulated fluorescent dye particles CF.

Confocal laser scanning microscopy (CLSM) was employed to observe and confirm the encapsulation of CF model drug particles in PLA microcages, with the results shown in Figure 6.7. In order to distinguish the different components, the shell polymer PLA was labelled with red fluorescent dye Nile red, while the encapsulated model drug CF particles displayed a green signal as its own fluorescent colour. At the same time, the bright field channel of CLSM of each specimen was recorded as well, providing another angle to verify the accommodation of model drug particles.

CLSM was first applied at the preparation stage when CF loaded PLA microcages were printed and embedded inside the microwell arrays of patterned PDMS stamp after detaching the flat PDMS, whose results were demonstrated in Figure 6.7 a-d). The red channel (Figure 6.7 a)) showed the empty space inside PLA polymers where located the CF particles exhibited in Figure 6.7 b), which was confirmed in the overlaid channel. Besides, it is clearly displayed in the bright field channel (Figure 6.7 c)) that dye particles were fixed inside the area of microwells without setting on walls in between. In addition, the CF loaded printed PLA microcages dispersions were also characterized via CLSM (Figure 6.7 e-h)), aiming at confirming the sealing and leakage of the printed microcages. It is worth mentioning that these CF loaded PLA microcages had been incubated in DI water for 1 hour followed by three times washing steps to guarantee the non-encapsulated hydrophilic CF particles had completely been dissolved and removed, and moreover, all the microcages were imaged while floating and suspending in aquatic condition. In general, Figure 6.7 e) showed that every PLA microcage had hollow space occupied by green CF particles (Figure 6.7 f)) as confirmed in the red-green overlaid channel of Figure 6.7 g). Especially, Figure 6.7 h) evidently demonstrated that the CF model drug crystals, displayed as dark dots, were remained and located at the position of each microcage, indicating the well-sealing and non-leakage of printed PLA microcages. Moreover, one of the side-position-up microcages in Figure 6.7 e-h) was magnified and focused as Figure 6.7 i-l) presented. The red channel (Figure 6.7 i)) detailed showed that the empty area was located

in the middle of the microcage structure where also the green particles (Figure 6.7 j)) stayed. In addition, the overlaid channel (Figure 6.7 k)) proved that the encapsulated CF particles emerged only inside the core of PLA microcages instead of appearing on the surface of the polymer shell or randomly distributed in the bulk polymer, indicating the formation of a core-shell like structure. However, the fluorescent channels were only a thin cross-section of the microcage, while the bright field channel further provided the additional information that a large amount of model drug particles could be encapsulated in the individual microcage as the dark and dense area exhibited in the Figure 6.7 l).

In order to achieve a passive release behaviour, biodegradable and biocompatible polymer polycaprolactone (PCL) was selected to blend with PLA to increase the release rate of the encapsulated microcages due to the lower water permeability of PCL than PLA.⁴⁷⁸ Since both PLA and PCL can be easily dissolved in organic solvent of chloroform, the PLA-PCL blended polymer solutions can be simply obtained by mixing PLA and PCL chloroform solutions. By changing the blending ratios, the final selected polymer solutions for printing microcages were PLA:PCL=9:1, 8:2, 7:3. Although more PCL contents could be mixed with PLA, the dip-coated polymer films can hardly be smooth and homogenous when the PCL component reached 40%.

Besides, one of the most crucial requirements for the successful printing of microcages was controlling the heating and pressing temperature when PDMS stamp, polymer film and flat PDMS were in the sandwiched structure. Figure 6.8 demonstrated the morphology of the polymer films of the sandwiched structure after being heated, pressed at various temperature, and further transferred onto the gelatin-coated glass slide. When the pressing temperature was lower than the polymer melting point of 140°C (Figure 6.8 a)), the thin films cannot be separated into microcage. Instead, a PLA microchamber array film would be transferred onto the gelatin-coated glass slide. While when the heated temperature was a bit higher than the melting point at 160°C (Figure 6.8 c)), the microcages printing

procedures can still be succeeded, with the morphology of transferred microcages similar to the one printed at the melting point (Figure 6.8 b)). However, when the sandwiched structure was heated and pressed at a higher temperature of 180°C as shown in Figure 6.8 d), some of the melted PLA were attached to flat PDMS which would not in the capsule shape after cooling down, and only partial microcages were embedded in microwells of PDMS stamp and being transferred onto the glass slide by gelatin.

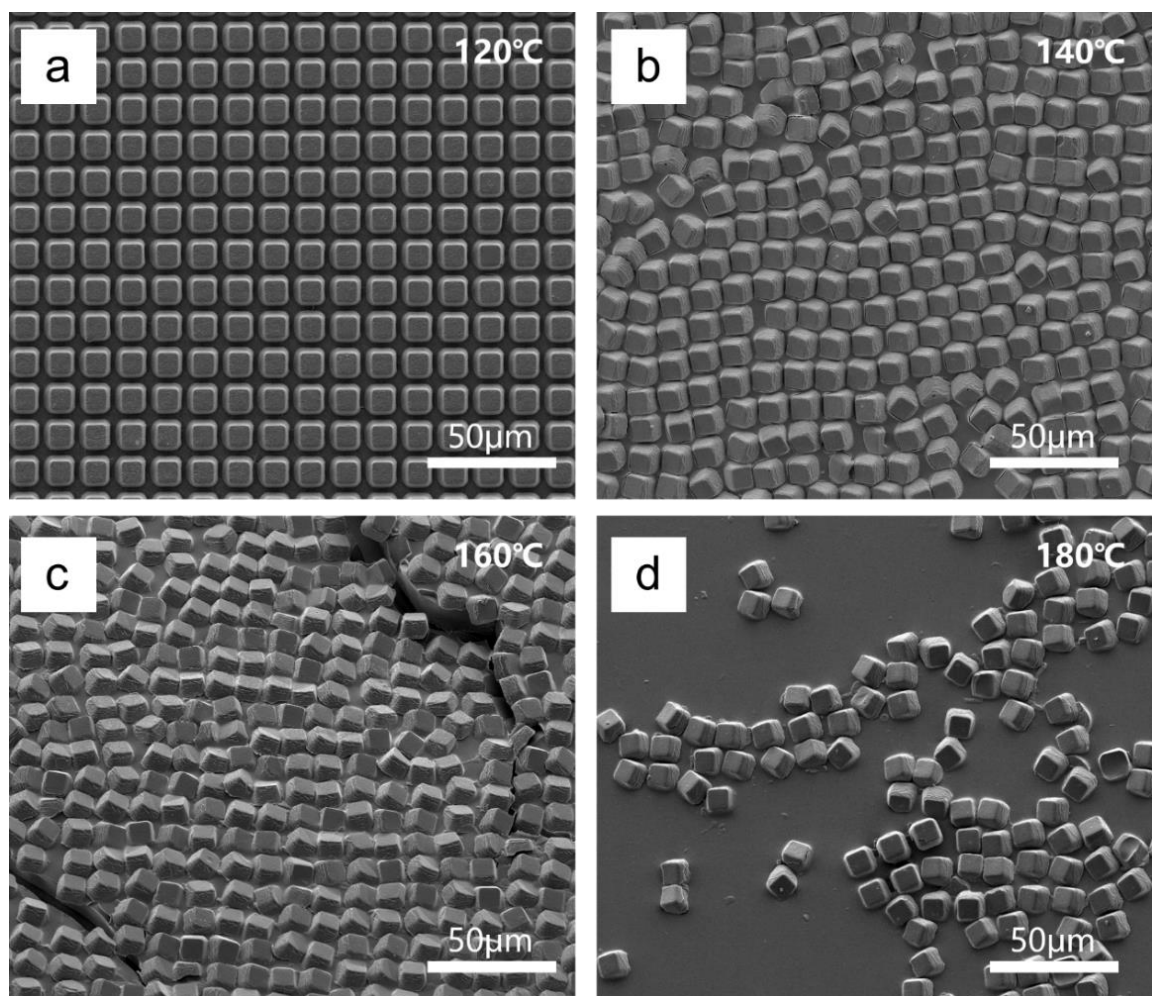


Figure 6.8 After the sandwiched structure of PDMS template - polymer films - flat PDMS being heated and pressed at the different structure and lifting over the flat PDMS, the resulted structure transferred onto a glass slide by gelatin. a) Heated and pressed at 120°C. The PLA polymer films were not separated by the wall of microwells due to the low temperature. b) Heated and pressed at 140°C. The temperature reached the melting temperature of PLA, thus the PLA films were separated and the individual microcages were forms. c) Heated and pressed at 160°C. The results were similar to b) in that the individual microcages were successfully printed. d) Heated and pressed at 180°C. The temperature was so high that some of the melted PLA were attached to flat PDMS and only partial microcages were embedded in microwells of PDMS stamp and being transferred onto a glass slide by gelatin.

Therefore, the melting point of afore prepared PLA and PCL blended polymer, as the key parameters to print microcages, needed to be characterized, whose thermal properties were evaluated and compared with pure PLA and PCL via DSC. After removing the thermal history in the first heating cycle, the thermal behaviours of all the above polymers were demonstrated in Figure 6.9.

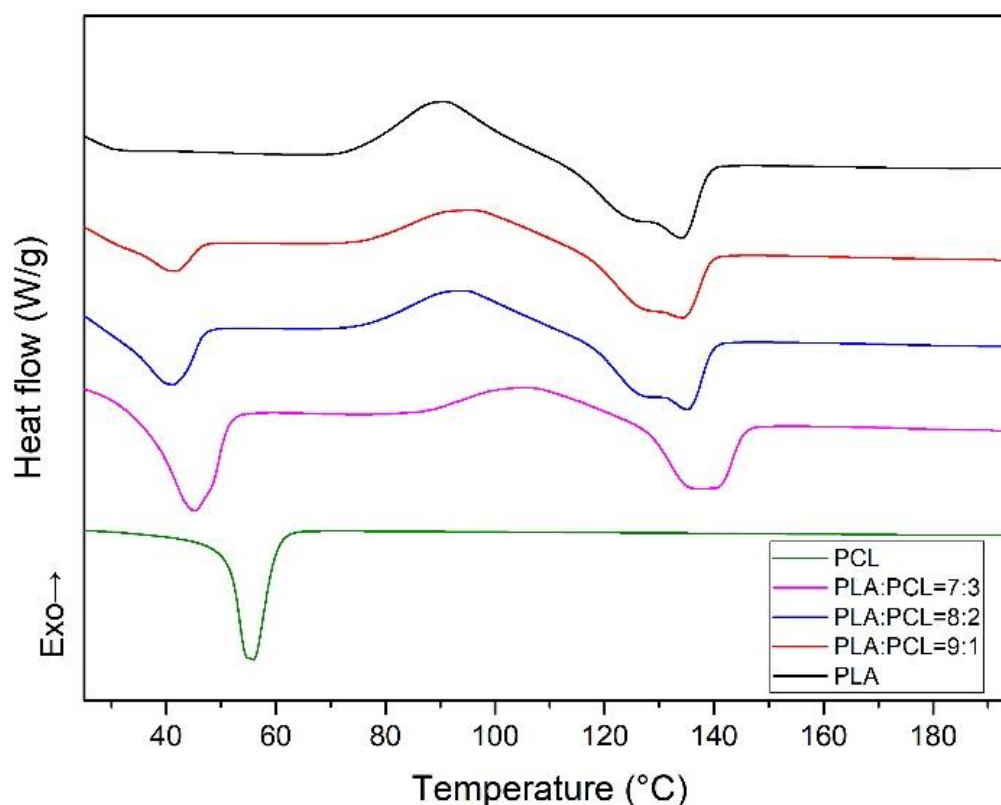


Figure 6.9 DSC results of PLA, PCL and PLA/PCL blends at different blending ratios.

For pure PCL, only one endothermic peak was observed, demonstrating the melting point at around 55°C. While for pure PLA, an exothermic crystallization peak can be found at about 92 °C. Besides, at around 135°C, the endothermic melting peak of PLA can be clearly observed. For the blending polymer of PLA and PCL, two individual endothermic peaks can be found, indicating the coexistence of heterogeneous polymer phases. With the increase of PCL ratios in the blending polymer, the left endothermic peak moves towards the melting point of pure PCL, while the right endothermic peak moves rightward, departing from the melting point of PLA.

Since the melting point of PLA-PCL blended polymers had a similar melting point as PLA, it is feasible to apply the same printing procedures and conditions as preparing PLA microcages for synthesizing PLA-PCL microcages after simply replacing the polymer solution from pure PLA to PLA-PCL blended polymer solutions. Figure 6.10 showed the SEM images of printed microcages made of PLA and PLA-PCL blended polymers at different ratios.

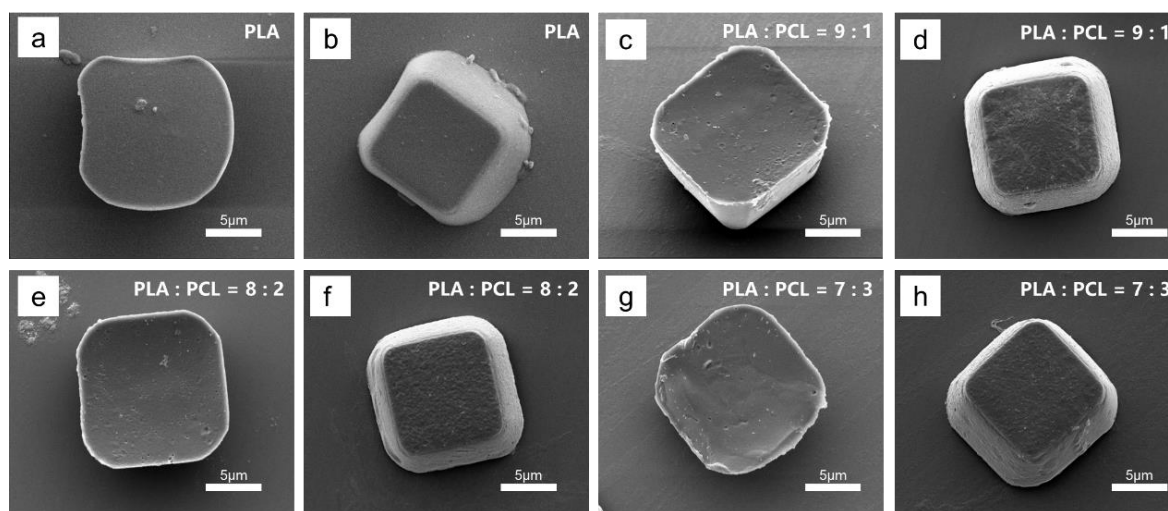


Figure 6.10 The SEM images of printed microcages made of PLA and PLA-PCL blended polymers at different ratios. a, b) microcages made of pure PLA. c, d) microcages made of PLA:PCL=9:1. e, f) microcages made of PLA:PCL=8:2. g, h) microcages made of PLA:PCL=7:3.

As shown in Figure 6.10, the printed microcages made of any polymers were almost identical both in size and shape. When observing the detailed morphology, the printed microcages made of pure PLA had a complete and smooth surface as Figure 6.10 a, b) showed, while for the microcages comprising 10% of PCL (Figure 6.10 c, d)), there were some small bumps emerged due to the phase separation between PLA and PCL, but the surface was flat and complete. When the PCL content reached 20% (Figure 6.10 e, f)), the surface morphology of the microcage was similar to PLA:PCL=9:1 ones, with complete surface and small pores. However, the microcages made of 70% PLA and 30% PCL showed an unsmooth surface, though still complete, indicating the PCL content was melted and flowed on the surface before due to the phase separation. Generally, the SEM results revealed that the identical microcages made of various polymers were successfully

prepared, and although the detailed surface morphologies were different, the drug particles had been completely encapsulated and sealed inside microcages.

6.4. Release Experiment of Drug-loaded Microcages

After confirming the successful preparation of printed biodegradable microcages as well as the encapsulation of CF model drug particles, the release kinetics of the microcages were further studied.

5,6-carboxyfluorescein (CF) has been widely accepted as the model drug for delivery system thanks to its physicochemical properties including the small molecular weight, the good water solubility as well as the stable fluorescent signals, which offer the possibilities to trace the location of labelled sample and analyse the release behaviours of drug delivery vehicles. Here, CF was encapsulated into printed microcages made of biodegradable polymers in order to study and examine the permeability of the microcage polymer shell. Figure 6.11 demonstrated the release behaviours of CF encapsulated microcages made of biodegradable polymers for up to 28 days.

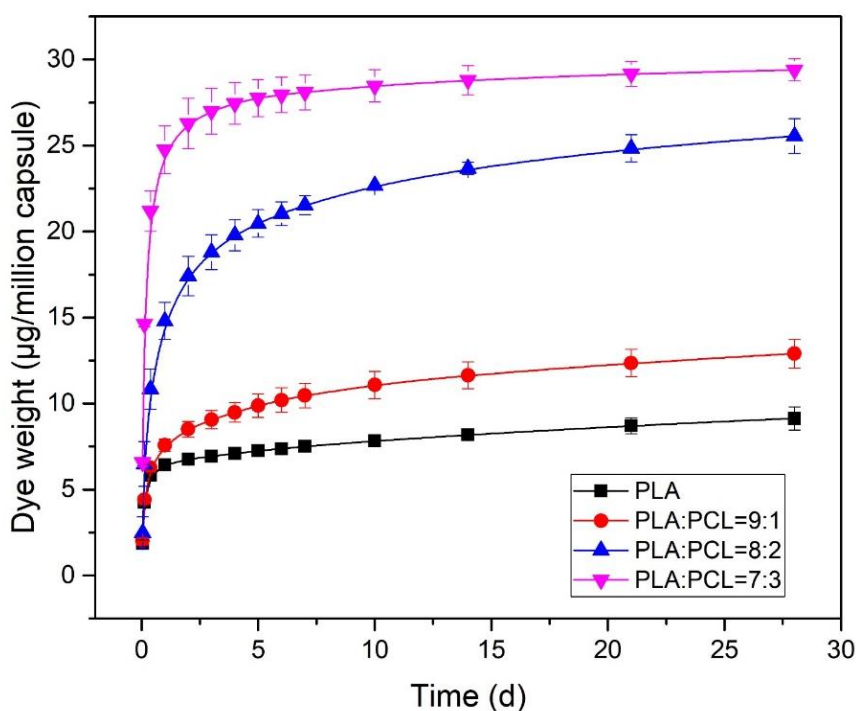


Figure 6.11 Release curve of biodegradable microcages at different PLA and PCL blending ratios.

Generally, the printed microcages made of polymers with higher PCL component tended to release the encapsulated CF particles faster as expected. Based on the dye release curve in Figure 6.11, it can be easily observed that the CF particle encapsulation amount was approximately 30 μg per million microcages, which was calculated that averagely 30 pg CF particles were loaded into individual microcages, indicating a relatively high encapsulating capacity.

During the first 24 hours of incubation, a burst release of encapsulated CF was observed in all groups, which could be caused by multiple factors. On the one hand, the unwell-sealed CF may not be fully washed out, even after all the samples of the four groups had been incubated at 37°C for 1 hour in water and three washing steps to remove the loaded drug in flawed microcages. On the other hand, the intensive incubation solution replacement would accelerate the release rate as well. While for the microcage incubation group of 70% PLA, the burst release was, to a large extent, contributed by the permeability of the designed polymer shell itself. Moreover, the release rate of this group was significantly higher than the other three groups with almost 80% encapsulated dye particles were diffused out.

After one-day release activity, the release curves of all four groups gradually went up steadily since the dye release rate tend to be dominated by the permeability of microcage shell constitution. While at the same time, manual operation inaccuracy would also affect the release curve that the incomplete replacement of the microcage incubation supernatant of the last time point was not fully replaced in order to avoid contacting the microcage precipitation. However, the PLA:PCL=7:3 group was an exception that the release rate decrease was originated from the inadequate amount of encapsulated CF particles, in other words, the drug diffusion rate was unsaturated. Basically, from day 1 till day 7, samples of all four group was maintained releasing cargos though in different speed, that the group of PLA:PCL=8:2 released around 22% of the overall encapsulated amount while the group of

PLA:PCL=7:3, PLA:PCL=9:1 and pure PLA had 11.15%, 9.64% and 3.55% loaded dye released within 6 days, respectively.

From day 7 to day 28, the release curve of all samples became almost linear as the dye release rate became nearly constant, indicating a main influence of the diffusion activity and less effect from flawed microcage as well as the manual operation inaccuracy. The release curve of the group PLA:PCL=7:3 among this period was getting almost levelled with 98% of CF released until day 28, since most of the loaded cargos had been released in the first week due to the highest polymer permeability. Therefore, PLA:PCL=8:2 group, with the second most PCL content, released CF particles at the highest rate as 35.8% of encapsulated drugs released within 3 weeks. However, as incubation time increased, the release rate slightly declined due to the drug encapsulation amount differences between individual microcages so that some microcages would finish the release activity earlier. In addition, when the blending ratio of PLA to PCL came to 9:1, the CF release rate became moderate that 17.8% was released from day 7 to day 28 and totally about 43% was released after 4-week incubation. While the slowest release increment of pure PLA group denoted the lowest diffusion rate of CF model drug, with only 9% of particles released during the 3 weeks and overall 30.46% in the whole followed 4-week period.

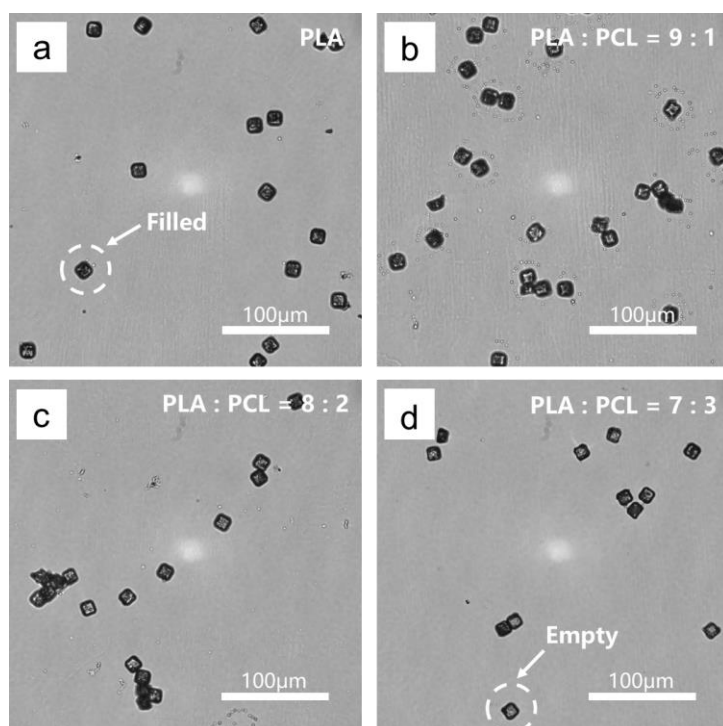


Figure 6.12 Optical images of CF loaded microcage of different PLA and PCL components after 4 weeks release experiment in PBS solutions at 37°C. a) pure PLA. b) PLA:PCL = 9:1. c) PLA:PCL = 8:2. d) PLA:PCL = 7:3.

Optical microscopy was applied to facilitate a better and straightforward observation of the release results of printed microcages made of PLA and PCL blends after 4 weeks of incubation in PBS solutions since the encapsulated dye particle can be easily and qualitatively examined through the transparent biodegradable polymer films, whose results were demonstrated in Figure 6.12. Generally, after the 28 days incubation, PLA microcages still retained a large amount of CF particles inside each microcages, as shown in Figure 6.12 a). For the microcages made of blended polymers of PLA:PCL=9:1, Figure 6.12 b) showed that a portion of loaded CF had been released from the microcages, but there were still many particles that remained inside microcages. When the PCL content enhanced to 20%, Figure 6.12 c) illustrated that some of the microcages still had CF particles loaded, although there were many microcages that had released most of the encapsulated CF. Moreover, significant differences emerged in the optical images of Figure 6.12 d) that when the polymer shell of printed microcages came to PLA-PCL=:7:3, many empty microcages can be easily observed, indicating most of CF particles had been diffused out of the microcages.

6.5. Conclusions

Identical microcages made of biodegradable polymers (PLA and PCL in various blended ratios) are successfully printed and prepared based on microarray structured. Besides, the printed PLA microcages can retain the dry method loaded CF model drug particle, which demonstrates the capability for the encapsulation of small and hydrophilic cargos. Moreover, the encapsulated CF was controlled released by varying the water permeability of the microcage polymer shells that high water permeability polymer PCL was blended with low permeability PLA in different ratios. The release curve of prepared biodegradable CF encapsulated microcages further reveals that with the increase of PCL contents in the microcage shell, the model drug release rate becomes faster. In addition, the overall amount of CF particles encapsulated in every million microcages is about 30 μg , which is calculated as 30 pg in each microcage, indicating that the printed biodegradable microcages can accommodate chemical compounds in a highly efficient way.

It is noteworthy to address that the appearance of the microcages prepared in this work is just an example, as the size and the shape of printed microcages are determined not only by the lithographed template, which can be predesigned in various structures,³⁷ but also by the casted microarray structure on the surface of PDMS stamp, whose resolution limit is in the range of 100-200 nm.⁴⁷³ Moreover, the lithographed structure of microarrays has also been extensively studied in the fields ranging from lab-on-chip,³³⁴ sensing,⁵⁰³ electronics,³³⁵ optics,³³⁶ and so on. Since the PDMS stamp cast from microarray structured template is reusable, it is strongly believed that the monodisperse microcages printing technique possesses industrially relevant advantages in reproducibility, scalability, and consistency of physicochemical properties of microencapsulated products.⁵⁰⁴

However, there were still many challenges for the printing of biodegradable microcages to overcome. The most significant problem was to guarantee the approximately constant drug loading amount in each microwell. Theoretically, each microwell has the same empty

volume to trap the drug crystals. While in practice, the amount of drug loaded is influenced by various factors including the particle size, the spreading time and pressure, the thickness of the polymer layer coated on the PDMS stamp and so forth. Fortunately, these problems can be solved to some extent. Currently the thickness of the polymer layer is manually dip-coated, causing the variation of thickness of the polymer films. The employment of machine can greatly solve this problem as every time the lifting speed and condition can be the same to minimize the variation, so does the drug spreading time and pressure. Additionally, the loaded drug crystals were manually milled into smaller size with wide size distribution. By using grinding machine and filtering procedures, the drug crystal size distribution can be narrowed, enabling more constant loading amount in each microwells.

Moreover, the microcages presented in this chapter had solid structure due to the special microarray structure and hot pressing techniques, which blocked the ultrasonic triggered release route. One feasible way to overcome this limitation would be employing microarray structures of different specification, such as more deep microwells or larger period. Current hot-press techniques can only prepare microcages with size around 5 μm , for smaller dimension, more advance and precise equipment should be employed.

Unlike microfluidic techniques that can precisely loading different drugs and polymers in one microcapsule, the proposed microcage printing technique can only prepare simple polymer-drug one layer structure. Though this structure would be sufficient for the requirement of majority of applications, it is of great importance to develop the method for loading drugs in different layers for special occasions. One straightforward way is to load drug into microcages of smaller dimension, while using these smaller microcages as the model drug to be encapsulated in a larger microcage, thus forming double layer of microcages. Furthermore, by using smaller microcage with different drug and repeating using larger microcages to encapsulate smaller microcages multiple times, more complex but versatile microcage structures can be achieved.

7. Precursor Ceramics Assisted Templating of Minified Microarray

Structure

7.1. Introduction

Microstructures are increasingly important as components in a variety of fields ranging from microfluidics,⁵⁰⁵ drug delivery,⁴⁴⁵ genetic analyze⁵⁰⁶ to tissue engineering⁵⁰⁷ and sensing areas.⁵⁰⁸ The fabrication of microstructures with controlled and defined geometries has been considered as one of the most challenging parts of micro- and nanotechnology. The achievement of the special geometries is usually determined by the technology applied for the preparation, which would influence the overall performance of the materials.⁵⁰⁹ A multitude of top-down and bottom-up techniques have been proposed to achieve the size and shape-controlled and defined geometries.⁵¹⁰

The most common applied top-down approach is based on photolithography with the advantages of cost-effective and fast fabrication, as the entire substrate surface is simultaneously patterned. However, the optical diffraction effect puts a limitation on the achieved lithography resolution.⁴⁸ Though the lithographed resolution can be enhanced by applying approaches of electrons or ion-based lithography to less than 50 nm, their line-by-line pattern generation process leads to a relatively small throughput.^{49,50} Scanning probe lithographic technique such as dip-pen nanolithography (DPN) and scanning tunnel microscopy (STM) are also widely implemented as a top-down method for generating controlled and defined geometries.^{511,512} Although the definition of DPN can reach sub 15 nm,⁵¹³ and STM can position individual atoms in the sub-nanometer range,⁵¹⁴ they are not appropriate for high-volume fabrication due to their serial lithograph mode.

While the bottom-up methods that widely employed are patterned self-assembly process using topographically/chemically patterned templating substrates and bio templates. One of the representative systems of topographically patterned substrates is

block copolymer (BCP) systems, providing a versatile way to produce ordered nanoscale structure in the range of 10-200nm.⁵¹ However, the requirement of specialized polymer component and the assistance of external fields are challenging issues for most BCP-based templating schemes.⁵² Bio-templating is another newly developed bottom-up technique that has the advantages of natural, ecofriendly, and cost-effective with a great resolution of less than 100nm.⁵⁰⁹ Nevertheless, several limitations of the bio-templating approach of lack of long-range order in the final product because of its intrinsic morphological defects, and in some cases neither predictable nor repeatable still need to be overcome.⁵¹⁰ Moreover, another common disadvantage of the above fabrication techniques is the requirement of expensive and unportable specialized equipment. Therefore, a cost-effective and easily accessible fabrication method that owns the possibility of large area and high-volume pattern fabrications is in high demand.

One of the feasible ways to overcome the massive manufacture challenge is by using soft lithography, which is another inexpensive and facile technique to transfer different types of both microscale and nanoscale structures onto planar, curved or other flexible substrates, essentially based on printing, moulding and embossing with an elastomeric stamp.⁷⁵ Common soft lithography methods include microcontact printing,⁵¹⁵ replica moulding,⁵¹⁶ microtransfer moulding,⁵¹⁷ micromoulding in capillary,⁵¹⁸ nanotransferring printing⁵¹⁹ and so forth. Especially, replica moulding (REM) is an efficient and cost-effective approach for the fabrication of size and shape-controlled and defined microstructures on the surface of various of soft materials parallelly on large areas with relatively low cost.

Generally, REM employs a hard silicon substrate or other solid patterned surfaces as the master template prepared with traditional lithography technique, which is moulded and cast by an elastomer poly (dimethyl siloxane) (PDMS) to form a solid but elastomeric crosslinked PDMS polymer stamp, containing $-\text{Si}-(\text{CH}_3)_2-\text{O}-$ structural unit. PDMS provides a variety of merits including the achievement of an atomic-level contact due to the

elastomeric properties, commercialized product with acceptable price, optical transparency, and protect the fragile structures during separation.⁵²⁰ After peeling off the master substrate, a reversed surface structure of the master template is successfully transferred on the top of the PDMS surface with elevated regions of the stamp correspond to indented regions of the template master. Therefore, the polymers re-replicated from the patterned surface of the PDMS stamp would present an extremely similar (several nanometers deviation) to the geometries of the original master template.⁵¹⁶ Compared with conventional microstructure fabrication techniques, REM comprises numerous advantages. For example, REM is capable of embossing over relatively large areas quickly and simultaneously rather than line-by-line serial processes. Besides, the stamp using REM techniques can fabricate moulds, replicas, and patterned surface for many repeating times (>50) potentially at atomic level resolutions.⁷⁴ Moreover, the elastomeric stamp of REM allows the pattern to be transferred onto non-planar surfaces, and the structured materials are not limited to e-beam sensitive materials.⁵²¹

Until now, a variety of work has been presented for structuring organic polymers with micropatterns by REM techniques for application in microfluidic and photovoltaic industries.^{522,523} However, the devices made of most of the organic polymers can hardly survive in harsh environments as they lack properties such as high-temperature tolerance, corrosion resistance and other extreme conditions.⁵²⁴ Therefore, the development of various fabrication methods of inorganic ceramic microstructures would continuously be of great importance. Potentially, transferring the preceramic polymers to ceramics by pyrolysis is one of the feasible routes for fabricating inorganic ceramic microstructures with REM techniques.⁵²⁵

In this work, a novel UV and thermal dual curable precursor ceramics, provided by our collaborator – Jie Kong's group in Northwest Polytechnical University, Xi'an, China, is employed for the fabrication of inorganic ceramic films. The precursor material is structured

with microarray structures by an original patterned PDMS template using a special soft lithography technique of replica moulding method, followed by step heating and pyrolysis processes, resulting in the proportional shrunk sized ceramic film with similar microarray patterns. The fabricated ceramic film is further applied as the new master template to cast the PDMS stamp, thus achieving microarray structures of the same geometries as the original template but in a minified specification. Moreover, this replica cycle can be repeated multiple times to produce proportionally minimized microarray geometries. Therefore, this simple and effective method shows significant potentials to pave a novel route for the fabrication and manipulation of size and shape-controlled microarray structures in a cost-effective way.

7.2. Replica Moulding Method for Preparing Minified Microarray Structures

The general concept of fabricating microarray structures of shrunk size using the soft lithography technique of the replica moulding method is schematically demonstrated in Figure 7.1. Generally, the preparation process is initiated with a patterned PDMS stamp with microarray structures that are fabricated following the preparing method demonstrated in 3.2.1. The PDMS stamp, either with microwell or micropillar array structures, is applied to structure the novel precursor ceramic polymer, which is further pyrolyzed into ceramic film with reversed microarray structure and smaller dimension compared with the initial PDMS template. The detailed description of the templating and pyrolysis will be presented in section 7.2.2. After that, the patterned ceramic film becomes the master template for casting PDMS stamp, resulting in a new PDMS stamp template of identical surface structure with original PDMS stamp but in a smaller specification. Following the same procedures above, the new PDMS stamp of shrunk size can be employed for another cycle of the fabrication of PSO film, enabling the templating of proportionally minified microarray structures, as shown in Figure 7.1.

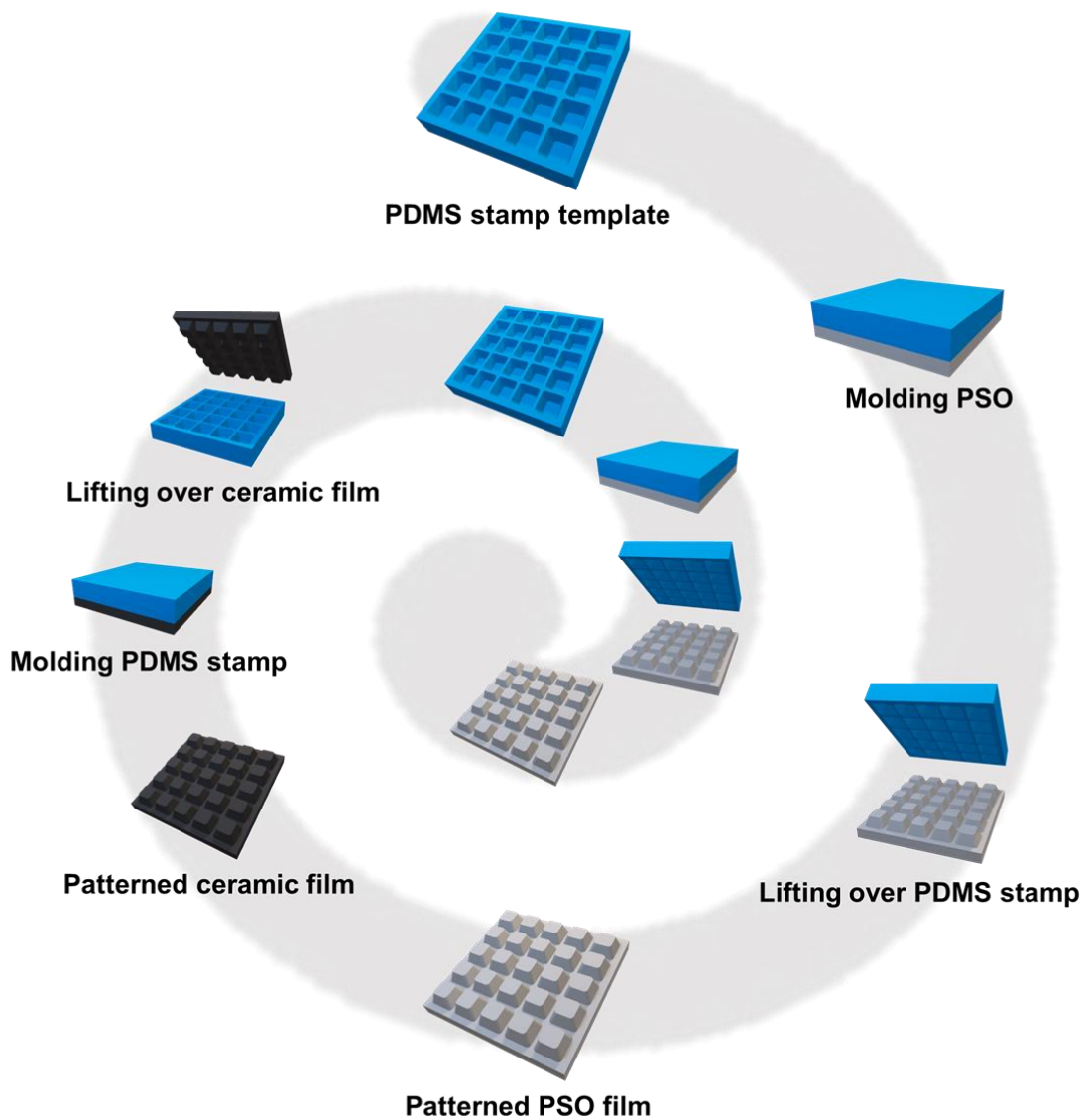


Figure 7.1 Schematic illustration of the process of preparing proportionally shrunk microarray structure.

Therefore, with this soft lithography technique of replica moulding method, proportionally smaller sized inorganic films, as well as PDMS stamp templates, can be quickly and simply achieved in a cost-effective way by further repeating this spiral cycle more times, without the requirement of costly and complicated lithography equipment and procedures.

7.2.1. Design and Synthesis of Precursor Ceramics

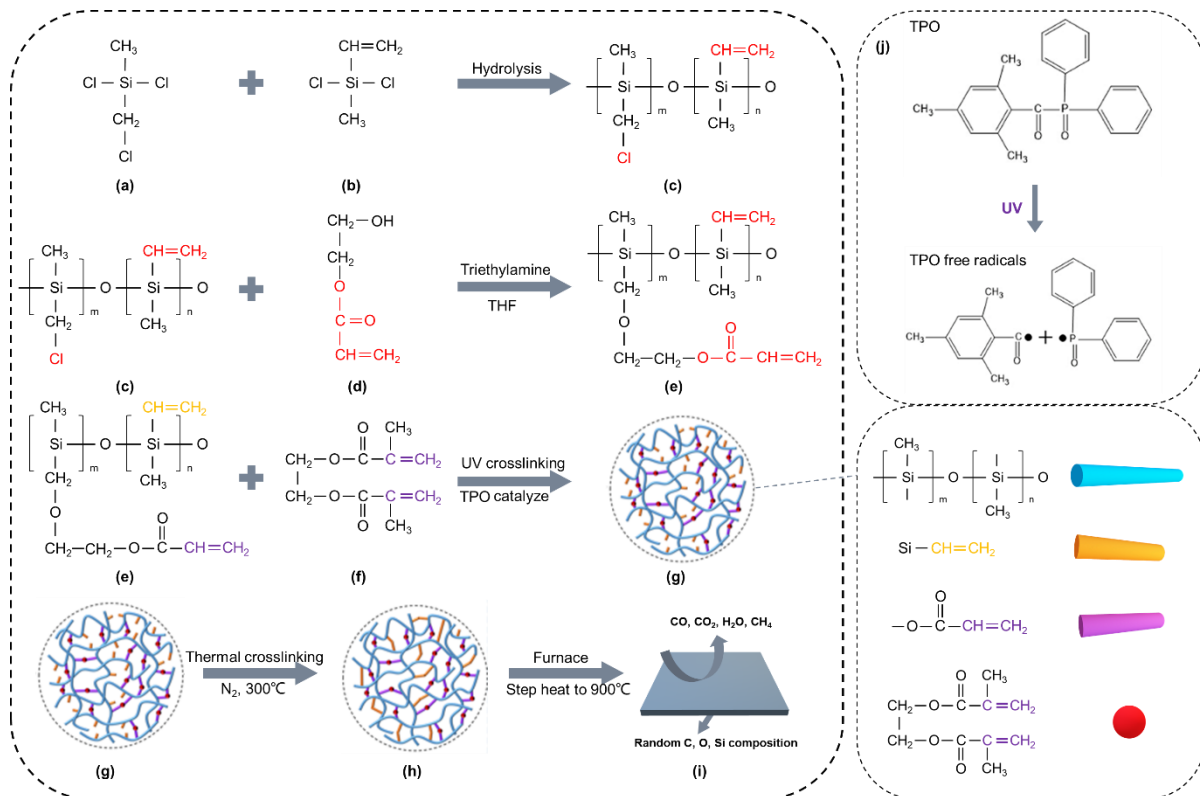


Figure 7.2 The synthesis route of inorganic ceramics. (a) Dichloro (chloromethyl) methylsilane, (b) Dichloromethylvinylsilane, (c) Polysiloxane, (d) Hydroxyethyl acrylate, (e) UV-PSO, (f) Ethylene glycol dimethacrylate (g) UV cured precursor, (h) UV and thermal dual-cured precursor, (i) prepared ceramics, (j) the formation of TPO free radicals under UV light.

As shown in Figure 7.2, the synthesis route of inorganic ceramics is initiated with the hydrolysis and condensation reactions between dichloro (chloromethyl) methylsilane and dichloromethylvinylsilane (Figure 7.2 (a) and (b)), forming the polysiloxane (PSO) which serves as the main chain of the precursor ceramics. This PSO polymer provides an unsaturated hydrocarbon radical vinyl ($-\text{CH}=\text{CH}_2$) as well as a chloro group ($-\text{Cl}$) as red colour labelled in Figure 7.2 (c). The chloro group of PSO is then etherified with hydroxyethyl acrylate (HEMA, Figure 7.2 (d)) in the organic solvent tetrahydrofuran (THF) at alkaline conditions provided by the triethylamine (Et_3N), result in the UV-PSO with two vinyl ($-\text{CH}=\text{CH}_2$) groups as shown in red colour in Figure 7.2 (e). After that, diester ethylene glycol dimethacrylate (EGDMA), commonly employed in free radical copolymer crosslinking reactions, is added into UV-PSO to provide two symmetric vinyl ($-\text{CH}=\text{CH}_2$) groups. In addition, the photo initiator diphenyl(2,4,6-trimethylbenzoyl) phosphine oxide

(TPO) is also introduced into UV-PSO which can provide free radicals under the radiation of UV light as shown in Figure 7.2 (j). It is noteworthy to address that the mixture of UV-PSO, EGDMA and TPO should be carefully stored in a dark environment avoiding illumination by the sun or other light sources. The crosslinking of the prepolymer mixture is first initiated by the radiation of UV light, which triggers the generation of TPO free radicals and the double bond addition reactions. At this stage, the vinyl groups of both UV-PSO and EGDMA (labelled in purple in Figure 7.2 (e) and (f)) are crosslinked, leading to an interconnected 3D polymeric network (Figure 7.2 (g)). Here, the addition of EGDMA can not only be served as a crosslinker but also provide more crosslinking active positions and accelerate the rate of the reaction. After the UV curing, the liquid mixtures are solidified which is further heated in the tube furnace for thermal crosslinking. The thermal curing reaction takes place at around 300°C under the N₂ atmosphere, where the vinyl group on the main chains (Si- vinyl) are opened and connected so that the crosslinking rate is significantly enhanced, as shown in Figure 7.2 (h). Finally, the inorganic ceramics (Figure 7.2 (i)) of proportionally shrunk size are successfully fabricated after the pyrolysis process that the UV and thermal dual crosslinked polymers are step-heated up to 900 °C to decompose the organic composition. During the pyrolysis process, small gas molecules such as CO, CO₂, H₂O and CH₄ were generated and removed, leaving only ceramics with the randomly compounded composition of C, Si, and O.

7.2.2. Preparation of Minified Inorganic Microarray Structures

The achievement of the ceramic microarray structure with shrunk size involves the application of the precursor material, whose synthesis routes, as well as general properties, have been introduced in 7.2.1. By taking the advantage of both the crosslinking solidification and the size-shrink properties of the material, the shrink-sized ceramic microarray structure can be fabricated with a special soft lithography technique of replica moulding method, which has been schematically demonstrated in Figure 7.3.

This work first time propose the idea of combining the dual curable and pyrolysis-shrink properties of precursor ceramics with microarray structures for getting proportionally minified specification for multiple times through PDMS soft lithography. With this proposed approach, people can get shortcut to achieve proportionally minified structure beyond microarray structures. One of the largest advantages of the replica moulding technique is that it is a cost-effective method without the requirement of expensive and special equipment, which enables the widely applications among researchers. Besides, this replica moulding technique is a high-volume pattern fabrication method as a large area can be replicated and transferred at each time. In addition, this technique can transfer the structure efficiently with high accuracy. By repeating the technique multiple times, proportionally minified structure can be easily achieved. Moreover, unlike common organic template, the inorganic template produced in this replica moulding technique can survive in environment, like high temperature, corrosion resistance and other extreme conditions, thus can be applied in broader areas with harsh environment.

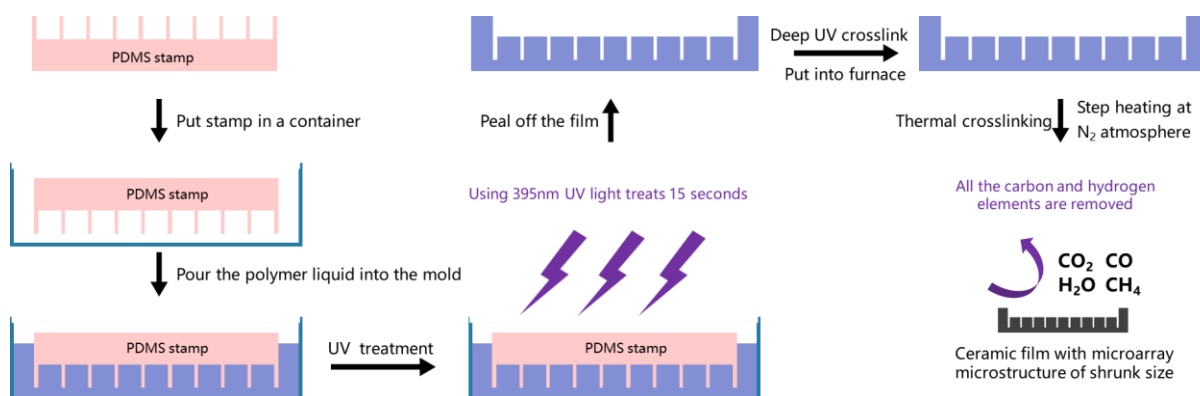


Figure 7.3 Schematic demonstration of the process for fabricating ceramic microarray films.

A patterned PDMS stamp with microarray surface structures is employed for the fabrication of inorganic films as shown in Figure 7.3. The PDMS stamp is placed in a container or other substrates with the patterned side face the bottom. After that, the liquid solution of UV-PSO mixtures is dropped and poured on the side of PDMS so that the liquid can be automatically spread onto the overall surface of the patterned PDMS by the capillary forces. The UV curing is activated by vertically illuminating the PDMS stamp and the UV-

PSO mixture with UV light at the wavelength of 395 nm generated by a 10-watt UV torch. There are two times UV crosslinking processes. The first one is aiming at solidifying the prepolymer with about 30% of the crosslinking rate after about 15-second radiation. After the solidification, the PDMS stamp is peeled off, leaving a freestanding film with reversed microarray structures. While in the second UV curing procedure, the freestanding patterned film is further and deep cured under the illumination of the same UV light for 6 hours to maximize the crosslinking rate. After that, the UV cured freestanding film is then thermally crosslinked in a tube furnace at 300°C for 2 hours, followed with pyrolysis process by step heating the prepolymer up to 900°C to decompose the organic components in the polymeric structures, result in a proportional size shrunk inorganic ceramic film with microarray structures. The specified tube furnace setup protocol for thermal crosslinking and step heating pyrolysis of UV crosslinked microarray films is listed in Table 7-1 below.

Table 7-1 The setup details of the tube furnace for the heat treatment of UV-crosslinked film.

	Ramp speed (°C/min)	Target temperature (°C)	Incubation time (h)
Step 1	1	150	1
Step 2	1	350	1
Step 3	1.5	25	0.5
Step 4	1	500	2
Step 5	1	700	1
Step 6	1	900	2
Step 7	1.5	700	0.5
Step 8	1.5	500	30
Step 9	Naturally	Room temperature	/

It is worth noting that in Figure 7.3, the PDMS stamp is selected as microwell array surface morphology as an example for demonstration, stamps of other geometries like micropillar arrays are also fit for the fabricating process with the same procedures.

7.3. Characterization of Shrink-Sized Microarray Structures

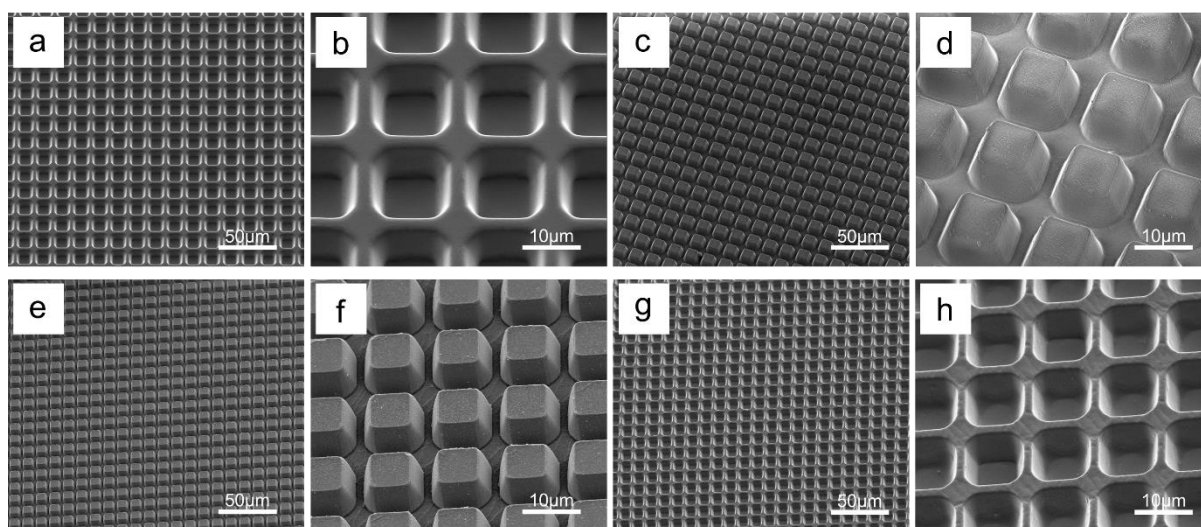


Figure 7.4 The surface morphology of a,b) original patterned PDMS stamp with microwell array surface structure. c,d) micropillar array film made of UV cured precursor polymer moulded from a,b) before the tube furnace pyrolysis. e,f) the inorganic film pyrolyzed from c,d) with shrink-sized micropillar array surface structure. g,h) new PDMS stamp with shrink-sized microwell array surface structure cast from e,f).

SEM is applied to evaluate the surface morphology of the original employed patterned PDMS stamp, the fabricated micropillar array films before and after the tube furnace pyrolysis processes as well as the new patterned PDMS stamp, with the results shown in Figure 7.4. The applied original PDMS stamp has perfect and complete periodic microwell array structures without any contaminations (Figure 7.4 a) and b)), thus serves as an excellent template for replica moulding of UV-PSO polymers. The morphology of UV-cured and solidified precursor micropillar array films are presented in Figure 7.4 c) and d), whose surface is complete and smooth with every individual truncated pyramid-shaped micropillars perfectly transferred and arranged into arrays without losing any structural details. After the thermal crosslinking as well as the pyrolysis processes, the ceramic micropillar array films are successfully obtained with the surface geometries shown in Figure 7.4 e) and f), where micropillars are clearly observed, arranging perfectly and periodically as arrays similar to the UV-PSO film before heat treatment but in a proportionally smaller size. The surface of the ceramic pillar is almost as smooth as the original UV-PSO film without losing any pillar details, while the surface between pillars

presents some defects that random streamline that may cause by the inhomogeneous gas flow in the tube furnace, which can be avoided by optimizing the gas flow velocity. These defects are also reflected in the PDMS stamp replica of the micropillar array ceramic film, as demonstrated in Figure 7.4 g) and h) that some randomly distributed grooves emerge on the surface of the new PDMS stamp, indicating a high sensitivity of this replica moulding technique. Whereas in general, it is found that the new PDMS template has an excellent reversed periodical microwell array structure of its inorganic template. Furthermore, it is calculated that the period of the micropillar array films is shrunk from 16 μm to 11.7 μm before and after the pyrolysis, respectively. In other words, the period of ceramic micropillar array films becomes 73% of the original UV-PSO micropillar array films.

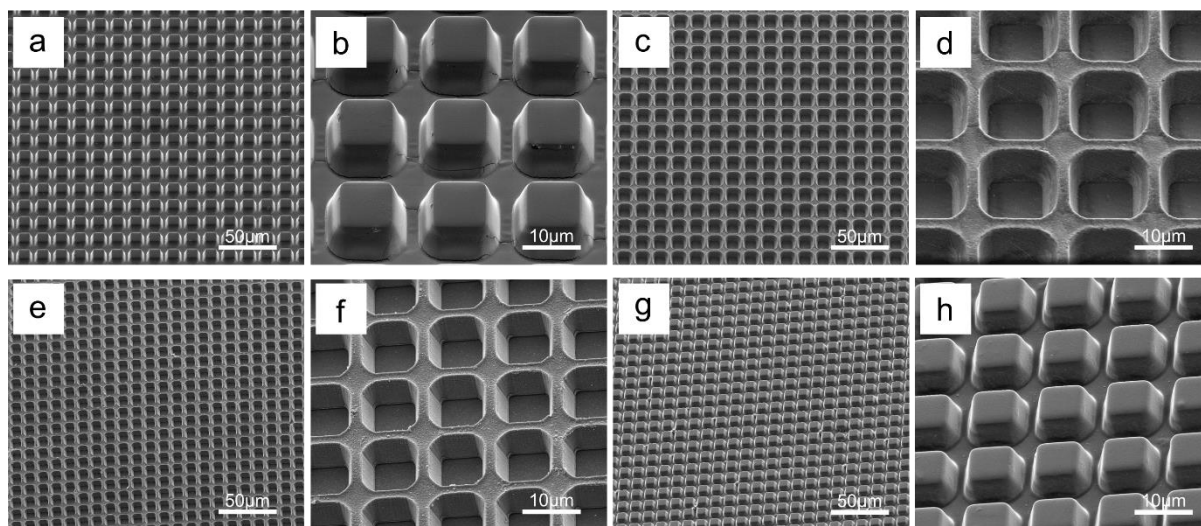


Figure 7.5 The surface morphology of a,b) original patterned PDMS stamp with micropillar array structure. c,d) microwell array film made of UV cured precursor polymer moulded from a,b) before the tube furnace pyrolysis. e,f) the inorganic film pyrolyzed from c,d) with shrink-sized microwell array structure. g,h) new PDMS stamp with shrunken micropillar array surface structure cast from e,f).

Similar results can be found in the microwell array films made of inorganic ceramics when the applied PDMS stamp is changed to patterned micropillar array structures, as shown in Figure 7.5. The employed patterned PDMS stamp has the exact same specifications but reversed structure of the PDMS stamp used for preparing micropillar arrays, as shown in Figure 7.5 a) and b). The PDMS stamp with micropillar arrays also has a smooth surface and highly periodic structures. The morphology of UV crosslinked

precursor polymer replica of the PDMS stamp is shown in Figure 7.5 c) and d) that perfectly ordered microwell arrays are formed on the clean and complete surfaces. Figure 7.5 e) and f) demonstrate the morphology of inorganic ceramic microwell array films after thermal crosslinking and pyrolysis in the tube furnace. The ceramic films at this stage still retain the periodic microwell array structures in relatively large surface areas, and also, present a shrunk specification. This ceramic film with microwell arrays surface structures can also be served as the template for moulding new PDMS stamps whose surface geometry is shown in Figure 7.5 g) and h). Here, the new PDMS replica presents a perfect micropillar array morphology with clean and smooth surfaces displayed both on and between the micropillars, indicating the potential as the template for further replica moulding. In addition, it is noteworthy to mention that the specification of the inorganic ceramic microwell array films has the same shrunk rate as the micropillar array ones, with the period of the UV cured precursor microwell array films shrink 27% from 16 μm to 11.7 μm after pyrolysis process.

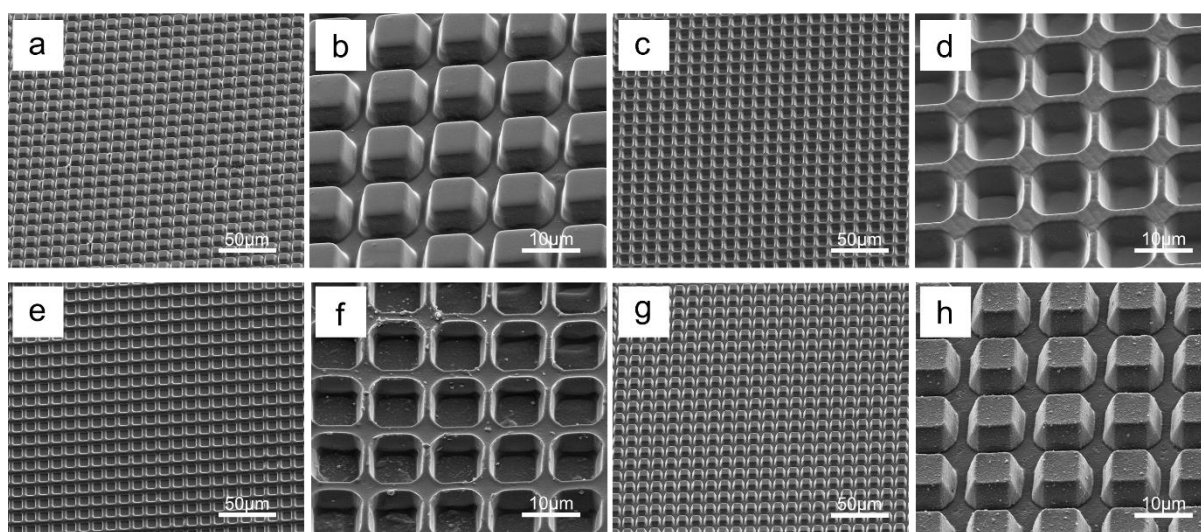


Figure 7.6 The surface morphology of a,b) the new patterned PDMS stamp with micropillar array structure. c,d) the new patterned PDMS stamp with microwell array structure. e,f) microwell array film made of UV cured precursor polymer moulded from a,b) before the tube furnace pyrolysis. g,h) microwell array film made of UV cured precursor polymer moulded from c,d) before the tube furnace pyrolysis.

Employing the shrink-sized PDMS stamp cast from the microarray structured ceramic film as the template, UV-PSO film with reversed microarray structures can be further fabricated, as demonstrated in Figure 7.6. Comparing with the PDMS stamp (Figure 7.6 a)

and b)), the UV crosslinked and solidified PSO film has a completely reversed microwell array surface structure without losing many details despite some contamination presented on the surface as shown in Figure 7.6 e) and f). Similarly, the UV-PSO micropillar array replica (Figure 7.6 g) and h)) from shrink-sized microwell array PDMS stamp (Figure 7.6 c) and d)) also ideally restore the reversed structure that even the randomly distributed grooves on the PDMS template are reflected to some extent. In general, the UV-PSO microarray film can be applied for another pyrolysis and PDMS casting procedures to further obtain two-time-shrunk microarray structures. Although a certain degree of structural detail loss is always inevitable during each replica moulding process, it is revealed that an extremely low structure loss can be achieved with this “PDMS stamp-UV PSO-ceramic film-PDMS stamp” spiral soft lithography cycle method.

7.4. Conclusions

This work introduces a simple, efficient, and cost-effective soft lithography method of replica moulding technique to fabricate minified microarray structures with the assistance of novel UV and thermal dual curable precursor ceramics. The special micropillar and microwell array microstructures of the selected PDMS template are successfully replicated and transferred onto the surface of UV crosslinked and solidified UV-PSO in high resolutions. In addition, the inorganic ceramic films with minified microarray structures are successfully fabricated after thermal crosslinking and pyrolysis processes. The specification of the microarray structures of the inorganic ceramic films are significant shrinks compared with the patterned UV crosslinked precursor ceramics and the original PDMS stamp, as the period of the microarray structure varies from 16 μm to 11.7 μm for heat untreated and heat-treated films, respectively. Moreover, a new PDMS stamp with minified microarray structures is obtained by using the resulted ceramic film as the master template. The new minified PDMS has the same function as the original PDMS template that can structure precursor ceramic material with minified microarray structures.

It is noteworthy to mention that this work just proves the feasibility of the soft lithography technique for the fabrication of minified microarray structure by demonstrating a cycle of the replica moulding processes. While the overall goal of this work is to generate a series of inorganic ceramic films thus producing microarray structures of proportionally minified size in different degrees. Therefore, with one lithographed master template with predetermined size and shape, many replicas of the designed master template of proportionally different size and the same geometries can be easily duplicated, indicating an efficient and cost-effective approach for fabricating size and shape-controlled geometries.

Although the proposed soft lithography techniques of replica moulding methods owns a variety of advantages, the limitations of the techniques also need to be considered. One of the largest disadvantages was that the replicated and transferred structures can only be proportionally shrunk, in other words, the original structure must be produced by other lithography techniques and the fabricated cannot be changed during the replica processes. This is an inherent limitation of the technique that can not be overcome. While another significant drawback was that the shrunk size after each fabrication cycle can not be adjusted as the shrunk proportion is the inherent properties of the precursor ceramics themselves. However, this drawback is expected to be solved when applying and combining different precursor ceramics that owns different shrinking properties.

8. General Conclusions and Outlooks

8.1. Conclusions

In this thesis, microarray structures were applied to provide periodic micropatterns to a variety of materials, including stimuli-responsive polyelectrolytes, biodegradable and hydrophobic polymer PLA and PCL and their combination as well as polysiloxane, in order to overcome the challenges in sensing, drug delivery areas and microfabrication. As a result of this work, several multidisciplinary applications are achieved.

The preparation of an inexpensive and portable multi-sensing platform based on structured microarray films is achieved. Given the property of microarray structure that diffraction patterns can be generated when illuminated by laser light, any external stimuli that contribute to the deformation of stimuli-responsive microarray films will be accurately and efficiently reflected on diffraction patterns. To sense the external stimuli, Microarray structures were combined with stimuli-responsive polymers, producing PAA/PAH PEC micropillar array films as well as PCL microchamber array films.

- 1) The ability of PAA/PAH PEC micropillar array films for sensing pH was investigated. Both PAA and PAH weak polyelectrolytes whose ionizations are intimately associated with pH. The results showed that the pH solution variations induce shrink and swell behaviours in the PEC microstructure, which, therefore, alter the resulting diffraction patterns. RCWA simulation results proved that all the changes of the diffraction pattern were attributed to the induced changes of microarray geometry rather than optical constants of PEC, with simulations agreeing well with experimental results.
- 2) Since the presence of divalent ions can induce chelation with PAA leading to the reduction of charge repulsion, the ions sensing potential of PAA/PAH PEC micropillar array films were also explored. The results showed that divalent metal

ions can lead to reversible shrinkage of PEC micropillar arrays films, allowing multiple times detections and were confirmed by RCWA simulations.

- 3) PCL is micro-structured into microchamber arrays for sensing temperature, with the results showing when the temperature surpasses the melting point of PCL, the viscous flow-induced microstructure elimination would emerge, causing the loss of light scattering properties which is consistent with RCWA simulations.

In addition, the successful encapsulation and biologically stimulated release of small hydrophilic molecules are implemented by fabricating microchamber array films made of hydrophobic and biodegradable polymer blends of PCL and PLA. In the results, PCL microchamber array films can be efficiently degraded by lipase PS at a concentration of 0.5 mg/ml within 5 hours. The degradation behaviours of PCL microchamber arrays can be conveniently and real-time checked based on the time of full degradation time and the disappearance of laser diffraction patterns, enabling the ability for sensing enzymes. With the decrease in lipase concentration, the degradation time becomes prolonged. The addition of PLA significantly decreases the permeability of PCL films, enabling the encapsulation of small and hydrophilic molecule CF, as an envisaged model drug, in a high amount of about 11 pg per microchamber, which can be enzymatically controlled released under the presence of lipase PS within 26 hours.

Moreover, a novel biodegradable drug delivery vehicle of microcages was first time fabricated, which not only can encapsulate small and hydrophilic molecules in a non-liquid fashion, but also have a uniform size distribution with homogeneous predesigned shape. The microcages were made of biodegradable polymers PLA and PCL of various blending ratios, enabling the encapsulation of small and hydrophilic cargo CF. The release rate of microcages can be controlled by adjusting the blending ratio of PLA and PCL that with the increase of PCL contents in the microcage shell, the release rate of CF become faster. It is noteworthy to address that the model drug CF was loaded in dry loading method, with the

overall loaded amount in every million microcages reaching about 30 μg , or calculated as 30 pg in each microcages, indicating that the printed biodegradable microcages can accommodate chemical compounds in a highly efficient way.

Furthermore, a simple, efficient, and cost-effective soft lithography method of replica moulding technique is introduced for the microfabrication of minified microarray structures with the assistance of novel UV and thermal dual curable precursor ceramics. Generally, periodical micropillar and microwell array microstructures of the selected PDMS template are successfully replicated and transferred onto the surface of UV crosslinked and solidified UV-PSO in high resolutions. In addition, the inorganic ceramic films with minified microarray structures are successfully fabricated after thermal crosslinking and pyrolysis processes, with the period of the microarray structure of the ceramic shrinks 27% from 16 μm to 11.7 μm compared with untreated UV-crosslinked precursor material. Moreover, a new PDMS stamp with minified microarray structures is obtained by using the resulted ceramic film as the master template. The new minified PDMS has the same function as the original PDMS template that can be applied for precursor ceramic material microfabrication.

8.2. Outlooks

This thesis investigates the potential multidisciplinary application of microarrays structures when transferred and imprinted with different polymers, such as sensing platforms, 2D drug delivery films, 3D microcages, as well as structuring templates, showing great versatility. However, more applications can be achieved by adjusting the combined materials with different properties. Besides, some improvements and explorations of the fabricated micropillar or microchamber array films, biodegradable microcages and templating minified microarray structures demonstrated in this thesis are required in the future.

The sensing of environmental changes of pH, ions and temperature are merely some examples of what the sensing platform of microarray structure can achieve. A multitude of

other reversible and irreversible external stimuli sensing properties can be realized by changing the types and/or compositions of polymers being structured into microarrays. For example, the crosslinked polyelectrolytes PMMA can be fabricated into microarray structures for sensing pH value ranging from pH 4 to pH 8.⁴⁴¹ Besides, enzymes might be introduced into these polymers to enable sensing chemical species.⁴⁴² In addition, different polyelectrolyte complex combinations for various sensing ranges can be further explored. The minimum concentration of ions that can be measured by PEC micropillar films are also worth exploring. Moreover, the possibility of sensing multiple factors at the same time can also be performed by the employment of different PEC micropillar films at the same time. In other word, the microarray structure reveals a unique chance to further incorporate different functional and responsive polymers into one entity. Ultimately, an inexpensive, convenient and portable multi-sensing platform can be fabricated by combining the stimuli-responsive properties of different materials which provides the opportunities to determine multiple external stimuli in real-time. Also, sensor arrays might be utilized in the future in combination with multivariant data analysis to increase sensitivity towards isolated species and for quantification of the amounts of single species. After gathering sufficient experimental data, special simulation models and algorithms can be establish for better guidance and prediction of the practical applications.

The truncated quadrangular pyramid shape of microcages can be further printed into different size and shape which are determined not only by the predesigned lithographed template,³⁷ but also by the casted microarray structure on the surface of the PDMS stamp, whose resolution limit is in the range of 100-200 nm.⁴⁷³ While the size of PLA microcages printed from PDMS stamp in this work is around 15 μm , indicating huge potentials to be fabricated into a smaller size. By the introduction of microarray stamp made of other low surface tension but with high hardness materials, the potential microcage specifications can be further decreased.

In addition, the architectural difference between microcages and microcages is that although cargos are wrapped by shell polymers, there is no empty space inside microcages to form a distinctive core-shell structure as microcages did. The special microcage structure is formed since high printing temperature was employed to melt the shell polymers so that the individual microcages can be separated and sealed. However, it is believed in the future, when the printing of microcages was performed by programmed machines instead of manually pressing, individual core-shell structured microcages can be separated and sealed owing to the high pressing pressure. The proposed microcage printing technique can be easily industrialized. The simple fabrication processes of microcages also enables the scale-up massive production of microcages with the assistance of auto-streamlines.

Moreover, the release of encapsulated cargos from PLA microcages was achieved simply by the diffusions in this work. While the release rate was controlled by adjusting the composition of wrapping polymers and result in different permeabilities. Other triggered release methods of microcages are required to be investigated. For instance, using near-infrared laser as release triggers by incorporating gold nanoparticle into polymer shell.²⁶ Or release the encapsulated cargos via the biodegradation of wrapping polymer.⁵²⁶ In addition, by incorporating magnetic nanoparticles or chemically modify the polymer surface, the targeted delivery of drugs can be achieved. Though further experiment is also needed to evaluate the safety and activity of microcages against cells *in vitro* and *in vivo* before applying in drug delivery fields, especially to determine optimal drug concentration for the release. the appropriate drug concentration for the treatment varies from diseases, and is commonly decided in the phase I clinic trial. While in order to control the amount of drug release at specific time range, changing the polymer composition would be a feasible way to control the release rate. Also, the release concentration can also adjusted by using different number of microcages and different area of microchamber array films.

Furthermore, the loaded cargo selected in this work is merely an envisaged model drug 5,6-carboxyfluorescein with the benefits of tracing and quantifying. Now that the fundamental properties of the biodegradable microchamber array films as well as microcages have been initially acknowledged and confirmed, a real pharmaceutical drug can be encapsulated in microchamber array films and microcages, whose release kinetics, pharmaceutical abilities for the disease treatment *in vitro* and *in vivo* should also be further investigated and explored. Current size of present microcages are too large to be injected in blood circulation for drug delivery. However, it is an appropriate size for localized drug delivery. For example, dexamethasone, as one of the glucocorticoids, can be encapsulated into microcages. These drug loaded microcages can be injected into joint cavity, which cannot be internalized by cells or excluded from the joint, enabling a sustained local dexamethasone release, indicating great potentials for the treatment of arthritis. When the microcages can be printed into smaller size, the intravenous injection is possible and the potential deliverable drug area can be significantly expanded. Other practical drug formulations such as external paste, gels and so forth can be feasible options.

Although biodegradable microchamber array films cannot be applied as flexible as microcages, its special 2D structure indeed have advantages in special drug delivery areas. For example, the drug loaded microchamber array films can be wrapped surrounding implant or stents, and sustained release anti-inflammatory or anti-bacterial drugs around the wounds. In addition, the thin microchamber array films can also be rolled into biodegradable threads for surgery suture with extra function of releasing drugs that helps recovery. The function of trigger release can be added into the microarray films as well, expanding its potentially for designed and remote controlled drug release.

For the microfabrication of microarray structures, this work just proves the feasibility of the soft lithography technique by demonstrating a cycle of the replica moulding processes. Though the resolutions of the replica are relatively high with almost all the details reflected

in this initial cycle, the structural deviation cannot be thoroughly avoided. This problem would be accumulated and magnified with the increasing number of replica cycles and up to a threshold where the loss of resolution becomes unacceptable. Therefore, in the future, it is of great importance to explore that replica threshold thus determining the limitation of this microfabrication technique. In addition, as the shrinking degree of precursor ceramic varied with the specific compositions, the properties of different precursor ceramics should be tested, enabling more desired and optional minified structures.

References

- (1) Whitehead, K. A.; Colligon, J. S.; Verran, J. The Production of Surfaces of Defined Topography and Chemistry for Microbial Retention Studies, Using Ion Beam Sputtering Technology. *Int. Biodeterior. Biodegrad.* **2004**, *54* (2–3), 143–151. <https://doi.org/10.1016/j.ibiod.2004.03.010>.
- (2) Whitehead, K. A.; Colligon, J.; Verran, J. Retention of Microbial Cells in Substratum Surface Features of Micrometer and Sub-Micrometer Dimensions. *Colloids Surfaces B Biointerfaces* **2005**, *41* (2–3), 129–138. <https://doi.org/10.1016/j.colsurfb.2004.11.010>.
- (3) Lejeune, M.; Chartier, T.; Dossou-Yovo, C.; Noguera, R. Ink-Jet Printing of Ceramic Micro-Pillar Arrays. *J. Eur. Ceram. Soc.* **2009**, *29* (5), 905–911. <https://doi.org/10.1016/j.jeurceramsoc.2008.07.040>.
- (4) Seto, M.; Westra, K.; Brett, M. Arrays of Self-Sealed Microchambers and Channels. *J. Mater. Chem.* **2002**, *12* (8), 2348–2351. <https://doi.org/10.1039/b204598m>.
- (5) Pimpin, A.; Srituravanich, W. Reviews on Micro- and Nanolithography Techniques and Their Applications. *Eng. J.* **2012**, *16* (1), 37–55. <https://doi.org/10.4186/ej.2012.16.1.37>.
- (6) Kim, K.; Xu, X.; Guo, J.; Fan, D. L. Ultrahigh-Speed Rotating Nanoelectromechanical System Devices Assembled from Nanoscale Building Blocks. *Nat. Commun.* **2014**, *5*, 1–9. <https://doi.org/10.1038/ncomms4632>.
- (7) Hui, C. Y.; Jagota, A.; Lin, Y. Y.; Kramer, E. J. Constraints on Microcontact Printing Imposed by Stamp Deformation. *Langmuir* **2002**, *18* (4), 1394–1407. <https://doi.org/10.1021/la0113567>.
- (8) Bozorgzadeh, F.; Sahrai, M. Laser-Induced Diffraction Grating in Asymmetric Double Quantum Well Nanostructure. *Laser Phys. Lett.* **2019**, *16* (3). <https://doi.org/10.1088/1612-202X/ab0101>.
- (9) Yap, C. Y.; Chua, C. K.; Dong, Z. L.; Liu, Z. H.; Zhang, D. Q.; Loh, L. E.; Sing, S. L. Review of Selective Laser Melting: Materials and Applications. *Appl. Phys. Rev.* **2015**, *2* (4). <https://doi.org/10.1063/1.4935926>.
- (10) Khodier, S. A. Measurement of Wire Diameter by Optical Diffraction. *Opt. Laser Technol.* **2004**, *36* (1), 63–67. [https://doi.org/10.1016/S0030-3992\(03\)00134-8](https://doi.org/10.1016/S0030-3992(03)00134-8).
- (11) Zhang, F.; Wang, C.; Yin, K.; Dong, X. R.; Song, Y. X.; Tian, Y. X.; Duan, J. A. Quasi-Periodic Concave Microlens Array for Liquid Refractive Index Sensing Fabricated by Femtosecond Laser Assisted with Chemical Etching. *Sci. Rep.* **2018**, *8* (1), 1–10. <https://doi.org/10.1038/s41598-018-20807-1>.
- (12) Xu, Z.; Han, K.; Khan, I.; Wang, X.; Liu, G. L. Liquid Refractive Index Sensing Independent of Opacity Using an Optofluidic Diffraction Sensor. *Opt. Lett.* **2014**, *39* (20), 6082. <https://doi.org/10.1364/ol.39.006082>.
- (13) Ma, Z.; Merkus, H. G.; De Smet, J. G. A. E.; Heffels, C.; Scarlett, B. New Developments in Particle Characterization by Laser Diffraction: Size and Shape. *Powder Technol.* **2000**, *111* (1–2), 66–78. [https://doi.org/10.1016/S0032-5910\(00\)00242-4](https://doi.org/10.1016/S0032-5910(00)00242-4).

- (14) Yu, F.; Yao, D.; Knoll, W. Oligonucleotide Hybridization Studied by a Surface Plasmon Diffraction Sensor (SPDS). *Nucleic Acids Res.* **2004**, *32* (9). <https://doi.org/10.1093/nar/gnh067>.
- (15) Lee, Y. J.; Pruzinsky, S. A.; Braun, P. V. Glucose-Sensitive Inverse Opal Hydrogels: Analysis of Optical Diffraction Response. *Langmuir* **2004**, *20* (8), 3096–3106. <https://doi.org/10.1021/la035555x>.
- (16) Bai, W.; Spivak, D. A. A Double-Imprinted Diffraction-Grating Sensor Based on a Virus-Responsive Super-Aptamer Hydrogel Derived from an Impure Extract. *Angew. Chemie - Int. Ed.* **2014**, *53* (8), 2095–2098. <https://doi.org/10.1002/anie.201309462>.
- (17) Ulery, A. L.; Flynn, R.; Parra, R. Appropriate Preservation of Dairy Wastewater Samples for Environmental Analysis. *Environ. Monit. Assess.* **2004**, *95* (1–3), 117–124. <https://doi.org/10.1023/B:EMAS.0000029892.53599.81>.
- (18) Hoogenboom, G. *Measuring the Natural Environment*, Second Edi.; Cambridge University Press, 2005; Vol. 45. <https://doi.org/10.2135/cropsci2005.0014br>.
- (19) Krasteva, N.; Fogel, Y.; Bauer, R. E.; Müllen, K.; Joseph, Y.; Matsuzawa, N.; Yasuda, A.; Vossmeier, T. Vapor Sorption and Electrical Response of Au-Nanoparticle-Dendrimer Composites. *Adv. Funct. Mater.* **2007**, *17* (6), 881–888. <https://doi.org/10.1002/adfm.200600598>.
- (20) Gao, Y.; Li, X.; Serpe, M. J. Stimuli-Responsive Microgel-Based Etalons for Optical Sensing. *RSC Adv.* **2015**, *5* (55), 44074–44087. <https://doi.org/10.1039/c5ra02306h>.
- (21) Kiryukhin, M. V.; Man, S. M.; Gorelik, S. R.; Subramanian, G. S.; Low, H. Y.; Sukhorukov, G. B. Fabrication and Mechanical Properties of Microchambers Made of Polyelectrolyte Multilayers. *Soft Matter* **2011**, *7* (14), 6550–6556. <https://doi.org/10.1039/c1sm05101f>.
- (22) Antipina, M. N.; Kiryukhin, M. V.; Skirtach, A. G.; Sukhorukov, G. B. Micropackaging via Layer-by-Layer Assembly: Microcapsules and Microchamber Arrays. *Int. Mater. Rev.* **2014**, *59* (4), 224–244. <https://doi.org/10.1179/1743280414Y.0000000030>.
- (23) Decher, G.; Schmitt, J. Fine-Tuning of the Film Thickness of Ultrathin Multilayer Films Composed of Consecutively Alternating Layers of Anionic and Cationic Polyelectrolytes. *Trends Colloid Interface Sci. VI* **2007**, *89*, 160–164. <https://doi.org/10.1007/bfb0116302>.
- (24) Delcea, M.; Möhwald, H.; Skirtach, A. G. Stimuli-Responsive LbL Capsules and Nanoshells for Drug Delivery. *Adv. Drug Deliv. Rev.* **2011**, *63* (9), 730–747. <https://doi.org/10.1016/j.addr.2011.03.010>.
- (25) Gao, C.; Donath, E.; Moya, S.; Dudnik, V.; Möhwald, H. Elasticity of Hollow Polyelectrolyte Capsules Prepared by the Layer-by-Layer Technique. *Eur. Phys. J. E* **2001**, *5* (1), 21–27. <https://doi.org/10.1007/s101890170083>.
- (26) Kiryukhin, M. V.; Gorelik, S. R.; Man, S. M.; Subramanian, G. S.; Antipina, M. N.; Low, H. Y.; Sukhorukov, G. B. Individually Addressable Patterned Multilayer Microchambers for Site-Specific Release-on-Demand. *Macromol. Rapid Commun.* **2013**, *34* (1), 87–93. <https://doi.org/10.1002/marc.201200564>.

- (27) Volodkin, D. V.; Larionova, N. I.; Sukhorukov, G. B. Protein Encapsulation via Porous CaCO₃ Microparticles Templating. *Biomacromolecules* **2004**, *5* (5), 1962–1972. <https://doi.org/10.1021/bm049669e>.
- (28) Lomova, M. V.; Brichkina, A. I.; Kiryukhin, M. V.; Vasina, E. N.; Pavlov, A. M.; Gorin, D. A.; Sukhorukov, G. B.; Antipina, M. N. Multilayer Capsules of Bovine Serum Albumin and Tannic Acid for Controlled Release by Enzymatic Degradation. *ACS Appl. Mater. Interfaces* **2015**, *7* (22), 11732–11740. <https://doi.org/10.1021/acsami.5b03263>.
- (29) Sukhorukov, G. B.; Donath, E.; Moya, S.; Susha, A. S.; Voigt, A.; Hartmann, J.; Möhwald, H. Microencapsulation by Means of Step-Wise Adsorption of Polyelectrolytes. *J. Microencapsul.* **2000**, *17* (2), 177–185. <https://doi.org/10.1080/026520400288418>.
- (30) Georgieva, R.; Moya, S.; Hin, M.; Mitlöhner, R.; Donath, E.; Kiesewetter, H.; Möhwald, H.; Bäuml, H. Permeation of Macromolecules into Polyelectrolyte Microcapsules. *Biomacromolecules* **2002**, *3* (3), 517–524. <https://doi.org/10.1021/bm010164n>.
- (31) Craik, D. J.; Fairlie, D. P.; Liras, S.; Price, D. The Future of Peptide-Based Drugs. *Chem. Biol. Drug Des.* **2013**, *81* (1), 136–147. <https://doi.org/10.1111/cbdd.12055>.
- (32) Abbaspourrad, A.; Datta, S. S.; Weitz, D. A. Controlling Release from PH-Responsive Microcapsules. *Langmuir* **2013**, *29* (41), 12697–12702. <https://doi.org/10.1021/la403064f>.
- (33) Hsieh, W. C.; Chang, C. P.; Gao, Y. L. Controlled Release Properties of Chitosan Encapsulated Volatile Citronella Oil Microcapsules by Thermal Treatments. *Colloids Surfaces B Biointerfaces* **2006**, *53* (2), 209–214. <https://doi.org/10.1016/j.colsurfb.2006.09.008>.
- (34) Finotelli, P. V.; Da Silva, D.; Sola-Penna, M.; Rossi, A. M.; Farina, M.; Andrade, L. R.; Takeuchi, A. Y.; Rocha-Leão, M. H. Microcapsules of Alginate/Chitosan Containing Magnetic Nanoparticles for Controlled Release of Insulin. *Colloids Surfaces B Biointerfaces* **2010**, *81* (1), 206–211. <https://doi.org/10.1016/j.colsurfb.2010.07.008>.
- (35) Pavlov, A. M.; Saez, V.; Copley, A.; Graves, J.; Sukhorukov, G. B.; Mason, T. J. Controlled Protein Release from Microcapsules with Composite Shells Using High Frequency Ultrasound - Potential for in Vivo Medical Use. *Soft Matter* **2011**, *7* (9), 4341–4347. <https://doi.org/10.1039/c0sm01536a>.
- (36) Gai, M.; Kurochkin, M. A.; Li, D.; Khlebtsov, B. N.; Dong, L.; Tarakina, N.; Poston, R.; Gould, D. J.; Frueh, J.; Sukhorukov, G. B. In-Situ NIR-Laser Mediated Bioactive Substance Delivery to Single Cell for EGFP Expression Based on Biocompatible Microchamber-Arrays. *J. Control. Release* **2018**, *276* (January), 84–92. <https://doi.org/10.1016/j.jconrel.2018.02.044>.
- (37) Acharya, G.; Shin, C. S.; McDermott, M.; Mishra, H.; Park, H.; Kwon, I. C.; Park, K. The Hydrogel Template Method for Fabrication of Homogeneous Nano/Microparticles. *J. Control. Release* **2010**, *141* (3), 314–319. <https://doi.org/10.1016/j.jconrel.2009.09.032>.
- (38) Acharya, G.; Shin, C. S.; Vedantham, K.; McDermott, M.; Rish, T.; Hansen, K.; Fu, Y.; Park, K. A Study of Drug Release from Homogeneous PLGA Microstructures. *J. Control. Release* **2010**, *146* (2), 201–206. <https://doi.org/10.1016/j.jconrel.2010.03.024>.

- (39) Allison, S. D. Analysis of Initial Burst in PLGA Microparticles. *Expert Opin. Drug Deliv.* **2008**, *5* (6), 615–628. <https://doi.org/10.1517/17425247.5.6.615>.
- (40) Decher, G. Fuzzy Nanoassemblies: Toward Layered Polymeric Multicomposites. *Science (80-.)*. **1997**, *277* (5330), 1232–1237. <https://doi.org/10.1126/science.277.5330.1232>.
- (41) Sukhorukov, G. B.; Donath, E.; Davis, S.; Lichtenfeld, H.; Caruso, F.; Popov, V. I.; Möhwald, H. Stepwise Polyelectrolyte Assembly on Particle Surfaces: A Novel Approach to Colloid Design. *Polym. Adv. Technol.* **1998**, *9* (10–11), 759–767. [https://doi.org/10.1002/\(SICI\)1099-1581\(199810\)9:10/11<759::AID-PAT846>3.0.CO;2-Q](https://doi.org/10.1002/(SICI)1099-1581(199810)9:10/11<759::AID-PAT846>3.0.CO;2-Q).
- (42) Yaqoob Khan, A.; Talegaonkar, S.; Iqbal, Z.; Jalees Ahmed, F.; Krishan Khar, R. Multiple Emulsions: An Overview. *Curr. Drug Deliv.* **2006**, *3* (4), 429–443. <https://doi.org/10.2174/156720106778559056>.
- (43) Lee, T. Y.; Ku, M.; Kim, B.; Lee, S.; Yang, J.; Kim, S. H. Microfluidic Production of Biodegradable Microcapsules for Sustained Release of Hydrophilic Actives. *Small* **2017**, *13* (29), 1–11. <https://doi.org/10.1002/sml.201700646>.
- (44) G. B. Sukhorukov, E. Donath, S. M. Microencapsulation by Means of Step-Wise Adsorption of Polyelectrolytes. *J. Microencapsul.* **2000**, *17* (2), 177–185. <https://doi.org/10.1080/026520400288418>.
- (45) Thorne, M. F.; Simkovic, F.; Slater, A. G. Production of Monodisperse Polyurea Microcapsules Using Microfluidics. *Sci. Rep.* **2019**, *9* (1), 1–7. <https://doi.org/10.1038/s41598-019-54512-4>.
- (46) Pohlmann, A. R.; Fonseca, F. N.; Paese, K.; Detoni, C. B.; Coradini, K.; Beck, R. C.; Guterres, S. S. Poly(ϵ -Caprolactone) Microcapsules and Nanocapsules in Drug Delivery. *Expert Opin. Drug Deliv.* **2013**, *10* (5), 623–638. <https://doi.org/10.1517/17425247.2013.769956>.
- (47) Lignel, S.; Salsac, A. V.; Drelich, A.; Leclerc, E.; Pezron, I. Water-in-Oil Droplet Formation in a Flow-Focusing Microsystem Using Pressure- and Flow Rate-Driven Pumps. *Colloids Surfaces A Physicochem. Eng. Asp.* **2017**, *531* (May), 164–172. <https://doi.org/10.1016/j.colsurfa.2017.07.065>.
- (48) Fourkas, J. T. Nanoscale Photolithography with Visible Light. *J. Phys. Chem. Lett.* **2010**, *1* (8), 1221–1227. <https://doi.org/10.1021/jz1002082>.
- (49) Henry, M. D.; Shearn, M. J.; Chhim, B.; Scherer, A. Ga⁺ Beam Lithography for Nanoscale Silicon Reactive Ion Etching. *Nanotechnology* **2010**, *21* (24). <https://doi.org/10.1088/0957-4484/21/24/245303>.
- (50) Vieu, C.; Carcenac, F.; Pépin, A.; Chen, Y.; Mejias, M.; Lebib, A.; Manin-Ferlazzo, L.; Couraud, L.; Launois, H. Electron Beam Lithography: Resolution Limits and Applications. *Appl. Surf. Sci.* **2000**, *164* (1–4), 111–117. [https://doi.org/10.1016/S0169-4332\(00\)00352-4](https://doi.org/10.1016/S0169-4332(00)00352-4).
- (51) Lazzari, M.; Arturo López-Quintela, M. Block Copolymers as a Tool for Nanomaterial Fabrication. *Adv. Mater.* **2003**, *15* (19), 1583–1594. <https://doi.org/10.1002/adma.200300382>.

- (52) Park, C.; Yoon, J.; Thomas, E. L. Enabling Nanotechnology with Self Assembled Block Copolymer Patterns. *Polymer (Guildf)*. **2003**, *44* (22), 6725–6760. <https://doi.org/10.1016/j.polymer.2003.08.011>.
- (53) Zhai, L. Stimuli-Responsive Polymer Films. *Chem. Soc. Rev.* **2013**, *42* (17), 7148–7160. <https://doi.org/10.1039/c3cs60023h>.
- (54) Ionov, L. Actively-Moving Materials Based on Stimuli-Responsive Polymers. *J. Mater. Chem.* **2010**, *20* (17), 3382–3390. <https://doi.org/10.1039/b922718k>.
- (55) Su, S.; Ali, M. M.; Filipe, C. D. M.; Li, Y.; Pelton, R. Microgel-Based Inks for Paper-Supported Biosensing Applications. *Biomacromolecules* **2008**, *9* (3), 935–941. <https://doi.org/10.1021/bm7013608>.
- (56) Hendrickson, G. R.; Lyon, L. A. Bioresponsive Hydrogels for Sensing Applications. *Soft Matter* **2009**, *5* (1), 29–35. <https://doi.org/10.1039/b811620b>.
- (57) Stuart, M. A. C.; Huck, W. T. S.; Genzer, J.; Müller, M.; Ober, C.; Stamm, M.; Sukhorukov, G. B.; Szleifer, I.; Tsukruk, V. V.; Urban, M.; Winnik, F.; Zauscher, S.; Luzinov, I.; Minko, S. Emerging Applications of Stimuli-Responsive Polymer Materials. *Nat. Mater.* **2010**, *9* (2), 101–113. <https://doi.org/10.1038/nmat2614>.
- (58) Wei, M.; Gao, Y.; Li, X.; Serpe, M. J. Stimuli-Responsive Polymers and Their Applications. *Polym. Chem.* **2017**, *8* (1), 127–143. <https://doi.org/10.1039/c6py01585a>.
- (59) Morillon, V.; Debeaufort, F.; Capelle, M.; Blond, G.; Voilley, A. Influence of the Physical State of Water on the Barrier Properties of Hydrophilic and Hydrophobic Films. *J. Agric. Food Chem.* **2000**, *48* (1), 11–16. <https://doi.org/10.1021/jf990809z>.
- (60) Tong, W.; Song, X.; Gao, C. Layer-by-Layer Assembly of Microcapsules and Their Biomedical Applications. *Chem. Soc. Rev.* **2012**, *41* (18), 6103–6124. <https://doi.org/10.1039/c2cs35088b>.
- (61) Hu, Q.; Katti, P. S.; Gu, Z. Enzyme-Responsive Nanomaterials for Controlled Drug Delivery. *Nanoscale* **2014**, *6* (21), 12273–12286. <https://doi.org/10.1039/c4nr04249b>.
- (62) Lemmouchi, Y.; Schacht, E.; Kageruka, P.; De Deken, R.; Diarra, B.; Diall, O.; Geerts, S. Biodegradable Polyesters for Controlled Release of Trypanocidal Drugs: In Vitro and in Vivo Studies. *Biomaterials* **1998**, *19* (20), 1827–1837. [https://doi.org/10.1016/S0142-9612\(98\)00074-X](https://doi.org/10.1016/S0142-9612(98)00074-X).
- (63) Gan, Z.; Liang, Q.; Zhang, J.; Jing, X. Enzymatic Degradation of Poly(ϵ -Caprolactone) Film in Phosphate Buffer Solution Containing Lipases. *Polym. Degrad. Stab.* **1997**, *56* (2), 209–213. [https://doi.org/10.1016/S0141-3910\(96\)00208-X](https://doi.org/10.1016/S0141-3910(96)00208-X).
- (64) Darwis, D.; Mitomo, H.; Enjoji, T.; Yoshii, F.; Makuuchi, K. Enzymatic Degradation of Radiation Crosslinked Poly(ϵ -Caprolactone). *Polym. Degrad. Stab.* **1998**, *62* (2), 259–265. [https://doi.org/10.1016/S0141-3910\(98\)00005-6](https://doi.org/10.1016/S0141-3910(98)00005-6).
- (65) Kweon, H. Y.; Yoo, M. K.; Park, I. K.; Kim, T. H.; Lee, H. C.; Lee, H. S.; Oh, J. S.; Akaike, T.; Cho, C. S. A Novel Degradable Polycaprolactone Networks for Tissue Engineering. *Biomaterials* **2003**, *24* (5), 801–808. [https://doi.org/10.1016/S0142-9612\(02\)00370-8](https://doi.org/10.1016/S0142-9612(02)00370-8).

- (66) Cheng, Z.; Teoh, S. H. Surface Modification of Ultra Thin Poly (ϵ -Caprolactone) Films Using Acrylic Acid and Collagen. *Biomaterials* **2004**, *25* (11), 1991–2001. <https://doi.org/10.1016/j.biomaterials.2003.08.038>.
- (67) Brode, G. L.; Koleske, J. V. Lactone Polymerization and Polymer Properties. *J. Macromol. Sci. Part A - Chem.* **1972**, *6* (6), 1109–1144. <https://doi.org/10.1080/10601327208056888>.
- (68) Ulery, B. D.; Nair, L. S.; Laurencin, C. T. Biomedical Applications of Biodegradable Polymers. *J. Polym. Sci. Part B Polym. Phys.* **2011**, *49* (12), 832–864. <https://doi.org/10.1002/polb.22259>.
- (69) Kim, S. Y.; Lee, Y. M. Taxol-Loaded Block Copolymer Nanospheres Composed of Methoxy Poly(Ethylene Glycol) and Poly(ϵ -Caprolactone) as Novel Anticancer Drug Carriers. *Biomaterials* **2001**, *22* (13), 1697–1704. [https://doi.org/10.1016/S0142-9612\(00\)00292-1](https://doi.org/10.1016/S0142-9612(00)00292-1).
- (70) Kumari, A.; Yadav, S. K.; Yadav, S. C. Biodegradable Polymeric Nanoparticles Based Drug Delivery Systems. *Colloids Surfaces B Biointerfaces* **2010**, *75* (1), 1–18. <https://doi.org/10.1016/j.colsurfb.2009.09.001>.
- (71) Kim, H. W.; Knowles, J. C.; Kim, H. E. Hydroxyapatite/Poly(ϵ -Caprolactone) Composite Coatings on Hydroxyapatite Porous Bone Scaffold for Drug Delivery. *Biomaterials* **2004**, *25* (7–8), 1279–1287. <https://doi.org/10.1016/j.biomaterials.2003.07.003>.
- (72) Middleton, J. C.; Tipton, A. J. Synthetic Biodegradable Polymers as Orthopedic Devices. *Biomaterials* **2000**, *21* (23), 2335–2346. [https://doi.org/10.1016/S0142-9612\(00\)00101-0](https://doi.org/10.1016/S0142-9612(00)00101-0).
- (73) Herrero-Herrero, M.; Gómez-Tejedor, J. A.; Vallés-Lluch, A. PLA/PCL Electrospun Membranes of Tailored Fibres Diameter as Drug Delivery Systems. *Eur. Polym. J.* **2018**, *99* (January), 445–455. <https://doi.org/10.1016/j.eurpolymj.2017.12.045>.
- (74) Gates, B. D.; Whitesides, G. M. Replication of Vertical Features Smaller than 2 Nm by Soft Lithography. *J. Am. Chem. Soc.* **2003**, *125* (49), 14986–14987. <https://doi.org/10.1021/ja0367647>.
- (75) Xia, Y.; Whitesides, G. M. Soft Lithography. *Angew. Chemie - Int. Ed.* **1998**, *37* (5), 550–575. [https://doi.org/10.1002/\(sici\)1521-3773\(19980316\)37:5<550::aid-anie550>3.3.co;2-7](https://doi.org/10.1002/(sici)1521-3773(19980316)37:5<550::aid-anie550>3.3.co;2-7).
- (76) Lankalapalli, S.; Kolapalli, V. R. M. Polyelectrolyte Complexes: A Review of Their Applicability in Drug Delivery Technology. *Indian J. Pharm. Sci.* **2009**, *71* (5), 481. <https://doi.org/10.4103/0250-474X.58165>.
- (77) Meka, V. S.; Sing, M. K. G.; Pichika, M. R.; Nali, S. R.; Kolapalli, V. R. M.; Kesharwani, P. A. Comprehensive Review on Polyelectrolyte Complexes. *Drug Discov. Today* **2017**, *22* (11), 1697–1706. <https://doi.org/10.1016/j.drudis.2017.06.008>.
- (78) Manning, G. S. Counterion Binding in Polyelectrolyte Theory. *Acc. Chem. Res.* **1979**, *12* (12), 443–449. <https://doi.org/10.1021/ar50144a004>.
- (79) Dakhara, S. L.; Anajwala, C. C. Polyelectrolyte Complex: A Pharmaceutical Review. *Syst.*

- Rev. Pharm.* **2010**, *1* (2), 121–127. <https://doi.org/10.4103/0975-8453.75046>.
- (80) Solis, F. J.; Olvera De La Cruz, M. Collapse of Flexible Polyelectrolytes in Multivalent Salt Solutions. *J. Chem. Phys.* **2000**, *112* (4), 2030–2035. <https://doi.org/10.1063/1.480763>.
- (81) Burke, S. E.; Barrett, C. J. Controlling the Physicochemical Properties of Weak Polyelectrolyte Multilayer Films through Acid/Base Equilibria. *Pure Appl. Chem.* **2004**, *76* (7–8), 1387–1398. <https://doi.org/10.1351/pac200476071387>.
- (82) Po, H. N.; Senozan, N. M. The Henderson-Hasselbalch Equation: Its History and Limitations. *J. Chem. Educ.* **2001**, *78* (11), 1499–1503. <https://doi.org/10.1021/ed078p1499>.
- (83) Exner, G.; Marudova, M.; Sotirov, S.; Marinova, A.; Viraneva, A.; Pilicheva, B.; Bodurov, I.; Vlaeva, I.; Uzunova, Y.; Yovcheva, T. Multilayered Polyelectrolyte Structures with Potential for Intracavity Drug Delivery Systems. *Appl. Surf. Sci.* **2019**, *493* (July), 620–627. <https://doi.org/10.1016/j.apsusc.2019.07.039>.
- (84) Shaikh, S. M. R.; Nasser, M. S.; Hussein, I.; Benamor, A.; Onaizi, S. A.; Qiblawey, H. Influence of Polyelectrolytes and Other Polymer Complexes on the Flocculation and Rheological Behaviors of Clay Minerals: A Comprehensive Review. *Sep. Purif. Technol.* **2017**, *187*, 137–161. <https://doi.org/10.1016/j.seppur.2017.06.050>.
- (85) Van Haver, L.; Nayar, S. Polyelectrolyte Flocculants in Harvesting Microalgal Biomass for Food and Feed Applications. *Algal Res.* **2017**, *24*, 167–180. <https://doi.org/10.1016/j.algal.2017.03.022>.
- (86) Ge, Q.; Wang, P.; Wan, C.; Chung, T. S. Polyelectrolyte-Promoted Forward Osmosis-Membrane Distillation (FO-MD) Hybrid Process for Dye Wastewater Treatment. *Environ. Sci. Technol.* **2012**, *46* (11), 6236–6243. <https://doi.org/10.1021/es300784h>.
- (87) Rembaum, A.; Sélégny, E. *Polyelectrolytes and Their Applications*; Springer Science & Business Media, 2012; Vol. 2.
- (88) Michaels, A. S. POLYELECTROLYTE COMPLEXES. *Ind. Eng. Chem.* **1965**, *57* (10), 32–40. <https://doi.org/10.1021/ie50670a007>.
- (89) Michaels, A. S.; Miekka, R. G. Polycation-Polyanion Complexes: Preparation and Properties of Poly-(Vinylbenzyltrimethylammonium) Poly-(Styrenesulfonate). *J. Phys. Chem.* **1961**, *65* (10), 1765–1773. <https://doi.org/10.1021/j100827a020>.
- (90) Thünemann, A. F.; Müller, M.; Dautzenberg, H.; Joanny, J.-F.; Löwen, H. Polyelectrolyte Complexes. In *Polyelectrolytes with defined molecular architecture II*; Springer, 2004; pp 113–171. <https://doi.org/10.1007/b11350>.
- (91) Zhao, Q.; An, Q. F.; Ji, Y.; Qian, J.; Gao, C. Polyelectrolyte Complex Membranes for Pervaporation, Nanofiltration and Fuel Cell Applications. *J. Memb. Sci.* **2011**, *379* (1–2), 19–45. <https://doi.org/10.1016/j.memsci.2011.06.016>.
- (92) Sappidi, P.; Natarajan, U. Polyelectrolyte Conformational Transition in Aqueous Solvent Mixture Influenced by Hydrophobic Interactions and Hydrogen Bonding Effects: PAA-Water-Ethanol. *J. Mol. Graph. Model.* **2016**, *64*, 60–74.

- <https://doi.org/10.1016/j.jmngm.2015.12.004>.
- (93) Moya, S. E.; Ilie, A.; Bendall, J. S.; Hernandez-Lopez, J. L.; Ruiz-García, J.; Huck, W. T. S. Assembly of Polyelectrolytes on CNTs by Van Der Waals Interactions and Fabrication of LBL Polyelectrolyte/CNT Composites. *Macromol. Chem. Phys.* **2007**, *208* (6), 603–608. <https://doi.org/10.1002/macp.200600530>.
- (94) Sadman, K.; Wang, Q.; Chen, Y.; Keshavarz, B.; Jiang, Z.; Shull, K. R. Influence of Hydrophobicity on Polyelectrolyte Complexation. *Macromolecules* **2017**, *50* (23), 9417–9426. <https://doi.org/10.1021/acs.macromol.7b02031>.
- (95) Hofs, B.; De Keizer, A.; Stuart, M. A. C. On the Stability of (Highly Aggregated) Polyelectrolyte Complexes Containing a Charged-Block-Neutral Diblock Copolymer. *J. Phys. Chem. B* **2007**, *111* (20), 5621–5627. <https://doi.org/10.1021/jp0714318>.
- (96) Pergushov, D. V.; Müller, A. H. E.; Schacher, F. H. Micellar Interpolyelectrolyte Complexes. *Chem. Soc. Rev.* **2012**, *41* (21), 6888–6901. <https://doi.org/10.1039/c2cs35135h>.
- (97) Tsuchida, E. Formation of Polyelectrolyte Complexes and Their Structures. *J. Macromol. Sci. Part A* **1994**, *31* (1), 1–15. <https://doi.org/10.1080/10601329409349713>.
- (98) Shovsky, A.; Varga, I.; Makuška, R.; Claesson, P. M. Formation and Stability of Water-Soluble, Molecular Polyelectrolyte Complexes: Effects of Charge Density, Mixing Ratio, and Polyelectrolyte Concentration. *Langmuir* **2009**, *25* (11), 6113–6121. <https://doi.org/10.1021/la804189w>.
- (99) Bakeev, K. N.; Izumrudov, V. A.; Kuchanov, S. I.; Zezin, A. B.; Kabanov, V. A. Kinetics and Mechanism of Interpolyelectrolyte Exchange and Addition Reactions. *Macromolecules* **1992**, *25* (17), 4249–4254. <https://doi.org/10.1021/ma00043a003>.
- (100) Mueller, A. H. E.; Yan, D.; Wulkow, M. Molecular Parameters of Hyperbranched Polymers Made by Self-Condensing Vinyl Polymerization. 1. Molecular Weight Distribution. *Macromolecules* **1997**, *30* (23), 7015–7023. <https://doi.org/10.1021/ma9619187>.
- (101) Kabanov, V. A.; Zezin, A. B.; Izumrudov, V. A.; Bronich, T. K.; Bakeev, K. N. Cooperative Interpolyelectrolyte Reactions. *Die Makromol. Chemie* **1985**, *13* (S19851), 137–155. <https://doi.org/10.1002/macp.1985.020131985111>.
- (102) Dautzenberg, H. Polyelectrolyte Complex Formation in Highly Aggregating Systems. 1. Effect of Salt: Polyelectrolyte Complex Formation in the Presence of NaCl. *Macromolecules* **1997**, *30* (25), 7810–7815. <https://doi.org/10.1021/ma970803f>.
- (103) Zezin, A. B.; Kabanov, V. A. A New Class of Complex Water-Soluble Polyelectrolytes. *Russ. Chem. Rev.* **1982**, *51* (9), 833–855. <https://doi.org/10.1070/rc1982v051n09abeh002921>.
- (104) Tsuchida, E.; Osada, Y.; Sanada, K. Interaction of Poly(Styrene Sulfonate) With Polycations Carrying Charges in the Chain Backbone. *J Polym Sci Part A-1 Polym Chem* **1972**, *10* (11), 3397–3404. <https://doi.org/10.1002/pol.1972.170101124>.
- (105) Izumrudov, V. A.; Bronich, T. K.; Zezin, A. B.; Kabanov, V. A. Kinetics and Mechanism of Intermacromolecular Reactions in Polyelectrolyte Solutions. *J. Polym. Sci. Polym. Lett. Ed.*

- 1985**, 23 (8), 439–444. <https://doi.org/10.1002/pol.1985.130230808>.
- (106) Dautzenberg, H.; Karibyants, N. Polyelectrolyte Complex Formation in Highly Aggregating Systems. Effect of Salt: Response to Subsequent Addition of NaCl. *Macromol. Chem. Phys.* **1999**, 200 (1), 118–125. [https://doi.org/10.1002/\(SICI\)1521-3935\(19990101\)200:1<118::AID-MACP118>3.0.CO;2-K](https://doi.org/10.1002/(SICI)1521-3935(19990101)200:1<118::AID-MACP118>3.0.CO;2-K).
- (107) Berger, J.; Reist, M.; Mayer, J. M.; Felt, O.; Peppas, N. A.; Gurny, R. Structure and Interactions in Covalently and Ionically Crosslinked Chitosan Hydrogels for Biomedical Applications. *Eur. J. Pharm. Biopharm.* **2004**, 57 (1), 19–34. [https://doi.org/10.1016/S0939-6411\(03\)00161-9](https://doi.org/10.1016/S0939-6411(03)00161-9).
- (108) Gåserød, O.; Smidsrød, O.; Skjåk-Bræk, G. Microcapsules of Alginate-Chitosan - I. A Quantitative Study of the Interaction between Alginate and Chitosan. *Biomaterials* **1998**, 19 (20), 1815–1825. [https://doi.org/10.1016/S0142-9612\(98\)00073-8](https://doi.org/10.1016/S0142-9612(98)00073-8).
- (109) Tanaka, T.; Sun, S. T.; Nishio, I.; Swislow, G.; Shah, A. Phase Transitions In Ionic Gels. *Ferroelectrics* **1980**, 30 (1), 97. <https://doi.org/10.1080/00150198008209494>.
- (110) Jin, X.; Hsieh, Y. Lo. PH-Responsive Swelling Behavior of Poly(Vinyl Alcohol)/Poly(Acrylic Acid) Bi-Component Fibrous Hydrogel Membranes. *Polymer (Guildf)*. **2005**, 46 (14), 5149–5160. <https://doi.org/10.1016/j.polymer.2005.04.066>.
- (111) Mauser, T.; Déjugnat, C.; Sukhorukov, G. B. Reversible PH-Dependent Properties of Multilayer Microcapsules Made of Weak Polyelectrolytes. *Macromol. Rapid Commun.* **2004**, 25 (20), 1781–1785. <https://doi.org/10.1002/marc.200400331>.
- (112) Luo, Y.; Wang, Q. Recent Development of Chitosan-Based Polyelectrolyte Complexes with Natural Polysaccharides for Drug Delivery. *Int. J. Biol. Macromol.* **2014**, 64, 353–367. <https://doi.org/10.1016/j.ijbiomac.2013.12.017>.
- (113) McCall, P. M.; Srivastava, S.; Perry, S. L.; Kovar, D. R.; Gardel, M. L.; Tirrell, M. V. Partitioning and Enhanced Self-Assembly of Actin in Polypeptide Coacervates. *Biophys. J.* **2018**, 114 (7), 1636–1645. <https://doi.org/10.1016/j.bpj.2018.02.020>.
- (114) Anraku, Y.; Kishimura, A.; Kamiya, M.; Tanaka, S.; Nomoto, T.; Toh, K.; Matsumoto, Y.; Fukushima, S.; Sueyoshi, D.; Kano, M. R.; Urano, Y.; Nishiyama, N.; Kataoka, K. Systemically Injectable Enzyme-Loaded Polyion Complex Vesicles as in Vivo Nanoreactors Functioning in Tumors. *Angew. Chemie - Int. Ed.* **2016**, 55 (2), 560–565. <https://doi.org/10.1002/anie.201508339>.
- (115) Zhao, M.; Eghtesadi, S. A.; Dawadi, M. B.; Wang, C.; Huang, S.; Seymore, A. E.; Vogt, B. D.; Modarelli, D. A.; Liu, T.; Zacharia, N. S. Partitioning of Small Molecules in Hydrogen-Bonding Complex Coacervates of Poly(Acrylic Acid) and Poly(Ethylene Glycol) or Pluronic Block Copolymer. *Macromolecules* **2017**, 50 (10), 3818–3830. <https://doi.org/10.1021/acs.macromol.6b02815>.
- (116) Bawa, P.; Pillay, V.; Choonara, Y. E.; Du Toit, L. C.; Ndesendo, V. M. K.; Kumar, P. A. Composite Polyelectrolytic Matrix for Controlled Oral Drug Delivery. *AAPS PharmSciTech* **2011**, 12 (1), 227–238. <https://doi.org/10.1208/s12249-010-9576-8>.
- (117) Insua, I.; Majok, S.; Peacock, A. F. A.; Krachler, A. M.; Fernandez-Trillo, F. Preparation and

- Antimicrobial Evaluation of Polyion Complex (PIC) Nanoparticles Loaded with Polymyxin B. *Eur. Polym. J.* **2017**, *87*, 478–486. <https://doi.org/10.1016/j.eurpolymj.2016.08.023>.
- (118) Srinivas, L.; Ramana Murthy, K. V. Preparation and Evaluation of Polyelectrolyte Complexes for Oral Controlled Drug Delivery. *Asian J. Pharm.* **2010**, *4* (1), 69–78. <https://doi.org/10.4103/0973-8398.63977>.
- (119) Srivastava, S.; Andreev, M.; Levi, A. E.; Goldfeld, D. J.; Mao, J.; Heller, W. T.; Prabhu, V. M.; De Pablo, J. J.; Tirrell, M. V. Gel Phase Formation in Dilute Triblock Copolyelectrolyte Complexes. *Nat. Commun.* **2017**, *8*, 1–9. <https://doi.org/10.1038/ncomms14131>.
- (120) Zhao, Q.; Lee, D. W.; Ahn, B. K.; Seo, S.; Kaufman, Y.; Israelachvili, J. N.; Waite, J. H. Underwater Contact Adhesion and Microarchitecture in Polyelectrolyte Complexes Actuated by Solvent Exchange. *Nat. Mater.* **2016**, *15* (4), 407–412. <https://doi.org/10.1038/nmat4539>.
- (121) Hamano, T.; Teramoto, A.; Lizuka, E.; Abe, K. Effects of Polyelectrolyte Complex (PEC) on Human Periodontal Ligament Fibroblast (HPLF) Function. I. Three-Dimensional Structure of HPLF Cultured on PEC. *J. Biomed. Mater. Res.* **1998**, *41* (2), 257–269. [https://doi.org/10.1002/\(SICI\)1097-4636\(199808\)41:2<257::AID-JBM11>3.0.CO;2-I](https://doi.org/10.1002/(SICI)1097-4636(199808)41:2<257::AID-JBM11>3.0.CO;2-I).
- (122) Coimbra, P.; Ferreira, P.; de Sousa, H. C.; Batista, P.; Rodrigues, M. A.; Correia, I. J.; Gil, M. H. Preparation and Chemical and Biological Characterization of a Pectin/Chitosan Polyelectrolyte Complex Scaffold for Possible Bone Tissue Engineering Applications. *Int. J. Biol. Macromol.* **2011**, *48* (1), 112–118. <https://doi.org/10.1016/j.ijbiomac.2010.10.006>.
- (123) Araujo, J. V.; Davidenko, N.; Danner, M.; Cameron, R. E.; Best, S. M. Novel Porous Scaffolds of PH Responsive Chitosan/Carrageenan-Based Polyelectrolyte Complexes for Tissue Engineering. *J. Biomed. Mater. Res. - Part A* **2014**, *102* (12), 4415–4426. <https://doi.org/10.1002/jbm.a.35128>.
- (124) Caruso, F.; Caruso, R. A.; Möhwald, H. Nanoengineering of Inorganic and Hybrid Hollow Spheres by Colloidal Templating. *Science (80-.)*. **1998**, *282* (5391), 1111–1114. <https://doi.org/10.1126/science.282.5391.1111>.
- (125) Donath, E.; Sukhorukov, G. B.; Caruso, F.; Davis, S. A.; Möhwald, H. Novel Hollow Polymer Shells by Colloid-Templated Assembly of Polyelectrolytes. *Angew. Chemie Int. Ed.* **1998**, *37* (16), 2201–2205. [https://doi.org/10.1002/\(sici\)1521-3773\(19980904\)37:16<2201::aid-anie2201>3.0.co;2-e](https://doi.org/10.1002/(sici)1521-3773(19980904)37:16<2201::aid-anie2201>3.0.co;2-e).
- (126) Schlenoff, J. B.; Ly, H.; Li, M. Charge and Mass Balance in Polyelectrolyte Multilayers. *J. Am. Chem. Soc.* **1998**, *120* (30), 7626–7634. <https://doi.org/10.1021/ja980350+>.
- (127) Zhai, L.; Cebeci, F. C.; Cohen, R. E.; Rubner, M. F. Stable Superhydrophobic Coatings from Polyelectrolyte Multilayers. *Nano Lett.* **2004**, *4* (7), 1349–1353. <https://doi.org/10.1021/nl049463j>.
- (128) Graul, T. W.; Li, M.; Schlenoff, J. B. Ion Exchange in Ultrathin Films. *J. Phys. Chem. B* **1999**, *103* (14), 2718–2723. <https://doi.org/10.1021/jp983049o>.
- (129) Sukhishvili, S. A. Responsive Polymer Films and Capsules via Layer-by-Layer Assembly. *Curr. Opin. Colloid Interface Sci.* **2005**, *10* (1–2), 37–44.

- <https://doi.org/10.1016/j.cocis.2005.05.001>.
- (130) Sukhorukov, G. B.; Donath, E.; Lichtenfeld, H.; Knippel, E.; Knippel, M.; Budde, A.; Möhwald, H. Layer-by-Layer Self Assembly of Polyelectrolytes on Colloidal Particles. *Colloids Surfaces A Physicochem. Eng. Asp.* **1998**, *137* (1–3), 253–266. [https://doi.org/10.1016/S0927-7757\(98\)00213-1](https://doi.org/10.1016/S0927-7757(98)00213-1).
- (131) Schoeler, B.; Kumaraswamy, G.; Caruso, F. Investigation of the Influence of Polyelectrolyte Charge Density on the Growth of Multilayer Thin Films by LBLma011349p.Pdf. *Macromolecules*. 2002, pp 889–897.
- (132) Voigt, U.; Jaeger, W.; Findenegg, G. H.; Klitzing, R. V. Charge Effects on the Formation of Multilayers Containing Strong Polyelectrolytes. *J. Phys. Chem. B* **2003**, *107* (22), 5273–5280. <https://doi.org/10.1021/jp0256488>.
- (133) Park, S. Y.; Barrett, C. J.; Rubner, M. F.; Mayes, A. M. Anomalous Adsorption of Polyelectrolyte Layers. *Macromolecules* **2001**, *34* (10), 3384–3388. <https://doi.org/10.1021/ma001601d>.
- (134) Shiratori, S. S.; Rubner, M. F. PH-Dependent Thickness Behavior of Sequentially Adsorbed Layers of Weak Polyelectrolytes. *Macromolecules* **2000**, *33* (11), 4213–4219. <https://doi.org/10.1021/ma991645q>.
- (135) Rojas, O. J.; Ernstsson, M.; Neuman, R. D.; Claesson, P. M. Effect of Polyelectrolyte Charge Density on the Adsorption and Desorption Behavior on Mica. *Langmuir* **2002**, *18* (5), 1604–1612. <https://doi.org/10.1021/la0155698>.
- (136) Steitz, R.; Jaeger, W.; Klitzing, R. V. Influence of Charge Density and Ionic Strength on the Multilayer Formation of Strong Polyelectrolytes. *Langmuir* **2001**, *17* (15), 4471–4474. <https://doi.org/10.1021/la010168d>.
- (137) Voigt, U.; Khrenov, V.; Tauer, K.; Hahn, M.; Jaeger, W.; Von Klitzing, R. The Effect of Polymer Charge Density and Charge Distribution on the Formation of Multilayers. *J. Phys. Condens. Matter* **2003**, *15* (1). <https://doi.org/10.1088/0953-8984/15/1/327>.
- (138) V. Klitzing, R. Internal Structure of Polyelectrolyte Multilayer Assemblies. *Phys. Chem. Chem. Phys.* **2006**, *8* (43), 5012–5033. <https://doi.org/10.1039/b607760a>.
- (139) Van Der Schee, H. A.; Lyklema, J. A Lattice Theory of Polyelectrolyte Adsorption. *J. Phys. Chem.* **1984**, *88* (26), 6661–6667. <https://doi.org/10.1021/j150670a031>.
- (140) Ruths, J.; Essler, F.; Decher, G.; Riegler, H. Polyelectrolytes. I: Polyanion/Polycation Multilayers at the Air/Monolayer/Water Interface as Elements for Quantitative Polymer Adsorption Studies and Preparation of Hetero-Superlattices on Solid Surfaces. *Langmuir* **2000**, *16* (23), 8871–8878. <https://doi.org/10.1021/la000257a>.
- (141) Salomäki, M.; Tervasmäki, P.; Areva, S.; Kankare, J. The Hofmeister Anion Effect and the Growth of Polyelectrolyte Multilayers. *Langmuir* **2004**, *20* (9), 3679–3683. <https://doi.org/10.1021/la036328y>.
- (142) Fischer, P.; Laschewsky, A. Layer-by-Layer Adsorption of Identically Charged Polyelectrolytes. *Macromolecules* **2000**, *33* (3), 1100–1102.

- <https://doi.org/10.1021/ma991447z>.
- (143) Becker, A. L.; Johnston, A. P. R.; Caruso, F. Layer-by-Layer-Assembled Capsules and Films for Therapeutic Delivery. *Small* **2010**, *6* (17), 1836–1852. <https://doi.org/10.1002/smll.201000379>.
- (144) Vilela, C.; Figueiredo, A. R. P.; Silvestre, A. J. D.; Freire, C. S. R. Multilayered Materials Based on Biopolymers as Drug Delivery Systems. *Expert Opin. Drug Deliv.* **2017**, *14* (2), 189–200. <https://doi.org/10.1080/17425247.2016.1214568>.
- (145) Izumrudov, V. A.; Mussabayeva, B. K.; Murzagulova, K. B. Polyelectrolyte Multilayers: Preparation and Applications. *Russ. Chem. Rev.* **2018**, *87* (2), 192–200. <https://doi.org/10.1070/rcr4767>.
- (146) Mandal, B. B.; Mann, J. K.; Kundu, S. C. Silk Fibroin/Gelatin Multilayered Films as a Model System for Controlled Drug Release. *Eur. J. Pharm. Sci.* **2009**, *37* (2), 160–171. <https://doi.org/10.1016/j.ejps.2009.02.005>.
- (147) Mohanta, V.; Madras, G.; Patil, S. Albumin-Mediated Incorporation of Water-Insoluble Therapeutics in Layer-by-Layer Assembled Thin Films and Microcapsules. *J. Mater. Chem. B* **2013**, *1* (37), 4819–4827. <https://doi.org/10.1039/c3tb20592d>.
- (148) Cho, Y.; Lee, J. B.; Hong, J. Controlled Release of an Anti-Cancer Drug from DNA Structured Nano-Films. *Sci. Rep.* **2014**, *4*, 4–8. <https://doi.org/10.1038/srep04078>.
- (149) Monge, C.; Almodóvar, J.; Boudou, T.; Picart, C. Spatio-Temporal Control of LbL Films for Biomedical Applications: From 2D to 3D. *Adv. Healthc. Mater.* **2015**, *4* (6), 811–830. <https://doi.org/10.1002/adhm.201400715>.
- (150) Vergaro, V.; Papadia, P.; Leporatti, S.; De Pascali, S. A.; Fanizzi, F. P.; Ciccarella, G. Synthesis of Biocompatible Polymeric Nano-Capsules Based on Calcium Carbonate: A Potential Cisplatin Delivery System. *J. Inorg. Biochem.* **2015**, *153*, 284–292. <https://doi.org/10.1016/j.jinorgbio.2015.10.014>.
- (151) Sousa, F.; Kreft, O.; Sukhorukov, G. B.; Möhwald, H.; Kokol, V. Biocatalytic Response of Multi-Layer Assembled Collagen/Hyaluronic Acid Nanoengineered Capsules. *J. Microencapsul.* **2014**, *31* (3), 270–276. <https://doi.org/10.3109/02652048.2013.834995>.
- (152) Van Natta, F. J.; Hill, J. W.; Carothers, W. H. Studies of Polymerization and Ring Formation. XXIII. ϵ -Caprolactone and Its Polymers. *J. Am. Chem. Soc.* **1934**, *56* (2), 455–457. <https://doi.org/10.1021/ja01317a053>.
- (153) Labet, M.; Thielemans, W. Synthesis of Polycaprolactone: A Review. *Chem. Soc. Rev.* **2009**, *38* (12), 3484–3504. <https://doi.org/10.1039/b820162p>.
- (154) Braud, C.; Devarieux, R.; Atlan, A.; Ducos, C.; Michel Vert. Capillary Zone Electrophoresis in Normal or Reverse Polarity Separation Modes for the Analysis of Hydroxy Acid Oligomers in Neutral Phosphate Buffer. *J. Chromatogr. B Biomed. Appl.* **1998**, *706* (1), 73–82. [https://doi.org/10.1016/S0378-4347\(97\)00468-4](https://doi.org/10.1016/S0378-4347(97)00468-4).
- (155) Mahapatro, A.; Kumar, A.; Gross, R. A. Mild, Solvent-Free ω -Hydroxy Acid Polycondensations Catalyzed by *Candida Antarctica* Lipase B. *Biomacromolecules* **2004**,

- 5 (1), 62–68. <https://doi.org/10.1021/bm0342382>.
- (156) Dong, H.; Wang, H. Da; Cao, S. G.; Shen, J. C. Lipase-Catalyzed Polymerization of Lactones and Linear Hydroxyesters. *Biotechnol. Lett.* **1998**, *20* (10), 905–908. <https://doi.org/10.1023/A:1005482232687>.
- (157) Sisson, A. L.; Ekinici, D.; Lendlein, A. The Contemporary Role of ϵ -Caprolactone Chemistry to Create Advanced Polymer Architectures. *Polymer (Guildf)*. **2013**, *54* (17), 4333–4350. <https://doi.org/10.1016/j.polymer.2013.04.045>.
- (158) Dechy-Cabaret, O.; Martin-Vaca, B.; Bourissou, D. Controlled Ring-Opening Polymerization of Lactide and Glycolide. *Chem. Rev.* **2004**, *104* (12), 6147–6176. <https://doi.org/10.1021/cr040002s>.
- (159) Sinha, V. R.; Bansal, K.; Kaushik, R.; Kumria, R.; Trehan, A. Poly- ϵ -Caprolactone Microspheres and Nanospheres: An Overview. *Int. J. Pharm.* **2004**, *278* (1), 1–23. <https://doi.org/10.1016/j.ijpharm.2004.01.044>.
- (160) Chandra, R.; Rustgi, R. Biodegradable Polymers. *Prog. Polym. Sci.* **1998**, *23* (7), 1273–1335. [https://doi.org/10.1016/S0079-6700\(97\)00039-7](https://doi.org/10.1016/S0079-6700(97)00039-7).
- (161) Okada, M. Chemical Syntheses of Biodegradable Polymers. *Prog. Polym. Sci.* **2002**, *27* (1), 87–133. [https://doi.org/10.1016/S0079-6700\(01\)00039-9](https://doi.org/10.1016/S0079-6700(01)00039-9).
- (162) Nishide, H.; Toyota, K.; Kimura, M. Effects of Soil Temperature and Anaerobiosis on Degradation of Biodegradable Plastics in Soil and Their Degrading Microorganisms. *Soil Sci. Plant Nutr.* **1999**, *45* (4), 963–972. <https://doi.org/10.1080/00380768.1999.10414346>.
- (163) Vert, M. Degradable and Bioresorbable Polymers in Surgery and in Pharmacology: Beliefs and Facts. *J. Mater. Sci. Mater. Med.* **2009**, *20* (2), 437–446. <https://doi.org/10.1007/s10856-008-3581-4>.
- (164) Sun, H.; Mei, L.; Song, C.; Cui, X.; Wang, P. The in Vivo Degradation, Absorption and Excretion of PCL-Based Implant. *Biomaterials* **2006**, *27* (9), 1735–1740. <https://doi.org/10.1016/j.biomaterials.2005.09.019>.
- (165) Liu, L.; Li, S.; Garreau, H.; Vert, M. Selective Enzymatic Degradations of Poly(L-Lactide) and Poly(ϵ -Caprolactone) Blend Films. *Biomacromolecules* **2000**, *1* (3), 350–359. <https://doi.org/10.1021/bm000046k>.
- (166) Gan, Z.; Yu, D.; Zhong, Z.; Liang, Q.; Jing, X. Enzymatic Degradation of Poly(ϵ -Caprolactone)/Poly(DL-Lactide) Blends in Phosphate Buffer Solution. *Polymer (Guildf)*. **1999**, *40* (10), 2859–2862. [https://doi.org/10.1016/S0032-3861\(98\)00549-7](https://doi.org/10.1016/S0032-3861(98)00549-7).
- (167) Fukuzaki, H.; Yoshida, M.; Asano, M.; Kumakura, M.; Mashimo, T.; Yuasa, H.; Imai, K.; Hidetoshi, Y. Synthesis of Low-Molecular-Weight Copoly(l-Lactic Acid/ ϵ -Caprolactone) by Direct Copolycondensation in the Absence of Catalysts, and Enzymatic Degradation of the Polymers. *Polymer (Guildf)*. **1990**, *31* (10), 2006–2014. [https://doi.org/10.1016/0032-3861\(90\)90031-S](https://doi.org/10.1016/0032-3861(90)90031-S).
- (168) Cook, W. J.; Cameron, J. A.; Bell, J. P.; Huang, S. J. Scanning Electron Microscopic Visualization of Biodegradation of Polycaprolactones by Fungi. *J. Polym. Sci. Polym. Lett.*

- Ed.* **1981**, *19* (4), 159–165. <https://doi.org/10.1002/pol.1981.130190402>.
- (169) Benedict, C. V.; Cook, W. J.; Jarrett, P.; Cameron, J. A.; Huang, S. J.; Bell, J. P. Fungal Degradation of Polycaprolactones. *J. Appl. Polym. Sci.* **1983**, *28* (1), 327–334. <https://doi.org/10.1002/app.1983.070280128>.
- (170) Mochizuki, M.; Hirano, M.; Kanmuri, Y.; Kudo, K.; Tokiwa, Y. Hydrolysis of Polycaprolactone Fibers by Lipase: Effects of Draw Ratio on Enzymatic Degradation. *J. Appl. Polym. Sci.* **1995**, *55* (2), 289–296. <https://doi.org/10.1002/app.1995.070550212>.
- (171) Lam, C. X. F.; Savalani, M. M.; Teoh, S. H.; Hutmacher, D. W. Dynamics of in Vitro Polymer Degradation of Polycaprolactone-Based Scaffolds: Accelerated versus Simulated Physiological Conditions. *Biomed. Mater.* **2008**, *3* (3). <https://doi.org/10.1088/1748-6041/3/3/034108>.
- (172) Fukushima, K.; Feijoo, J. L.; Yang, M. C. Comparison of Abiotic and Biotic Degradation of PDLLA, PCL and Partially Miscible PDLLA/PCL Blend. *Eur. Polym. J.* **2013**, *49* (3), 706–717. <https://doi.org/10.1016/j.eurpolymj.2012.12.011>.
- (173) Iwamoto, A.; Tokiwa, Y. Enzymatic Degradation of Plastics Containing Polycaprolactone. *Polym. Degrad. Stab.* **1994**, *45* (2), 205–213. [https://doi.org/10.1016/0141-3910\(94\)90138-4](https://doi.org/10.1016/0141-3910(94)90138-4).
- (174) Cho, K.; Lee, J.; Xing, P. Enzymatic Degradation of Blends of Poly(ϵ -Caprolactone) and Poly(Styrene-Co-Acrylonitrile) by Pseudomonas Lipase. *J. Appl. Polym. Sci.* **2001**, *83* (4), 868–879. <https://doi.org/10.1002/app.10084>.
- (175) Peng, H.; Ling, J.; Liu, J.; Zhu, N.; Ni, X.; Shen, Z. Controlled Enzymatic Degradation of Poly(ϵ -Caprolactone)-Based Copolymers in the Presence of Porcine Pancreatic Lipase. *Polym. Degrad. Stab.* **2010**, *95* (4), 643–650. <https://doi.org/10.1016/j.polymdegradstab.2009.12.005>.
- (176) Williams, D. F. On the Mechanisms of Biocompatibility. *Biomaterials* **2008**, *29* (20), 2941–2953. <https://doi.org/10.1016/j.biomaterials.2008.04.023>.
- (177) Guarino, V.; Gentile, G.; Sorrentino, L.; Ambrosio, L. *Polycaprolactone: Synthesis, Properties, and Applications*, 2017. <https://doi.org/10.1002/0471440264.pst658>.
- (178) Avérous, L. Biodegradable Multiphase Systems Based on Plasticized Starch: A Review. *J. Macromol. Sci. - Polym. Rev.* **2004**, *44* (3), 231–274. <https://doi.org/10.1081/MC-200029326>.
- (179) Jiang, H.; Wang, X. B.; Li, C. Y.; Li, J. S.; Xu, F. J.; Mao, C.; Yang, W. T.; Shen, J. Improvement of Hemocompatibility of Polycaprolactone Film Surfaces with Zwitterionic Polymer Brushes. *Langmuir* **2011**, *27* (18), 11575–11581. <https://doi.org/10.1021/la202101q>.
- (180) Varde, N. K.; Pack, D. W. Microspheres for Controlled Release Drug Delivery. *Expert Opin. Biol. Ther.* **2004**, *4* (1), 35–51. <https://doi.org/10.1517/14712598.4.1.35>.
- (181) Dash, T. K.; Konkimalla, V. B. Poly- ϵ -Caprolactone Based Formulations for Drug Delivery and Tissue Engineering: A Review. *J. Control. Release* **2012**, *158* (1), 15–33.

- <https://doi.org/10.1016/j.jconrel.2011.09.064>.
- (182) Benoit, M. A.; Baras, B.; Gillard, J. Preparation and Characterization of Protein-Loaded Poly(ϵ -Caprolactone) Microparticles for Oral Vaccine Delivery. *Int. J. Pharm.* **1999**, *184* (1), 73–84. [https://doi.org/10.1016/S0378-5173\(99\)00109-X](https://doi.org/10.1016/S0378-5173(99)00109-X).
- (183) Mundargi, R. C.; Srirangarajan, S.; Agnihotri, S. A.; Patil, S. A.; Ravindra, S.; Setty, S. B.; Aminabhavi, T. M. Development and Evaluation of Novel Biodegradable Microspheres Based on Poly(d,l-Lactide-Co-Glycolide) and Poly(ϵ -Caprolactone) for Controlled Delivery of Doxycycline in the Treatment of Human Periodontal Pocket: In Vitro and in Vivo Studies. *J. Control. Release* **2007**, *119* (1), 59–68. <https://doi.org/10.1016/j.jconrel.2007.01.008>.
- (184) Yuan, B.; Jiang, X.; Chen, Y.; Guo, Q.; Wang, K.; Meng, X.; Huang, Z.; Wen, X. Metastatic Cancer Cell and Tissue-Specific Fluorescence Imaging Using a New DNA Aptamer Developed by Cell-SELEX. *Talanta* **2017**, *170* (2), 56–62. <https://doi.org/10.1016/j.talanta.2017.03.094>.
- (185) Pinto Reis, C.; Neufeld, R. J.; Ribeiro, A. J.; Veiga, F. Nanoencapsulation I. Methods for Preparation of Drug-Loaded Polymeric Nanoparticles. *Nanomedicine Nanotechnology, Biol. Med.* **2006**, *2* (1), 8–21. <https://doi.org/10.1016/j.nano.2005.12.003>.
- (186) Woodruff, M. A.; Hutmacher, D. W. The Return of a Forgotten Polymer - Polycaprolactone in the 21st Century. *Prog. Polym. Sci.* **2010**, *35* (10), 1217–1256. <https://doi.org/10.1016/j.progpolymsci.2010.04.002>.
- (187) Eatemadi, A.; Daraee, H.; Aiyelabegan, H. T.; Negahdari, B.; Rajeian, B.; Zarghami, N. Synthesis and Characterization of Chrysin-Loaded PCL-PEG-PCL Nanoparticle and Its Effect on Breast Cancer Cell Line. *Biomed. Pharmacother.* **2016**, *84*, 1915–1922. <https://doi.org/10.1016/j.biopha.2016.10.095>.
- (188) Jiang, Y.; Lu, H.; Dag, A.; Hart-Smith, G.; Stenzel, M. H. Albumin-Polymer Conjugate Nanoparticles and Their Interactions with Prostate Cancer Cells in 2D and 3D Culture: Comparison between PMMA and PCL. *J. Mater. Chem. B* **2016**, *4* (11), 2017–2027. <https://doi.org/10.1039/c5tb02576a>.
- (189) Schlesinger, E.; Ciaccio, N.; Desai, T. A. Polycaprolactone Thin-Film Drug Delivery Systems: Empirical and Predictive Models for Device Design. *Mater. Sci. Eng. C* **2015**, *57*, 232–239. <https://doi.org/10.1016/j.msec.2015.07.027>.
- (190) Ramgopal, Y.; Mondal, D.; Venkatraman, S. S.; Godbey, W. T.; Yuen, G. Y. Controlled Release of Complexed DNA from Polycaprolactone Film: Comparison of Lipoplex and Polyplex Release. *J. Biomed. Mater. Res. - Part B Appl. Biomater.* **2009**, *89* (2), 439–447. <https://doi.org/10.1002/jbm.b.31231>.
- (191) Holländer, J.; Genina, N.; Jukarainen, H.; Khajeheian, M.; Rosling, A.; Mäkilä, E.; Sandler, N. Three-Dimensional Printed PCL-Based Implantable Prototypes of Medical Devices for Controlled Drug Delivery. *J. Pharm. Sci.* **2016**, *105* (9), 2665–2676. <https://doi.org/10.1016/j.xphs.2015.12.012>.
- (192) Grossen, P.; Witzigmann, D.; Sieber, S.; Huwyler, J. PEG-PCL-Based Nanomedicines: A

- Biodegradable Drug Delivery System and Its Application. *J. Control. Release* **2017**, *260* (April), 46–60. <https://doi.org/10.1016/j.jconrel.2017.05.028>.
- (193) Langer, R.; Vacanti, J. P. Tissue Engineering. *Science (80-.)* **1993**, *260* (5110), 920–926. <https://doi.org/10.1126/science.8493529>.
- (194) Sitharaman, B.; Shi, X.; Walboomers, X. F.; Liao, H.; Cuijpers, V.; Wilson, L. J.; Mikos, A. G.; Jansen, J. A. In Vivo Biocompatibility of Ultra-Short Single-Walled Carbon Nanotube/Biodegradable Polymer Nanocomposites for Bone Tissue Engineering. *Bone* **2008**, *43* (2), 362–370. <https://doi.org/10.1016/j.bone.2008.04.013>.
- (195) Dalton, P. D.; Woodfield, T.; Hutmacher, D. W. Snapshot: Polymer Scaffolds for Tissue Engineering. *Biomaterials* **2009**, *30* (4), 701–702. [https://doi.org/10.1016/S0142-9612\(08\)00900-9](https://doi.org/10.1016/S0142-9612(08)00900-9).
- (196) Yoshimoto, H.; Shin, Y. M.; Terai, H.; Vacanti, J. P. A Biodegradable Nanofiber Scaffold by Electrospinning and Its Potential for Bone Tissue Engineering. *Biomaterials* **2003**, *24* (12), 2077–2082. [https://doi.org/10.1016/S0142-9612\(02\)00635-X](https://doi.org/10.1016/S0142-9612(02)00635-X).
- (197) Fomby, P.; Cherlin, A. J.; Hadjizadeh, A.; Doillon, C. J.; Sueblinvong, V.; Weiss, D. J.; Bates, J. H. T.; Gilbert, T.; Liles, W. C.; Lutzko, C.; Rajagopal, J.; Prockop, D. J.; Chambers, D.; Giangreco, A.; Keating, A.; Kotton, D.; Lelkes, P. I.; Wagner, D. E.; Prockop, D. J. Stem Cells and Cell Therapies in Lung Biology and Diseases: Conference Report. *Ann. Am. Thorac. Soc.* **2010**, *12* (3), 181–204. <https://doi.org/10.1002/term>.
- (198) Martin, J. L.; Norris, B. J.; Murphy, E.; Crowe, J. A. Medical Device Development: The Challenge for Ergonomics. *Appl. Ergon.* **2008**, *39* (3), 271–283. <https://doi.org/10.1016/j.apergo.2007.10.002>.
- (199) Ruckh, T. T.; Kumar, K.; Kipper, M. J.; Papat, K. C. Osteogenic Differentiation of Bone Marrow Stromal Cells on Poly(ϵ -Caprolactone) Nanofiber Scaffolds. *Acta Biomater.* **2010**, *6* (8), 2949–2959. <https://doi.org/10.1016/j.actbio.2010.02.006>.
- (200) Cheng, L.; Lei, L.; Guo, S. In Vitro and in Vivo Evaluation of Praziquantel Loaded Implants Based on PEG/PCL Blends. *Int. J. Pharm.* **2010**, *387* (1–2), 129–138. <https://doi.org/10.1016/j.ijpharm.2009.12.010>.
- (201) Kovalevsky, G.; Barnhart, K. Norplant and Other Implantable Contraceptives. *Clinical Obstetrics and Gynecology*. 2001, pp 92–100. <https://doi.org/10.1097/00003081-200103000-00012>.
- (202) Catanzano, O.; Acierno, S.; Russo, P.; Cervasio, M.; Del Basso De Caro, M.; Bolognese, A.; Sammartino, G.; Califano, L.; Marenzi, G.; Calignano, A.; Acierno, D.; Quaglia, F. Melt-Spun Bioactive Sutures Containing Nanohybrids for Local Delivery of Anti-Inflammatory Drugs. *Mater. Sci. Eng. C* **2014**, *43*, 300–309. <https://doi.org/10.1016/j.msec.2014.07.012>.
- (203) Jing, X.; Mi, H. Y.; Huang, H. X.; Turng, L. S. Shape Memory Thermoplastic Polyurethane (TPU)/Poly(ϵ -Caprolactone) (PCL) Blends as Self-Knotting Sutures. *J. Mech. Behav. Biomed. Mater.* **2016**, *64*, 94–103. <https://doi.org/10.1016/j.jmbbm.2016.07.023>.
- (204) Croisier, F.; Atanasova, G.; Poumay, Y.; Jérôme, C. Polysaccharide-Coated PCL Nanofibers for Wound Dressing Applications. *Adv. Healthc. Mater.* **2014**, *3* (12), 2032–2039.

- <https://doi.org/10.1002/adhm.201400380>.
- (205) Jung, S. M.; Yoon, G. H.; Lee, H. C.; Shin, H. S. Chitosan Nanoparticle/PCL Nanofiber Composite for Wound Dressing and Drug Delivery. *J. Biomater. Sci. Polym. Ed.* **2015**, *26* (4), 252–263. <https://doi.org/10.1080/09205063.2014.996699>.
- (206) Augustine, R.; Kalarikkal, N.; Thomas, S. Electrospun PCL Membranes Incorporated with Biosynthesized Silver Nanoparticles as Antibacterial Wound Dressings. *Appl. Nanosci.* **2016**, *6* (3), 337–344. <https://doi.org/10.1007/s13204-015-0439-1>.
- (207) Farah, S.; Anderson, D. G.; Langer, R. Physical and Mechanical Properties of PLA, and Their Functions in Widespread Applications — A Comprehensive Review. *Adv. Drug Deliv. Rev.* **2016**, *107*, 367–392. <https://doi.org/10.1016/j.addr.2016.06.012>.
- (208) Narayanan, N.; Roychoudhury, P. K.; Srivastava, A. L (+) Lactic Acid Fermentation and Its Product Polymerization. *Electron. J. Biotechnol.* **2004**, *7* (2). <https://doi.org/10.2225/vol7-issue2-fulltext-7>.
- (209) Aydin, R. S. T. *Plant Oil Renewable Resources as Green Alternatives in Polymer Science*; Kaplan, D. L., Ed.; Springer Berlin Heidelberg: Berlin, Heidelberg, 2017; Vol. 94. <https://doi.org/10.1007/978-3-662-03680-8>.
- (210) Jamshidian, M.; Tehrany, E. A.; Imran, M.; Jacquot, M.; Desobry, S. Poly-Lactic Acid: Production, Applications, Nanocomposites, and Release Studies. *Compr. Rev. Food Sci. Food Saf.* **2010**, *9* (5), 552–571. <https://doi.org/10.1111/j.1541-4337.2010.00126.x>.
- (211) Vink, E. T. H.; Davies, S. Life Cycle Inventory and Impact Assessment Data for 2014 Ingeo® Polylactide Production. *Ind. Biotechnol.* **2015**, *11* (3), 167–180. <https://doi.org/10.1089/ind.2015.0003>.
- (212) Ahmed, J.; Varshney, S. K. Polylactides—Chemistry, Properties and Green Packaging Technology: A Review. *Int. J. Food Prop.* **2011**, *14* (1), 37–58. <https://doi.org/10.1080/10942910903125284>.
- (213) Carothers, W. H.; Borough, G. L.; Natta, F. J. Studies of Polymerization and Ring Formation. X. The Reversible Polymerization of Six-Membered Cyclic Esters. *J. Am. Chem. Soc.* **1932**, *54* (2), 761–772. <https://doi.org/10.1021/ja01341a046>.
- (214) Lasprilla, A. J. R.; Martinez, G. A. R.; Lunelli, B. H.; Jardini, A. L.; Filho, R. M. Poly-Lactic Acid Synthesis for Application in Biomedical Devices - A Review. *Biotechnol. Adv.* **2012**, *30* (1), 321–328. <https://doi.org/10.1016/j.biotechadv.2011.06.019>.
- (215) Ajioka, M.; Enomoto, K.; Suzuki, K.; Yamaguchi, A. Basic Properties of Polylactic Acid Produced by The. *Bull. Chem. Soc. Jpn.* 1995, pp 2125–2131.
- (216) Moon, S. II; Lee, C. W.; Miyamoto, M.; Kimura, Y. Melt Polycondensation of L-Lactic Acid with Sn(II) Catalysts Activated by Various Proton Acids: A Direct Manufacturing Route to High Molecular Weight Poly(L-Lactic Acid). *J. Polym. Sci. Part A Polym. Chem.* **2000**, *38* (9), 1673–1679. [https://doi.org/10.1002/\(SICI\)1099-0518\(20000501\)38:9<1673::AID-POLA33>3.0.CO;2-T](https://doi.org/10.1002/(SICI)1099-0518(20000501)38:9<1673::AID-POLA33>3.0.CO;2-T).
- (217) Cheng, Y.; Deng, S.; Chen, P.; Ruan, R. Polylactic Acid (PLA) Synthesis and Modifications:

- A Review. *Front. Chem. China* **2009**, *4* (3), 259–264. <https://doi.org/10.1007/s11458-009-0092-x>.
- (218) Inside, L.; Access, G.; April, E. A Literature Review of Poly (Lactic Acid). **2014**, *9* (2), 1–10. <https://doi.org/1566-2543/01/0400-0063/0>.
- (219) Madhavan Nampoothiri, K.; Nair, N. R.; John, R. P. An Overview of the Recent Developments in Polylactide (PLA) Research. *Bioresour. Technol.* **2010**, *101* (22), 8493–8501. <https://doi.org/10.1016/j.biortech.2010.05.092>.
- (220) Hartmann, M. H. High Molecular Weight Polylactic Acid Polymers. *Biopolym. from Renew. Resour.* **1998**, 367–411. https://doi.org/10.1007/978-3-662-03680-8_15.
- (221) Lassalle, V. L.; Ferreira, M. L. Lipase-Catalyzed Synthesis of Polylactic Acid: An Overview of the Experimental Aspects. *J. Chem. Technol. Biotechnol.* **2008**, *83* (11), 1493–1502. <https://doi.org/10.1002/jctb.1994>.
- (222) Shibryaeva, L. S.; Krashennnikov, V. G.; Gorshenev, V. N. Thermal Properties of Porous Polylactide. *Polym. Sci. - Ser. A* **2019**, *61* (2), 162–174. <https://doi.org/10.1134/S0965545X19020123>.
- (223) Auras, R.; Harte, B.; Selke, S. An Overview of Polylactides as Packaging Materials. *Macromol. Biosci.* **2004**, *4* (9), 835–864. <https://doi.org/10.1002/mabi.200400043>.
- (224) Auras, R.; Lim, L. T.; Selke, S. E. M.; Tsuji, H. *Poly(Lactic Acid): Synthesis, Structures, Properties, Processing, and Applications*; John Wiley & Sons, 2010; Vol. 10. <https://doi.org/10.1002/9780470649848>.
- (225) Ikada, Y.; Jamshidi, K.; Tsuji, H.; Hyon, S. H. Stereocomplex Formation between Enantiomeric Poly(Lactides). *Macromolecules* **1987**, *20* (4), 904–906. <https://doi.org/10.1021/ma00170a034>.
- (226) Fang, Q.; Hanna, M. A. Rheological Properties of Amorphous and Semicrystalline Polylactic Acid Polymers. *Ind. Crops Prod.* **1999**, *10* (1), 47–53. [https://doi.org/10.1016/S0926-6690\(99\)00009-6](https://doi.org/10.1016/S0926-6690(99)00009-6).
- (227) Park, K. I.; Xanthos, M. A Study on the Degradation of Polylactic Acid in the Presence of Phosphonium Ionic Liquids. *Polym. Degrad. Stab.* **2009**, *94* (5), 834–844. <https://doi.org/10.1016/j.polymdegradstab.2009.01.030>.
- (228) Bergsma, J. E.; Rozema, F. R.; Bos, R. R. M.; Boering, G.; de Bruijn, W. C.; Pennings, A. J. In Vivo Degradation and Biocompatibility Study of in Vitro Pre-Degraded as-Polymerized Polylactide Particles. *Biomaterials* **1995**, *16* (4), 267–274. [https://doi.org/10.1016/0142-9612\(95\)93253-A](https://doi.org/10.1016/0142-9612(95)93253-A).
- (229) Mohanty, A. K.; Misra, M.; Drzal, L. T.; Selke, S. E.; Harte, B. R.; Hinrichsen, G. Natural Fibers, Biopolymers, and Biocomposites.
- (230) Lunt, J. Large-Scale Production, Properties and Commercial Applications of Poly Lactic Acid Polymers. *Polym. Degrad. Stab.* **1998**, *59* (1–3), 145–152. [https://doi.org/10.1016/s0141-3910\(97\)00148-1](https://doi.org/10.1016/s0141-3910(97)00148-1).
- (231) Hamad, K.; Kaseem, M.; Yang, H. W.; Deri, F.; Ko, Y. G. Properties and Medical

- Applications of Polylactic Acid: A Review. *Express Polym. Lett.* **2015**, *9* (5), 435–455.
<https://doi.org/10.3144/expresspolymlett.2015.42>.
- (232) Qi, X.; Ren, Y.; Wang, X. New Advances in the Biodegradation of Poly(Lactic) Acid. *Int. Biodeterior. Biodegrad.* **2017**, *117*, 215–223. <https://doi.org/10.1016/j.ibiod.2017.01.010>.
- (233) Pranamuda, H.; Tokiwa, Y.; Tanaka, H. Polylactide Degradation by an Amycolatopsis Sp. *Appl. Environ. Microbiol.* **1997**, *63* (4), 1637–1640.
<https://doi.org/10.1128/aem.63.4.1637-1640.1997>.
- (234) Pranamuda, H.; Tokiwa, Y. Degradation of Poly(L-Lactide) by Strains Belonging to Genus Amycolatopsis. *Biotechnol. Lett.* **1999**, *21* (10), 901–905.
<https://doi.org/10.1023/A:1005547326434>.
- (235) Nakamura, K.; Tomita, T.; Abe, N.; Kamio, Y. Purification and Characterization of an Extracellular Poly(L-Lactic Acid) Depolymerase from a Soil Isolate, Amycolatopsis Sp. Strain K104-1. *Appl. Environ. Microbiol.* **2001**, *67* (1), 345–353.
<https://doi.org/10.1128/AEM.67.1.345-353.2001>.
- (236) Tomita, K.; Kuroki, Y.; Nagai, K. Isolation of Thermophiles Degrading Poly(L-Lactic Acid). *J. Biosci. Bioeng.* **1999**, *87* (6), 752–755. [https://doi.org/10.1016/S1389-1723\(99\)80148-0](https://doi.org/10.1016/S1389-1723(99)80148-0).
- (237) Torres, A.; Li, S. M.; Roussos, S.; Vert, M. Screening of Microorganisms for Biodegradation of Poly(Lactic Acid) and Lactic Acid-Containing Polymers. *Appl. Environ. Microbiol.* **1996**, *62* (7), 2393–2397. <https://doi.org/10.1128/aem.62.7.2393-2397.1996>.
- (238) Lipsa, R.; Tudorachi, N.; Darie-Nita, R. N.; Oprică, L.; Vasile, C.; Chiriac, A. Biodegradation of Poly(Lactic Acid) and Some of Its Based Systems with Trichoderma Viride. *Int. J. Biol. Macromol.* **2016**, *88*, 515–526. <https://doi.org/10.1016/j.ijbiomac.2016.04.017>.
- (239) Jarerat, A.; Tokiwa, Y. Degradation of Poly(L-Lactide) by a Fungus. *Macromol. Biosci.* **2001**, *1* (4), 136–140. [https://doi.org/10.1002/1616-5195\(20010601\)1:4<136::AID-MABI136>3.0.CO;2-3](https://doi.org/10.1002/1616-5195(20010601)1:4<136::AID-MABI136>3.0.CO;2-3).
- (240) Karamanlioglu, M.; Houlden, A.; Robson, G. D. Isolation and Characterisation of Fungal Communities Associated with Degradation and Growth on the Surface of Poly(Lactic) Acid (PLA) in Soil and Compost. *Int. Biodeterior. Biodegrad.* **2014**, *95* (PB), 301–310.
<https://doi.org/10.1016/j.ibiod.2014.09.006>.
- (241) Lim, H. A.; Raku, T.; Tokiwa, Y. Hydrolysis of Polyesters by Serine Proteases. *Biotechnol. Lett.* **2005**, *27* (7), 459–464. <https://doi.org/10.1007/s10529-005-2217-8>.
- (242) Kawai, F. Polylactic Acid (PLA)-Degrading Microorganisms and PLA Depolymerases. *ACS Symp. Ser.* **2010**, *1043*, 405–414. <https://doi.org/10.1021/bk-2010-1043.ch027>.
- (243) Kawai, F.; Nakadai, K.; Nishioka, E.; Nakajima, H.; Ohara, H.; Masaki, K.; Iefuji, H. Different Enantioselectivity of Two Types of Poly(Lactic Acid) Depolymerases toward Poly(L-Lactic Acid) and Poly(D-Lactic Acid). *Polym. Degrad. Stab.* **2011**, *96* (7), 1342–1348.
<https://doi.org/10.1016/j.polymdegradstab.2011.03.022>.
- (244) Tokiwa, Y.; Jarerat, A. Biodegradation of Poly(L-Lactide). *Biotechnol. Lett.* **2004**, *26* (10),

- 771–777. <https://doi.org/10.1023/B:BILE.0000025927.31028.e3>.
- (245) Jarerat, A.; Tokiwa, Y.; Tanaka, H. Poly(L-Lactide) Degradation by *Kibdelosporangium Aridum*. *Biotechnol. Lett.* **2003**, *25* (23), 2035–2038. <https://doi.org/10.1023/B:BILE.0000004398.38799.29>.
- (246) Bergström, J. S.; Hayman, D. An Overview of Mechanical Properties and Material Modeling of Polylactide (PLA) for Medical Applications. *Ann. Biomed. Eng.* **2016**, *44* (2), 330–340. <https://doi.org/10.1007/s10439-015-1455-8>.
- (247) Tsuji, H.; Hyon, S. H.; Ikada, Y. Stereocomplex Formation between Enantiomeric Poly(Lactic Acid)s. 3. Calorimetric Studies on Blend Films Cast from Dilute Solution. *Macromolecules* **1991**, *24* (20), 5651–5656. <https://doi.org/10.1021/ma00020a026>.
- (248) Uhrich, K. E.; Cannizzaro, S. M.; Langer, R. S.; Shakesheff, K. M. ChemInform Abstract: Polymeric Systems for Controlled Drug Release. *ChemInform* **2010**, *31* (3), no-no. <https://doi.org/10.1002/chin.200003275>.
- (249) Gupta, B.; Revagade, N.; Hilborn, J. Poly(Lactic Acid) Fiber: An Overview. *Prog. Polym. Sci.* **2007**, *32* (4), 455–482. <https://doi.org/10.1016/j.progpolymsci.2007.01.005>.
- (250) Yamane, H.; Sasai, K. Effect of the Addition of Poly(D-Lactic Acid) on the Thermal Property of Poly(L-Lactic Acid). *Polymer (Guildf)*. **2003**, *44* (8), 2569–2575. [https://doi.org/10.1016/S0032-3861\(03\)00092-2](https://doi.org/10.1016/S0032-3861(03)00092-2).
- (251) Henton, D. E.; Gruber, P.; Lunt, J.; Randall, J. Polylactic Acid Technology. *Nat. Fibers, Biopolym. Biocomposites* **2005**, *12*, 527–577. [https://doi.org/10.1002/1521-4095\(200012\)12:23<1841::aid-adma1841>3.3.co;2-5](https://doi.org/10.1002/1521-4095(200012)12:23<1841::aid-adma1841>3.3.co;2-5).
- (252) Kulkarni, R. K.; Pani, K. C.; Neuman, C.; Leonard, F. *Polylactic Acid for Surgical Implants*; WALTER REED ARMY MEDICAL CENTER WASHINGTON DC ARMY MEDICAL BIOMECHANICAL ...; 1966; Vol. 93. <https://doi.org/10.1001/archsurg.1966.01330050143023>.
- (253) Mitragotri, S.; Burke, P. A.; Langer, R. Overcoming the Challenges in Administering Biopharmaceuticals: Formulation and Delivery Strategies. *Nat. Rev. Drug Discov.* **2014**, *13* (9), 655–672. <https://doi.org/10.1038/nrd4363>.
- (254) Valantin, M. A.; Aubron-Olivier, C.; Ghosn, J.; Laglenne, E.; Pauchard, M.; Schoen, H.; Bousquet, R.; Katz, P.; Costagliola, D.; Katlama, C. Polylactic Acid Implants (New-Fill)® to Correct Facial Lipoatrophy in HIV-Infected Patients: Results of the Open-Label Study VEGA. *Aids* **2003**, *17* (17), 2471–2477. <https://doi.org/10.1097/00002030-200311210-00009>.
- (255) Edlund, U.; Albertsson, A. C. Degradable Polymer Microspheres for Controlled Drug Delivery. In *Advances in Polymer Science*; Springer Berlin Heidelberg: Berlin, Heidelberg, 2002; Vol. 157, pp 67–112. https://doi.org/10.1007/3-540-45734-8_3.
- (256) Coelho, J. F.; Ferreira, P. C.; Alves, P.; Cordeiro, R.; Fonseca, A. C.; Góis, J. R.; Gil, M. H. Drug Delivery Systems: Advanced Technologies Potentially Applicable in Personalized Treatments. *EPMA J.* **2010**, *1* (1), 164–209. <https://doi.org/10.1007/s13167-010-0001-x>.

- (257) Lee, B. K.; Yun, Y.; Park, K. PLA Micro- and Nano-Particles. *Adv. Drug Deliv. Rev.* **2016**, *107*, 176–191. <https://doi.org/10.1016/j.addr.2016.05.020>.
- (258) Sah, E.; Sah, H. Recent Trends in Preparation of Poly(Lactide-Co-Glycolide) Nanoparticles by Mixing Polymeric Organic Solution with Antisolvent. *J. Nanomater.* **2015**, *2015*. <https://doi.org/10.1155/2015/794601>.
- (259) Wischke, C.; Schwendeman, S. P. Principles of Encapsulating Hydrophobic Drugs in PLA/PLGA Microparticles. *Int. J. Pharm.* **2008**, *364* (2), 298–327. <https://doi.org/10.1016/j.ijpharm.2008.04.042>.
- (260) Lambert, G.; Fattal, E.; Couvreur, P. Nanoparticulate Systems for the Delivery of Antisense Oligonucleotides. *Adv. Drug Deliv. Rev.* **2001**, *47* (1), 99–112. [https://doi.org/10.1016/S0169-409X\(00\)00116-2](https://doi.org/10.1016/S0169-409X(00)00116-2).
- (261) Lu, Y.; Sturek, M.; Park, K. Microparticles Produced by the Hydrogel Template Method for Sustained Drug Delivery. *Int. J. Pharm.* **2014**, *461* (1–2), 258–269. <https://doi.org/10.1016/j.ijpharm.2013.11.058>.
- (262) Tan, M. L.; Choong, P. F. M.; Dass, C. R. Recent Developments in Liposomes, Microparticles and Nanoparticles for Protein and Peptide Drug Delivery. *Peptides* **2010**, *31* (1), 184–193. <https://doi.org/10.1016/j.peptides.2009.10.002>.
- (263) Thermet, A.; Rollier, C.; Zoulim, F.; Trepo, C.; Cova, L. Progress in DNA Vaccine for Prophylaxis and Therapy of Hepatitis B. *Vaccine* **2003**, *21* (7–8), 659–662. [https://doi.org/10.1016/S0264-410X\(02\)00575-3](https://doi.org/10.1016/S0264-410X(02)00575-3).
- (264) Guillon, C.; Mayol, K.; Terrat, C.; Compagnon, C.; Primard, C.; Charles, M. H.; Delair, T.; Munier, S.; Verrier, B. Formulation of HIV-1 Tat and P24 Antigens by PLA Nanoparticles or MF59 Impacts the Breadth, but Not the Magnitude, of Serum and Faecal Antibody Responses in Rabbits. *Vaccine* **2007**, *25* (43), 7491–7501. <https://doi.org/10.1016/j.vaccine.2007.08.060>.
- (265) Liu, Y.; Chen, X.; Wang, L.; Yang, T.; Yuan, Q.; Ma, G. Surface Charge of PLA Microparticles in Regulation of Antigen Loading, Macrophage Phagocytosis and Activation, and Immune Effects in Vitro. *Particuology* **2014**, *17*, 74–80. <https://doi.org/10.1016/j.partic.2014.02.006>.
- (266) Gupta, R. K.; Goswami, D. G.; Singh, R. R.; Surolia, A.; Panda, A. K. Soybean Agglutinin Coated PLA Particles Entrapping Candidate Vaccines Induces Enhanced Primary and Sustained Secondary Antibody Response from Single Point Immunization. *Eur. J. Pharm. Sci.* **2012**, *45* (3), 282–295. <https://doi.org/10.1016/j.ejps.2011.11.022>.
- (267) Kumar, G.; Shafiq, N.; Malhotra, S. Drug-Loaded PLGA Nanoparticles for Oral Administration: Fundamental Issues and Challenges Ahead. *Crit. Rev. Ther. Drug Carrier Syst.* **2012**, *29* (1), 149–182. <https://doi.org/10.1615/critrevtherdrugcarriersyst.v29.i2.20>.
- (268) Hsu, C. H.; Cui, Z.; Mumper, R. J.; Jay, M. Preparation and Characterization of Novel Coenzyme Q10 Nanoparticles Engineered from Microemulsion Precursors. *AAPS PharmSciTech* **2003**, *4* (3), 1–12. <https://doi.org/10.1208/pt040332>.
- (269) Kamaly, N.; Xiao, Z.; Valencia, P. M.; Radovic-Moreno, A. F.; Farokhzad, O. C. Targeted

- Polymeric Therapeutic Nanoparticles: Design, Development and Clinical Translation. *Chem. Soc. Rev.* **2012**, *41* (7), 2971–3010. <https://doi.org/10.1039/c2cs15344k>.
- (270) Sah, H.; Thoma, L. A.; Desu, H. R.; Sah, E.; Wood, G. C. Concepts and Practices Used to Develop Functional PLGA-Based Nanoparticulate Systems. *Int. J. Nanomedicine* **2013**, *8*, 747–765. <https://doi.org/10.2147/IJN.S40579>.
- (271) Dhandayuthapani, B.; Yoshida, Y.; Maekawa, T.; Kumar, D. S. Polymeric Scaffolds in Tissue Engineering Application: A Review. *Int. J. Polym. Sci.* **2011**, *2011* (ii). <https://doi.org/10.1155/2011/290602>.
- (272) Nair, L. S.; Laurencin, C. T. Biodegradable Polymers as Biomaterials. *Prog. Polym. Sci.* **2007**, *32* (8–9), 762–798. <https://doi.org/10.1016/j.progpolymsci.2007.05.017>.
- (273) Kloxin, A. M.; Kloxin, C. J.; Bowman, C. N.; Anseth, K. S. Mechanical Properties of Cellularly Responsive Hydrogels and Their Experimental Determination. *Adv. Mater.* **2010**, *22* (31), 3484–3494. <https://doi.org/10.1002/adma.200904179>.
- (274) Patrício, T.; Domingos, M.; Gloria, A.; Bártolo, P. Characterisation of PCL and PCL/PLA Scaffolds for Tissue Engineering. *Procedia CIRP* **2013**, *5*, 110–114. <https://doi.org/10.1016/j.procir.2013.01.022>.
- (275) Schmid, J.; Wallkamm, B.; Hämmerle, C. H. F.; Gogolewski, S.; Lang, N. P. The Significance of Angiogenesis in Guided Bone Regeneration: A Case Report of a Rabbit Experiment. *Clinical Oral Implants Research*. 1997, pp 244–248. <https://doi.org/10.1034/j.1600-0501.1997.080311.x>.
- (276) Haaparanta, A. M.; Järvinen, E.; Cengiz, I. F.; Ellä, V.; Kokkonen, H. T.; Kiviranta, I.; Kellomäki, M. Preparation and Characterization of Collagen/PLA, Chitosan/PLA, and Collagen/Chitosan/PLA Hybrid Scaffolds for Cartilage Tissue Engineering. *J. Mater. Sci. Mater. Med.* **2014**, *25* (4), 1129–1136. <https://doi.org/10.1007/s10856-013-5129-5>.
- (277) Dai, W.; Kawazoe, N.; Lin, X.; Dong, J.; Chen, G. The Influence of Structural Design of PLGA/Collagen Hybrid Scaffolds in Cartilage Tissue Engineering. *Biomaterials* **2010**, *31* (8), 2141–2152. <https://doi.org/10.1016/j.biomaterials.2009.11.070>.
- (278) Kinoshita, Y.; Kobayashi, M.; Fukuoka, S.; Yokoya, S.; Ikada, Y. Reconstruction of Jaw Bones Using Poly(L-Lactic Acid) Mesh and Transplantation of Particulate Cancellous Bone and Marrow: Long-Term Observation Of 40 Cases. *Int J Oral Maxillofac Surg* **2003**, *32* (2), 117–120.
- (279) Rezwan, K.; Chen, Q. Z.; Blaker, J. J.; Boccaccini, A. R. Biodegradable and Bioactive Porous Polymer/Inorganic Composite Scaffolds for Bone Tissue Engineering. *Biomaterials* **2006**, *27* (18), 3413–3431. <https://doi.org/10.1016/j.biomaterials.2006.01.039>.
- (280) Chia, H. N.; Wu, B. M. Recent Advances in 3D Printing of Biomaterials. *J. Biol. Eng.* **2015**, *9* (1), 1–14. <https://doi.org/10.1186/s13036-015-0001-4>.
- (281) Gross, B. C.; Erkal, J. L.; Lockwood, S. Y.; Chen, C.; Spence, D. M. Evaluation of 3D Printing and Its Potential Impact on Biotechnology and the Chemical Sciences. *Anal. Chem.* **2014**, *86* (7), 3240–3253. <https://doi.org/10.1021/ac403397r>.

- (282) Serra, T.; Ortiz-Hernandez, M.; Engel, E.; Planell, J. A.; Navarro, M. Relevance of PEG in PLA-Based Blends for Tissue Engineering 3D-Printed Scaffolds. *Mater. Sci. Eng. C* **2014**, *38* (1), 55–62. <https://doi.org/10.1016/j.msec.2014.01.003>.
- (283) da Silva, D.; Kaduri, M.; Poley, M.; Adir, O.; Krinsky, N.; Shainsky-Roitman, J.; Schroeder, A. Biocompatibility, Biodegradation and Excretion of Polylactic Acid (PLA) in Medical Implants and Theranostic Systems. *Chem. Eng. J.* **2018**, *340* (January), 9–14. <https://doi.org/10.1016/j.cej.2018.01.010>.
- (284) Saeed, S. M.; Mirzadeh, H.; Zandi, M.; Barzin, J. Designing and Fabrication of Curcumin Loaded PCL/PVA Multi-Layer Nanofibrous Electrospun Structures as Active Wound Dressing. *Prog. Biomater.* **2017**, *6* (1–2), 39–48. <https://doi.org/10.1007/s40204-017-0062-1>.
- (285) Ignatova, M.; Manolova, N.; Markova, N.; Rashkov, I. Electrospun Non-Woven Nanofibrous Hybrid Mats Based on Chitosan and PLA for Wound-Dressing Applications. *Macromol. Biosci.* **2009**, *9* (1), 102–111. <https://doi.org/10.1002/mabi.200800189>.
- (286) Perumal, G.; Pappuru, S.; Chakraborty, D.; Maya Nandkumar, A.; Chand, D. K.; Doble, M. Synthesis and Characterization of Curcumin Loaded PLA—Hyperbranched Polyglycerol Electrospun Blend for Wound Dressing Applications. *Mater. Sci. Eng. C* **2017**, *76*, 1196–1204. <https://doi.org/10.1016/j.msec.2017.03.200>.
- (287) Ignatova, M.; Manolova, N.; Rashkov, I. Novel Antibacterial Fibers of Quaternized Chitosan and Poly(Vinyl Pyrrolidone) Prepared by Electrospinning. *Eur. Polym. J.* **2007**, *43* (4), 1112–1122. <https://doi.org/10.1016/j.eurpolymj.2007.01.012>.
- (288) Casper, C. L.; Yamaguchi, N.; Kiick, K. L.; Rabolt, J. F. Functionalizing Electrospun Fibers with Biologically Relevant Macromolecules. *Biomacromolecules* **2005**, *6* (4), 1998–2007. <https://doi.org/10.1021/bm050007e>.
- (289) Karami, Z.; Rezaeian, I.; Zahedi, P.; Abdollahi, M. Preparation and Performance Evaluations of Electrospun Poly(ϵ - Caprolactone), Poly(Lactic Acid), and Their Hybrid (50/50) Nanofibrous Mats Containing Thymol as an Herbal Drug for Effective Wound Healing. *J. Appl. Polym. Sci.* **2013**, *129* (2), 756–766. <https://doi.org/10.1002/app.38683>.
- (290) Cutright, D. E.; Hunsuck, E. E. Tissue Reaction to the Biodegradable Polylactic Acid Suture. *Oral Surgery, Oral Med. Oral Pathol.* **1971**, *31* (1), 134–139. [https://doi.org/10.1016/0030-4220\(71\)90044-2](https://doi.org/10.1016/0030-4220(71)90044-2).
- (291) Lou, C. W.; Yao, C. H.; Chen, Y. S.; Hsieh, T. C.; Lin, J. H.; Hsing, W. H. Manufacturing and Properties of PLA Absorbable Surgical Suture. *Text. Res. J.* **2008**, *78* (11), 958–965. <https://doi.org/10.1177/0040517507087856>.
- (292) Liu, S.; Wu, G.; Zhang, X.; Yu, J.; Liu, M.; Zhang, Y.; Wang, P.; Yin, X.; Zhang, J.; Li, F.; Zhang, M. Preparation and Properties of Poly (Lactic Acid) (PLA) Suture Loaded with PLA Microspheres Enclosed Drugs (PM-Ds). *J. Text. Inst.* **2019**, *110* (11), 1596–1605. <https://doi.org/10.1080/00405000.2019.1610999>.
- (293) Cruz, J.; Rana, S.; Figueiro, R.; Guedes, R. Designing Artificial Anterior Cruciate Ligaments Based on Novel Fibrous Structures. *Fibers Polym.* **2014**, *15* (1), 181–186.

- <https://doi.org/10.1007/s12221-014-0181-4>.
- (294) Santoro, M.; Shah, S. R.; Walker, J. L.; Mikos, A. G. Poly(Lactic Acid) Nanofibrous Scaffolds for Tissue Engineering. *Adv. Drug Deliv. Rev.* **2016**, *107*, 206–212. <https://doi.org/10.1016/j.addr.2016.04.019>.
- (295) Verran, J.; Packer, A.; Kelly, P.; Whitehead, K. A. The Retention of Bacteria on Hygienic Surfaces Presenting Scratches of Microbial Dimensions. *Lett. Appl. Microbiol.* **2010**, *50* (3), 258–263. <https://doi.org/10.1111/j.1472-765X.2009.02784.x>.
- (296) Brueck, S. R. J. Optical and Interferometric Lithography -Nanotechnology Enablers. *Proc. IEEE* **2005**, *93* (10), 1704–1721. <https://doi.org/10.1109/JPROC.2005.853538>.
- (297) Pease, R. F.; Chou, S. Y. Lithography and Other Patterning Techniques for Future Electronics. *Proc. IEEE* **2008**, *96* (2), 248–270. <https://doi.org/10.1109/JPROC.2007.911853>.
- (298) Gates, B. D.; Xu, Q.; Stewart, M.; Ryan, D.; Willson, C. G.; Whitesides, G. M. New Approaches to Nanofabrication: Molding, Printing, and Other Techniques. *Chem. Rev.* **2005**, *105* (4), 1171–1196. <https://doi.org/10.1021/cr030076o>.
- (299) Sanders, D. P. Advances in Patterning Materials for 193 Nm Immersion Lithography. *Chem. Rev.* **2010**, *110* (1), 321–360. <https://doi.org/10.1021/cr900244n>.
- (300) Liebmann, L. W.; Mansfield, S. M.; Wong, A. K.; Lavin, M. A.; Leipold, W. C.; Dunham, T. G. TCAD Development for Lithography Resolution Enhancement. *IBM J. Res. Dev.* **2001**, *45* (5), 651–665. <https://doi.org/10.1147/rd.455.0651>.
- (301) Wagner, C.; Harned, N. EUV Lithography: Lithography Gets Extreme. *Nat. Photonics* **2010**, *4* (1), 24–26. <https://doi.org/10.1038/nphoton.2009.251>.
- (302) Altissimo, M. E-Beam Lithography for Micro-/Nanofabrication. *Biomicrofluidics* **2010**, *4* (2). <https://doi.org/10.1063/1.3437589>.
- (303) Tseng, A. A. Recent Developments in Nanofabrication Using Focused Ion Beams. *Small* **2005**, *1* (10), 924–939. <https://doi.org/10.1002/smll.200500113>.
- (304) Solak, H. H.; David, C.; Gobrecht, J.; Golovkina, V.; Cerrina, F.; Kim, S. O.; Nealey, P. F. Sub-50 Nm Period Patterns with EUV Interference Lithography. *Microelectron. Eng.* **2003**, *67–68*, 56–62. [https://doi.org/10.1016/S0167-9317\(03\)00059-5](https://doi.org/10.1016/S0167-9317(03)00059-5).
- (305) Lu, C.; Lipson, R. H. Interference Lithography: A Powerful Tool for Fabricating Periodic Structures. *Laser Photonics Rev.* **2010**, *4* (4), 568–580. <https://doi.org/10.1002/lpor.200810061>.
- (306) Jang, J. H.; Ullal, C. K.; Maldovan, M.; Gorishnyy, T.; Kooi, S.; Koh, C. Y.; Thomas, E. L. 3D Micro- and Nanostructures via Interference Lithography. *Adv. Funct. Mater.* **2007**, *17* (16), 3027–3041. <https://doi.org/10.1002/adfm.200700140>.
- (307) Schiff, H. Nanoimprint Lithography: An Old Story in Modern Times? A Review. *J. Vac. Sci. Technol. B Microelectron. Nanom. Struct.* **2008**, *26* (2), 458–480. <https://doi.org/10.1116/1.2890972>.

- (308) Chou, S. Y. Nanoimprint Lithography and Lithographically Induced Self-Assembly. *MRS Bull.* **2001**, *26* (7), 512–517. <https://doi.org/10.1557/mrs2001.122>.
- (309) Chou, S. Y.; Krauss, P. R. Imprint Lithography with Sub-10 Nm Feature Size and High Throughput. *Microelectron. Eng.* **1997**, *35* (1–4), 237–240. [https://doi.org/10.1016/S0167-9317\(96\)00097-4](https://doi.org/10.1016/S0167-9317(96)00097-4).
- (310) Schiff, H.; Urwyler, P.; Kristiansen, P. M.; Gobrecht, J. Nanoimprint Lithography Process Chains for the Fabrication of Micro- and Nanodevices. *J. Micro/Nanolithography, MEMS, MOEMS* **2014**, *13* (3), 031303. <https://doi.org/10.1117/1.jmm.13.3.031303>.
- (311) Schiff, H. Nanoimprint Lithography: 2D or Not 2D? A Review. *Appl. Phys. A* **2015**, 415–435. <https://doi.org/10.1007/s00339-015-9106-3>.
- (312) Moharam, M. G.; Gaylord, T. K. Rigorous Coupled-Wave Analysis of Metallic Surface-Relief Gratings. *J. Opt. Soc. Am. A* **1986**, *3* (11), 1780. <https://doi.org/10.1364/josaa.3.001780>.
- (313) Moharam, M. G.; Gaylord, T. K. Rigorous Coupled-Wave Analysis of Planar-Grating Diffraction. *J. Opt. Soc. Am.* **1981**, *71* (7), 811. <https://doi.org/10.1364/JOSA.71.000811>.
- (314) Nielsen, R.; Cones, F.; Kelly, R. *Electromagnetic Theory of Gratings*; Petit, R., Ed.; Topics in Current Physics; Springer Berlin Heidelberg: Berlin, Heidelberg, 1980; Vol. 22. <https://doi.org/10.1007/978-3-642-81500-3>.
- (315) Peng, S.; Morris, G. M. Efficient Implementation of Rigorous Coupled-Wave Analysis for Surface-Relief Gratings. *J. Opt. Soc. Am. A* **1995**, *12* (5), 1087. <https://doi.org/10.1364/josaa.12.001087>.
- (316) Botten, I. C.; Craig, M. S.; McPhedran, R. C.; Adams, J. L.; Andrewartha, J. R. The Dielectric Lamellar Diffraction Grating. *Opt. Acta (Lond)*. **1981**, *28* (3), 413–428. <https://doi.org/10.1080/713820571>.
- (317) Gaylord, T. K.; Moharam, M. G. Analysis and Applications of Optical Diffraction by Gratings. *Proc. IEEE* **1985**, *73* (5), 894–937. <https://doi.org/10.1109/PROC.1985.13220>.
- (318) Moharam, M. G.; Gaylord, T. K. Rigorous Coupled-Wave Analysis of Grating Diffraction - E-Mode Polarization and Losses. *J. Opt. Soc. Am.* **1983**, *73* (4), 451–455. <https://doi.org/10.1364/JOSA.73.000451>.
- (319) Moharam, M. G.; Gaylord, T. K. Diffraction Analysis of Dielectric Surface-Relief Gratings. *J. Opt. Soc. Am.* **1982**, *72* (10), 1385–1392. <https://doi.org/10.1364/JOSA.72.001385>.
- (320) Moharam, M. G. Coupled-Wave Analysis Of Two-Dimensional Dielectric Gratings. In *Holographic Optics: Design and Applications*; Cindrich, I., Ed.; 1988; Vol. 0883, p 8. <https://doi.org/10.1117/12.944119>.
- (321) Moharam, M. G.; Gaylord, T. K.; Pommet, D. A.; Grann, E. B. Stable Implementation of the Rigorous Coupled-Wave Analysis for Surface-Relief Gratings: Enhanced Transmittance Matrix Approach. *J. Opt. Soc. Am. A* **1995**, *12* (5), 1077. <https://doi.org/10.1364/JOSAA.12.001077>.
- (322) Liu, S. Estimation of the Convergence Order of Rigorous Coupled-Wave Analysis for

- Binary Gratings in Optical Critical Dimension Metrology. *Opt. Eng.* **2012**, *51* (8), 081504. <https://doi.org/10.1117/1.oe.51.8.081504>.
- (323) Li, L. New Formulation of the Fourier Modal Method for Crossed Surface-Relief Gratings. *J. Opt. Soc. Am. A* **1997**, *14* (10), 2758. <https://doi.org/10.1364/JOSAA.14.002758>.
- (324) Li, L. Use of Fourier Series in the Analysis of Discontinuous Periodic Structures. *J. Opt. Soc. Am. A* **1996**, *13* (9), 1870. <https://doi.org/10.1364/josaa.13.001870>.
- (325) Lalanne, P. Improved Formulation of the Coupled-Wave Method for Two-Dimensional Gratings. *J. Opt. Soc. Am. A* **1997**, *14* (7), 1592. <https://doi.org/10.1364/josaa.14.001592>.
- (326) Kim, H.; Lee, I.-M.; Lee, B. Extended Scattering-Matrix Method for Efficient Full Parallel Implementation of Rigorous Coupled-Wave Analysis. *J. Opt. Soc. Am. A* **2007**, *24* (8), 2313. <https://doi.org/10.1364/josaa.24.002313>.
- (327) Nagai, H.; Murakami, Y.; Yokoyama, K.; Tamiya, E. High-Throughput PCR in Silicon Based Microchamber Array. *Biosens. Bioelectron.* **2001**, *16* (9–12), 1015–1019. [https://doi.org/10.1016/S0956-5663\(01\)00248-2](https://doi.org/10.1016/S0956-5663(01)00248-2).
- (328) Nagai, H.; Murakami, Y.; Morita, Y.; Yokoyama, K.; Tamiya, E. Development of a Microchamber Array for Picoliter PCR. *Anal. Chem.* **2001**, *73* (5), 1043–1047. <https://doi.org/10.1021/ac000648u>.
- (329) Hattori, K.; Yoshimitsu, R.; Sugiura, S.; Maruyama, A.; Ohnuma, K.; Kanamori, T. Masked Plasma Oxidation: Simple Micropatterning of Extracellular Matrix in a Closed Microchamber Array. *RSC Adv.* **2013**, *3* (39), 17749–17754. <https://doi.org/10.1039/c3ra42976h>.
- (330) Moriguchi, H.; Takahashi, K.; Sugio, Y.; Wakamoto, Y.; Inoue, I.; Jimbo, Y.; Yasuda, K. On-Chip Neural Cell Cultivation Using Agarose-Microchamber Array Constructed by a Photothermal Etching Method. *Electr. Eng. Japan (English Transl. Denki Gakkai Ronbunshi)* **2004**, *146* (2), 37–42. <https://doi.org/10.1002/eej.10215>.
- (331) Sugiura, S.; Edahiro, J. I.; Kikuchi, K.; Sumaru, K.; Kanamori, T. Pressure-Driven Perfusion Culture Microchamber Array for a Parallel Drug Cytotoxicity Assay. *Biotechnol. Bioeng.* **2008**, *100* (6), 1156–1165. <https://doi.org/10.1002/bit.21836>.
- (332) Ermakov, A.; Lim, S. H.; Gorelik, S.; Kauling, A. P.; de Oliveira, R. V. B.; Castro Neto, A. H.; Glukhovskoy, E.; Gorin, D. A.; Sukhorukov, G. B.; Kiryukhin, M. V. Polyelectrolyte–Graphene Oxide Multilayer Composites for Array of Microchambers Which Are Mechanically Robust and Responsive to NIR Light. *Macromol. Rapid Commun.* **2019**, *40* (5), 1700868. <https://doi.org/10.1002/marc.201700868>.
- (333) Gai, M.; Frueh, J.; Kudryavtseva, V. L.; Yashchenok, A. M.; Sukhorukov, G. B. Polylactic Acid Sealed Polyelectrolyte Multilayer Microchambers for Entrapment of Salts and Small Hydrophilic Molecules Precipitates. *ACS Appl. Mater. Interfaces* **2017**, *9* (19), 16536–16545. <https://doi.org/10.1021/acsami.7b03451>.
- (334) Chen, X.; Cui, D. F.; Liu, C. C.; Li, H. Microfluidic Chip for Blood Cell Separation and Collection Based on Crossflow Filtration. *Sensors Actuators, B Chem.* **2008**, *130* (1), 216–221. <https://doi.org/10.1016/j.snb.2007.07.126>.

- (335) Prehn, R.; Abad, L.; Sánchez-Molas, D.; Duch, M.; Sabaté, N.; Del Campo, F. J.; Muñoz, F. X.; Compton, R. G. Microfabrication and Characterization of Cylinder Micropillar Array Electrodes. *J. Electroanal. Chem.* **2011**, *662* (2), 361–370. <https://doi.org/10.1016/j.jelechem.2011.09.002>.
- (336) Reitzenstein, S.; Forchel, A. Quantum Dot Micropillars. *J. Phys. D. Appl. Phys.* **2010**, *43* (3). <https://doi.org/10.1088/0022-3727/43/3/033001>.
- (337) Lalanne, P.; Morris, G. M. Antireflection Behavior of Silicon Subwavelength Periodic Structures for Visible Light. *Nanotechnology* **1997**, *8* (2), 53–56. <https://doi.org/10.1088/0957-4484/8/2/002>.
- (338) Li, H. Y.; Dauriac, V.; Thibert, V.; Senechal, H.; Peltre, G.; Zhang, X. X.; Descroix, S. Micropillar Array Chips toward New Immunodiagnosis. *Lab Chip* **2010**, *10* (19), 2597–2604. <https://doi.org/10.1039/c005034b>.
- (339) Marinas, M.; Sa, E.; Rojas, M. M.; Moalem, M.; Urbano, F. J.; Guillou, C.; Rallo, L. A Nuclear Magnetic Resonance (^1H and ^{13}C) and Isotope Ratio Mass Spectrometry ($\delta^{13}\text{C}$, $\delta^2\text{H}$ and $\delta^{18}\text{O}$) Study of Andalusian Olive Oils. *Rapid Commun. Mass Spectrom.* **2010**, *24*, 1457–1466. <https://doi.org/10.1002/rcm>.
- (340) Kotov, N. A.; Winter, J. O.; Clements, I. P.; Jan, E.; Timko, B. P.; Campidelli, S.; Pathak, S.; Mazzatenta, A.; Lieber, C. M.; Prato, M.; Bellamkonda, R. V.; Silva, G. A.; Kam, N. W. S.; Patolsky, F.; Ballerini, L. Nanomaterials for Neural Interfaces. *Adv. Mater.* **2009**, *21* (40), 3970–4004. <https://doi.org/10.1002/adma.200801984>.
- (341) Myllymaa, S.; Pirinen, S.; Myllymaa, K.; Suvanto, M.; Pakkanen, T. A.; Pakkanen, T. T.; Lappalainen, R. Improving Electrochemical Performance of Flexible Thin Film Electrodes with Micropillar Array Structures. *Meas. Sci. Technol.* **2012**, *23* (12). <https://doi.org/10.1088/0957-0233/23/12/125701>.
- (342) Shuai, X.; Zhu, P.; Zeng, W.; Hu, Y.; Liang, X.; Zhang, Y.; Sun, R.; Wong, C. P. Highly Sensitive Flexible Pressure Sensor Based on Silver Nanowires-Embedded Polydimethylsiloxane Electrode with Microarray Structure. *ACS Appl. Mater. Interfaces* **2017**, *9* (31), 26314–26324. <https://doi.org/10.1021/acsami.7b05753>.
- (343) Cheng, D.; Sridharamurthy, S. S.; Hunter, J. T.; Park, J. S.; Abbott, N. L.; Jiang, H. A Sensing Device Using Liquid Crystal in a Micropillar Array Supporting Structure. *J. Microelectromechanical Syst.* **2009**, *18* (5), 973–982. <https://doi.org/10.1109/JMEMS.2009.2029977>.
- (344) Ge, X.; Leng, Y.; Lu, X.; Ren, F.; Wang, K.; Ding, Y.; Yang, M. Bacterial Responses to Periodic Micropillar Array. *J. Biomed. Mater. Res. - Part A* **2015**, *103* (1), 384–396. <https://doi.org/10.1002/jbm.a.35182>.
- (345) Gai, M.; Frueh, J.; Girard-Egrot, A.; Rebaud, S.; Doumeche, B.; He, Q. Micro-Contact Printing of PEM Thin Films: Effect of Line Tension and Surface Energies. *RSC Adv.* **2015**, *5* (64), 51891–51899. <https://doi.org/10.1039/C5RA08456C>.
- (346) Jin, M.; Feng, X.; Xi, J.; Zhai, J.; Cho, K.; Feng, L.; Jiang, L. Super-Hydrophobic PDMS Surface with Ultra-Low Adhesive Force. *Macromol. Rapid Commun.* **2005**, *26* (22), 1805–

1809. <https://doi.org/10.1002/marc.200500458>.
- (347) Gai, M.; Frueh, J.; Kudryavtseva, V. L.; Mao, R.; Kiryukhin, M. V.; Sukhorukov, G. B. Patterned Microstructure Fabrication: Polyelectrolyte Complexes vs Polyelectrolyte Multilayers. *Sci. Rep.* **2016**, *6* (October), 1–11. <https://doi.org/10.1038/srep37000>.
- (348) Schnäckel, A.; Hiller, S.; Reibetanz, U.; Donath, E. Fluorescent Bead Arrays by Means of Layer-by-Layer Polyelectrolyte Adsorption. *Soft Matter* **2007**, *3* (2), 200–206. <https://doi.org/10.1039/b612117a>.
- (349) PALADE, G. E. A Study of Fixation for Electron Microscopy. *J. Exp. Med.* **1952**, *95* (3), 285–298. <https://doi.org/10.1084/jem.95.3.285>.
- (350) Srivastava, S. K.; Verma, R.; Gupta, B. D. Surface Plasmon Resonance Based Fiber Optic Sensor for the Detection of Low Water Content in Ethanol. *Sensors Actuators, B Chem.* **2011**, *153* (1), 194–198. <https://doi.org/10.1016/j.snb.2010.10.038>.
- (351) Boyde, A. *Scanning Electron Microscopy of Bone*; Springer Series in Optical Sciences; Springer Berlin Heidelberg: Berlin, Heidelberg, 2019; Vol. 1914. https://doi.org/10.1007/978-1-4939-8997-3_31.
- (352) Kotula, P. G.; Keenan, M. R.; Michael, J. R. Automated Analysis of SEM X-Ray Spectral Images: A Powerful New Microanalysis Tool. *Microsc. Microanal.* **2003**, *9* (1), 1–17. <https://doi.org/10.1017/S1431927603030058>.
- (353) Danilatos, G. D.; Robinson, V. N. E. Principles of Scanning Electron Microscopy at High Specimen Chamber Pressures. *Scanning* **1979**, *2* (2), 72–82. <https://doi.org/10.1002/sca.4950020202>.
- (354) Escovitz, W. H.; Fox, T. R.; Levi Setti, R. Scanning Transmission Ion Microscope with a Field Ion Source. *Proc. Natl. Acad. Sci. U. S. A.* **1975**, *72* (5), 1826–1828. <https://doi.org/10.1073/pnas.72.5.1826>.
- (355) Orloff, J. H.; Swanson, L. W. Study of a Field-ionization Source for Microprobe Applications. *J. Vac. Sci. Technol.* **1975**, *12* (6), 1209–1213. <https://doi.org/10.1116/1.568497>.
- (356) Seliger, R. L.; Ward, J. W.; Wang, V.; Kubena, R. L. A High-Intensity Scanning Ion Probe with Submicrometer Spot Size. *Appl. Phys. Lett.* **1979**, *34* (5), 310–312. <https://doi.org/10.1063/1.90786>.
- (357) Puretz, J.; Orloff, J.; Swanson, L. An Application Of Focused Ion Beams To Electron Beam Testing Of Integrated Circuits. In *Electron-Beam, X-Ray, and Ion-Beam Techniques for Submicrometer Lithographies III*; Wagner, A., Ed.; 1984; Vol. 0471, p 38. <https://doi.org/10.1117/12.942318>.
- (358) Wirth, R. Focused Ion Beam (FIB) Combined with SEM and TEM : Advanced Analytical Tools for Studies of Chemical Composition , Microstructure and Crystal Structure in Geomaterials on a Nanometre Scale. *Chem. Geol.* **2009**, *261* (3–4), 217–229. <https://doi.org/10.1016/j.chemgeo.2008.05.019>.
- (359) Sezen, M. Focused Ion Beams (FIB) — Novel Methodologies and Recent Applications for

- Multidisciplinary Sciences. *Mod. Electron Microsc. Phys. Life Sci.* **2016**.
<https://doi.org/10.5772/61634>.
- (360) Orloff, J.; Swanson, L. W.; Utlaut, M. Fundamental Limits to Imaging Resolution for Focused Ion Beams. *J. Vac. Sci. Technol. B Microelectron. Nanom. Struct.* **1996**, *14* (6), 3759–3763. <https://doi.org/10.1116/1.588663>.
- (361) Castaldo, V.; Hagen, C. W.; Rieger, B.; Kruit, P. Sputtering Limits versus Signal-to-Noise Limits in the Observation of Sn Balls in a Ga⁺ Microscope. *J. Vac. Sci. Technol. B Microelectron. Nanom. Struct.* **2008**, *26* (6), 2107–2115.
<https://doi.org/10.1116/1.3013306>.
- (362) Drobne, D.; Milani, M.; Lešer, V.; Tatti, F. Surface Damage Induced by FIB Milling and Imaging of Biological Samples Is Controllable. *Microsc. Res. Tech.* **2007**, *70* (10), 895–903. <https://doi.org/10.1002/jemt.20494>.
- (363) McKendrick, K. G. *Principles and Applications of Photochemistry*, John Wiley & Sons, 1989; Vol. 36. <https://doi.org/10.1080/09500348914551321>.
- (364) Becker, J. S.; Matusch, A.; Depboylu, C.; Dobrowolska, J.; Zoriy, M. V. Quantitative Imaging of Selenium, Copper, and Zinc in Thin Sections of Biological Tissues (Slugs-Genus Arion) Measured by Laser Ablation Inductively Coupled Plasma Mass Spectrometry. *Anal. Chem.* **2007**, *79* (16), 6074–6080.
<https://doi.org/10.1021/ac0700528>.
- (365) Liebmann, L. W.; Robinson, J. A.; Mann, K. G. A Dual Beam Total Internal Reflection Fluorescence Spectrometer for Dynamic Depth Resolved Measurements of Biochemical Liquid-Solid Interface Binding Reactions in Opaque Solvents. *Rev. Sci. Instrum.* **1991**, *62* (9), 2083–2092. <https://doi.org/10.1063/1.1142371>.
- (366) Koenig, K.; Schneckenburger, H. Laser-Induced Autofluorescence for Medical Diagnosis. *J. Fluoresc.* **1994**, *4* (1), 17–40. <https://doi.org/10.1007/BF01876650>.
- (367) Kumar, C. V.; Asuncion, E. H. DNA Binding Studies and Site Selective Fluorescence Sensitization of an Anthryl Probe. *J. Am. Chem. Soc.* **1993**, *115* (19), 8547–8553.
<https://doi.org/10.1021/ja00072a004>.
- (368) Lakowicz, J. R. *Principles of Fluorescence Spectroscopy*, Springer US: Boston, MA, 2006.
<https://doi.org/10.1007/978-0-387-46312-4>.
- (369) Zehentbauer, F. M.; Moretto, C.; Stephen, R.; Thevar, T.; Gilchrist, J. R.; Pokrajac, D.; Richard, K. L.; Kiefer, J. Fluorescence Spectroscopy of Rhodamine 6G: Concentration and Solvent Effects. *Spectrochim. Acta - Part A Mol. Biomol. Spectrosc.* **2014**, *121*, 147–151.
<https://doi.org/10.1016/j.saa.2013.10.062>.
- (370) Thompson, R. *Fluorescent Probes, Labels, and Sensors*, 2012.
- (371) Murray, J. M.; Appleton, P. L.; Swedlow, J. R.; Waters, J. C. Evaluating Performance in Three-Dimensional Fluorescence Microscopy. *J. Microsc.* **2007**, *228* (3), 390–405.
<https://doi.org/10.1111/j.1365-2818.2007.01861.x>.
- (372) Lichtman, J. W.; Conchello, J. A. Fluorescence Microscopy. *Nat. Methods* **2005**, *2* (12),

- 910–919. <https://doi.org/10.1038/nmeth817>.
- (373) Wei, X. S.; Cruickshank, D. G. M.; Mulgrew, B.; Riera-Palou, F. IV. Ἀμόρφωτα, No. I.— on a Case of Superficial Colour Presented by a Homogeneous Liquid Internally Colourless. *Philos. Trans. R. Soc. London* **1845**, *135* (3), 143–145. <https://doi.org/10.1098/rstl.1845.0004>.
- (374) Stokes, G. G.; Stokes, G. G. On the Change of Refrangibility of Light. *Math. Phys. Pap.* **2010**, *142*, 267–414. <https://doi.org/10.1017/cbo9780511702266.012>.
- (375) Denis Semwogerere, E. R. W. Separating Blue Whiting (*Micromesistius Poutassou* Risso , 1826) from Myctophid Targets Using Multi-Frequency Methods. In *Encyclopedia of Biomaterial and Biomedical Engineering*, 2005; p 97. <https://doi.org/10.1081/E-EBBE-120024153>.
- (376) Bunney, P. E.; Zink, A. N.; Holm, A. A.; Billington, C. J.; Kotz, C. M. Orexin Activation Counteracts Decreases in Nonexercise Activity Thermogenesis (NEAT) Caused by High-Fat Diet. *Physiol. Behav.* **2017**, *176* (10), 139–148. <https://doi.org/10.1016/j.physbeh.2017.03.040>.
- (377) Paddock, S. W. Principles and Practices of Laser Scanning Confocal Microscopy. *Appl. Biochem. Biotechnol. - Part B Mol. Biotechnol.* **2000**, *16* (2), 127–149. <https://doi.org/10.1385/mb:16:2:127>.
- (378) Minsky, M. Memoir on Inventing the Confocal Scanning Microscope. *Scanning* **1988**, *10* (4), 128–138. <https://doi.org/10.1002/sca.4950100403>.
- (379) Udupa, G.; Singaperumal, M.; Sirohi, R. S.; Kothiyal, M. P. Characterization of Surface Topography by Confocal Microscopy: I. Principles and the Measurement System. *Meas. Sci. Technol.* **2000**, *11* (3), 305–314. <https://doi.org/10.1088/0957-0233/11/3/320>.
- (380) Coda, S.; Thillainayagam, A. V. State of the Art in Advanced Endoscopic Imaging for the Detection and Evaluation of Dysplasia and Early Cancer of the Gastrointestinal Tract. *Clin. Exp. Gastroenterol.* **2014**, *7* (1), 133–150. <https://doi.org/10.2147/CEG.S58157>.
- (381) Caldwell, D. E.; Korber, D. R.; Lawrence, J. R. *Confocal Laser Microscopy and Digital Image Analysis in Microbial Ecology*, 1992; Vol. 12. https://doi.org/10.1007/978-1-4684-7609-5_1.
- (382) González, S.; Tannous, Z. Real-Time, in Vivo Confocal Reflectance Microscopy of Basal Cell Carcinoma. *J. Am. Acad. Dermatol.* **2002**, *47* (6), 869–874. <https://doi.org/10.1067/mjd.2002.124690>.
- (383) Guilak, F.; Ratcliffe, A.; Mow, V. C. Chondrocyte Deformation and Local Tissue Strain in Articular Cartilage: A Confocal Microscopy Study. *J. Orthop. Res.* **1995**, *13* (3), 410–421. <https://doi.org/10.1002/jor.1100130315>.
- (384) Pellett, P. A.; Sun, X.; Gould, T. J.; Rothman, J. E.; Xu, M.-Q.; Corrêa, I. R.; Bewersdorf, J. Two-Color STED Microscopy in Living Cells. *Biomed. Opt. Express* **2011**, *2* (8), 2364. <https://doi.org/10.1364/boe.2.002364>.
- (385) Pawley, J. B. Fundamental Limits in Confocal Microscopy. In *Handbook of Biological*

- Confocal Microscopy: Third Edition*; Springer US: Boston, MA, 2006; pp 20–42.
https://doi.org/10.1007/978-0-387-45524-2_2.
- (386) Wilson, T. The Role of the Pinhole in Confocal Imaging System. *Handb. Biol. Confocal Microsc.* **1995**, *2* (2), 167–182. https://doi.org/10.1007/978-1-4757-5348-6_11.
- (387) Brakenhoff, G. J.; Blom, P.; Barends, P. Confocal Scanning Light Microscopy with High Aperture Immersion Lenses. *J. Microsc.* **1979**, *117* (2), 219–232.
<https://doi.org/10.1111/j.1365-2818.1979.tb01178.x>.
- (388) Tien, A. C.; Backus, S.; Kapteyn, H.; Murnane, M.; Mourou, G. Short-Pulse Laser Damage in Transparent Materials as a Function of Pulse Duration. *Phys. Rev. Lett.* **1999**, *82* (19), 3883–3886. <https://doi.org/10.1103/PhysRevLett.82.3883>.
- (389) Szabó, Á.; Szendi-Szatmári, T.; Ujlaky-Nagy, L.; Rádi, I.; Vereb, G.; Szöllősi, J.; Nagy, P. The Effect of Fluorophore Conjugation on Antibody Affinity and the Photophysical Properties of Dyes. *Biophys. J.* **2018**, *114* (3), 688–700. <https://doi.org/10.1016/j.bpj.2017.12.011>.
- (390) Verdonck, E.; Schaap, K.; Thomas, L. C. A Discussion of the Principles and Applications of Modulated Temperature DSC (MTDSC). *Int. J. Pharm.* **1999**, *192* (1), 3–20.
[https://doi.org/10.1016/S0378-5173\(99\)00267-7](https://doi.org/10.1016/S0378-5173(99)00267-7).
- (391) Picollo, M.; Aceto, M.; Vitorino, T. UV-Vis Spectroscopy. *Phys. Sci. Rev.* **2019**, *4* (4), 1–14.
<https://doi.org/10.1515/psr-2018-0008>.
- (392) Gauglitz, G. Ultraviolet and Visible Spectroscopy. *Handb. Anal. Tech.* **2008**, *1–2*, 419–463.
<https://doi.org/10.1002/9783527618323.ch16>.
- (393) Altemose, I. Evolution of Instrumentation for UV-Visible Spectrophotometry Part I. *J. Chem. Educ.* **1986**, *63* (9). <https://doi.org/10.1021/ed063pA216>.
- (394) Schawlow, A. L.; Townes, C. H. Infrared and Optical Masers. *Phys. Rev.* **1958**, *112* (6), 1940–1949. <https://doi.org/10.1103/PhysRev.112.1940>.
- (395) Steinvall, O. Review of Laser Sensing Devices and Systems. *Technol. Opt. Countermeas. II; Femtosecond Phenom. II; Passiv. Millimetre-Wave Terahertz Imaging II* **2005**, 5989, 598903. <https://doi.org/10.1117/12.638187>.
- (396) Beutel, S.; Henkel, S. In Situ Sensor Techniques in Modern Bioprocess Monitoring. *Appl. Microbiol. Biotechnol.* **2011**, *91* (6), 1493–1505. <https://doi.org/10.1007/s00253-011-3470-5>.
- (397) Jiang, X.; Gao, H.; Zhang, X.; Pang, J.; Li, Y.; Li, K.; Wu, Y.; Li, S.; Zhu, J.; Wei, Y.; Jiang, L. Highly-Sensitive Optical Organic Vapor Sensor through Polymeric Swelling Induced Variation of Fluorescent Intensity. *Nat. Commun.* **2018**, *9* (1), 1–9.
<https://doi.org/10.1038/s41467-018-06101-8>.
- (398) Feng, J.; Wen, W.; Wei, X.; Jiang, X.; Cao, M.; Wang, X.; Zhang, X.; Jiang, L.; Wu, Y. Random Organic Nanolaser Arrays for Cryptographic Primitives. *Adv. Mater.* **2019**, *31* (36), 1–9. <https://doi.org/10.1002/adma.201807880>.
- (399) Ruan, C.; Zeng, K.; Grimes, C. A. A Mass-Sensitive PH Sensor Based on a Stimuli-Responsive Polymer. *Anal. Chim. Acta* **2003**, *497* (1–2), 123–131.

- <https://doi.org/10.1016/j.aca.2003.08.051>.
- (400) He, W.; Frueh, J.; Hu, N.; Liu, L.; Gai, M.; He, Q. Guidable Thermophoretic Janus Micromotors Containing Gold Nanocolorifiers for Infrared Laser Assisted Tissue Welding. *Adv. Sci.* **2016**, *3* (12), 1600206. <https://doi.org/10.1002/adv.201600206>.
- (401) Paczesnya, D.; Tarapata, G.; Michał, M.; Jachowicz, R. The Capacitive Sensor for Liquid Level Measurement Made with Ink-Jet Printing Technology. *Procedia Eng.* **2015**, *120*, 731–735. <https://doi.org/10.1016/j.proeng.2015.08.776>.
- (402) Gai, M.; Frueh, J.; Kudryavtseva, V. L.; Mao, R.; Kiryukhin, M. V.; Sukhorukov, G. B. Patterned Microstructure Fabrication: Polyelectrolyte Complexes vs Polyelectrolyte Multilayers. *Sci. Rep.* **2016**, *6*, 1–6. <https://doi.org/10.1038/srep37000>.
- (403) Schaaf, P.; Schlenoff, J. B. Saloplastics: Processing Compact Polyelectrolyte Complexes. *Adv. Mater.* **2015**, *27* (15), 2420–2432. <https://doi.org/10.1002/adma.201500176>.
- (404) Semesi, I. S.; Kangwe, J.; Björk, M. Alterations in Seawater PH and CO₂ Affect Calcification and Photosynthesis in the Tropical Coralline Alga, *Hydrolithon* Sp. (Rhodophyta). *Estuar. Coast. Shelf Sci.* **2009**, *84* (3), 337–341. <https://doi.org/10.1016/j.ecss.2009.03.038>.
- (405) Sanguansri, P.; Augustin, M. A. Nanoscale Materials Development – a Food Industry Perspective. *Trends Food Sci. Technol.* **2006**, *17* (10), 547–556. <https://doi.org/10.1016/j.tifs.2006.04.010>.
- (406) Chen, Y.; Wang, X.; Hong, M.; Erramilli, S.; Mohanty, P. Surface-Modified Silicon Nano-Channel for Urea Sensing. *Sensors Actuators, B Chem.* **2008**, *133* (2), 593–598. <https://doi.org/10.1016/j.snb.2008.03.033>.
- (407) Rydzek, G.; Pakdel, A.; Witecka, A.; Awang Shri, D. N.; Gaudière, F.; Nicolosi, V.; Mokarian-Tabari, P.; Schaaf, P.; Boulmedais, F.; Ariga, K. PH-Responsive Saloplastics Based on Weak Polyelectrolytes: From Molecular Processes to Material Scale Properties. *Macromolecules* **2018**, *51* (12), 4424–4434. <https://doi.org/10.1021/acs.macromol.8b00609>.
- (408) Cranford, S. W.; Buehler, M. J. Critical Cross-Linking to Mechanically Couple Polyelectrolytes and Flexible Molecules. *Soft Matter* **2013**, *9* (4), 1076–1090. <https://doi.org/10.1039/c2sm27055b>.
- (409) Schönhoff, M.; Bieker, P. Linear and Exponential Growth Regimes of Multilayers of Weak Polyelectrolytes in Dependence on PH. *Macromolecules* **2010**, *43* (11), 5052–5059. <https://doi.org/10.1021/ma1007489>.
- (410) Antipov, A. A.; Sukhorukov, G. B.; Leporatti, S.; Radtchenko, I. L.; Donath, E.; Möhwald, H. Polyelectrolyte Multilayer Capsule Permeability Control. *Colloids Surfaces A Physicochem. Eng. Asp.* **2002**, *198–200*, 535–541. [https://doi.org/10.1016/S0927-7757\(01\)00956-6](https://doi.org/10.1016/S0927-7757(01)00956-6).
- (411) Frueh, J.; Gai, M.; Halstead, S.; He, Q. Structure and Thermodynamics of Polyelectrolyte Complexes. In *Polyelectrolyte: Thermodynamics and Rheology*, S. Visakh, Bayraktar, Oguz, Pico, G. A., Ed.; Springer Berlin Heidelberg: Berlin, Heidelberg, 2014; pp 19–86. https://doi.org/10.1007/978-3-319-01680-1_2.

- (412) Donath, E.; Sukhorukov, G. B.; Caruso, F.; Davis, S. A.; Möhwald, H. Novel Hollow Polymer Shells by Colloid-Templated Assembly of Polyelectrolytes. *Angew. Chemie Int. Ed.* **1998**, *37*(16), 2201–2205. [https://doi.org/10.1002/\(sici\)1521-3773\(19980904\)37:16<2201::aid-anie2201>3.0.co;2-e](https://doi.org/10.1002/(sici)1521-3773(19980904)37:16<2201::aid-anie2201>3.0.co;2-e).
- (413) OVERBEEK, J. T.; VOORN, M. J. Phase Separation in Polyelectrolyte Solutions; Theory of Complex Coacervation. *J. Cell. Physiol. Suppl.* **1957**, *49* (Suppl 1), 7–22; discussion, 22–26. <https://doi.org/10.1002/jcp.1030490404>.
- (414) Dobrynin, A. V.; Colby, R. H.; Rubinstein, M. Scaling Theory of Polyelectrolyte Solutions. *Macromolecules* **1995**, *28* (6), 1859–1871. <https://doi.org/10.1021/ma00110a021>.
- (415) Cranford, S. W.; Ortiz, C.; Buehler, M. J. Mechanomutable Properties of a PAA/PAH Polyelectrolyte Complex: Rate Dependence and Ionization Effects on Tunable Adhesion Strength. *Soft Matter* **2010**, *6* (17), 4175–4188. <https://doi.org/10.1039/c0sm00095g>.
- (416) Connal, L. A.; Li, Q.; Quinn, J. F.; Tjipto, E.; Caruso, F.; Qiao, G. G. PH-Responsive Poly(Acrylic Acid) Core Cross-Linked Star Polymers: Morphology Transitions in Solution and Multilayer Thin Films. *Macromolecules* **2008**, *41* (7), 2620–2626. <https://doi.org/10.1021/ma7019557>.
- (417) Van Der Vegte, E. W.; Hadziioannou, G. Scanning Force Microscopy with Chemical Specificity: An Extensive Study of Chemically Specific Tip-Surface Interactions and the Chemical Imaging of Surface Functional Groups. *Langmuir* **1997**, *13* (16), 4357–4368. <https://doi.org/10.1021/la970025k>.
- (418) Petrov, A. I.; Antipov, A. A.; Sukhorukov, G. B. Base-Acid Equilibria in Polyelectrolyte Systems: From Weak Polyelectrolytes to Interpolyelectrolyte Complexes and Multilayered Polyelectrolyte Shells. *Macromolecules* **2003**, *36* (26), 10079–10086. <https://doi.org/10.1021/ma034516p>.
- (419) Clark, S. L.; Hammond, P. T. Role of Secondary Interactions in Selective Electrostatic Multilayer Deposition. *Langmuir* **2000**, *16* (26), 10206–10214. <https://doi.org/10.1021/la000418a>.
- (420) Itano, K.; Choi, J.; Rubner, M. F. Mechanism of the PH-Induced Discontinuous Swelling/Deswelling Transitions of Poly(Allylamine Hydrochloride)-Containing Polyelectrolyte Multilayer Films. *Macromolecules* **2005**, *38* (8), 3450–3460. <https://doi.org/10.1021/ma047667g>.
- (421) Annaka, M.; Tokita, M.; Tanaka, T.; Tanaka, S.; Nakahira, T. The Gel That Memorizes Phases. *J. Chem. Phys.* **2000**, *112* (1), 471–477. <https://doi.org/10.1063/1.480638>.
- (422) Choi, J.; Rubner, M. F. Influence of the Degree of Ionization on Weak Polyelectrolyte Multilayer Assembly. *Macromolecules* **2005**, *38* (1), 116–124. <https://doi.org/10.1021/ma048596o>.
- (423) Hiller, J.; Rubner, M. F. Reversible Molecular Memory and PH-Switchable Swelling Transitions in Polyelectrolyte Multilayers. *Macromolecules* **2003**, *36* (11), 4078–4083. <https://doi.org/10.1021/ma025837o>.
- (424) Yukikazu, T.; Nihat, B. A.; Rose, D.; Takashi, E.; Alexander, G.; Mehran, K.; Taro, O.;

- Kazunori, T.; Guoqiang, W.; Xiaohong, Y.; Toyochi, T. First Order Phase Transition and Evidence for Frustrations in Polyampholytic Gels. *Phys. Rev. Lett.* **1999**, *82* (24), 4863–4865. <https://doi.org/10.1103/PhysRevLett.82.4863>.
- (425) Piper, D. W.; Fenton, B. H. PH Stability and Activity Curves of Pepsin with Special Reference to Their Clinical Importance. *Gut* **1965**, *6* (5), 506–508. <https://doi.org/10.1136/gut.6.5.506>.
- (426) Kawano, K.; Hamaguchi, K.; Masuda, S.; Tomida, T. Binding Properties of a Water-Soluble Chelating Polymer with Divalent Metal Ions Measured by Ultrafiltration. Poly(α -Acethylaminoacrylic Acid). *Ind. Eng. Chem. Res.* **2002**, *41* (20), 5079–5084. <https://doi.org/10.1021/ie0200050>.
- (427) Whittinghill, K. A.; Hobbie, S. E. Effects of PH and Calcium on Soil Organic Matter Dynamics in Alaskan Tundra. *Biogeochemistry* **2012**, *111* (1–3), 569–581. <https://doi.org/10.1007/s10533-011-9688-6>.
- (428) Bolland, M. J.; Avenell, A.; Baron, J. A.; Grey, A.; MacLennan, G. S.; Gamble, G. D.; Reid, I. R. Effect of Calcium Supplements on Risk of Myocardial Infarction and Cardiovascular Events: Meta-Analysis. *BMJ* **2010**, *341* (7767), 289. <https://doi.org/10.1136/bmj.c3691>.
- (429) Kriwet, B.; Kissel, T. Interactions between Bioadhesive Poly(Acrylic Acid) and Calcium Ions. *Int. J. Pharm.* **1996**, *127* (2), 135–145. [https://doi.org/10.1016/0378-5173\(95\)04098-6](https://doi.org/10.1016/0378-5173(95)04098-6).
- (430) Amore Bonapasta, A.; Buda, F.; Colombet, P. Interaction between Ca Ions and Poly(Acrylic Acid) Chains in Macro-Defect-Free Cements: A Theoretical Study. *Chem. Mater.* **2001**, *13* (1), 64–70. <https://doi.org/10.1021/cm000505o>.
- (431) Ooya, T.; Eguchi, M.; Ozaki, A.; Yui, N. Carboxyethylester-Polyrotaxanes as a New Calcium Chelating Polymer: Synthesis, Calcium Binding and Mechanism of Trypsin Inhibition. *Int. J. Pharm.* **2002**, *242* (1–2), 47–54. [https://doi.org/10.1016/S0378-5173\(02\)00139-4](https://doi.org/10.1016/S0378-5173(02)00139-4).
- (432) Gormley, R.; Walshe, T.; Hussey, K.; Butler, F. The Effect of Fluctuating vs. Constant Frozen Storage Temperature Regimes on Some Quality Parameters of Selected Food Products. *LWT - Food Sci. Technol.* **2002**, *35* (2), 190–200. <https://doi.org/10.1006/fstl.2001.0837>.
- (433) Higl, B.; Kurtmann, L.; Carlsen, C. U.; Ratjen, J.; Först, P.; Skibsted, L. H.; Kulozik, U.; Risbo, J. Impact of Water Activity, Temperature, and Physical State on the Storage Stability of *Lactobacillus Paracasei* Ssp. *Paracasei* Freeze-Dried in a Lactose Matrix. *Biotechnol. Prog.* **2007**, *23* (4), 794–800. <https://doi.org/10.1021/bp070089d>.
- (434) Ozdemir, M.; Floros, J. D. Active Food Packaging Technologies. *Crit. Rev. Food Sci. Nutr.* **2004**, *44* (3), 185–193. <https://doi.org/10.1080/10408690490441578>.
- (435) Zhang, B.; Kahrizi, M. High-Temperature Resistance Fiber Bragg Grating Temperature Sensor Fabrication. *IEEE Sens. J.* **2007**, *7* (4), 586–591. <https://doi.org/10.1109/JSEN.2007.891941>.
- (436) Nguyen, L. V.; Hwang, D.; Moon, S.; Moon, D. S.; Chung, Y. High Temperature Fiber Sensor with High Sensitivity Based on Core Diameter Mismatch. *Opt. Express* **2008**, *16* (15), 11369. <https://doi.org/10.1364/oe.16.011369>.

- (437) Yang, Y.; Yang, F.; Wang, H.; Yang, W.; Jin, W. Temperature-Insensitive Hydrogen Sensor with Polarization-Maintaining Photonic Crystal Fiber-Based Sagnac Interferometer. *J. Light. Technol.* **2015**, *33* (12), 2566–2571. <https://doi.org/10.1109/JLT.2014.2375362>.
- (438) Gai, M.; Frueh, J.; Tao, T.; Petrov, A. V.; Petrov, V. V.; Shesterikov, E. V.; Tverdokhlebov, S. I.; Sukhorukov, G. B. Polylactic Acid Nano- and Microchamber Arrays for Encapsulation of Small Hydrophilic Molecules Featuring Drug Release via High Intensity Focused Ultrasound. *Nanoscale* **2017**, *9* (21), 7063–7070. <https://doi.org/10.1039/c7nr01841j>.
- (439) Shah, A. A.; Schultz, B.; Zhang, W.; Glotzer, S. C.; Solomon, M. J. Actuation of Shape-Memory Colloidal Fibres of Janus Ellipsoids. *Nat. Mater.* **2015**, *14* (1), 117–124. <https://doi.org/10.1038/nmat4111>.
- (440) Tikhodeev, S. G.; Yablonskii, A. L.; Muljarov, E. A.; Gippius, N. A.; Ishihara, T. Quasiguidded Modes and Optical Properties of Photonic Crystal Slabs. *Phys. Rev. B - Condens. Matter Mater. Phys.* **2002**, *66* (4), 451021–4510217. <https://doi.org/10.1103/PhysRevB.66.045102>.
- (441) Kozlovskaya, V.; Kharlampieva, E.; Mansfield, M. L.; Sukhishvili, S. A. Poly(Methacrylic Acid) Hydrogel Films and Capsules: Response to PH and Ionic Strength, and Encapsulation of Macromolecules. *Chem. Mater.* **2006**, *18* (2), 328–336. <https://doi.org/10.1021/cm0517364>.
- (442) Teng, F.; Wang, X.; Shen, C.; Li, S. A Micro Glucose Sensor Based on Direct Prototyping Mesoporous Carbon Electrode. *Microsyst. Technol.* **2015**, *21* (6), 1337–1343. <https://doi.org/10.1007/s00542-014-2159-y>.
- (443) Pu, J.; Wang, X.; Xu, R.; Komvopoulos, K. Highly Stretchable Microsupercapacitor Arrays with Honeycomb Structures for Integrated Wearable Electronic Systems. *ACS Nano* **2016**, *10* (10), 9306–9315. <https://doi.org/10.1021/acsnano.6b03880>.
- (444) Nakao, M.; Inoue, S.; Yoshinobu, T.; Iwasaki, H. High-Resolution PH Imaging Sensor for Microscopic Observation of Microorganisms. *Sensors Actuators, B Chem.* **1996**, *34* (1–3), 234–239. [https://doi.org/10.1016/S0925-4005\(96\)01903-X](https://doi.org/10.1016/S0925-4005(96)01903-X).
- (445) Zhang, J.; Sun, R.; Desouza-Edwards, A. O.; Frueh, J.; Sukhorukov, G. B. Microchamber Arrays Made of Biodegradable Polymers for Enzymatic Release of Small Hydrophilic Cargos. *Soft Matter* **2020**, *16* (9), 2266–2275. <https://doi.org/10.1039/c9sm01856e>.
- (446) Timin, A. S.; Litvak, M. M.; Gorin, D. A.; Atochina-Vasserman, E. N.; Atochin, D. N.; Sukhorukov, G. B. Cell-Based Drug Delivery and Use of Nano- and Microcarriers for Cell Functionalization. *Adv. Healthc. Mater.* **2018**, *7* (3), 1–19. <https://doi.org/10.1002/adhm.201700818>.
- (447) Skirtach, A. G.; Dejugnat, C.; Braun, D.; Susha, A. S.; Rogach, A. L.; Parak, W. J.; Möhwald, H.; Sukhorukov, G. B. The Role of Metal Nanoparticles in Remote Release of Encapsulated Materials. *Nano Lett.* **2005**, *5* (7), 1371–1377. <https://doi.org/10.1021/nl050693n>.
- (448) Xiong, R.; Raemdonck, K.; Peynshaert, K.; Lentacker, I.; De Cock, I.; Demeester, J.; De Smedt, S. C.; Skirtach, A. G.; Braeckmans, K. Comparison of Gold Nanoparticle Mediated

- Photoporation: Vapor Nanobubbles Outperform Direct Heating for Delivering Macromolecules in Live Cells. *ACS Nano* **2014**, *8* (6), 6288–6296. <https://doi.org/10.1021/nn5017742>.
- (449) Peppas, N. A.; Van Blarcom, D. S. Hydrogel-Based Biosensors and Sensing Devices for Drug Delivery. *J. Control. Release* **2016**, *240*, 142–150. <https://doi.org/10.1016/j.jconrel.2015.11.022>.
- (450) Nguyen, N. T.; Shaegh, S. A. M.; Kashaninejad, N.; Phan, D. T. Design, Fabrication and Characterization of Drug Delivery Systems Based on Lab-on-a-Chip Technology. *Adv. Drug Deliv. Rev.* **2013**, *65* (11–12), 1403–1419. <https://doi.org/10.1016/j.addr.2013.05.008>.
- (451) Gorodzha, S. N.; Muslimov, A. R.; Syromotina, D. S.; Timin, A. S.; Tcvetkov, N. Y.; Lepik, K. V.; Petrova, A. V.; Surmeneva, M. A.; Gorin, D. A.; Sukhorukov, G. B.; Surmenev, R. A. A Comparison Study between Electrospun Polycaprolactone and Piezoelectric Poly(3-Hydroxybutyrate-Co-3-Hydroxyvalerate) Scaffolds for Bone Tissue Engineering. *Colloids Surfaces B Biointerfaces* **2017**, *160*, 48–59. <https://doi.org/10.1016/j.colsurfb.2017.09.004>.
- (452) Parakhonskiy, B. V.; Yashchenok, A. M.; Konrad, M.; Skirtach, A. G. Colloidal Micro- and Nano-Particles as Templates for Polyelectrolyte Multilayer Capsules. *Adv. Colloid Interface Sci.* **2014**, *207* (1), 253–264. <https://doi.org/10.1016/j.cis.2014.01.022>.
- (453) Gao, C.; Leporatti, S.; Moya, S.; Donath, E.; Möhwald, H. Swelling and Shrinking of Polyelectrolyte Microcapsules in Response to Changes in Temperature and Ionic Strength. *Chem. - A Eur. J.* **2003**, *9* (4), 915–920. <https://doi.org/10.1002/chem.200390113>.
- (454) Zhou, J.; Moya, S.; Ma, L.; Gao, C.; Shen, J. Polyelectrolyte Coated PLGA Nanoparticles: Templatation and Release Behavior. *Macromol. Biosci.* **2009**, *9* (4), 326–335. <https://doi.org/10.1002/mabi.200800188>.
- (455) Hu, S. H.; Tsai, C. H.; Liao, C. F.; Liu, D. M.; Chen, S. Y. Controlled Rupture of Magnetic Polyelectrolyte Microcapsules for Drug Delivery. *Langmuir* **2008**, *24* (20), 11811–11818. <https://doi.org/10.1021/la801138e>.
- (456) Yashchenok, A. M.; Delcea, M.; Videnova, K.; Jares-Erijman, E. A.; Jovin, T. M.; Konrad, M.; Möhwald, H.; Skirtach, A. G. Enzyme Reaction in the Pores of CaCO₃ Particles upon Ultrasound Disruption of Attached Substrate-Filled Liposomes. *Angew. Chemie - Int. Ed.* **2010**, *49* (44), 8116–8120. <https://doi.org/10.1002/anie.201003244>.
- (457) Skirtach, A. G.; Muñoz Javier, A.; Kreft, O.; Köhler, K.; Piera Alberola, A.; Möhwald, H.; Parak, W. J.; Sukhorukov, G. B. Laser-Induced Release of Encapsulated Materials inside Living Cells. *Angew. Chemie - Int. Ed.* **2006**, *45* (28), 4612–4617. <https://doi.org/10.1002/anie.200504599>.
- (458) Peer, D.; Karp, J. M.; Hong, S.; Farokhzad, O. C.; Margalit, R.; Langer, R. Nanocarriers as an Emerging Platform for Cancer Therapy. *Nat. Nanotechnol.* **2007**, *2* (12), 751–760. <https://doi.org/10.1038/nnano.2007.387>.

- (459) Johnston, A. P. R.; Cortez, C.; Angelatos, A. S.; Caruso, F. Layer-by-Layer Engineered Capsules and Their Applications. *Curr. Opin. Colloid Interface Sci.* **2006**, *11* (4), 203–209. <https://doi.org/10.1016/j.cocis.2006.05.001>.
- (460) Luo, D.; Gould, D. J.; Sukhorukov, G. B. Local and Sustained Activity of Doxycycline Delivered with Layer-by-Layer Microcapsules. *Biomacromolecules* **2016**, *17* (4), 1466–1476. <https://doi.org/10.1021/acs.biomac.6b00070>.
- (461) Zou, A.; Yang, Y.; Cheng, J.; Garamus, V. M.; Li, N. Construction and Characterization of a Novel Sustained-Release Delivery System for Hydrophobic Pesticides Using Biodegradable Polydopamine-Based Microcapsules. *J. Agric. Food Chem.* **2018**, *66* (25), 6262–6268. <https://doi.org/10.1021/acs.jafc.8b00877>.
- (462) Sofos, S. S.; Shokrollahi, K. *Book Review*; Springer Science & Business Media, 2013; Vol. 71. <https://doi.org/10.1097/sap.0b013e31825c76ca>.
- (463) Ng, K. Y. B.; Mingels, R.; Morgan, H.; Macklon, N.; Cheong, Y. In Vivo Oxygen, Temperature and PH Dynamics in the Female Reproductive Tract and Their Importance in Human Conception: A Systematic Review. *Hum. Reprod. Update* **2018**, *24* (1), 15–34. <https://doi.org/10.1093/HUMUPD/DMX028>.
- (464) Bouhemad, B.; Zhang, M.; Lu, Q.; Rouby, J. J. Clinical Review: Bedside Lung Ultrasound in Critical Care Practice. *Crit. Care* **2007**, *11* (1), 1–9. <https://doi.org/10.1186/cc5668>.
- (465) Yin, N.; Hu, L.; Xiao, Z. B.; Liu, C.; Chen, W. Z.; Roberts, N.; Chen, J. Y.; Wang, Z. B. Factors Influencing Thermal Injury to Skin and Abdominal Wall Structures in HIFU Ablation of Uterine Fibroids. *Int. J. Hyperth.* **2018**, *34* (8), 1298–1303. <https://doi.org/10.1080/02656736.2018.1433880>.
- (466) Hu, J.; Zhang, G.; Liu, S. Enzyme-Responsive Polymeric Assemblies, Nanoparticles and Hydrogels. *Chem. Soc. Rev.* **2012**, *41* (18), 5933–5949. <https://doi.org/10.1039/c2cs35103j>.
- (467) Ulijn, R. V. Enzyme-Responsive Materials: A New Class of Smart Biomaterials. *J. Mater. Chem.* **2006**, *16* (23), 2217–2225. <https://doi.org/10.1039/b601776m>.
- (468) de la Rica, R.; Aili, D.; Stevens, M. M. Enzyme-Responsive Nanoparticles for Drug Release and Diagnostics. *Adv. Drug Deliv. Rev.* **2012**, *64* (11), 967–978. <https://doi.org/10.1016/j.addr.2012.01.002>.
- (469) Chen, D. R.; Bei, J. Z.; Wang, S. G. Polycaprolactone Microparticles and Their Biodegradation. *Polym. Degrad. Stab.* **2000**, *67* (3), 455–459. [https://doi.org/10.1016/S0141-3910\(99\)00145-7](https://doi.org/10.1016/S0141-3910(99)00145-7).
- (470) Gai, M.; Frueh, J.; Tao, T.; Petrov, A. V.; Petrov, V. V.; Shesterikov, E. V.; Tverdokhlebov, S. I.; Sukhorukov, G. B. Polylactic Acid Nano- and Microchamber Arrays for Encapsulation of Small Hydrophilic Molecules Featuring Drug Release via High Intensity Focused Ultrasound. *Nanoscale* **2017**, *9* (21), 7063–7070. <https://doi.org/10.1039/C7NR01841J>.
- (471) Hammond, P. T. Form and Function in Multilayer Assembly: New Applications at the Nanoscale. *Adv. Mater.* **2004**, *16* (15 SPEC. ISS.), 1271–1293. <https://doi.org/10.1002/adma.200400760>.

- (472) Kiryukhin, M. V.; Man, S. M.; Tonoyan, A.; Low, H. Y.; Sukhorukov, G. B. Adhesion of Polyelectrolyte Multilayers: Sealing and Transfer of Microchamber Arrays. *Langmuir* **2012**, *28* (13), 5678–5686. <https://doi.org/10.1021/la3003004>.
- (473) Gai, M.; Frueh, J.; Sukhorukov, G. B.; Girard-Egrot, A.; Rebaud, S.; Doumeche, B.; He, Q. Microcontact Printing of Polyelectrolyte Multilayer Thin Films: Glass-Viscous Flow Transition Based Effects and Hydration Methods. *Colloids Surfaces A Physicochem. Eng. Asp.* **2015**, *483*, 271–278. <https://doi.org/10.1016/j.colsurfa.2015.05.009>.
- (474) Coulembier, O.; Degée, P.; Hedrick, J. L.; Dubois, P. From Controlled Ring-Opening Polymerization to Biodegradable Aliphatic Polyester: Especially Poly(β -Malic Acid) Derivatives. *Prog. Polym. Sci.* **2006**, *31* (8), 723–747. <https://doi.org/10.1016/j.progpolymsci.2006.08.004>.
- (475) Chawla, J. S.; Amiji, M. M. Biodegradable Poly(ϵ -Caprolactone) Nanoparticles for Tumor-Targeted Delivery of Tamoxifen. *Int. J. Pharm.* **2002**, *249* (1–2), 127–138. [https://doi.org/10.1016/S0378-5173\(02\)00483-0](https://doi.org/10.1016/S0378-5173(02)00483-0).
- (476) Huebner, K. D.; Shrive, N. G.; Frank, C. B. Dexamethasone Inhibits Inflammation and Cartilage Damage in a New Model of Post-Traumatic Osteoarthritis. *J. Orthop. Res.* **2014**, *32* (4), 566–572. <https://doi.org/10.1002/jor.22568>.
- (477) Wang, Q.; Jiang, J.; Chen, W.; Jiang, H.; Zhang, Z.; Sun, X. Targeted Delivery of Low-Dose Dexamethasone Using PCL-PEG Micelles for Effective Treatment of Rheumatoid Arthritis. *J. Control. Release* **2016**, *230*, 64–72. <https://doi.org/10.1016/j.jconrel.2016.03.035>.
- (478) Shogren, R. Water Vapor Permeability of Biodegradable Polymers. *J. Environ. Polym. Degrad.* **1997**, *5* (2), 91–95. <https://doi.org/10.1007/BF02763592>.
- (479) Wu, D.; Zhang, Y.; Zhang, M.; Zhou, W. Phase Behavior and Its Viscoelastic Response of Polylactide/Poly(ϵ -Caprolactone) Blend. *Eur. Polym. J.* **2008**, *44* (7), 2171–2183. <https://doi.org/10.1016/j.eurpolymj.2008.04.023>.
- (480) Sukhorukov, G.; Fery, A.; Möhwald, H. Intelligent Micro- and Nanocapsules. *Prog. Polym. Sci.* **2005**, *30* (8–9), 885–897. <https://doi.org/10.1016/j.progpolymsci.2005.06.008>.
- (481) Xie, X.; Zhang, W.; Abbaspourrad, A.; Ahn, J.; Bader, A.; Bose, S.; Vegas, A.; Lin, J.; Tao, J.; Hang, T.; Lee, H.; Iverson, N.; Bisker, G.; Li, L.; Strano, M. S.; Weitz, D. A.; Anderson, D. G. Microfluidic Fabrication of Colloidal Nanomaterials–Encapsulated Microcapsules for Biomolecular Sensing. *Nano Lett.* **2017**, *17* (3), 2015–2020. <https://doi.org/10.1021/acs.nanolett.7b00026>.
- (482) Hou, J. T.; Ren, W. X.; Li, K.; Seo, J.; Sharma, A.; Yu, X. Q.; Kim, J. S. Fluorescent Bioimaging of PH: From Design to Applications. *Chem. Soc. Rev.* **2017**, *46* (8), 2076–2090. <https://doi.org/10.1039/c6cs00719h>.
- (483) Longstreet, A. R.; McQuade, D. T. Organic Reaction Systems: Using Microcapsules and Microreactors to Perform Chemical Synthesis. *Acc. Chem. Res.* **2013**, *46* (2), 327–338. <https://doi.org/10.1021/ar300144x>.
- (484) Song, J.; Chen, H. Preparation of Aroma Microcapsules with Sodium Alginate and Tetradecylallyldimethylammonium Bromide (TADAB) and Its Potential Applications in

- Cosmetics. *Flavour Fragr. J.* **2018**, *33* (2), 160–165. <https://doi.org/10.1002/ffj.3411>.
- (485) Yu, X.; Zhao, Z.; Nie, W.; Deng, R.; Liu, S.; Liang, R.; Zhu, J.; Ji, X. Biodegradable Polymer Microcapsules Fabrication through a Template-Free Approach. *Langmuir* **2011**, *27* (16), 10265–10273. <https://doi.org/10.1021/la201944s>.
- (486) Bysell, H.; Månsson, R.; Hansson, P.; Malmsten, M. Microgels and Microcapsules in Peptide and Protein Drug Delivery. *Adv. Drug Deliv. Rev.* **2011**, *63* (13), 1172–1185. <https://doi.org/10.1016/j.addr.2011.08.005>.
- (487) Ding, Y.; Li, W.; Zhang, F.; Liu, Z.; Zanjaniadeh Ezazi, N.; Liu, D.; Santos, H. A. Electrospun Fibrous Architectures for Drug Delivery, Tissue Engineering and Cancer Therapy. *Adv. Funct. Mater.* **2019**, *29* (2), 1–35. <https://doi.org/10.1002/adfm.201802852>.
- (488) Park, S. Bin; Lih, E.; Park, K. S.; Joung, Y. K.; Han, D. K. Biopolymer-Based Functional Composites for Medical Applications. *Prog. Polym. Sci.* **2017**, *68*, 77–105. <https://doi.org/10.1016/j.progpolymsci.2016.12.003>.
- (489) Shchukin, D. G.; Patel, A. A.; Sukhorukov, G. B.; Lvov, Y. M. Nanoassembly of Biodegradable Microcapsules for DNA Encasing. *J. Am. Chem. Soc.* **2004**, *126* (11), 3374–3375. <https://doi.org/10.1021/ja036952x>.
- (490) Youan, B. B. C.; Jackson, T. L.; Dickens, L.; Hernandez, C.; Owusu-Ababio, G. Protein Release Profiles and Morphology of Biodegradable Microcapsules Containing an Oily Core. *J. Control. Release* **2001**, *76* (3), 313–326. [https://doi.org/10.1016/S0168-3659\(01\)00445-X](https://doi.org/10.1016/S0168-3659(01)00445-X).
- (491) Seok Kwon, O.; Jang, J.; Bae, J. A Review of Fabrication Methods and Applications of Novel Tailored Microcapsules. *Curr. Org. Chem.* **2013**, *17* (1), 3–13. <https://doi.org/10.2174/138527213805289196>.
- (492) Whitesides, G. M. The Origins and the Future of Microfluidics. *Nature* **2006**, *442* (7101), 368–373. <https://doi.org/10.1038/nature05058>.
- (493) Wang, J. T.; Wang, J.; Han, J. J. Fabrication of Advanced Particles and Particle-Based Materials Assisted by Droplet-Based Microfluidics. *Small* **2011**, *7* (13), 1728–1754. <https://doi.org/10.1002/smll.201001913>.
- (494) Shah, R. K.; Shum, H. C.; Rowat, A. C.; Lee, D.; Agresti, J. J.; Utada, A. S.; Chu, L. Y.; Kim, J. W.; Fernandez-Nieves, A.; Martinez, C. J.; Weitz, D. A. Designer Emulsions Using Microfluidics. *Mater. Today* **2008**, *11* (4), 18–27. [https://doi.org/10.1016/S1369-7021\(08\)70053-1](https://doi.org/10.1016/S1369-7021(08)70053-1).
- (495) Anderson, J. M.; Shive, M. S. Biodegradation and Biocompatibility of PLA and PLGA Microspheres. *Adv. Drug Deliv. Rev.* **2012**, *64* (SUPPL.), 72–82. <https://doi.org/10.1016/j.addr.2012.09.004>.
- (496) Chee, M. J. K.; Ismail, J.; Kammer, H. W.; Kummerloöwe, C. Study on Miscibility of PEO and PCL in Blends with PHB by Solution Viscometry. *Polymer (Guildf)* **2001**, *43* (4), 1235–1239. [https://doi.org/10.1016/S0032-3861\(01\)00725-X](https://doi.org/10.1016/S0032-3861(01)00725-X).
- (497) Torres-Huerta, A. M.; Palma-Ramírez, D.; Domínguez-Crespo, M. A.; Del Angel-López,

- D.; De La Fuente, D. Comparative Assessment of Miscibility and Degradability on PET/PLA and PET/Chitosan Blends. *Eur. Polym. J.* **2014**, *61*, 285–299. <https://doi.org/10.1016/j.eurpolymj.2014.10.016>.
- (498) Hutmacher, D. W.; Schantz, T.; Zein, I.; Ng, K. W.; Teoh, S. H.; Tan, K. C. Mechanical Properties and Cell Cultural Response of Polycaprolactone Scaffolds Designed and Fabricated via Fused Deposition Modeling. *J. Biomed. Mater. Res.* **2001**, *55* (2), 203–216. [https://doi.org/10.1002/1097-4636\(200105\)55:2<203::AID-JBM1007>3.0.CO;2-7](https://doi.org/10.1002/1097-4636(200105)55:2<203::AID-JBM1007>3.0.CO;2-7).
- (499) Chang, S. H.; Lee, H. J.; Park, S.; Kim, Y.; Jeong, B. Fast Degradable Polycaprolactone for Drug Delivery. *Biomacromolecules* **2018**, *19* (6), 2302–2307. <https://doi.org/10.1021/acs.biomac.8b00266>.
- (500) Tyler, B.; Gullotti, D.; Mangraviti, A.; Utsuki, T.; Brem, H. Polylactic Acid (PLA) Controlled Delivery Carriers for Biomedical Applications. *Adv. Drug Deliv. Rev.* **2016**, *107*, 163–175. <https://doi.org/10.1016/j.addr.2016.06.018>.
- (501) Grémare, A.; Guduric, V.; Bareille, R.; Heroguez, V.; Latour, S.; L'heureux, N.; Fricain, J. C.; Catros, S.; Le Nihouannen, D. Characterization of Printed PLA Scaffolds for Bone Tissue Engineering. *J. Biomed. Mater. Res. - Part A* **2018**, *106* (4), 887–894. <https://doi.org/10.1002/jbm.a.36289>.
- (502) Ahmed, M. K.; Mansour, S. F.; Al-Wafi, R.; Afifi, M.; Uskoković, V. Gold as a Dopant in Selenium-Containing Carbonated Hydroxyapatite Fillers of Nanofibrous ϵ -Polycaprolactone Scaffolds for Tissue Engineering. *Int. J. Pharm.* **2020**, *577* (October 2019). <https://doi.org/10.1016/j.ijpharm.2019.118950>.
- (503) Zhang, J.; Gai, M.; Ignatov, A. V.; Dyakov, S. A.; Wang, J.; Gippius, N. A.; Frueh, J.; Sukhorukov, G. B. Stimuli-Responsive Microarray Films for Real-Time Sensing of Surrounding Media, Temperature, and Solution Properties via Diffraction Patterns. *ACS Appl. Mater. Interfaces* **2020**, *12* (16), 19080–19091. <https://doi.org/10.1021/acsami.0c05349>.
- (504) Berkland, C.; Pollauf, E.; Varde, N.; Pack, D. W.; Kim, K. Monodisperse Liquid-Filled Biodegradable Microcapsules. *Pharm. Res.* **2007**, *24* (5), 1007–1013. <https://doi.org/10.1007/s11095-006-9197-9>.
- (505) Situma, C.; Hashimoto, M.; Soper, S. A. Merging Microfluidics with Microarray-Based Bioassays. *Biomol. Eng.* **2006**, *23* (5), 213–231. <https://doi.org/10.1016/j.bioeng.2006.03.002>.
- (506) Cha, Y. J.; Park, S. M.; You, R.; Kim, H.; Yoon, D. K. Microstructure Arrays of DNA Using Topographic Control. *Nat. Commun.* **2019**, *10* (1), 1–8. <https://doi.org/10.1038/s41467-019-10540-2>.
- (507) Cavo, M.; Scaglione, S. Scaffold Microstructure Effects on Functional and Mechanical Performance: Integration of Theoretical and Experimental Approaches for Bone Tissue Engineering Applications. *Mater. Sci. Eng. C* **2016**, *68*, 872–879. <https://doi.org/10.1016/j.msec.2016.07.041>.
- (508) Pan, L.; Chortos, A.; Yu, G.; Wang, Y.; Isaacson, S.; Allen, R.; Shi, Y.; Dauskardt, R.; Bao, Z.

- An Ultra-Sensitive Resistive Pressure Sensor Based on Hollow-Sphere Microstructure Induced Elasticity in Conducting Polymer Film. *Nat. Commun.* **2014**, *5*.
<https://doi.org/10.1038/ncomms4002>.
- (509) Selvakumar, R.; Seethalakshmi, N.; Thavamani, P.; Naidu, R.; Megharaj, M. Recent Advances in the Synthesis of Inorganic Nano/Microstructures Using Microbial Biotemplates and Their Applications. *RSC Adv.* **2014**, *4* (94), 52156–52169.
<https://doi.org/10.1039/c4ra07903e>.
- (510) Sotiropoulou, S.; Sierra-Sastre, Y.; Mark, S. S.; Batt, C. A. Biotemplated Nanostructured Materials. *Chem. Mater.* **2008**, *20* (3), 821–834. <https://doi.org/10.1021/cm702152a>.
- (511) Liu, G.; Petrosko, S. H.; Zheng, Z.; Mirkin, C. A. Evolution of Dip-Pen Nanolithography (DPN): From Molecular Patterning to Materials Discovery. *Chem. Rev.* **2020**, *120* (13), 6009–6047. <https://doi.org/10.1021/acs.chemrev.9b00725>.
- (512) Grafström, S. Photoassisted Scanning Tunneling Microscopy. *J. Appl. Phys.* **2002**, *91* (3), 1717–1753. <https://doi.org/10.1063/1.1432113>.
- (513) Salaita, K.; Wang, Y.; Mirkin, C. A. Applications of Dip-Pen Nanolithography. *Nat. Nanotechnol.* **2007**, *2* (3), 145–155. <https://doi.org/10.1038/nnano.2007.39>.
- (514) Ko, W.; Ma, C.; Nguyen, G. D.; Kolmer, M.; Li, A. P. Atomic-Scale Manipulation and In Situ Characterization with Scanning Tunneling Microscopy. *Adv. Funct. Mater.* **2019**, *29* (52), 1–24. <https://doi.org/10.1002/adfm.201903770>.
- (515) Perl, A.; Reinhoudt, D. N.; Huskens, J. Microcontact Printing: Limitations and Achievements. *Adv. Mater.* **2009**, *21* (22), 2257–2268.
<https://doi.org/10.1002/adma.200801864>.
- (516) Xia, Y.; McClelland, J. J.; Gupta, R.; Qin, D.; Zhao, X.-M.; Sohn, L. L.; Celotta, R. J.; Whitesides, G. M. Replica Molding Using Polymeric Materials: A Practical Step toward Nanomanufacturing. *Adv. Mater.* **1997**, *9* (2), 147–149.
<https://doi.org/10.1002/adma.19970090211>.
- (517) Zhao, X.; Xia, Y.; Whitesides, G. M. Fabrication of Three-Dimensional Micro-Structures: Microtransfer Molding. *Adv. Mater.* **1996**, *8* (10), 837–840.
<https://doi.org/10.1002/adma.19960081016>.
- (518) Kim, E.; Xia, Y.; Whitesides, G. M. Polymer Microstructures Formed by Moulding in Capillaries. *Nature* **1995**, *376* (6541), 581–584. <https://doi.org/10.1038/376581a0>.
- (519) Zaumseil, J.; Meitl, M. A.; Hsu, J. W. P.; Acharya, B. R.; Baldwin, K. W.; Loo, Y. L.; Rogers, J. A. Three-Dimensional and Multilayer Nanostructures Formed by Nanotransfer Printing. *Nano Lett.* **2003**, *3* (9), 1223–1227. <https://doi.org/10.1021/nl0344007>.
- (520) Qin, D.; Xia, Y.; Whitesides, G. M. Soft Lithography for Micro- and Nanoscale Patterning. *Nat. Protoc.* **2010**, *5* (3), 491–502. <https://doi.org/10.1038/nprot.2009.234>.
- (521) Xia, Y.; Kim, E.; Zhao, X.-M.; Rogers, J. A.; Prentiss, M.; Whitesides, G. M. Complex Optical Surfaces Formed by Replica Molding Against Elastomeric Masters. *Science (80-.)*. **1996**, *273* (5273), 347–349. <https://doi.org/10.1126/science.273.5273.347>.

- (522) Credi, C.; Pintossi, D.; Bianchi, C. L.; Levi, M.; Griffini, G.; Turri, S. Combining Stereolithography and Replica Molding: On the Way to Superhydrophobic Polymeric Devices for Photovoltaics. *Mater. Des.* **2017**, *133*, 143–153. <https://doi.org/10.1016/j.matdes.2017.07.068>.
- (523) Snyder, J.; Rin Son, A.; Hamid, Q.; Sun, W. Fabrication of Microfluidic Manifold by Precision Extrusion Deposition and Replica Molding for Cell-Laden Device. *J. Manuf. Sci. Eng. Trans. ASME* **2016**, *138*(4), 1–11. <https://doi.org/10.1115/1.4031551>.
- (524) Pham, T. A.; Kim, D. P.; Lim, T. W.; Park, S. H.; Yang, D. Y.; Lee, K. S. Three-Dimensional SiCN Ceramic Microstructures via Nano-Stereolithography of Inorganic Polymer Photoresists. *Adv. Funct. Mater.* **2006**, *16*(9), 1235–1241. <https://doi.org/10.1002/adfm.200600009>.
- (525) Lee, H. J.; Yoon, T. H.; Kim, D. P. Fabrication of Microfluidic Channels Derived from a UV/Thermally Cured Preceramic Polymer via a Soft Lithographic Technique. *Microelectron. Eng.* **2007**, *84*(12), 2892–2895. <https://doi.org/10.1016/j.mee.2007.03.002>.
- (526) Liu, G.; Lin, G.; Lin, X.; Zhou, H.; Chen, H.; Hao, L.; Zhou, X. Enzyme and PH Dual-Responsive Avermectin Nano-Microcapsules for Improving Its Efficacy. *Environ. Sci. Pollut. Res.* **2019**, *26*(24), 25107–25116. <https://doi.org/10.1007/s11356-019-05804-9>.

Publications

1. **Zhang, J.**; Sun, R.; Desouza-Edwards, A. O.; Frueh, J.; Sukhorukov, G. B. Microchamber Arrays Made of Biodegradable Polymers for Enzymatic Release of Small Hydrophilic Cargos. *Soft Matter* **2020**, *16* (9), 2266–2275.
2. **Zhang, J.**; Gai, M.; Ignatov, A. V.; Dyakov, S. A.; Wang, J.; Gippius, N. A.; Frueh, J.; Sukhorukov, G. B. Stimuli-Responsive Microarray Films for Real-Time Sensing of Surrounding Media, Temperature, and Solution Properties via Diffraction Patterns. *ACS Appl. Mater. Interfaces* **2020**, *12* (16), 19080–19091.
3. **Zhang, J.**; Sun, R.; Kudryavtseva, V. L.; Gould, D. J.; Sukhorukov, G. B. Fabrication of identical biodegradable microcages with predesigned shape printed from microarrays for controlled release of small hydrophilic molecules. (*Ready for submission*)
4. **Zhang, J.**; Sun, Z.; Sun, R.; Jie, K.; Sukhorukov, G. B. Templating of inorganic microarray films and minified microarray structures via soft lithography. (*In preparation*)
5. Ermakov, A. V.; Kudryavtseva, V. L.; Demina, P. A.; Verkhovskii, R. A.; **Zhang, J.**; Lengert, E. V.; Sapelkin, A. V.; Goryacheva, I. Y.; Sukhorukov, G. B. Site-Specific Release of Reactive Oxygen Species from Ordered Arrays of Microchambers Based on Polylactic Acid and Carbon Nanodots. *J. Mater. Chem. B* **2020**, *8* (35), 7977–7986.
6. Kudryavtseva, V.; Boi, S.; Read, J.; Guillemet, R.; **Zhang, J.**; Udalov, A.; Shesterikov, E.; Tverdokhlebov, S.; Pastorino, L.; Gould, D. J.; et al. Biodegradable Defined Shaped Printed Polymer Microcapsules for Drug Delivery. *ACS Appl. Mater. Interfaces* **2021**. <https://doi.org/10.1021/acsami.0c21607>.